PHD

Investigation of Rab-GAPs as links between insulin signalling and GLUT4 translocation

Roche, Lucy

Award date:
2013

Awarding institution:
University of Bath

Investigation of Rab-GAPs as links between insulin signalling and GLUT4 translocation

Lucy Mary Roche

A thesis submitted for the degree of Doctor of Philosophy

University of Bath

Department of Biology and Biochemistry

May 2013

Abstract

TBC1D1 and TBC1D4 are Rab-GTPase Activating Proteins (Rab-GAPs) expressed in insulin-responsive tissues. Both proteins are involved in mechanisms which regulate basal levels of glucose transport and have been identified as targets of insulin and AMP-dependant kinase (AMPK) signalling pathways, which regulate GLUT4 translocation to the plasma membrane in muscle.

We have characterised the C2C12 muscle cell model retrovirally expressing HA-epitope tagged GLUT4 in order to investigate how distinct signalling pathways regulate GLUT4 trafficking. Insulin-stimulation and treatment with the AMPK-activator (AICAR) increased the levels of GLUT4 at the plasma membrane by two-fold in C2C12 myotubes. Insulin-stimulation and activation of AMPK mobilised GLUT4 in to the actively cycling pool. However, our data revealed that insulin-stimulation or AMPK activation resulted in distinct effects on GLUT4 trafficking parameters at steady-state. Insulin increased GLUT4 exocytosis (k_{ex}) of this cycling pool. Activation of AMPK inhibited GLUT4 internalisation (k_{en}). The combined effect of insulin-stimulation and AMPK-activation was synergistic and led to increased GLUT4 cell surface levels above those obtained with either treatment alone. Insulin-stimulation and AMPK activation in combination resulted in a partially additive effect on the size of the actively recycling GLUT4 pool and further enhanced k_{ex} of this cycling pool.

Kinetic studies were performed to measure the effect of TBC1D1 and TBC1D4 knockdown on GLUT4 trafficking in C2C12 myotubes. siRNA-mediated knockdown of TBC1D4 did not affect the basal levels of cell surface GLUT4. Knockdown of TBC1D1 increased cell surface levels of GLUT4 in basal and in insulin-stimulated C2C12 myotubes. The knockdown increased the release of GLUT4 in to the actively recycling pool. By contrast TBC1D1 knockdown did not change the levels of GLUT4 at the plasma membrane that occur in the presence of the AMPK-activator (AICAR). Our results support a model whereby TBC1D1 inactivation by signalling-dependant phosphorylation is required for

GLUT4 translocation, but with insulin and AICAR having separate and distinguishable effects on the released GLUT4.

Acknowledgments

I would like to express my gratitude to my supervisor Professor Geoff Holman for giving me the opportunity to carry out this PhD in his laboratory and for all the help, encouragement and supervision over the last four years. This thesis would not have been possible without his advice and guidance. I would also like to express my appreciation to my co-supervisor Francoise Koumanov for all her support, advice and useful discussions throughout this project. Funding for this research project has been provided by the BBSRC and Astra Zeneca.

I would also like to thank Anna Marley my project supervisor at AstraZeneca for her support and valued input during this project. I am also thankful for the opportunity to spend a few months at AstraZeneca in order to carry out the Taqman expression analysis detailed in Chapter 3. During my time working at Astra Zeneca I am very grateful to Alison Davies, Henry Brown and Carol, and also Linda Härndahl and Phil Chapman who kindly gave up their time and expertise to help me to complete these studies. I also thank Daniel Fazakerley for his help and patience teaching me the GLUT4 trafficking assays. I would also like to thank Jim Caunt who has kindly lent his time and expertise helping me to obtain images of C2C12 myotubes using the the IN-Cell Analyser system.

I wish to thank all of the staff and students past and present I have worked with at the University of Bath, Department of Biology and Biochemistry. In Lab 1.37 (Francoise, Judith, Daniel, Paul, Joe, Jim, Ying, Vinit, Rich and Samantha) it has been a great pleasure to work alongside such a great group of people for the past four years. I would also like to thank my friends and fellow PhD students in Lab 0.44. In particular, to Laura, for her friendship and support over the years and to Gail, for all her encouragement throughout this writing process. I'd also like to thank all of the committee members and PhD students in PGBio. They have each helped make my time in Bath more fun and interesting. Finally, I would like to thank my parents for their love, support and encouragement over the last four years and to Sam for his endless support and understanding.

Table of Contents

List of Tables

List of Figures

Nomenclature

aa	Amino acid
AA	Antibiotic Antimycotic
ACC	Acetyl CoA Carboxylase
AESBF	4-(2-Aminoethyl) benzenesulfonyl fluoride hydrochloride
AGG	Antibody Generation Group
AICAR	5-Aminoimidazole-4-carboxamide ribonucleotide
AMP	AMP-activated Protein
AMPK	AMP-activated Protein Kinase
APS	Ammonium Persulphate
AS160	Akt(PKB) substrate of 160 kDa
ATP	Adenosine-5'-Triphosphate
B2M	Beta-2-microglobulin
BCA	Bicinchroninic Acid
BMI	Body mass index
bp	Base pairs
BSA	Bovine Serum Albumin
CaM	Calmodulin
CAMK	Ca2+-Calmodulin protein kinase
CAMKK	Ca2+-Calmodulin protein kinase kinase
CBD	Calmodulin binding domian
cDNA	Complementary DNA
C-terminus	Carboxy-terminus
CVD	Cardio vascular disease
CYP A	Cyclophilin A
d H_2O	Distilled H_2O
Da	Dalton
DAG	Diacylglycerol
dd H_2O	Double Distilled H_2O
DEPC	diethyl pyro carbonate
DMEM	Dulbecco's Modified Essential Medium

DMSO	Dimethylsulfoxide
DNA	Deoxyribonucleic acid
dNTP	Deoxyribonucleotides
DTT	Dithiothreitol
E. coli	Escherichia Coli
ECL	Enhanced Chemi-luminescence
EDL	Extensor Digitorum Longus
EDTA	Ethylenediaminetetraacetic Acid
EGTA	Ethyleneglycoltetraacetic Acid
EPI	Epitrochlearis
EV	Empty Vector
FATPs	Fatty Acid Transporter Proteins
FBS	Foetal Bovine Serum
F moles	Femto-moles
FFA	Free fatty acids
g	Grams
g	Gravity
GA	Glutaldehyde
GAP	GTPase-activating Protein
GAPDH	Glyceraldehyde 3-phosphate dehydrogenase
GAS	Gastrocnemius
GDP	Guanosine diphosphate
GEF	Guanosine exchange factor
GFP	Green Fluorescent Protein
GLUT	Facilitative Glucose Transporter
GS	Goat Serum
GSV	GLUT4 storage vesicle
GTP	Guanosine triphosphate
Gus B	Beta Glucuronidase
HA	Hemagglutinin
HBS	HEPES-buffered saline
HEK	Human Embryonic Kidney

HEPES	4-(2-hydroxyethyl)-1-piperazineethanesulfonic acid
HPRT	Hypoxanthine phosphoribosyltransferase 1
HRP	Horse Radish Peroxidase
HS	Horse Serum
IgG	Immunoglobulin G
IR	Insulin Receptor
IR	Insulin receptor
IRAP	Insulin-responsive aminopeptidase
IRS	Insulin Receptor Substrate
IRS	Insulin receptor substrate 1-4
kb	Kilo base pair
kDa	Kilo Dalton
Kex	Rate constant for exocytosis
Kin	Rate constant for endocytosis
LB	Luria Broth
LCFA	Long chain fatty acids
M	Molar
mA	Milliamps
mg	Milligram
Min	Minutes
ml	Millilitre
mM	Millimolar
MPR	Mannose 6-phosphate receptor
mRNA	Messenger Ribonucleic acid
NEFA	Non-esterified fatty acid
ng	Nanogram
nM	Nanomolar
nm	Nanometer
N-terminus	Amino-terminus
PAS	Phospho-(Ser/Thr) Akt substrate
PBS	Phosphate Buffered Saline
PCR	Polymerase Chain Reaction

PDH	Pyruvate Deohydrogenase
PDK 1	Pyruvate dehydrogenase
PFA	Paraformaldehyde
PFK	Phosphofructokinase
PH domain	Plecstrin homology domain
PI3K	Phosphoinositide 3-kinase
PIP_2	Phosphatidylinositol (4,5)-bisphosphate
PIP_3	Phosphatidylinositol (3,4,5)-trisphosphate
PKB	Protein Kinase B
PKC	Protein Kinase C
PTB	Phosphotyrosine binding domain
QPCR	Quantitative
RCS	Recominant Congenic Strain
RLT	RNAeasy Lysis Buffer
rt	Real Time
RT-PCR	Reverse Transcription Polymerase Chain Reaction
SDS	Sodium Dodecyl Sulfate
SDS-PAGE	Sodium Dodecyl Sulfate - Polyacrylamide Gel Electrophoresis
sec	Seconds
SH2	Sr2-homology domain
siRNA	Small Interferring RNA
SOL	Soleus
T2DM	Type 2 Diabetes Militis
TA	Tibialis Anterior
TAE	Tris –acetate EDTA
TBP	TATA box binding protein
TBS	Tris-buffered saline
TCA	Tri-chloroacetic Acid
TEMED	N,N,N,N’-tetramethylethylenediamine
Tg	Transgenic Strain
TGN	Trans golgi network
TUG	

TV	Tubulo vesicular
UV	Ultraviolet
V	volts
VAMP	Vesicle associated membrane protein
w/v	Weight/Volume
WT	Wild type
µg	Microgram
µl	Microlitre
µM	Micromolar

1 Introduction

This thesis details the mechanisms that are involved in maintaining basal levels of glucose transport and which are involved in both insulin regulation and energy-status regulation of translocation of the glucose transporter GLUT4. It is widely considered that understanding these fundamental mechanisms can lead in turn to a greater understanding of factors that contribute to the insulin resistance that occurs in metabolic disease. Therefore, to put the thesis study into an appropriate context I introduce, in this chapter, a consideration of relevant aspects of obesity and type 2 diabetes.

1.1 Obesity

1.1.1 Classification

Obesity is defined by the World Health Organisation (WHO) as an abnormal or excessive fat accumulation that may impair health. In 2008, the number of overweight and obese adults worldwide had reached 1.4 billion. Body Mass Index (BMI) (kg/m^2) is the primary measurement used for the classification of obesity. An overweight individual is classified as having a BMI of over 25, and obesity is defined when the BMI is over 30. Obesity is described as a state of energy imbalance, where Individuals expend less energy than the food that they consume (Froguel & Boutin, 2001). A small percentage of severe obesity cases are the result of a number of monogenic mutations in the leptin–melanocortin system. These pathways are critical for the regulation of energy balance (Ranadive & Vaisse, 2008). However, in the majority of obesity cases, the disease is multifactorial associated with both genetic factors and environmental factors which include nutrition and lifestyle. The genetic component of common obesity is likely to be determined by a number of susceptibility genes (polygenic). These genetic and environmental factors interact with each other in complex ways to influence the development of the disease. Persistent obesity can lead to the dysregulation of glucose and fat metabolism, resulting in an array of clinical conditions collectively known as the metabolic syndrome (Misra & Khurana, 2008). These conditions include glucose intolerance, insulin resistance, dyslipidaemia and hypertension (Eckel, et al., 2005). All of these are

risk factors associated with the development of type 2 diabetes mellitus (T2DM) and cardiovascular disease (CVD). Furthermore, weight loss either through sustained lifestyle changes or surgical intervention can improve blood glucose levels which reduce the risk of developing the T2DM (Aucott, 2008).

1.1.2 Whole-body insulin resistance

Metabolic homeostasis is tightly regulated by two pancreatic hormones; these are glucagon and insulin. Glucagon is secreted from pancreatic alpha cells during the fasted state. Glucagon targets the liver and skeletal muscle cells and mediates the release of glucose from the glycogen stores a process known as glycogenolysis. In addition, glucagon targets adipose tissue and stimulates the up-regulation of lipolysis. In response to food intake, insulin is secreted from pancreatic beta cells to regulate the storage and utilisation of glucose in the liver and skeletal muscle. Skeletal muscle is the major site for post prandial glucose disposal. In addition, insulin stimulates the production of fatty acids and their storage in adipose tissue (Lazar, 2005).

Obesity is associated with insulin resistance. Insulin resistance is a metabolic state which describes how peripheral tissues fail to respond to normal levels of insulin. As a consequence, the production of insulin and its secretion from the pancreas increases. However, if insulin resistance persists, this can eventually lead to an elevation in blood glucose levels (hyperglycaemia) and free fatty-acids (FFA) (dyslipidaemia), which contribute to the development of T2DM. Equally, hyperglycaemia and dyslipidaemia can exacerbate an insulin-resistant state.

1.1.3 Metabolic Flexibility

The term ‘metabolic flexibility’ has been proposed to describe how muscle can dynamically switch between glucose and fat oxidation (Figure 1.1). This is related to fitness, body fat and insulin sensitivity. Lean individuals who regularly exercise are described as ‘metabolically flexible’. These individuals are able to switch between the utilisation of fatty acid in the fasted state and increased glucose oxidation during insulin stimulation. In contrast, individuals who are

obese and aerobically unfit are described as ‘metabolically inflexible’. These individuals have a blunted preference for fat oxidation during fasting and display an impaired insulin-stimulated glucose oxidation (Kelley, 2005). Furthermore, metabolic flexibility has been found to be an intrinsic property of muscle cells (Ukropcova, et al., 2005). Primary human muscle cells were isolated from a mixed population of donors. The metabolic phenotype *in vitro* was found to mirror the *in vivo* state of the donor. This study demonstrated that ‘metabolically inflexible’ muscle cells have a decreased ability to oxidise fatty acids in the presence of glucose. Furthermore, these muscle cells have a reduced capacity to increase fatty acid oxidation when treated with high concentration of the saturated fatty acid palmitate.

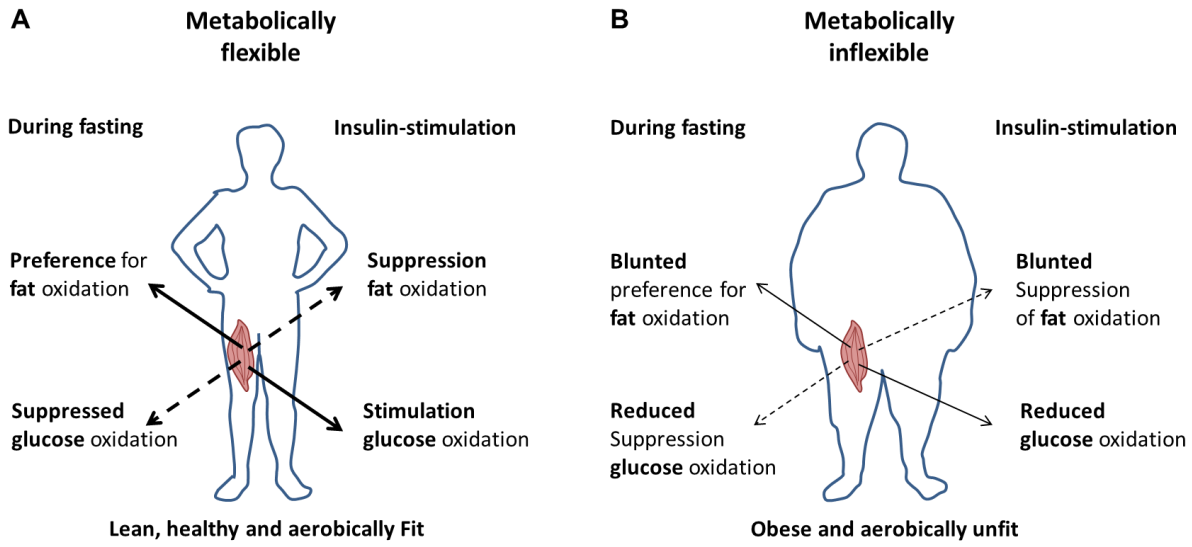

Figure 1.1: Metabolic Flexibility. The flexibility of skeletal muscle to switch between fat and glucose oxidation is related to fitness, insulin sensitivity and body fat. (A) An aerobically fit individual with preference for fat oxidation in the fasted state. Insulin stimulation inhibits fat oxidation and switches muscle to utilise glucose. (B) An aerobically unfit individual with a blunted fat oxidation in the fasted state reliance on glucose metabolism. The muscle is less sensitive to insulin and so there is a reduced stimulation for glucose oxidation and suppression of fat oxidation. This diagram has been adapted from (Kelley, 2005).

1.1.4 Glucose-fatty acid cycle

In 1964, Randle and co-workers proposed a mechanism which described the relationship between glucose and fatty acid utilisation in skeletal muscle (Randle, 1964). This model is known as the ‘Randle hypothesis’ and describes how nutrient levels independently determine the metabolic effects within the

cell. Circulatory FFAs are transported in to muscle cells to be oxidised which elevates cellular levels of Acetyl CoA and citrate. This results in the inhibition of Phosphofructokinase (PFK) and Pyruvate Dehydrogenase (PDH), enzymes which are involved in glycolysis and glucose utilisation. The relationship between elevated serum triglycerides, insulin sensitivity and T2DM has been widely investigated (Bergman & Ader, 2000). A European study conducted on a large cohort of healthy individuals, concluded that there was a negative correlation between levels of non-esterified fatty-acids (NEFA) and insulin sensitivity (Baldeweg, et al., 2000). In contrast, excess circulating glucose typically associated with insulin resistance could inhibit fatty acid oxidation. This is known as the reverse Randle cycle. This process is associated with individuals who are 'metabolically inflexible' (described in section 1.1.3).

1.1.5 Skeletal muscle classification

As skeletal muscle contributes extensively to metabolic interactions between glucose and fat metabolism, with differences in the interactions occurring in different muscle types, it is necessary to consider muscle type classification. Skeletal muscles are classed depending on their fibre type composition. There are four main muscle fibre types (Type I, IIA, IIB and IIX). Muscle fibres are defined by their strength of contraction (slow or fast) and resistance to fatigue (oxidative or glycolytic) which are correlated with sarcoplasmic reticulum development (poor or richly developed) and mitochondria content (abundant or few) respectively (Tasic, et al., 2003) (Schiaffino & Reggiani, 2011). Type I muscle fibres are slow twitch and have a high oxidative capacity. Type IIA, IIB and IIX are fast twitch glycolytic muscle fibres however type IIA fibres have an increased oxidative capacity and resistance to fatigue (Schiaffino & Reggiani, 2011). The Soleus muscle is a slow-twitch oxidative muscle composed of entirely type I and type IIA muscle fibres (Song, et al., 1999). The tibialis anterior (TA), extensor digitorum longus (EDL), epitrochlearis muscles (EPI) and flexor digitorum brevis (FDB) are fast-twitch and contain predominately type II fibres (Henriksen, et al., 1990). It has been suggested that fibre-type composition may affect how muscle responds to contraction-stimuli. In TA muscle the mitochondrial content is inversely correlated with the basal kinase

activity. For instance in glycolytic (white) TA muscle fibres the basal phosphorylation levels of the protein kinases AMPK, p38, p42 and p44 MAPK are significantly greater than in oxidative (red) TA fibres. Comparatively, the level of Akt phosphorylation was similar between the two fibres types (Ljubicic & Hood, 2008)

1.2 Fatty acid Transport

Fatty acids are elevated in the circulation either after the consumption of dietary long chain fatty acids (LCFA) esterified in triacylglycerol (TAG) or as a result of the lipolysis of fat stored in adipose tissue. Fatty-acids are a major fuel source for skeletal muscle during fasting and exercise. The uptake of fatty acids in to target tissues either occurs by means of passive diffusion across the plasma membrane or this process is facilitated through fatty-acid transporter proteins (FATPs). Insulin and muscle contraction mediate the translocation of FAT/CD36 present in intracellular vesicles to the plasma membrane in skeletal muscle to increase fatty-acid uptake (Bonen, et al., 2000). The oxidative soleus muscle expresses increased levels of fatty acid transport proteins FAT/CD36 and FABP proteins compared with the glycolytic flexor digitorum brevis (FDB) muscle. The increased expression of FATPs in the soleus muscle accounts for the increased rate of palmitate transport and oxidation in soleus muscle (Bonen, et al., 1998).

1.3 Glucose Transporters

1.3.1 The GLUT Family

Circulating glucose is removed from the blood stream by a family of glucose transporters (GLUTs). Glucose transporters are expressed on the surface of target tissues and function to facilitate the transfer of glucose across the plasma membrane. Glucose transporters are a group of homologous plasma membrane proteins comprised of 12 trans-membrane alpha helices (Figure 1.2). There are 14 GLUT family members to date (Thorens & Mueckler, 2009). These have been divided into three distinct sub classes (Joost, et al., 2002) (Table 1.1).

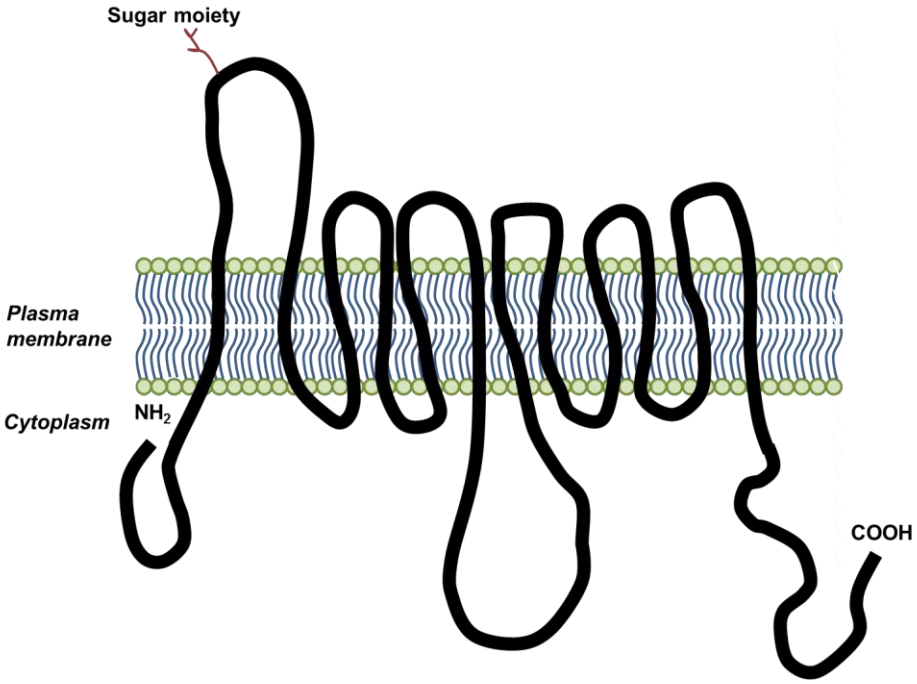

Figure 1.2: A schematic diagram of the GLUT4. There are 14 GLUT family members to date which are predicted to comprise of 12 trans-membrane alpha helices. The N and C Termini are located in the cytosol. The family has been divided into three distinct classes, which are outlined in Table 1.1. This diagram is modified from (Bryant, et al., 2002).

GLUT1 was isolated from human erythrocyte membranes and was the first transporter to be identified. In 1985, GLUT1 was characterised and successfully cloned (Mueckler, et al., 1985). GLUT1 is ubiquitously expressed in most tissues including in insulin-responsive tissues. Skeletal muscle, adipose and liver are the major tissues which contribute in whole-body post-prandial glucose disposal. The liver is responsible for the removal of approximately 7% of dietary glucose (Fernandes, et al., 2011). This is facilitated by the transporter GLUT2, which is localised at the cell surface. Skeletal muscle is responsible for the clearance of around 69% of dietary glucose and a further 7% is transported into adipose tissue (Fernandes, et al., 2011). In contrast to in the liver, it is well established that glucose transport into skeletal muscle and adipose tissue is regulated by insulin.

Table 1.1: Summary of the glucose transporter family (GLUT) members.

Class	Protein	Expression	Proposed Function
I	**GLUT 1**	Ubiquitous, erythrocytes, brain	Basal glucose uptake; transport across blood brain barriers
	GLUT 3	Brain; neuronal	Neuronal transport
	GLUT 4	Adipose, skeletal muscle and heart	Insulin-regulated transport in fat and muscle
	GLUT 2	Liver, islets, kidney, small intestine	High capacity low affinity transport
	GLUT 14	Testes	High sequence similarity to GLUT3
II	**GLUT 5**	Intestine, kidney, testis	Transport of fructose
	GLUT 7	Small intestine, colon, testis	Transport of fructose
	GLUT 9	Liver, kidney	
	GLUT 11	Heart, muscle	Muscle specific fructose transporter
III	**GLUT 6**	Spleen, leukocytes, brain	
	GLUT 8	Testes, blastocyst, brain, muscle, adipocytes	Insulin-responsive transport blastocyst. Fuel supply mature spermatozoa
	GLUT 10	Liver, pancreas	
	GLUT 12	Heart, prostate, mammary gland	
	HMIT 1	Brain	H^+/myo-inositol co-transporter

1.3.2 Glucose Transporter 4 (GLUT4)

1.3.2.1 Identification and cloning

It was in the 1950s that a direct role for insulin in the regulation of glucose-uptake into peripheral tissues was established (Levine & Goldstein, 1955). However, it wasn't until methods were developed to isolate adipose cells that it became possible to study the molecular mechanism of insulin action. In 1980, two independent research groups reported that insulin stimulation increased the glucose transport activity at the plasma membrane in adipose cells (Suzuki & Kono, 1980) (Cushman & Wardzala, 1980). Cushman and colleagues used a radiolabelled [^{3}H] cytochalasin b which binds to and inhibits glucose transporters. The use of [^{3}H] cytochalasin b demonstrated that upon insulin stimulation 'glucose transport systems' move (translocate) from an intracellular vesicular compartment to the plasma membrane in isolated rat adipocytes cells. In 1989, nearly a decade after the 'translocation hypothesis' was proposed, the elusive 'insulin-responsive glucose transporter' was cloned by several independent research groups (James, et al., 1989) (Birnbaum, 1989) (Charron,

et al., 1989) (Fukumoto, et al., 1989). This transporter was later referred to as GLUT4, the fourth member of the facilitative glucose transporter family (Figure 1.2). Subsequently, antibodies were developed against the specific glucose transporters and used to confirm that insulin stimulates the translocation of GLUT4 to the cell surface in adipose cells.

Since the cloning and identification of GLUT4, an extensive amount of research has been dedicated to understanding how insulin regulates the translocation of GLUT4 from specialised intracellular storage compartments to the plasma membrane in both adipose and muscle tissue. Several biochemical and immuno-cytochemical methods have been developed over the years for the studies of GLUT4 trafficking. These include subcellular-fractionation techniques, biotinylated bis-mannose photolabelling (Holman, et al., 1990) (Yang & Holman, 1993) (Koumanov, et al., 1998), electron and fluorescence-based microscopy (Ploug, et al., 1998) (Slot, et al., 1991) (Malide, et al., 2000) (Malide, et al., 1997) (Dawson, et al., 2001) (Ralston & Ploug, 1996). In more recent years, GLUT4 reporter constructs have been designed to contain a hemagglutinin (HA) or Myc tag in the first exofacial loop and can also have a C-Terminal GFP tag (HA/Myc GLUT4 GFP). These have been utilised to study GLUT4 trafficking in both adipose (Karylowski, et al., 2004) (Zeigerer, et al., 2002) (Govers, et al., 2004) (Shewan, et al., 2003) and in muscle cells (Hoehn, et al., 2008) (Fazakerely, et al., 2009) and in primary muscle (Lauritzen, et al., 2008) (Lauritzen, et al., 2006) (Lauritzen, et al., 2010).

1.3.2.2 The GLUT4 translocation hypothesis

The use of a cell impermeant bismannose photolabel 2-N-4(1-azi-2,2,2-trifluoroethyl) benzoyl-1,3-bis(D-manos-4-yloxy)-2-propylamine (ATB-BMPA) in combination with anti-GLUT4 and anti-GLUT1 specific antibodies have been used to quantify the abundance of glucose transporters at the cell surface in rat adipose and muscle cells. In non-stimulated rat adipose cells, GLUT1 and GLUT4 transporters are present at low levels at the plasma membrane. Following insulin stimulation the level of GLUT4 and GLUT1 at the cell surface are increased 15-20-fold and five-fold respectively. However, the increased level of GLUT4 transporters accounted for the majority of the insulin-stimulated

glucose transport activity (Holman, et al., 1990). Furthermore, in isolated rat soleus muscle cells insulin stimulates an 8-fold increase in GLUT4 at the cell surface compared to the non-stimulated state. The level of cell surface accessible GLUT4 was directly correlated with the increased glucose transport activity (Wilson & Cushman, 1994). Subsequently, it has been demonstrated that in adipose cells the cell surface level of GLUT1 is primarily responsible for basal cell glucose uptake (James & Piper, 1994).

1.3.2.3 GLUT4 intracellular localisation

The intracellular distribution of GLUT4 within the endosomal system was demonstrated in early studies using immuno-gold electron microscopy. A similar distribution pattern of GLUT4 has been observed in both adipose and muscle tissue (Malide, et al., 2000) (Slot, et al., 1991) (Slot, et al., 1991) (Ploug, et al., 1998). In non-stimulated white and brown adipose cells the majority of immuno-gold labelled GLUT4 is found located in tubular-vesicular (TV) structures within the cytoplasm, enriched near the *Trans* Golgi Network (TGN) and in endosomes (Malide, et al., 2000) (Slot, et al., 1991). Similarly, in muscle and heart, GLUT4 is located in small TV structures near to the sarcolemma and transverse tubular system and associated with larger endosomal depots in close proximity to the TGN (Slot, et al., 1991) (Ploug, et al., 1998).

Co-localisation studies using immuno-fluorescence microscopy revealed that a proportion of GLUT4 resides in large peri-nuclear structures which display partial overlap with mannose 6-phosphate receptor (M6PR), TGN 38-mannosidase II and giantin. These are cell compartment markers of late endosomes, TGN and Golgi respectively (Malide, et al., 1997) (Ploug, et al., 1998) (Ralston & Ploug, 1996). Furthermore, sub-cellular fractionation techniques together with immuno-adsorption of intracellular GLUT4 containing membranes has been used by several studies to identify proteins components which associate with GLUT4 storage compartment in rat adipocytes and 3T3-L1 cells. Major protein cargo constituents include the insulin-regulated amino peptidase (IRAP), sortilin, mannose-6-phosphate receptor (M6PR) and the transferrin receptor (TfR) (Kandror, et al., 1995) (Kandror & Pilch, 1996) (Morris, et al., 1998) (Hashiramoto & James, 2000) (Larance, et al., 2005). However, the

majority of GLUT4 is found present in a distinct vesicular population that resemble the TGN but which are segregated away from the Transferrin receptor (TfR) which a marker for constitutively recycling endosomes (Malide, et al., 1997) (Ploug, et al., 1998) (Ralston & Ploug, 1996) (Hashiramoto & James, 2000).

1.3.2.4 Insulin-stimulated GLUT4 trafficking

Immuno-cytochemical studies in adipose and cardiac muscle cells under basal conditions and following insulin stimulation provide further support for insulin-stimulated GLUT4 translocation. These results support the findings from earlier photo-labelling studies performed by (Holman, et al., 1990). These studies revealed that a relatively small amount of GLUT4 (approximately 1-5% of total labelled GLUT4) is immuno-located at the cell surface under basal conditions. In the insulin-stimulated state the proportion of GLUT4 at the plasma membrane increased to approximately 40% (Malide, et al., 2000) (Slot, et al., 1991). In addition, the amount of GLUT4 within the endocytic pathway and within clathrin coated vesicles/pits is increased in the continued presence of insulin (Slot, et al., 1991) (Slot, et al., 1991). These findings provided the first evidence that GLUT4 is continuously recycled with the plasma membrane and the main effect of insulin was to increase GLUT4 exocytosis.

The development and use of cell impermeable photo affinity glucose transporter labelling reagents has enabled the kinetics of endogenous GLUT4 recycling to be investigated under basal and insulin-stimulated steady-state conditions. Using these methods the rate for GLUT4 internalisation and exocytosis can be directly determined. Firstly, it was demonstrated that GLUT4 continuously recycles between the plasma membrane and a storage compartment in both non-stimulated and insulin-stimulated adipocytes (Yang, et al., 1992) (Jhun, et al., 1992). In the absence of insulin, GLUT4 is rapidly internalised from the cell surface and slowly recycled. The net effect is that the majority of GLUT4 transporters are sequestered within an intracellular compartment and absent from the plasma membrane pool.

The use of a bis-mannose photolabel, ATB-BMPA in 3T3-L1 adipocytes revealed that main effect of insulin was to increase GLUT4 transporter exocytosis (~9 fold) (Yang & Holman, 1993). In addition, the rate for GLUT4 endocytosis was reduced by ~30%. These findings contrast those of Juhn et al, who used the photo-reactive probe B3-GL in rat adipose cells. Here, they demonstrated that insulin exerts an equal effect to increase GLUT4 exocytosis and reduce GLUT4 endocytosis by approximately 3-fold (Jhun, et al., 1992). The action of insulin to stimulate GLUT4 exocytic pathways is also conserved in primary muscle cells. Using a biotinylated photolabel GP15, insulin stimulation has been shown to markedly increase GLUT4 exocytosis rate in both skeletal muscle and in rat cardiomyocytes (Karlsson, et al., 2009) (Yang & Holman, 2005). Furthermore, insulin stimulation did not alter the rate for GLUT4 endocytosis in cardiomyocytes (Yang & Holman, 2005). This is in contrast to the effect observed in adipose cells.

In 1994, Holman et al. identified several important features of GLUT4 trafficking behaviour based on modelling data from photo-labelling and sub-fractionation studies (Holman, et al., 1994). This study indicated that the behaviour of GLUT4 is inconsistent with a straightforward two-pool model (one intra-cellular compartment and the plasma membrane) but that a 3-pool model can more appropriately account for the experimental results. The presence of an additional pool can explain the initial rapid stimulation of GLUT4 translocation to the plasma membrane following insulin stimulation. Furthermore, recycling through two intracellular pools can account for the reduced steady-state $t_{1/2}$ values for GLUT4 exocytosis in the continued presence of insulin.

1.3.2.5 GLUT4 storage vesicular (GSV) compartment

In non-stimulated adipocyte cells, using immuno-fluorescence microscopy, a large proportion of GLUT4 is localised in punctate 50-80nm diameter vesicular structures (Malide, et al., 2000). These punctate GLUT4-containing structures co-localise with vesicles containing the vesicular SNAP (Soluble NSF Attachment Protein) REceptor (SNARE) protein, vesicle-associated membrane protein 2 (VAMP2). VAMP2 is a member of the VAMP/synaptobrevin family.

The primary function of SNARE proteins is to mediate vesicle fusion (Malide, et al., 1997) (Ralston & Ploug, 1996).

Further evidence for a distinct GLUT4 storage vesicular (GSV) compartment comes from biochemical studies performed in 3T3-L1 adipocytes using the transferrin (Tf) endosome ablation technique using Tf coupled-horse radish peroxidase (HRP)-3, 3'-diaminobenzidine (DAB). Briefly, 3T3-L1 adipocytes are first treated with a transferrin/HRP (Tf/HRP) conjugate. Following which cells are then incubated with DAB/peroxidise which results in the selective ablation of cellular compartments containing the TfR (Martin, et al., 1996) (Karylowski, et al., 2004). Using this method, it has been demonstrated that ~60% of GLUT4 is present within a distinct population of post-endocytic vesicles, enriched with VAMP2 (Martin, et al., 1996).

Sub cellular fractionation techniques have enabled the isolation and characterisation of GLUT4 storage vesicles (GSVs). Using this technique it has been discovered that GLUT4 resides in a population of homogenous GLUT4 vesicles that are distinct from other light microsomes in both adipose and muscle cells (Kandror, et al., 1995). GSVs have been further characterised into insulin-responsive and non-insulin-responsive, the former being defined by the presence of the protein cellugyrin. Cellugyrin is a homolog of the synaptic vesicle protein synaptogyrin. Approximately 50-60% of immuno-isolated GSVs are enriched with cellugyrin (Kupriyanova & Kandror, 2000). In addition, the protein IRAP is enriched within insulin-responsive GSVs isolated from non-stimulated adipocyte cells (Kupriyanova, et al., 2002). The expression of IRAP is up-regulated during adipocyte differentiation (Keller, 2003). Moreover, sortilin and low-density lipoprotein receptor-1 (LRP1) have been identified as major constituents of insulin-responsive GSVs. The expression of sortilin and LRP1 are also increased during adipocyte differentiation. Moreover, shRNA-mediated knockdown of sortilin (Shi & Kandror, 2005) or LRP1 (Jedrychowski, et al., 2010) in 3T3-L1 adipocytes significantly reduces total GLUT4 expression levels and subsequently decreases insulin-stimulated glucose uptake. Furthermore, the silencing of sortilin in 3T3-L1 cells impairs the formation of GLUT4 storage vesicles. More recently, siRNA-mediated knockdown of sortilin reduces GLUT4

translocation to the cell surface in C2C12 skeletal muscle cells (Tsuchiya, et al., 2010). Together, these findings indicate that IRAP, sortilin and LRP1 are major components of GSVs and are likely to be required for the stability of GSVs and involved in the regulation of insulin-dependent GLUT4 translocation.

In addition to the major cargo proteins outlined above, other ubiquitously expressed proteins are enriched within GSVs membranes and are involved in general membrane trafficking and fusion events. These include vesicle-associated membrane protein 2 (VAMP2), secretory carrier-associated membrane proteins (SCAMPs) and small GTP-binding proteins (Kandror & Pilch, 1996) (Laurie, et al., 1993). Furthermore, other studies have reported on several GSV associated proteins which are involved in regulating insulin-responsive GLUT4 translocation. These include the Rab-GTPase-activating protein AS160/TBC1D4 (Larance, et al., 2005), Tether-containing UBX domain for GLUT4 (TUG) (Bogan, et al., 2012) and the small ubiquitin regulated modifier (SUMO) conjugating enzyme Ubc9 (Liu, et al., 2007). In addition, rab proteins 2A, 4A, 8A, 8B, 10, 11 and 14 have been found to associate with GLUT4 storage vesicles (Larance, et al., 2005) (Miinea, et al., 2005) (Kaddai, et al., 2009). Rabs are part of a family of small GTPase proteins which regulate cellular processes involved in vesicle trafficking, membrane budding and fusion (Stenmark & Olkkonen, 2001). SiRNA-mediated depletion of rab 10 has been found to impair insulin-stimulated GLUT4 translocation to the cell surface in 3T3-L1 adipocytes (Sano, et al., 2007). In a recent study, employing total internal reflection fluorescence (TIRF) microscopy, it has been demonstrated that rab10 directly facilitates the translocation and docking of insulin-responsive GSVs to the plasma membrane (Chen, et al., 2012). Whereas, rabs 4, 8A and 14 mediate GLUT4 movement through specific routes of the general endocytic recycling pathway.

1.3.2.6 GLUT4 trafficking models

The intracellular trafficking route for GLUT4 can be partitioned into six discrete trafficking steps illustrated in Figure 1.3 (Larance, et al., 2008). These are the biogenesis of GSVs (trafficking of GLUT4 from the TGN to the GSV compartment and release of GSV from sequestration mechanisms), the

translocation/movement of GSVs to the cell surface (exocytosis), tethering (the low affinity interaction of GSVs and plasma membrane), docking (assembly of SNARE complex before fusion of the GSVs with the plasma membrane), fusion (the lipid bilayers of the GSVs and the plasma membrane combine) and endocytosis (the removal of GLUT4 from the cell surface and trafficking to the endosomal compartment). Additionally, as GLUT4 undergoes endocytosis it is sorted from the endosomes into vesicles associated with the general endosomal pathway. These vesicles undergo regulated constitutive trafficking and fusion with the plasma membrane. Therefore, it is likely that insulin can regulate any number of these discrete trafficking steps. However, the question is which of these steps of GLUT4 trafficking are the major sites of insulin action.

In 1994, Holman et al concluded that the original two-pool model (one intra-cellular compartment and the plasma membrane) could not accurately predict GLUT4 trafficking behaviour (Figure 1.4A). Instead a three-pool model could account for the fast transition from basal to insulin-stimulated steady state and the slower rate of GLUT4 recycling in the insulin-stimulated state (Figure 1.4B) (Holman, et al., 1994).

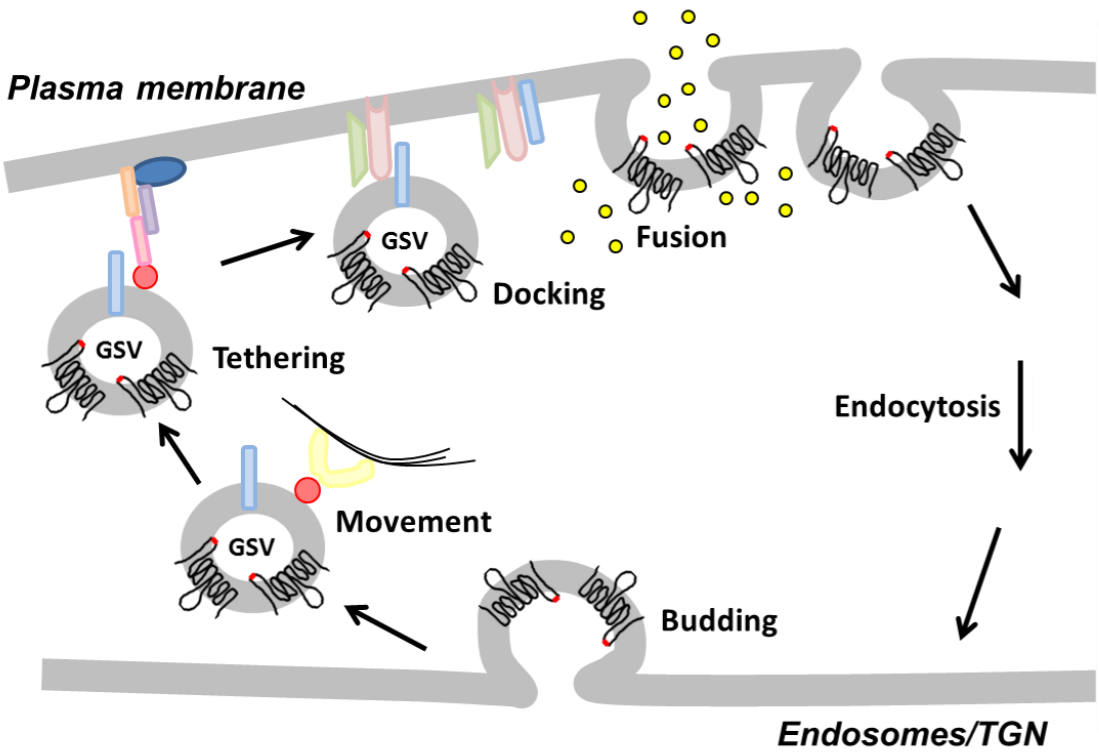

Figure 1.3: The trafficking routes of GLUT4. GLUT4 trafficking can be segregated into at least six processes: Exocytic processes: **Budding** of GSVs (release from sequestration mechanism or biogenesis of vesicles from endosomes/TGN), **movement** (transport of vesicles to the plasma membrane along microtubules and actin), **tethering** (interaction between GSVs and plasma membrane is mediated by a multisubunit tethering complex such as the exocyst complex), **docking** (assembly of the trans-SNARE complex), **fusion** (the merging of the GSV and plasma membrane lipid bilayers) and **endocytosis** (the retrieval of GLUT4 from the plasma membrane to the cell interior). Additionally, as GLUT4 undergoes endocytosis it is sorted from the endosomes into vesicles associated with the general endosomal pathway. These constitutive vesicles will also undergo regulated trafficking and fusion steps with the plasma membrane. This schematic has been adapted from (Larance, et al., 2008). Key: *Red circle* – Rab 10, *light yellow shape* – myosin motor proteins, Myo1C, *dark blue oval, orange, pink and purple oblongs* – subunits of the exocyst, *light blue oblong* – VAMP2, *pale pink and green shapes* – t-SNAREs, *yellow circles* – glucose.

More recently, the ectopic expression of exofacial epitope-tagged GLUT4 fusion proteins have been extensively used to study GLUT4 trafficking in both adipose and muscle cells. These GLUT4 reporter constructs contain a hemagglutinin (HA) or Myc tag in the first exofacial loop and can also have a C-Terminal GFP tag (HA/Myc-GLUT4-GFP). The exofacial (HA/Myc) tag allows for the rapid detection of GLUT4 which has been inserted into the plasma membrane. Firstly, using these reporter proteins the rate at which GLUT4 arrives at the cell surface can be measured as a function of time (transition kinetics). Secondly, several studies have used these reporter proteins to study the effect of insulin on

GLUT4 exocytic pathways at steady-state (Martin, et al., 2006) (Karylowski, et al., 2004) (Govers, et al., 2004) (Fazakerely, et al., 2009). For these studies intact live cells are labelled with a saturating concentration of purified anti-HA antibody. The concentration of antibody used is sufficient to label all HA-GLUT4 that appears at the cell surface. Thus, anti-HA accumulation (uptake) over time is a function of the rate of the exchange of GLUT4 between intracellular compartments and the plasma membrane (k_{ex}). In addition, the size of the GLUT4 recycling pool can be determined. Therefore, the effect of insulin on the release of GLUT4 from an intracellular storage in to the continuously recycling pool can be resolved.

Thus far, two distinctly different models of GLUT4 retention have been proposed. These are supported primarily from experimental data from studies performed in 3T3-L1 adipocytes. The GLUT4 retention models outlined below are depicted in Figure 1.4. The first model proposed by McGraw and colleagues details that intracellular GLUT4 traffic is governed by a dynamic system (Figure 1.4C). In this 'dynamic retention' model the actively cycling GLUT4 pool is governed by a very slow exocytosis rate to the cell surface and a rapid internalisation rate under basal conditions. Importantly, the entire insulin-responsive GLUT4 pool can eventually recycle with the plasma membrane in basal cells (Martin, et al., 2006) (Karylowski, et al., 2004). Insulin stimulation markedly increases k_{ex} for GLUT4 ~7-13 fold from 0.006-0.007 min^{-1} to 0.05-0.08 min^{-1} and concurrently, inhibits k_{en} (Karylowski, et al., 2004) (Martin, et al., 2006). A key feature of this model is that insulin solely regulates the rate of GLUT4 movement between the intracellular compartments and the plasma membrane.

Conversely, the second model pioneered by James and colleagues is one of 'GLUT4 static retention' (Govers, et al., 2004) (Coster, et al., 2004) (Figure 1.4D). The model for GLUT4 static retention is further supported by data from studies performed by Mastick and colleagues (Muretta, et al., 2008) (Brewer, et al., 2011). Govers et al. observed that only ~10% of the total GLUT4 pool is actively engaged in recycling with the plasma membrane in 3T3-L1 adipocytes under basal conditions. Intracellular GLUT4 is sequestered within specialised

static GLUT4 storage vesicles (GSV) away from the general endosomal recycling compartment (ERC). Insulin stimulation releases GLUT4 from a 'static retention mechanism' increasing cell surface GLUT4 levels thus, substantially increasing the amount of GLUT4 within the general recycling pathway. Furthermore, insulin stimulates a modest increase in k_{ex} for GLUT4 from 0.014 min^{-1} to 0.03 min^{-1} (Govers, et al., 2004) (Coster, et al., 2004). No effect on k_{en} was observed. More recently, direct analysis of GLUT4 dynamics using quantum dot technology has revealed the existence of a large stationary GLUT4 compartment in differentiated 3T3-L1 basal cells which further supports the model for 'static retention' (Fujita, et al., 2010).

The reason for the conflicting trafficking data and proposed GLUT4 trafficking models is yet to be determined. However, Muretta et al., discovered that the re-plating of confluent differentiated 3T3-L1 adipocytes (as performed in Martin et al, for microscopy based studies) increases the size of the basal GLUT4 recycling pool (Muretta, et al., 2008). It is therefore possible that re-plating of 3T3-L1 cells somehow affects adipogenic differentiation. In support of this, Govers et al observed that the 'static retention' capacity is not present in fibroblasts and is acquired during adipocyte differentiation (Govers, et al., 2004).

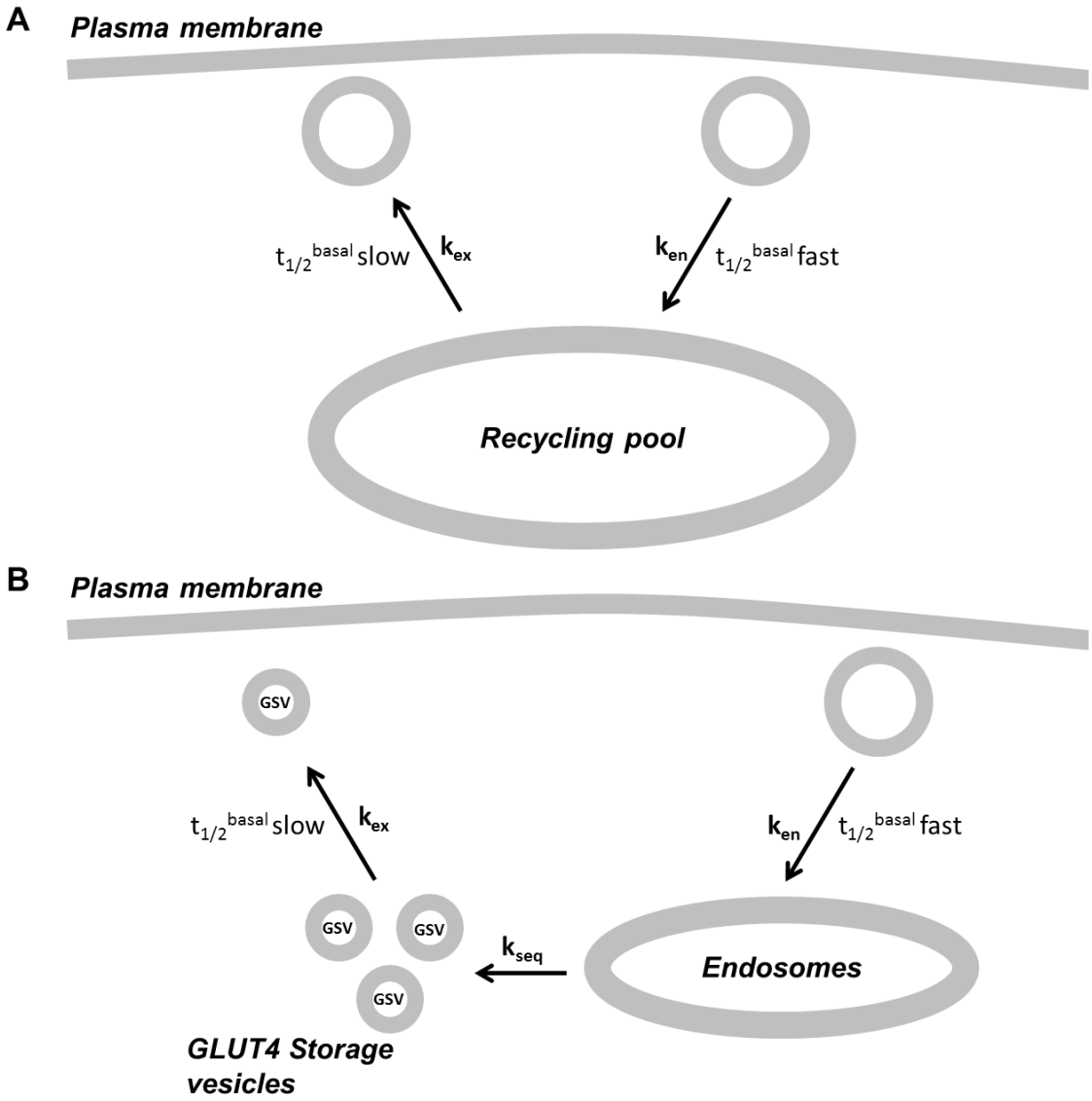
A
Plasma membrane
$t_{1/2}^{basal}$ slow
k_{ex}
k_{en}
$t_{1/2}^{basal}$ fast
Recycling pool
B
Plasma membrane
GSV
$t_{1/2}^{basal}$ slow
k_{ex}
k_{en}
$t_{1/2}^{basal}$ fast
GSV
GSV
GSV
k_{seq}
Endosomes
GLUT4 Storage vesicles

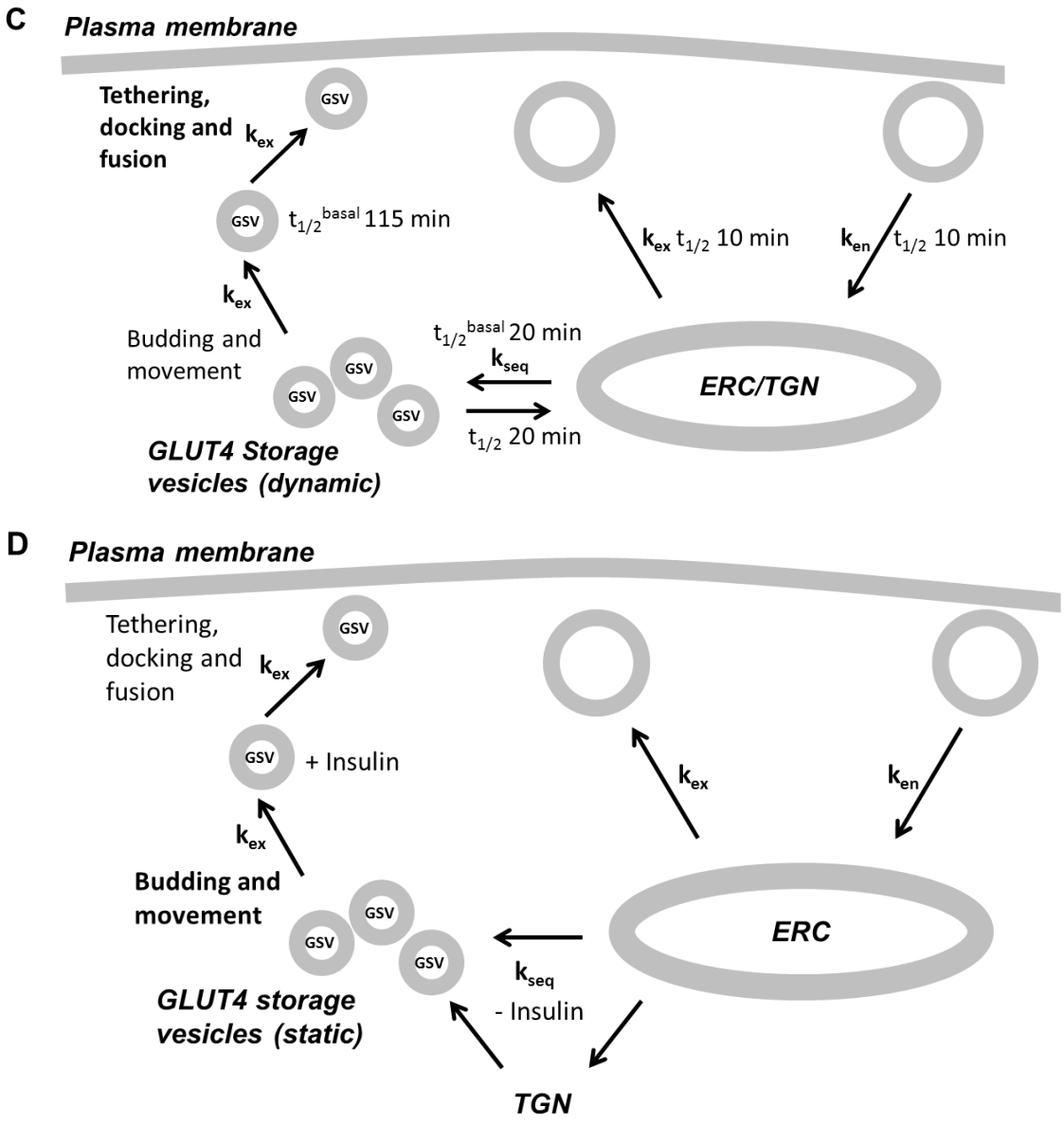

Figure 1.4: Models for GLUT4 trafficking. (A) The original two-pool model for GLUT4 recycling. In the two-pool model the plasma membrane GLUT4 pool is in equilibrium with one intracellular recycling pool. (B) In the three-pool model GLUT4 recycles through two intracellular compartments and the plasma membrane. The additional pool can account for the initial rapid stimulation of GLUT4 translocation to the plasma membrane following insulin stimulation and the slower steady-state $t_{1/2}$ value for GLUT4 exocytosis in the continued presence of insulin. (C) The dynamic-retention (three-pool) model proposed by Mcgraw and collegues. In the basal state, cell surface levels of GLUT4 are kept low from the slow movement of GLUT4 to the plasma membrane ($t_{1/2}$ 115 min) and the rapid retrieval back to endosomal recycling compartment (ERC). GLUT4 storage vesicles (GSVs) are in continual exchange with the endosomal recycling compartment. (D) The model of GLUT4 static retention (three-pool). In basal cells the majority of GLUT4 transporters are sequestered away from the ERC (via TGN) to a stationary non-cycling GSV compartment. This maintains the low cell surface levels of GLUT4 in the basal state. Insulin simulates the release of this GSV pool to the plasma membrane. This diagram has been adapted from (Larance, et al., 2008) (Karylowski, et al., 2004).

1.3.2.7 GLUT4 and T2DM

The dysregulation of insulin-stimulated glucose uptake into peripheral tissues is a major feature of T2DM. Insulin-stimulated glucose transport is decreased in human muscle from obese diabetic subjects compared with control individuals. This correlated with a reduced increase of GLUT4 transporters at the plasma membrane (Zierath et al., 1996). Furthermore, it has been reported that GLUT4 protein expression levels are decreased in both adipose and muscle tissues from diabetic rats compared with control rats (Kahn, 1992).

GLUT4 transgenic mouse models provide valuable information about the importance of GLUT4 expression in insulin-responsive tissues and the development of T2DM. Approximately half of heterozygous GLUT4 knock out (*GLUT4* $^{+/-}$) male mice developed moderate T2DM symptoms. This is correlated with the decreased abundance of GLUT4 in adipose and muscle tissues (Stenbit, et al., 1997). Furthermore, muscle-specific GLUT4 knockout mice (muscle-G4KO) develop severe insulin resistance and glucose intolerance. These mice exhibit significantly impaired basal and insulin-stimulated glucose transport (Zisman, et al., 2000). Furthermore, adipose-selective (adipose-G4KO) GLUT4 knockout mice display markedly impaired insulin-stimulated glucose transport (Abel, et al., 2001). Interestingly, even though GLUT4 levels were normal in muscle, adipose-G4KO mice displayed impaired *in vivo* glucose transport in muscle. Conversely, transgenic mice overexpressing GLUT4 selectively in skeletal muscle or adipose tissue display an increased enhanced basal and insulin-stimulated glucose utilisation.

1.4 Signalling pathways to GLUT4 translocation

Since the identification of GLUT4, a vast amount of research has been dedicated to further advance our understanding of how GLUT4 traffics from specialised intracellular storage compartments to the plasma membrane. As skeletal muscle is the major site of glucose disposal, it is therefore important to understand the mechanisms which regulate GLUT4 translocation in muscle. Here, we review the signalling pathways that regulate GLUT4 trafficking. A schematic is depicted in Figure 1.5.

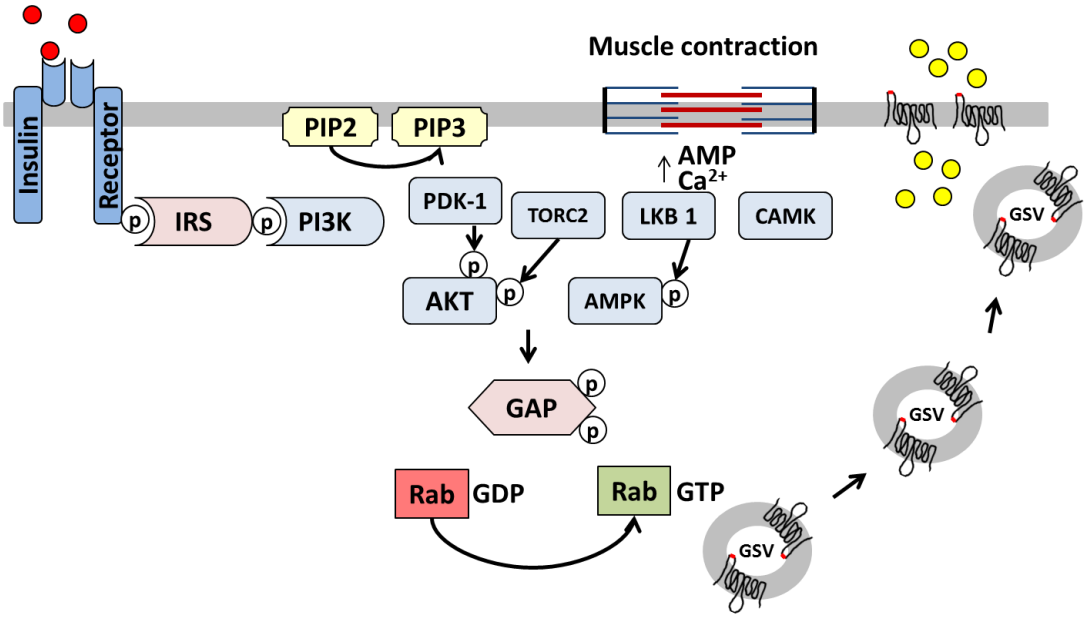

Figure 1.5: Insulin and contraction-mediated signalling pathways which lead to GLUT4 translocation. Insulin stimulation mediates a signalling cascade through insulin receptor substrates (IRS) and phosphatidyl inositol 3-kinase (PI3K) which leads to the activation of Akt via its phosphorylation by phosphoinositide dependant kinase 1(PDK-1) and mammalian target of rapamycin complex-2 (mTORC2). Activated Akt phosphorylates Rab-GTPase-activating proteins (Rab-GAP) which inactivates GAP activity towards associated rab proteins. This promotes the association of rab proteins with GTP and therefore in its active conformation. GTP-loaded rab proteins facilitate the translocation of GLUT4 storage vesicles (GSVs) and fusion with the plasma membrane. Muscle contraction results in the elevation of AMP and Ca^{2+} which through LKB1 and Ca^{2}+/calmodulin-dependant protein kinase-2 (CaMKII) phosphorylate and activate AMP-activated protein kinase (AMPK). These signalling cascades lead to the phosphorylation of Rab-GAP proteins and the translocation of GLUT4. This diagram has been adapted from (Sakamoto & Holman, 2008).

1.4.1 The Insulin signalling pathway

The binding of insulin to its receptors on the surface of insulin-responsive cells leads to the activation of complex downstream signalling cascades involved in cell metabolism (Watson & Pessin, 2006) (Bryant, et al., 2002)

1.4.1.1 The insulin Receptor

The insulin receptor (IR) is part of a large family of trans-membrane receptor tyrosine kinases. The IR is a heterotetrameric glycoprotein which is comprised of two extracellular α-subunits and two trans-membrane β-subunits. The β-subunits possess intrinsic tyrosine kinase activity. The binding of insulin to α-subunits initiates a conformational change in the insulin receptor. This induces intracellular β-subunit auto-phosphorylation of tyrosine residues and results in the activation of the tyrosine kinase domains. Activated tyrosine kinase domains transduce the insulin response through the recruitment and phosphorylation of an array of adaptor proteins. The best characterised are the insulin receptor substrates (IRS-1-4) proteins. However, others IR substrates include Shc, Clb, signal regulatory proteins (SIRPs) and adaptor protein with pleckstrin homology (PH) and Src homology 2 domains (APS) (White, 2002).

1.4.1.2 The insulin receptor substrates (IRS)

IRS proteins contain pleckstin homology (PH) and phosphotyrosine binding domains (PTB) domains situated at the N-terminus. PTB domains mediate interactions with the IR (White, 2002). IRS-1 and IRS-2 are proteins involved in maintaining normal glucose homeostasis. Transgenic mice deficient in IRS-1 (IRS-1 KO) are glucose intolerant and have an impaired insulin-stimulated glucose uptake (Araki, et al., 1994). In comparison, transgenic mice deficient in IRS-2 (IRS-2 KO) display a severe insulin resistance phenotype, associated with an impaired function of pancreatic β-cells (Withers, et al., 1998). IRS proteins contain multiple phosphotyrosine motifs which function as protein scaffolds for binding of Src homology 2 (SH2) domain-containing proteins (Sun, et al., 1991). IRS interacts with many SH2 domain containing proteins such the phosphatidyl inositol 3-kinase (PI3K) regulatory subunit p85, Grb-2 and SHP-2 (Boura-Halfon & Zick, 2009).

1.4.1.3 Phosphatidyl inositol 3-kinase (PI3K)

PI3K is a key intermediate in insulin-stimulated signalling responses leading to glucose transport. Early evidence for this arose from studies in adipocytes using the PI3K inhibitor, wortmannin (Clarke, et al., 1994) (Okada, et al., 1994). Furthermore, treatment with wortmannin inhibits insulin-stimulated cell surface levels of GLUT4 in L6 myotubes and muscle (Stockli, et al., 2008).

PI3Ks are signalling transducing enzymes involved in many cellular responses. PI3Ks phosphorylate inositol phospholipids at the 3'OH position to generate 3' phosphoinositides (3'PI). PI3Ks can be divided into three classes, I, II, III. Class I PI3Ks are further divided into two groups, class I_A PI3Ks and class I_B PI3Ks. Class I_A PI3Ks facilitate signalling responses downstream of the insulin and insulin-like growth factor (IGF) receptors (Cantley, 2002). Class I_A PI3Ks are heterodimers composed of a regulatory subunit (p85) and a catalytic subunit (p110). The regulatory subunit p85 of PI3Ks facilitate its interaction with adaptor proteins, directly associated with the insulin receptor. The class I_A PI3Ks preferentially catalyse the phosphorylation of membrane phosphatidylinositol (4, 5) bisphosphate (PI(4,5)P-2) (PIP2) to generate phosphatidylinositol (3, 4, 5) trisphosphate (PI(3,4,5)P-3) (PIP3) (Vanhaesebroeck & Alessi, 2000). PI3K signalling is modulated by the activity of two independent phosphatases. Src-Homology 2 (SH2) containing phosphatases (SHIPs) dephosphorylates PI(3,4,5)P-3 at the 5' position to generate PI(3,4)P-2. The lipid phosphatase PTEN, dephosphorylates at the 3' position to generate PI(4,5)P-2 (Cantley, 2002).

The accumulation of PIP3 at the cell membrane results in the recruitment of downstream signalling proteins which contain pleckstrin-homology (PH) domains. These include phosphoinositide-dependant protein kinase 1 (PDK-1) and isoforms of Akt, also known as protein kinase B (PKB). Activated PDK-1 phosphorylates and activates downstream serine/threonine kinases. Those of importance to insulin signalling are Akt and isoforms of atypical protein kinase C (aPKC) (Sajan, et al., 2006).

1.4.1.4 Akt/protein kinase b (PKB)

The serine/threonine kinase Akt is a major downstream effector of PI3K. The full activation of the serine/threonine kinase Akt requires phosphorylation at two distinct residues, threonine 308 and serine 473 (Alessi, et al., 1996). PIP3 in the plasma membrane recruits Akt and PDK-1 into close proximity. This facilitates PDK-1 phosphorylation of Akt on threonine 308 (Alessi, 2001). Mammalian target of Rapamycin (mTOR) in complex with rapamycin-insensitive companion of mTOR (raptor-mTOR protein complex (TORC2)) mediates serine 473 phosphorylation of Akt (Jacinto, et al., 2006).

The serine/threonine kinase Akt is a major downstream effector of PI3K. Insulin stimulation leads to the phosphorylation and activation of Akt which mediates GLUT4 translocation to the plasma membrane and increases glucose uptake (Franke, et al., 1995) (Alessi, et al., 1996). Akt has three isoforms Akt1/PKBα Akt2/PKBβ Akt3/PKBγ. Akt1 and Akt2 are expressed in adipose and muscle tissue (Kim, et al., 2000). Akt2 has been shown to be crucial for the regulation of normal glucose homeostasis. Transgenic mice deficient for Akt2 develop insulin resistance, hyperglycaemia and hyperinsulinemia (Cho, et al., 2001). Furthermore, Akt2 is essential for insulin-stimulated glucose uptake in muscle. *Ex vivo* insulin-stimulated glucose uptake was impaired in muscle from Akt2 knockout mice compared with control mice (Sakamoto, et al., 2006). In contrast, the over-expression of a constitutively active form of Akt increases GLUT4 translocation to the plasma membrane in 3T3-L1 adipocytes in the absence of insulin (Kohn, et al., 1996).

1.4.1.5 Protein kinase C (PKC)

There are three aPKC isoforms (PKC-ζ- λ- ι). PDK1 phosphorylates PKC-ζ, λ and ι on threonine residues 410, 411 and 403 respectively. RNAi mediated knock down of endogenous PKC-ζ or the viral expression of kinase inactive (KI) PKC-ζ has been found to significantly impair insulin-stimulated glucose uptake in L6 myotubes (Sajan, et al., 2006) (Sajan, et al., 2010).

1.4.1.6 Insulin resistance

Insulin resistance is a metabolic state which is caused by a range of factors which include hyperglycaemia, hyperinsulinemia, dyslipidaemia, inflammation and anti-inflammatory steroids. It is a complex condition and it still remains unclear whether there are discrete cellular mechanisms which regulate insulin resistance (Hoehn, et al., 2008).

High-fat diet (HFD) fed rodents provide robust models to study the effects of fatty acids on whole body metabolism and directly on insulin action in muscle. Mice fed on a HFD for 3-4 weeks impaired insulin-stimulated recruitment of GLUT4 to the cell surface and reduced glucose uptake in isolated soleus muscle compared to mice fed on a standard low-fat chow diet (Zeirath, et al., 1997). In addition, another study reported that high–fat feeding in mice for just 17 days was enough to impair insulin-stimulated glucose uptake in muscle (Hoehn, et al., 2008). Studies carried out in skeletal muscle cell models provide further information about the direct effect of the increased availability of fatty acids on insulin signalling. Treatment of L6 myotubes with palmitate significantly reduced insulin-stimulated cell surface levels of GLUT4 (Hoehn, et al., 2008) (Hoehn, et al., 2009). Additionally, Lee et al confirmed that treatment with palmitate reduced insulin-stimulated glucose uptake in L6 myotubes (Lee, et al., 2006). In addition treatment with palmitate reduced insulin-stimulated glycogen synthesis and glucose oxidation in C2C12 myotubes (Hirabara, et al., 2009).

Several studies support that a reduction in insulin-stimulated responses occurs through mechanisms that affect the levels of phosphorylated Akt. C2C12 myotubes treated with saturated fatty acids palmitate or stearate at a range of concentrations between 0.1-1 mM for between 16-24 hours inhibited insulin-stimulated Akt activation (Chavez, et al., 2003) (Hirabara, et al., 2009) (Tsuchiya, et al., 2010), but did not inhibit PI3K activity (Chavez, et al., 2003). However, in a study performed by Hoehn et al, low doses of palmitate (0.05- 0.3 mM) that were sufficient to significantly reduce insulin-stimulated cell surface levels of GLUT4 in L6 myotubes, did not affect the levels of phosphorylated IRS proteins or Akt (Hoehn, et al., 2008). Therefore, insulin resistance is associated with defects which occur through IRS-independent mechanisms.

The reduced fatty acid oxidative capacity of muscle from obese and insulin-resistant subjects is in part associated with the increased accumulation intracellular lipid-mediates (Holland, et al., 2007). In C2C12 or L6 myotubes, treatment with palmitate stimulated the accumulation of ceramide and diacylglycerol (DAG) (Chavez, et al., 2003) (Lee, et al., 2006). Furthermore, Chavez et al. demonstrated that increased levels of intramuscular ceramide impaired insulin action through inhibiting Akt activity (Chavez, et al., 2003). The inhibitory effect of palmitate on Akt phosphorylation was reversed in myotubes pre-treated with myriocin a serine palmitoyl transferase (SPT) inhibitor or cycloserine a citrate synthase inhibitor which are important enzymes regulating ceramide biosynthesis.

1.4.2 Contraction-mediated signalling.

It is well established that physical exercise is important and beneficial for overall fitness, body weight and for the management of T2DM. Acute exercise has been shown to enhance glucose uptake in muscle (Defronzo, et al., 1981) by mediating the translocation of GLUT4 from intracellular compartment to the plasma membrane (Douen, et al., 1990). Even though insulin-stimulated GLUT4 translocation is impaired in people with T2DM, exercise mediated GLUT4 translocation appears normal (Zeirath, et al., 1997). Our current understanding is that insulin and contraction mediate independent signalling mechanisms to regulate glucose disposal.

Contraction-mediated signalling activates multiple downstream signalling cascades which are independent of insulin/PI3K signalling (Funai & Cartee, 2009). Keys mediators include AMP-activated protein kinase (AMPK) (Hayashi, et al., 1998) (Musi, et al., 2001) and Ca^{2+} /calmodulin-dependant protein kinases (CaMK) (Funai & Cartee, 2008) (Funai & Cartee, 2009) (Witczak, et al., 2010) and atypical PKC.

1.4.2.1 AMP-activated protein kinase (AMPK)

The AMP-activated protein kinase (AMPK) is a mediator of hormonal signalling and is activated in response to exercise or cellular stress. The energy-status of a cell is determined by the abundance of adenosine mono-phosphate (AMP)

and adenosine tri-phosphate (ATP) nucleotides. Various stimuli activate AMPK by increasing the cellular ratio of AMP/ATP. AMPK detects discrete changes in the AMP/ATP ratio. Activated AMPK regulates mechanisms to restore the cellular energy balance (Hardie, 2004).

AMPK is a heterotrimeric protein which is comprised of a catalytic α-subunit along with regulatory scaffolding β-and nucleotide binding γ-subunits. The α-subunit possesses intrinsic serine/threonine kinase activity. There are multiple isoforms of each subunit. There are two α-subunits, α_1 and α_2. In addition there are two β-subunits β_1, β_2 and three γ-subunits γ_1, γ_2 and γ_3. The catalytic subunit α_2 isoform is found highly expressed in skeletal muscle and heart, whereas the AMPK-α_1 isoform is ubiquitously expressed in most tissues (Musi, et al., 2001). In addition, both α-subunits are expressed in C2C12 skeletal muscle cells (Niu, et al., 2010). The isoforms associate together to form 12 heterotrimeric protein complexes. These complexes exhibit differential tissue distribution patterns (Woods, et al., 2003). Only three of the 12 complexes are present in human skeletal muscle (α2β2γ1> α2β2γ3=α1β2γ1) (Wojtaszewski, et al., 2005). In addition, mouse skeletal muscle expresses predominately α2β2γ3 hetero-trimeric complexes (O'Neil et al., 2011).

The binding of AMP to the γ-subunit results in a conformational rearrangement in the AMPK complex. This facilitates the phosphorylation of γ-subunit at threonine 172 mediated by the serine/ threonine kinase, LKB1. The phosphorylation of AMPK is necessary for regulating AMPK activity (Shaw, et al., 2004) (Lizcano, et al., 2004). Muscle-specific knock-out of LKB1 (LKB1 KO) prevents contraction-mediated activation of AMPK-α_2. (Sakamoto, et al., 2004). *Ex vivo* muscle contraction does not directly stimulate LKB1 activity (Sakamoto et al., 2004). AMPK is allosterically activated by the binding of AMP to the γ-subunit which results in a conformation change to induce the phosphorylation of threonine 172 by LKB1.

Further evidence that AMPK activity directly stimulates glucose uptake in muscle comes from studies which utilise the adenosine analogue AICAR. AICAR, 5-Aminoimidazole-4-carboxamide 1-β-D-ribofuranoside is a cell-

permeable compound that can be phosphorylated in the target cell to ZMP, which mimics the activity of AMP. Treatment with AICAR increased the phosphorylation of AMPK at threonine 172 and stimulated glucose uptake in L6 myotubes (Sajan, et al., 2010). This is mediated by the increased levels of GLUT4 (Fazakerely, et al., 2009) (Sajan, et al., 2010) and GLUT1 transporters at the cell surface in L6 myotubes. In addition, treatment with AICAR increased the level of GLUT4 transporters at the cell surface and enhanced glucose transport in isolated muscle explants (Koistinen, et al., 2003) (Hayashi, et al., 1998) (Sajan, et al., 2010). Furthermore, the drug metformin has been shown to mimic AICAR's effect on muscle by significantly increasing both AMPK-α_1 and -α_2 catalytic activity in isolated rat skeletal muscle (Zhou, et al., 2001) (Sajan, et al., 2010) (Jorgensen, et al., 2004). Metformin is a biguanide hyperglycaemic drug which is widely administered to treat T2DM. The drug functions to reduce hepatic glucose production and to increase muscle glucose uptake.

AICAR-stimulated phosphorylation of AMPK and ACCβ and glucose uptake in muscle is dependent on the presence of the AMPK-α_2 isoform. AICAR-stimulated glucose uptake was significantly ablated in muscle from AMPK-α_2 knockout (AMPK-α_2 KO) mice but not affected in muscle from AMPK-α_1 knockout (AMPK-α_1 KO) mice. In contrast, contraction-mediated glucose uptake was not affected in either AMPK-α_2 or AMPK-α_1 KO mice (Jorgensen, et al., 2004). Even though contraction mediated phosphorylation of γ-subunit of AMPK at threonine 172 was impaired. Interestingly the protein expression level of the α_1-subunit was up-regulated in the skeletal muscle from AMPK-α_2 KO mice (Jorgensen, et al., 2004). There appears to be some functional redundancy between the two catalytic isoforms (α2/α1) of AMPK. Furthermore, contraction-mediated glucose uptake is only partially inhibited in mouse skeletal muscle expressing the kinase dead AMPK-α_2 kinase dead (AMPK-α_2 KD) or in L6 myotubes expressing the kinase-inactive (KI) dominant-negative AMPK-α_2 (AMPK-α_2 KI) (Sajan, et al., 2010).

AICAR allows us to study the downstream signalling effects of AMPK, a key regulator of energy balance. However, it is important to note that AICAR doesn't recapitulate the full extent of exercise signalling. Muscle contraction activates

complex cell signalling mechanisms and activation of AMPK only accounts for part of this. *In vitro* and *in situ* studies provide evidence that muscle contraction increases Akt activity and that this is dependent on signalling through PI3K (Kramer, et al., 2006). However, this pathway does not seem to contribute to contraction-stimulated glucose uptake (Funai & Cartee, 2009). *In vitro* contraction has also been shown to increase the phosphorylation of CaMKII at threonine 286 via an AMPK-independent signalling pathway. Contraction-stimulated phosphorylation of CaMKII was not affected in muscle pre-treated with compound C. Compound C (also known as dorsomorphin) is a small-molecule inhibitor of AMPK (Funai & Cartee, 2009). Compound C directly and reversibly inhibits AMPK and is competitive with ATP. Treatment with compound C led to only a partial inhibition of contraction-stimulated glucose transport. This indicated that AMPK-independent mechanisms can account for part of the stimulation of glucose transport. However, a significant portion is dependent on signalling via AMPK. Compound C has been reported to selectively inhibit the bone morphogenic protein (BMP) type I receptors ALK2, ALK3 and ALK6 (Yu, et al., 2008). The lack of specificity of compound C has limited its use.

1.4.2.2 Ca^{2+}/calmodulin-dependant protein kinases

An essential step in muscle contraction is the release of Ca^{2+} from ryanodine receptors at the sarcoplasmic reticulum. Exercise elevates the cytosolic concentrations of Ca^{2+}. Ca^{2+}/calmodulin-dependant protein kinase CaMKII, is regulated by Ca^{2+}/calmodulin, and is auto-phosphorylated upon binding. CaMKII has been implicated in the regulation of glucose uptake in muscle. *In vivo* muscle contraction induces CaMKII phosphorylation at threonine 286/287. Electrically-stimulated contraction but not insulin-stimulated glucose uptake was impaired in mouse muscle expressing a CaMKII specific inhibitory peptide compared with a control peptide (Witczak, et al., 2010).

1.4.2.3 PKC

PDK1 phosphorylates PKC-ζ, λ and ι on threonine residues 410, 411 and 403 respectively. Metformin and AICAR are reported to mediate the phosphorylation of atypical protein kinase C (aPKC) by PDK. AICAR and metformin stimulate

glucose uptake by increasing AMPK phosphorylation which activates downstream signalling pathways through ERK and aPKC. In support of this, when a kinase-inactive AMPK α2 is expressed in L6 myotubes, AICAR and metformin induced phosphorylation of AMPK, ERK and PKC-ζ were significantly impaired (Sajan, et al., 2010). In addition, muscle-specific KO of PKC-λ significantly inhibited AICAR and metformin but not exercise-stimulated 2DG uptake in vastus lateralis muscle (Sajan, et al., 2010).

1.4.2.4 Exercise and insulin sensitivity

In obese subjects moderate-intensity aerobic exercise improved insulin sensitivity and oxidative capacity which correlated with reduced intramuscular levels of ceramide and DAG. (Bruce, et al., 2006) (Dube, et al., 2008). In addition, a 16 week exercise intervention moderately increased the percentage of type I oxidative muscle fibres in vastus lateralis muscle (Dube, et al., 2008). As well as this, exercise and the drug metformin have been reported to significantly increase AMPK-α2 activity in muscle from T2DM subjects who have an impaired insulin-stimulated glucose uptake (Musi, et al., 2001).

Furthermore, numerous studies have reported additive effects of both AMPK-activators and insulin on glucose uptake and/or GLUT4 translocation in to muscle (Hayashi, et al., 1998) (Yang & Holman, 2005) (Yang & Holman, 2006) (Bergeron, et al., 1999) (Fazakerely, et al., 2009). Additionally, metformin has been shown to enhance basal and insulin-stimulated glucose uptake in skeletal muscle (Zhou, et al., 2001) and in L6 myotubes (Hundal, et al., 1992).

A vast amount of research is focused on finding potential therapeutic targets which increase insulin sensitivity and oxidative capacity of muscle. In which overcome insulin resistance associated with T2DM (Hawley & Lessard, 2008) (Maarbjerg, et al., 2011). It is important therefore to understand in detail how insulin- and contraction-mediated signalling regulates subsequent downstream signalling and membrane trafficking pathways which lead to the translocation of GLUT4.

1.5 Rab-GTPase Activating Proteins

1.5.1 Identification of AS160 (Akt Substrate of 160 kDa)/TBC1D4

AS160 is a protein of 160 kDa that was discovered in adipocytes as a novel phosphorylation substrate of Akt/PKB (Kane, et al., 2002). Phosphorylated AS160 was immuno-precipitated using a phosphorylated (serine/threonine) Akt antibody (PAS) from 3T3-L1 cells following insulin stimulation. The PAS antibody has been raised towards the phosphorylated Akt phospho-motif RXRXXpS/T and is used to detect Akt substrates. AS160 was predicted to contain a GTPase activating protein (GAP) domain (Kane, et al., 2002). In addition, AS160 contains two phosphotyrosine binding domains (PTB) which are situated at the N terminus. PTB domains are required for protein-protein interactions and are found to typically bind to phosphorylated tyrosine residues (Yan, et al., 2002). AS160 also possesses a calmodulin binding domain (CBD), situated just upstream from the GAP domain. AS160 was found to interact with Ca^{2+}/calmodulin based on co-immunoprecipitation analysis carried out in 3T3 L1 adipocytes (Kane & Lienhard, 2005).

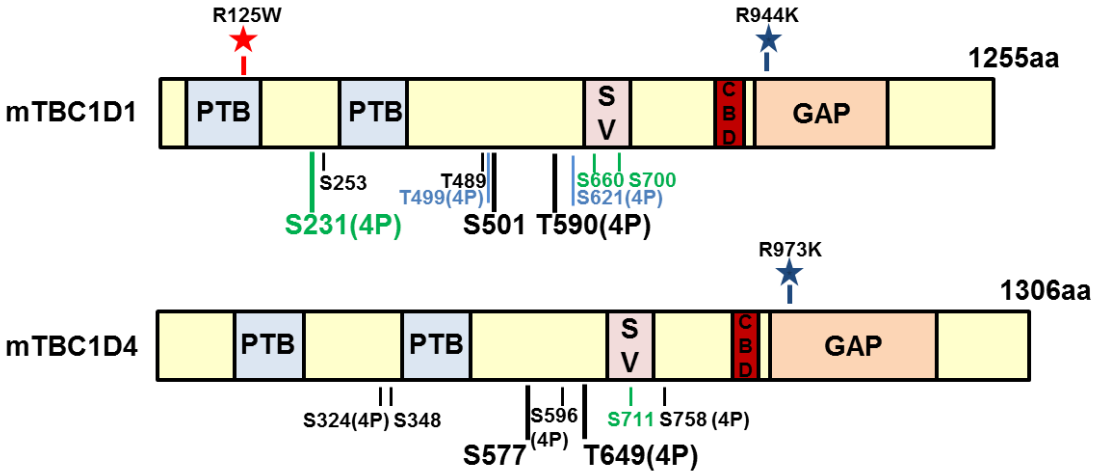

Figure 1.6: A schematic diagram of TBC1D1 and TBC1D4. TBC1D1 and TBC1D4 contain two phospho-tyrosine binding domains (PTB), a GTPase activating domain (GAP) and a calmodulin binding domain (CBD). There are appears two major splicing variants (SV). The long variant codes for an additional segment within the center of the protein. Insulin-stimulated phosphorylation sites are depicted in black. AMPK phosphorylation sites are displayed in green. Sites in blue are predicted Akt and AMPK phosphorylation sites. The R/K point mutation in the GAP domain inhibits its activity. The R125W mutation in TBC1D1 has been identified as a candidate causing severe familial obesity predisposition in humans, Diagram is modified from (Sakamoto & Holman, 2008).

AS160 is highly expressed in white adipose tissue, brown adipose tissue, brain, heart and in oxidative soleus muscle (Nagase, et al., 1998) (Taylor, et al., 2008). The expression of AS160 in the soleus muscle is greater compared to that in the glycolytic TA, EDL and gastrocnemius skeletal muscles. Therefore it appears to correlate with the increased oxidative capacity and insulin responsiveness of the soleus muscle.

AS160 is frequently referred to as TBC1D4 (tre-2/USP6, BUB2, cdc16 domain family member 4). Preceding its discovery as an Akt substrate, it was cloned from the brain (clone: KIAA 0603) as part of a series of studies which were carried out to sequence unidentified human genes. TBC1D4 belongs to a family of proteins which contain a highly conserved TBC domain which is located to a region of 180-200 amino acids at the C terminus (Nagase, et al., 1998). This domain shares significant homology to regions within ubiquitin specific protease 6, oncogene (tre-2/USP6) and the yeast cell cycle regulated phospho-protein (BUB2) and the yeast cell division cycle 16 protein (cdc16) (Richardson & Li, 1995). A schematic representation of TBC1D4 is depicted in Figure 1.6.

1.5.2 Identification of TBC1D1

Phylogeny analysis revealed that the closest relative of TBC1D4 is TBC1D1. TBC1D1 (tre-2/USP6, BUB2, cdc16 domain family member 1), was first identified by Richardson & Li. as a gene which was differentially regulated during mast cell development, highlighting its potential role in the cell cycle and cell differentiation (Richardson & Li, 1995). Phylogenetic data has indicated that TBC1D4 emerged after TBC1D1 in evolution during vertebrate development (Chen, et al., 2008). The two proteins are 47% identical and share similar protein domains including a TBC domain at the C-Terminus along with two N-Terminal PTB domains and a CBD domain (Roach, et al., 2007) (Figure 1.6).

TBC1D1 is expressed in skeletal muscle, heart and uterus (Stone, et al., 2002) (Chadt, et al., 2008). The highest levels of TBC1D1 protein are expressed in glycolytic TA and EDL muscles which contain predominately type II fibres. Lower expression levels are detected in oxidative soleus and in the gastrocnemius muscle. Furthermore, the expression of TBC1D1 is up-regulated

in C2C12 muscle cells during differentiation in to myotubes (Peck, et al., 2009). In comparison to TBC1D4, very little TBC1D1 is found to be expressed in adipose tissue (Taylor, et al., 2008) (Szekeres, et al., 2012).

1.5.3 Proposed function of Rab-GAPs

It is now well established that proteins which contain a TBC domain primarily function as a GAP for small GTPase rab proteins (Pan, et al., 2006). Rabs are part of a family of small GTPase proteins which regulate cellular processes involved in vesicle trafficking, membrane budding and fusion (Stenmark & Olkkonen, 2001). The rab family consists of more than 60 members and have been found to localise to discrete subcellular membrane compartments (Stenmark & Olkkonen, 2001). Rab proteins are found in two conformations, either in an ‘inactive state’ bound to guanoside diphosphate (GDP) or in an ‘active state’ bound to guanosine triphosphate (GTP) (Figure 1.7). The release of GDP and the subsequent binding to GTP is mediated by proteins known as guanosine nucleotide exchange factors (GEFs). Furthermore, activated GTP bound rab proteins associate with ‘effector’ proteins which regulate the diverse steps in vesicular trafficking. Conversely, Rab-GAP proteins function to accelerate the slow intrinsic hydrolysis (GTPase activity) of GTP to GDP on associated rab proteins. Therefore they are negative regulators of rab activity. The TBC1D4 and TBC1D1 GAP domains have been shown to exhibit catalytic activity towards rab proteins 2A, 8, 10 and 14. Furthermore, rab 10 has been shown to function downstream of TBC1D4 and is required for insulin-stimulated GLUT4 translocation in 3T3-L1 adipocytes (Sano, et al., 2007). In addition, rab 8A and rab 14 may be targets of AS160 in muscle cells and are found to co-localise with GLUT4 (Ishikura, et al., 2007). Additionally, these rab proteins have been found to be immuno-located on GLUT4 containing vesicles isolated from 3T3-L1 adipocytes (Miinea, et al., 2005) (Larance, et al., 2005).

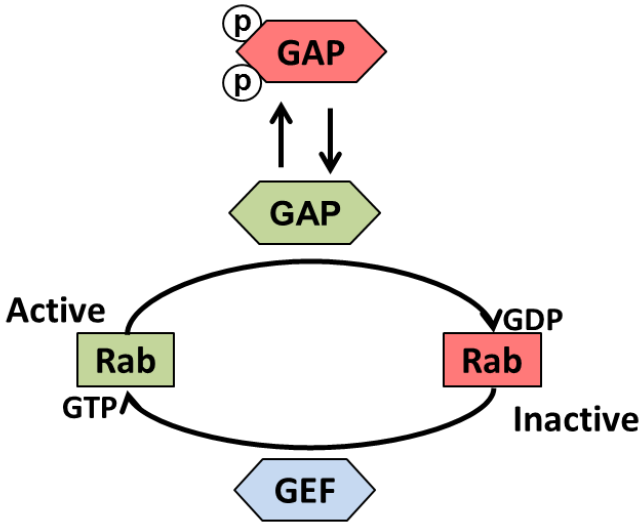

Figure 1.7: A schematic diagram of rab activity. Rab proteins exist in two conformations, either in an 'inactive state' (red) bound to GDP or in an 'active state' (green) bound to GTP. The release of GDP and the binding to GTP is mediated by proteins known as GEFs (blue). Rab-GAPs (TBC1D1 and TBC1D4) proteins (green) function to accelerate the slow intrinsic hydrolysis (GTPase activity) of GTP to GDP on associated rab proteins. It has proposed that the phosphorylation of the Rab-GAP suppresses its GAP activity (red) and as a result promotes the association of rab proteins with GTP and therefore in an active state.

Analysis of TBC1D4 revealed that it contains six potential Akt phosphorylation sites (Figure 1.6). Furthermore TBC1D4 was found to be phosphorylated at five of these sites in 3T3-L1 adipocytes following insulin stimulation. Of these sites four represent consensus motifs (RXRXXpS/T). These are located at serine 324 (318), serine 596 (588), threonine 649 (642) and threonine 758 (751) on mouse TBC1D4 (equivalent sites on human TBC1D4 are shown in brackets). A partial Akt phosphorylation motif is located at serine 577 (570) (Sano, et al., 2003) (Roach, et al., 2007). Similarly, TBC1D1 has been found to be phosphorylated at distinct sites in response to insulin stimulation. Two Akt phosphorylation sites originally detected in TBC1D4 are conserved in TBC1D1. These are threonine 590 (596) and serine 501 (507) which corresponded to threonine 649 (642) and serine 577 (570) on TBC1D4 respectively. Subsequently, other potential insulin-regulated phosphorylation sites on mouse TBC1D1 have been identified at serine 489 and threonine 499 in C2C12 muscle cells (Peck, et al., 2009) and at threonine 253 and serine 621 in TA muscle (Taylor, et al., 2008).

Several AMPK phosphorylation sites have been identified in TBC1D1. The most well studied site is the consensus motif at serine 231 (Stone, et al., 2002)

(Figure 1.6). A number of other AMPK sites have been identified in TBC1D1 at serine 660, serine 700 and threonine 499 and serine 621. These are phosphorylated in response to AICAR treatment in TA muscle. Furthermore, one predicted AMPK site has been identified in TBC1D4 at serine 711.

The identification of kinase modifiable sites led to the hypothesis that the phosphorylation of TBC1D4/TBC1D1 is important to inactivate the protein and inhibit its GAP activity. In basal cells, TBC1D4/TBC1D1 accelerates the slow intrinsic hydrolysis (GTPase activity) of GTP to GDP on associated rab proteins to switch off rab activity. Support for this hypothesis comes from studies carried out in 3T3-L1 adipocytes. Wild-type TBC1D4 or TBC1D4 4P (TBC1D4 mutated to alanine at four phosphorylation sites serine 318, serine 588, threonine 642 and serine 751, therefore removing its capacity to undergo phosphorylation) were expressed in 3T3-L1 adipocytes and the effects on GLUT4 translocation were assessed (Kane, et al., 2002) (Sano, et al., 2003). Insulin-stimulated cell surface GLUT4 levels were inhibited by approximately 80% in adipocytes over-expressing TBC1D4 4P. The TBC1D4 4P mutant completes with endogenous protein and functions as a ‘dominant-negative’ inhibitor of GLUT4 translocation. Insulin-stimulated cell surface levels of GLUT4 were rescued when cells were expressed with TBC1D4 4P simultaneously expressing an R/K point mutation which inactivated GAP activity (AS160 4P/RK). Therefore the inhibition on GLUT4 translocation was dependant on an active GAP domain.

It is important to note that the expression of TBC1D4 2P (TBC1D4 mutated at threonine 642 and serine 588) in 3T3-L1 adipocytes was able to reduce insulin-stimulated GLUT4 at the plasma membrane to the same extent as TBC1D4 4P. This indicated that threonine 642 and serine 588 are key sites within TBC1D4 which are phosphorylated by Akt and for the regulation of insulin-stimulated GLUT4 trafficking (Kane, et al., 2002) (Sano, et al., 2003).

Similarly, the ectopic expression of TBC1D1 3P (TBC1D1 mutated to alanine at four phosphorylation sites serine 489, serine 499, serine 501 and threonine 590) in 3T3 adipocytes inhibited insulin-stimulated GLUT4 at the cell surface (Roach, et al., 2007) (Peck, et al., 2009). Once again, this inhibition was

rescued when mutant proteins simultaneously expressed the catalytic dead mutation R/K. However, the expression of wild-type TBC1D1 also had an inhibitory effect on insulin-stimulated GLUT4 at the plasma membrane (Roach, et al., 2007). In contrast to TBC1D4, the expression of TBC1D1 in differentiated 3T3-L1 adipocytes is relatively low. Therefore, the expression of TBC1D1 may result in an increased level of active GAP which cannot be correctly regulated in these cells. In support of this, the inhibition on insulin-stimulated cell surface GLUT4 in 3T3-L1 cells was partially relieved by reducing the level of overexpression (Peck, et al., 2009). Furthermore, it has also been reported that over expression of wild-type TBC1D1 inhibited insulin-stimulated plasma membrane GLUT4 in L6 myoblasts (Park, et al., 2011). The expression of endogenous TBC1D1 is relatively low in L6 myoblasts. This supports the hypothesis that in cells where endogenous TBC1D1 is low, over expression may interfere with normal trafficking events leading to the inhibition of glucose transport. In addition, shRNA-mediated knockdown of TBC1D1 in 3T3 adipocytes did not affect insulin-stimulated cell surface GLUT4 levels (Chavez, et al., 2008).

1.5.4 Rab-GAPs and Obesity

A mutation in TBC1D1 to Tryptophan at Arginine 125 (TBC1D1 R125W) has been identified as a candidate causing severe familial obesity predisposition in females (Stone, et al., 2006) (Stone, et al., 2002). Further evidence for the association of TBC1D1 R125W and severe familial obesity was demonstrated within an independent French cohort (Meyre, et al., 2008). The mutation is found within the first phosphotyrosine-binding domain (PTB) domain (Figure 1.6). PTB domains are required for protein-protein interactions (Yan, et al., 2002). Therefore a mutation within this domain may alter TBC1D1 affinity for subsequent binding partners. In addition, a truncation mutant of *Tbc1d4* has also been identified and which causes severe postprandial hyperinsulinemia in humans (Dash, et al., 2009).

A further mutation of TBC1D1 has been discovered in certain chicken breeds with phenotypes for increased body weight and growth rate. Furthermore, a different genetic variant of *Tbc1d1* has been discovered in the lean

Swiss/Jackson Laboratory (SJL) mice strain. *Tbc1d1* was mapped to an obesity quantitative trait locus (QTL) *Nob1* (Chadt, et al., 2008). New Zealand obese (NZO) mice are a polygenic obesity model. They are susceptible to high fat diet induced obesity and develop symptoms of the metabolic syndrome (West & York, 1998). A backcross model of NZO mice with the lean SJL strain was established. Carriers of the NZO allele of Nob1 (*Nob1*^{NZO}) were susceptible to high fat diet induced diabetes (Kluge et al., 2000). The *Nob1*^{SJL} allele protected mice from diet induced obesity and confers leanness. TBC1D1 was found to be down regulated in skeletal muscle of the SJL mouse strain. This was the result of a 7 base-pair deletion in exon 18 which resulted in a frame-shift mutation and premature termination of the protein (Chadt, et al., 2008). Insulin-stimulated glucose uptake was impaired in EDL muscle from TBC1D1 deficient recombinant congenic B6.SJL-*Nob1*$^{SJL/SJL}$ mice. Furthermore, it was discovered that palmitate oxidation and the expression of genes including Fatty acid translocase (*Cd36),* Peroxisome proliferator activated receptor gamma co-activator 1 *(Ppargc1) and* Fatty acid binding protein (*Fabp3)* were increased in the soleus and EDL muscle from TBC1D1 deficient mice. These studies provide evidence that both TBC1D1 and TBC1D4 are involved in the regulation glucose metabolism. TBC1D1 may also play an important role in regulating fatty acid metabolism.

1.5.5 TBC1D1 and TBC1D4 role in skeletal muscle

As detailed in section 1.5.3, the early characterisation studies of TBC1D1 and TBC1D4 were performed in 3T3-L1 adipocyte cells. The results suggest that endogenous TBC1D1 may not play a significant role in insulin-stimulated GLUT4 trafficking in adipocytes. However, both TBC1D4 and TBC1D1 proteins are expressed in skeletal muscle and so it is of importance to further investigate their roles.

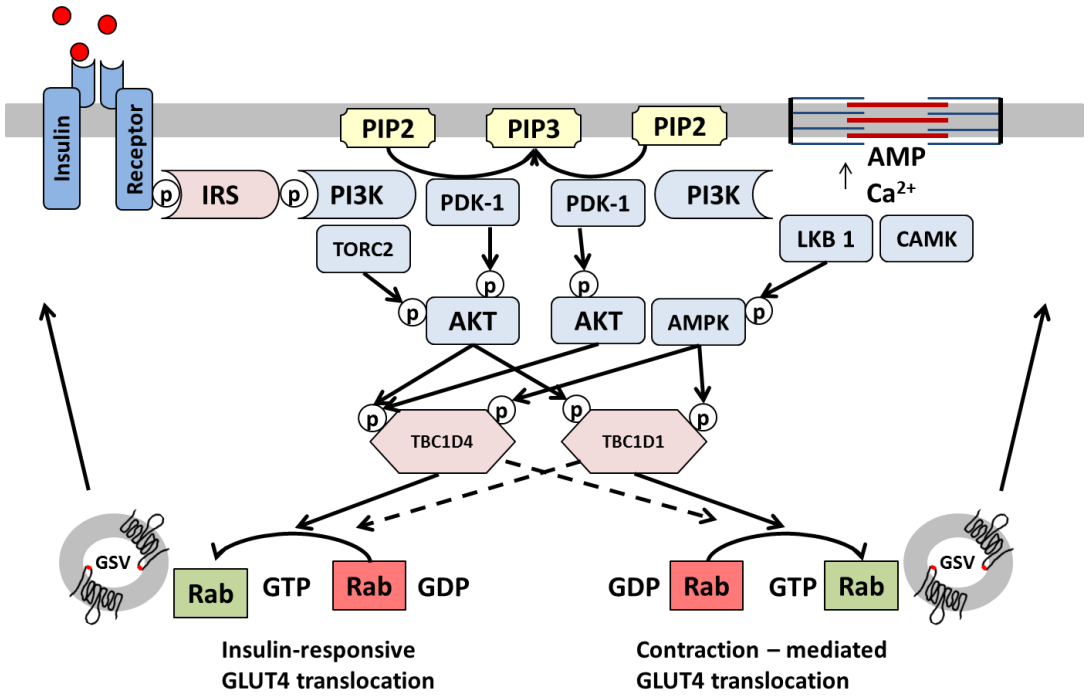

Figure 1.8: The regulation of TBC1D1 and TBC1D4 in skeletal muscle. Currently proposed insulin and contraction mediated signalling mechanisms leading to GLUT4 translocation in muscle. Insulin activates Akt via the canonical insulin receptor (IR) -insulin receptor substrate (IRS) -phosphatidyl inositol 3-kinase (PI3K) -phosphoinositide dependant kinase-1 (PDK-1) pathway. Activated Akt phosphorylates TBC1D4 and TBC1D1 primarily at threonine 649/642 and threonine 590/596 respectively. Muscle contraction elevates AMP and Ca^{2+} which through LKB1 and Ca^{2}+/calmodulin-dependant protein kinase-2 (CaMKII) activate AMP-activated protein kinase (AMPK). These signalling cascades result in the phosphorylation of TBC1D1 at threonine 590/596 and serine 231/237, serine 660, serine 700 and threonine 499 and serine 621 and TBC1D4 at serine 711. Muscle contraction also leads to the phosphorylation of TBC1D4 at threonine 649/642 via a PI 3-kinase dependent signalling mechanism.

1.5.5.1 Insulin-stimulated Glucose Transport

Insulin stimulation directly induces the phosphorylation of TBC1D4 and TBC1D1 detected using either the PAS antibody (Funai & Cartee, 2009) (Bruss, et al., 2005)(Kramer, et al., 2006) (Pehmoller, et al., 2009) (Vichaiwong, et al., 2010) or of TBC1D1 at threonine 596 using site-specific phospho-antibodies in skeletal muscles (EPI and EDL) (Pehmoller, et al., 2009) (Vichaiwong, et al., 2010). Furthermore, insulin-induced phosphorylation of TBC1D1 and TBC1D4 is dependent on signalling via PI3K pathways (Figure 1.8). Insulin-mediated phosphorylation and glucose uptake were impaired in muscle pre-treated with the PI 3-kinase inhibitor wortmannin (Kramer, et al., 2006) (Funai & Cartee, 2009)(Pehmoller, et al., 2009). Moreover, insulin-stimulated phosphorylation of TBC1D4 (detected using PAS) (Kramer, et al., 2006) and TBC1D1 at threonine

590 (Vichaiwong, et al., 2010) were significantly impaired in muscle from Akt2 KO mice compared to wild-type litter mates. These findings support the concept that both TBC1D4 and TBC1D1 are key intermediates downstream of insulin signalling. Furthermore, the over expression of TBC1D4 4P (S318A, S588A, T642A, S751A) in TA muscle using *in vivo* electroporation techniques impaired insulin-stimulated glucose uptake. This was dependant on TBC1D4 GAP activity, as the addition of the R/K mutation (which disrupts GAP activity) reversed the inhibitory effect (Kramer, et al., 2006). Thong et al., 2007 reported a similar inhibition of insulin-stimulated GLUT4 at the cell surface in L6 cells expressing the mutant protein TBC1D4 4P. Furthermore, mice with AS160/TBC1D4-Thr649Ala knockin mutation displayed impaired glucose disposal and insulin sensitivity. This coincided with a decreased insulin-stimulated glucose uptake and reduced cell surface GLUT4 levels in isolated muscles (Chen, et al., 2011). Conversely, the over expression TBC1D1 4P (TBC1D1 in which four phosphorylation sites had been mutated to alanine S231A, S499A, T590A, S621A) in TA did not affect insulin-stimulated glucose transport (An, et al., 2010). However, the over expression TBC1D1 R125W (TBC1D1 carrying the genetic mutation to associated with severe obesity) impaired insulin-stimulated glucose transport. The inhibition on glucose transport was rescued when TBC1D1 simultaneously expressed the R/K mutation which inactivated its GAP activity. These findings support the concept that both TBC1D4 and TBC1D1 are key signalling intermediates for insulin-mediated glucose transport. Intriguingly, the phosphorylation of TBC1D1 R125W detected with the PAS antibody was not impaired. Therefore, this raises important questions regarding the regulation of TBC1D1 through insulin-stimulated phosphorylation. Further investigations are required to determine how the R125W mutation affects the function of TBC1D1 and how this impairs insulin-regulated glucose transport in muscle leading to obesity.

1.5.5.2 Contraction-mediated Glucose Transport

It has been reported that other distinct signals that regulate GLUT4 translocation and glucose disposal including contraction and AICAR are mediated through the phosphorylation of TBC1D4 and TBC1D1 (Figure 1.8). Muscle contraction activates multiple downstream signalling pathways through

key mediators including AMPK and CAMKII. It is important to note that the PAS (phosphorylated Akt substrates) antibody which is used to detect downstream substrates of Akt signalling may also recognise AMPK phosphorylation motifs of (L/M)XRXXpS/T) and CaMKII motifs of HydXRXXpS/T. As detailed earlier TBC1D1 contains a number of AMPK phosphorylation sites (Figure 1.6). The most well studied site is the consensus motif at serine 231. TBC1D1 is phosphorylated at serine 237 (equivalent site in rat) in response to AICAR stimulation in L6 myotubes (Chen, et al., 2008). Furthermore, data from several studies have shown that phosphorylation of TBC1D1 at serine 231 is increased in response to *in situ* contraction or AICAR-treatment in skeletal muscle (Taylor, et al., 2008) (Vichaiwong, et al., 2010) (Pehmoller, et al., 2009). A number of other AMPK sites have been identified in TBC1D1 at serine 660, serine 700 and threonine 499 and serine 621. These are phosphorylated in response to AICAR-treatment in TA muscle (Vichaiwong, et al., 2010). The identification of TBC1D1 as an AMPK substrate supports a role for TBC1D1 as a downstream signalling intermediate of contraction signalling. In contrast only one AMPK site has been identified in TBC1D4 at serine 711. This site is phosphorylated in response to AICAR-treatment and contraction in mouse muscle (Treebak, et al., 2010).

In vivo exercise and contraction have been found to induce the phosphorylation of TBC1D4 and TBC1D1 (detected with PAS antibodies) (Bruss, et al., 2005) (Kramer, et al., 2006) (Funai & Cartee, 2009) and TBC1D4 at threonine 642 using a site-specific phospho-antibody (Kramer, et al., 2006) in GN, TA and EPI muscles. Furthermore, TBC1D1 is phosphorylated at serine 231 and at threonine 590 in response to *in situ* contraction or AICAR-stimulation in glycolytic muscles TA and EDL (Vichaiwong, et al., 2010) (Pehmoller, et al., 2009). Therefore, these results implicate both TBC1D1 and TBC1D4 Rab-GAPs as downstream signalling intermediates of contraction. In addition, the over expression of TBC1D4 4P (S318A, S588A, T642A, S751A) or TBC1D1 4P (S231A, S499A, T590A, S621A) in TA muscle inhibited contraction-mediated glucose uptake (An, et al., 2010) (Kramer, et al., 2006). This was reversed when GAP activity was disrupted with the R/K mutation. Thus, TBC1D1 and TBC1D4 could represent a convergent point for insulin- and contraction-regulated GLUT4 trafficking.

Interestingly, PI 3-kinase dependent signalling mechanisms were found to be essential for contraction-mediated phosphorylation of TBC1D4. Contraction-stimulated phosphorylation of TBC1D4 (detected using PAS antibody) was inhibited when muscle (EPI and TA) was treated with the PI3K inhibitor wortmannin (Bruss, et al., 2005) (Funai & Cartee, 2009). By contrast, contraction-mediated glucose transport and TBC1D1 phosphorylation (detected with PAS antibody) are facilitated via PI3K-independent mechanisms. These findings support the concept that TBC1D1 could predominately function to regulate contraction-mediated glucose disposal, at least in certain types of skeletal muscle. Taylor et al., 2008 demonstrated that *in vivo* injection of insulin or *in situ* contraction increased the phosphorylation of PAS-160 in TA, EDL and soleus muscles isolated from rat. Immuno-depletion of TBC1D4 from TA muscle lysates did not reduce PAS-160 and revealed that the major PAS band in TA muscle corresponded to TBC1D1. Furthermore, TBC1D1 is the major PAS band in EDL muscle (Pehmoller, et al., 2009). In contrast the major immuno-reactive band at 160 kDa in rat soleus muscle, gastrocnemius muscle and in adipocytes was confirmed to be TBC1D4 (Taylor, et al., 2008) (Lansey, et al., 2012).

The use of the muscle-specific transgenic mouse expressing inactive α2-AMPK isoform (AMPK-α2i Tg), muscle-specific AMPK-α_2 kinase dead (AMPK-α2 KD) and the whole body AMPK knockout (AMPK-α2 KO) mice models along with the development AMPK phosphorylation site-specific antibodies provide evidence that AMPK directly phosphorylates TBC1D1 and that this regulates glucose uptake in muscle. The AMPK-α2 catalytic isoform plays a functional role in regulating basal and contraction-stimulated levels of phosphorylated TBC1D1. In the AMPK-α2i Tg (Vichaiwong, et al., 2010) and the AMPK-α_2 KD mice (Pehmoller, et al., 2009) and whole body AMPK-α2 knockout mice (Frosig, et al., 2010) basal and contraction-stimulated phosphorylation of TBC1D1 was significantly reduced.

1.6 GLUT4 trafficking studies

Glucose transport into adipose and muscle cells is controlled through processes which regulate the rate at which GLUT4 is trafficked and inserted in to the plasma membrane and the rate GLUT4 is retrieved from the cell surface. The dysregulation of insulin-stimulated glucose uptake into peripheral tissues is a major feature of T2DM. Therefore, current research in part aims to find means by which glucose disposal in to muscle can be enhanced. This could be either through improving insulin sensitivity or discovering mechanisms which bypass insulin signalling altogether in cases of insulin resistance. Interestingly, exercise-mediated GLUT4 translocation and glucose disposal appears to be normal in insulin-resistant individuals. Furthermore, contraction or AMPK-activation in combination with insulin are additive to increase GLUT4 to the cell surface and enhance glucose uptake.

Both Rab-GAPs TBC1D1 and TBC1D4 are expressed in skeletal muscle and are phosphorylated in response to insulin and contraction stimulation. Therefore they have been identified as key intermediates linking upstream signalling pathways to downstream GLUT4 trafficking events. Furthermore, *Tbc1d1* has been identified as a candidate gene for obesity predisposition in some rare cases of severe obesity. In addition a truncation mutation of *Tbc1d4* has been identified to cause severe postprandial hyperinsulinemia in humans. Moreover, a different genetic mutation in *Tbc1d1* has been found to confer leanness in mice and protection from diet induced obesity. It is as yet unknown exactly how some of these mutations affect TBC1D1 function and how this impacts on normal metabolic pathways. Thus, it is of interest to further investigate the role of TBC1D1 and TBC1D4 with respect to GLUT4 trafficking in response to insulin- and/or contraction-mediated stimulation.

There have been many technical challenges associated with the investigation of GLUT4 trafficking in skeletal muscle. The abundance of cytoskeletal and structural proteins in muscle has made sub-cellular membrane fractionation procedures problematic for the analysis of GLUT4 intracellular distribution. Furthermore, there are difficulties associated with the isolation of single skeletal

muscle fibres which has impeded detailed kinetic analysis of endogenous GLUT4 trafficking using biotinylated photolabelling techniques. Therefore, alternative methods have been developed utilising the ectopic expression of epitope-tagged GLUT4. GLUT4 reporter constructs have been designed to contain a hemagglutinin (HA) or Myc tag in the first exofacial loop and can also have a C-Terminal GFP tag (HA/Myc GLUT4 GFP). The exofacial (HA/Myc) tag allows for the rapid detection of GLUT4 which has been inserted into the plasma membrane. In primary skeletal muscle tissue the expression of GLUT4-GFP has enabled more detailed investigations of GLUT4 translocation in response to insulin- and contraction-mediated signalling *in vivo* (Lauritzen, et al., 2008) (Lauritzen, et al., 2006). More recently, the transgenic expression of an exofacial-tagged GLUT4 (HA-GLUT4-GFP) in mice has enabled direct measurements of GLUT4 inserted into the cell membrane of intact single muscle fibres (Lizunov, et al., 2012) (Fazakerely, et al., 2009).

Immortal skeletal muscle cell lines (L6 cells and C2C12 myotubes) expressing exofacial tagged GLUT4 proteins have provided alternative model systems to study GLUT4 trafficking kinetics. In contrast to primary muscle cells, cell culture models can be efficiently manipulated through transduction and transfection techniques. Furthermore, large populations of cells can be obtained for detailed time-course investigations.

1.7 Experimental Design and Aims

The studies described in this thesis were completed in order to further enhance our understanding of how GLUT4 trafficking is regulated in response to insulin and AMPK-activation. Exercise-mediated GLUT4 translocation and glucose disposal appears to be normal in insulin-resistant individuals. Furthermore, contraction or AMPK-activation in combination with insulin are additive to increase glucose transport. A vast amount of research is focused on finding potential therapeutic targets which increase insulin sensitivity and oxidative capacity of muscle in order to overcome an insulin resistant state associated with T2DM and obesity. Therefore, an important overall aim of the work described in this thesis is to provide mechanistic evidence to support AMP-activated protein kinase and subsequent downstream signalling and membrane trafficking pathways leading to an alteration in GLUT4 translocation kinetics as important therapeutic targets.

The focus of these investigations is to address the importance of the Rab-GAPs TBC1D1 and TBC1D4 in muscle cells with regard to GLUT4 translocation. The Rab-GAP proteins TBC1D1 and TBC1D4 have been identified as potential downstream signalling intermediates which regulate GLUT4 translocation (Roach, et al., 2007). Several studies have demonstrated that TBC1D4 and TBC1D1 are phosphorylated in response to insulin and contraction stimulation in skeletal muscle (Kramer, et al., 2006) (Bruss, et al., 2005) (Funai & Cartee, 2008) (Funai & Cartee, 2009). It is generally accepted that the phosphorylation of these Rab-GAP proteins inhibits their function as negative regulators of GLUT4 trafficking and as a result any associated rab proteins would be in their active GTP-bound state. It has been recently proposed that TBC1D1 could be primarily responsible for regulating contraction-mediated glucose uptake in muscle (Funai & Cartee, 2009) (An, et al., 2010) (Pehmoller, et al., 2009) (Vichaiwong, et al., 2010). Several AMPK phosphorylation sites have been identified in TBC1D1. The most well studied site is the consensus motif at serine 231 (Stone, et al., 2002). However, whether TBC1D1 and TBC1D4 are both essential in muscle is not fully understood. In order to address this we have firstly comprehensively investigated the tissue-specific expression pattern

of TBC1D1 and TBC1D4 within different tissues using quantitative real-time PCR. Furthermore, we have quantified TBC1D1 and TBC1D4 protein levels in different muscles and other insulin-responsive tissues using western blotting techniques. At the time this project commenced there were no commercial antibodies available against TBC1D1 protein or TBC1D1 phosphorylated at serine 231 and so specific anti-serum was generated. It was therefore necessary to initially evaluate their use as potential tools for studying the role of TBC1D1 in AMPK-mediated GLUT4 translocation.

There is limited and in-conclusive evidence available to support the use of immortal skeletal muscle cell lines (L6 cells and C2C12 myotubes) to study GLUT4 trafficking kinetics. These muscle cell models are advantageous and can be easily manipulated to express exofacial tagged GLUT4 proteins to provide alternative *in vitro* model systems. Furthermore, they can be readily sourced and cultured with ease and so have great potential for industry applications. Therefore, the final aim of these investigations is to address whether immortal cell lines can provide a promising model for accurately measuring GLUT4 trafficking in muscle and if so, whether quantitative HA-GLUT4 trafficking assays can be optimised which may be useful as a reliable end-point tool for application in industry.

We have used the C2C12 muscle cell model to investigate how insulin stimulation and/or AMPK-activation affects the kinetics of GLUT4 trafficking. Our data support the current concepts that insulin stimulates the rapid release of GLUT4 to the plasma membrane and increases the rate of GLUT4 exocytosis (k_{ex}) at steady state. In addition, treatment with the AMPK-activator, AICAR, stimulates the slow accumulation of GLUT4 at the cell surface through the inhibition of GLUT4 endocytosis. Furthermore, our findings revealed that the combination of insulin plus AICAR treatments was synergistic to increase GLUT4 cell surface levels through increasing both the k_{ex} for GLUT4 and the size of the GLUT4 recycling compartment.

Finally, we have used siRNA-mediated knockdown to investigate the role of TBC1D1 and TBC1D4 in basal GLUT4 retention mechanisms. Furthermore, we have explored the potential involvement for TBC1D1 and TBC1D4 in insulin- and AMPK-mediated GLUT4 translocation. We have shown that TBC1D1 may play an important role in retention mechanisms which regulate basal cell surface levels of GLUT4.

2 Materials and Methods

2.1 Materials

2.1.1 Buffers and Solutions

Table 2.1: Laboratory material sources and list of abbreviations.

Company	Address	Abbreviation
Abcam	Cambridge, UK	ABM
BD	Oxford, UK	BD
Beckman Coulter	High Wycombe, Buck, UK	BEC
BMG Lab Tech	Aylesbury, Buck, UK	BMG
Bio-Rad	Hemel Hempstead, Herts, UK	BIO
CBS-Scientific	Del Mar, CA, USA	CBS
Celluliance Corporation	Norcross, GA, USA	CEL
Cell Signalling Technology	Hitchin, Herts, UK	CST
Clontech	Mountain View, CA, USA	CLO
Covance	Maidenhead, Berk, UK	COV
Electron Microscopy Sciences	Hatfield, PA, USA	EMS
Eppendorf	Stevenage, Herts, UK	EPP
Eurogentech	Southampton, UK	EUR
Fisher Thermo Scientific	Loughborough, Leis, UK	FIS
GE Healthcare	Little Chalfont, Buck, UK	GE
Greiner Bio-One	Stone house, Glos, UK	GRE
Life Technologies Ltd	Paisley, UK	LTC
Lonza	Tewkesbury, Glos, UK	LON
Merck Millipore	Watford, Herts, UK	MIL
Novo Nordisk	Crawley, W. Sus, UK	NOV
Promega	Southampton, UK	PRO
Peqlab	Southampton, UK	PEQ
Qiagen	Manchester, UK	QIA
Roche	Burgess Hill, W. Sus, UK	ROC
Sigma	Gillingham, Kent, UK	SIG
Symansis	Timaru, NZ	SYM
UVP	Cambridge, UK	UVP
VWR	Lutterworth, Leis, UK	VWR

Table 2.2: Buffers and solutions.

Name	Composition
BCA Reagent B	4% (w/v) $CuSO_4.5H_2O$
C2C12 normal growth media	Dulbecco's Modified Essential Medium (DMEM) (D6546, SIG),10% (v/v) Foetal Bovine Serum (FBS) (SIG), 50 units /ml penicillin, 50 µg/ml streptomycin (P4458,SIG), 2 mM L-glutamine (G7313, SIG)
C2C12 (HA-GLUT4) growth media	DMEM (SIG), 10% (v/v) FBS (SIG), 50 units/ml penicillin, 50 µg/ml streptomycin (SIG), 2 mM L-glutamine (SIG), 2 µg/ml (w/v) puromycin (540411, Calbiochem, MIL)
C2C12 differentiation media	DMEM (SIG), 5% (v/v) Horse Serum (HS) (SIG), 50 units/ml penicillin, 50 µg/ml streptomycin (SIG), 2 mM L-glutamine (SIG)
C2C12 serum-free media	DMEM (SIG), 0.2% (w/v) bovine serum albumin (BSA) (CEL), 2 mM L-glutamine (SIG)
C2C12 serum-free media (without bicarbonate)	11 mg/ml (w/v) GIBCO® DMEM (119 00-073, FIS), 20 mM (w/v) HEPES, 0.2% (w/v) BSA (CEL) (filter sterilised)
DEPC-treated ddH_2O (RNase-free)	1% (v/v) diethyl pyro carbonate (DEPC) (D5758, SIG) in ddH_2O (autoclaved)
Enhanced Chemi-luminescence buffer A	100 mM (w/v) Glycine (pH 10), 0.4 mM (w/v) luminol, 8 mM (w/v) 4-iodophenol
Enhanced Chemi-luminescence buffer B	0.12% (v/v) hydrogen peroxide
0.5% Glutaldehyde	25% (w/v) Glutaldehyde (16220, EMS) in 1x PBS
Quench solution (sterile)	50 mM Glycine (w/v) in 1x DPBS
Quench solution	50 mM Glycine (w/v) in 1x PBS
HA-GLUT4 Assay blocking buffer	1% (w/v) BSA (CEL), 3% (v/v) Goat serum (G9023, SIG, (±) 0.2% (w/v) saponin in PBS
HA-GLUT4 Assay antibody buffer	1% (w/v) BSA (CEL), (±) 0.025% (w/v) saponin in PBS
2x HBS	280 mM (W/V) NaCl, 50 mM (w/v) HEPES, 1.42 mM (w/v) Na_2HPO_4•7H2O (pH 7.05) Adjust pH to 7.05 with 10 M NaOH

HEK 293 cell growth media	DMEM (SIG),10% (v/v) FBS, 50 units/ml penicillin, 50 µg/ml streptomycin (SIG), 2 mM L-glutamine (SIG)
HEK 293 cell lysis buffer	50 mM (w/v) Tris-HCL (PH 7.4), 150 mM (w/v) NaCl, 1 mM (w/v) EDTA, 0.5% (v/v) Triton X-100
Luria broth	1% (w/v) Bacto tryptone, 0.5%(w/v) Bacto yeast extract, 0.5% (w/v) NaCl (pH 7.5, autoclaved)
3% Paraformaldehyde	16% paraformaldehyde (15710, EMS) in 1x PBS (foil wrapped)
1x Phosphate buffered saline (PBS)	12.5 mM (w/v) Na_2HPO_4, 154 mM (w/v) NaCl (pH 7.2)
1x PBS (RNase-free and sterile)	10x PBS (10468543, FIS) in DEPC-treated ddH_2O
1x DPBS (sterile)	10x Gibco® DPBS (14200-067, LTC) in autoclaved ddH_2O
Plat-E cell growth media	DMEM (SIG),10% (v/v) FBS (SIG) 50 units/ml penicillin, 50 µg/ml streptomycin (SIG), 2 mM L-glutamine (SIG) 10 µg/ml (w/v) blastocidin, 1 µg/ml puromycin (540411, Calbiochem, MIL)
Ponceau S stain	0.1% (w/v) Ponceau S, 3% (w/v) trichloroacetic acid (TCA)
Cell lysis buffer	20 mM (w/v) Tris-HCL (PH 7.4), 150 mM (w/v) NaCl ,1 mM (w/v) EDTA, 1 mM (w/v) EGTA, 1 % (v/v) Triton X-100
Resolving gel buffer	1.5 M (w/v) Tris HCl (pH 8.8), 0.4 % (w/v) SDS
3x Sample buffer	62.5 mM (w/v) Tris-HCl (pH 6.8), 2% (w/v) SDS, 10% (w/v) glycerol, 0.01% (w/v) bromophenol blue, 100 mM Dithiothreitol (DTT)
Stacking gel buffer	0.5 M (w/v) Tris HCl (pH 6.8), 0.4 % (w/v) SDS
SDS Electrophoresis buffer	25 mM (w/v) Tris HCL (pH 6.3), 0.2 M (w/v) glycine, 0.1% (w/v) SDS
SDS Transfer buffer	49 mM (w/v) Tris-HCl, 39 mM (w/v) glycine, 0.0375% (w/v) SDS, 20% (v/v) methanol

1x Tris buffered saline (1x TBS)	10 mM (w/v) Tris-HCl (pH 7.4), 154 mM (w/v) NaCl,
Tris buffered saline with Tween 20 (TBST)	10 mM (w/v) Tris-HCl (pH 7.4), 154 mM (w/v) NaCl, 0.1% (v/v) Tween 20
10x TAE	Tris-Acetate EDTA
1x TAE	Tris-Acetate EDTA

2.1.2 Antibodies

Cell and tissue lysates were resolved by SDS-PAGE and analysed using western blotting. A list of primary antibodies is detailed in Table 2.3.

Table 2.3: Primary Antibodies.

Antibody Name	**Dilution**	**Species**	**Source**
AMPK	1:1000 1% BSA	Rabbit	#2532, CEL
AKT2	1:1000	Rabbit	#3063, CEL
AS160	1:1000	Rabbit	#07-741, UPS, FIS
Monoclonal β Tubulin, clone	1:5000	Mouse	T0198, SIG
FLAG, clone M2	1:1000	Mouse	F3165, SIG
GAPDH	1:5000	Mouse	9484, ABM
GLUT 4	1:4000	Rabbit	In House
HA.11, clone 16B12	1:1000	Mouse	MMS 101P, COV
Phospho-ACC (serine 79)	1:1000	Rabbit	#07-303, MIL
Phospho-AMPK (threonine 172)	1:1000	Rabbit	#2535, CEL
Phospho-AKT (serine 473)	1:1000	Rabbit	#4058, CEL
Phospho-AS160 (threonine 642)	1:1000	Sheep	3028 P1, SYM
TBC1D1 AGG 4397	1:120	Rabbit	Astra Zeneca
TBC1D1 AGG 4398	1:170	Rabbit	Astra Zeneca
TBC1D1 AGG 4399	1:450	Rabbit	Astra Zeneca
TBC1D1 AGG 4400	1:280	Rabbit	Astra Zeneca
TBC1D1 AGG 4401	1:230	Rabbit	Astra Zeneca
TBC1D1 AGG 4402A	1:370	Rabbit	Astra Zeneca
TBC1D1 AGG 4402B	1:250	Rabbit	Astra Zeneca
TBC1D1 AGG 4403	1:280	Rabbit	Astra Zeneca
TBC1D1 AGG 4404	1:280	Rabbit	Astra Zeneca
TBC1D1 AGG 4405	1:220	Rabbit	Astra Zeneca
TBC1D1 H-AH	1:1000	Rabbit	Germany
TBC1D1 #4629	1:1000	Rabbit	#4629, CEL

Phospho-TBC1D1 AGG 4989	1:160	Rabbit	Astra Zeneca
Phospho-TBC1D1 AGG 4990	1:230	Rabbit	Astra Zeneca
Phospho-TBC1D1 AGG 4991	1:230	Rabbit	Astra Zeneca

Table 2.4: Secondary Antibodies.

Antibody Name	Dilution	Species	Source
anti-mouse, HRP conjugate	1: 4000	Goat	31430, FIS
anti-rabbit, HRP conjugate	1: 4000	Goat	AP187P, MIL
anti-sheep IgG, HRP conjugate	1: 4000		AP147P, MIL
Alexa Fluor 488 anti-mouse IgG	1: 100	Goat	A1101, FIS

2.1.2.1 Anti-TBC1D1 Antibody Generation

Specific anti-serum was raised against three different peptides sequences corresponding to rat TBC1D1 (AZ 3001724, AZ 3001725, and AZ 3001726) (Table 2.5, 2.1.2.2). The antibodies were generated by the Antibody Generation Group (AGG), Astra Zeneca, Macclesfield, UK as part of CASE PhD studentship between the University of Bath and Astra Zeneca. Three or four rabbits were injected with each peptide and affinity purified anti-serum from terminal bleeds were obtained.

2.1.2.2 Anti-TBC1D1 Phospho-specific Antibody

A phospho peptide matching the sequence around serine 237 of rat TBC1D1 was used to generate antibodies which would specifically recognise phosphorylated TBC1D1 (AZ 3003376) (Table 2.5). Three rabbits were injected with the peptide and anti-serum from terminal bleeds was obtained. Terminal bleeds were passed over a non-phosphorylated peptide column to isolate antibodies that do not recognise the phosphorylated peptide. The resulting flow through was then applied to a phospho-specific column in order to purify the phospho-specific antibodies. Antibodies were examined for specificity in western blots. These antibodies have been shown to display specificity by western blotting towards an in-vitro phosphorylated recombinant TBC1D1 N-terminal construct containing the two PTB domains of the protein (Fazakerely, 2010).

Table 2.5: Synthetic peptide sequences used to generate TBC1D1 antibodies. A sequence alignment comparing mouse and human TBC1D1 with the four epitopes of rat TBC1D1 used to generate 13 polyclonal antisera.

Antibody ID	Peptide	Mouse Sequence	Human Sequence
AGG 97-99 AZ 3001724	CEPDLRKSQPWDP	CEPDL**E**KSQPWDP	CEPEPGRSQQWDP
AGG 00-02B AZ 3001725	CDSPSRTEDYSE	Same	CDSSSRTEDYSE
AGG 03-05 AZ 3001726	QKLRPRNEQREN	Same	Same
AGG 89-91p AZ 3003376	CPMRKSFpSQPGLR		

2.1.3 Oligonucleotides and Taqman® Probes

2.1.3.1 PCR Primers

Two sets of exon-splicing PCR primers were designed against the regions flanking exons 11-12 of full-length *Tbc1d1* and synthesised (EUR). Primers were used to determine the qualitative expression pattern of splice variants of *Tbc1d1* in a panel of rodent tissues.

Table 2.6: PCR primers for qualitative reverse transcription (RT)-PCR experiments.

Name	Sequence 5' - 3'
Tbc1d1 exon flanking primers 1	Fwd. taagtaacaccagcaaagagct Rev. tgaataatcttcatatctgct
Tbc1d1 exon flanking primers 2	Fwd. tctgtcccggggcaataaagcc Rev. tcggaggaatatctgctcca

2.1.3.2 SiRNA Oligonucleotides

SiRNA Oligonucleotides were purchased from Dharmacon (FIS).

Table 2.7: siRNA Oligo-nucleotides.

Name	Product	Ordering number/sequence
Control	ON-TARGET plus Non Targeting SMART pool	D-001810-10
Knockdown of *Tbc1d1*	siGENOME siRNA mouse *Tbc1d1*	D-040360-01 GAUCAGAGGUCAUAUUUAAUU
Knockdown of *Tbc1d4*	siGENOME mouse *Tbc1d4* SMART pool	M-040174-01

2.1.3.3 Taqman Probes

Predesigned Applied Biosystems® Taqman® gene expression assays were purchased (Invitrogen, LTC). TaqMan® gene expression assays consist of a pair of unlabelled PCR primers and TaqMan® probe with a FAM™ label on the 5' end and minor groove binder (MGB) non-fluorescent quencher (NFQ) on the 3' end. Rat *Tbc1d4* assay was designed using in-house primer design software (Astra Zeneca) and synthesised (EUR).

Table 2.8: Taqman® probes for real-time quantitative PCR experiments.

Gene	Gene Name	Assay ID
Tbc1d1	*TBC1 (tre-2/USP6, BUB2, cdc16 domain family, member 1*	Rn 01413271.m1
Tbc1d1	*TBC1 (tre-2/USP6, BUB2, cdc16 domain family, member 1*	Mm 00497989.m1
TBC1D1	*TBC1 (tre-2/USP6, BUB2, cdc16 domain family, member 1*	Hs 00207999.m1
Tbc1d4	*TBC1 domain family, member 4*	Rn
Tbc1d4	*TBC1 domain family, member 4*	Mm 00557659.m1
TBC1D4	*TBC1 domain family, member 4*	Hs 00411484.m1
Hprt	*Hypoxanthine phosphoribosyltransferase 1*	Rn 01527840.m1
Hprt	*Hypoxanthine phosphoribosyltransferase 1*	Mm 01324427.m1
B2m	*Beta-2-microglobulin*	Rn 00560865.m1
B2M	*Beta-2-microglobulin*	Hs
Gus B	*Glucuronidase, beta*	Rn 00566655.m1
Gus B	*Glucuronidase, beta*	Mm 00446953.m1
GUS B	*Glucuronidase, beta*	Hs
Tbp	*TATA box binding protein*	Mm 00446971.m1
CYP A	*Cyclophilin A*	Hs
Myo g	*Myogenin*	Mm 00446194.m1
Myo d	*Myogenic differentiation 1*	Mm 00440387.m1

2.1.4 Animals

Adult male Wistar rats weighing ~200-240 g and adult male mice were used for the isolation of tissue samples. Tissues harvested from rats were used for the preparation of protein lysates and extraction of total RNA. Mouse tissues were used for the preparation of protein lysates. All animals were fed *ad libitum* a standard laboratory chow and housed in a 12h: 12h light dark cycle. Procedures involving use of animal material conformed to UK Home Office Guidelines on

the Operation of the Animals (Scientific Procedures) Act and were approved by the University of Bath Animal Care and Use Committee.

2.2 Experimental Methods

2.2.1 Molecular Biology Methods

2.2.1.1 Determining DNA/RNA Concentration

The concentration of DNA/RNA within samples was determined by absorbance at the wavelengths 260/280 nm. Absorbance measurements were made with a Bio Photometer UV spectrophotometer (EPP), using quartz cuvettes or using the Nano Drop ND-1000 Spectrophotometer (FIS). A selection of RNA samples were visualised using agarose gel electrophoresis as described in 2.2.1.3.

2.2.1.2 Plasmids

HA-tagged GLUT4 cloned into the retroviral vector pBabe was provided by Professor David James. Full-length *Tbc1d1* and *As160/Tbc1d4* cloned into the pcDNA3, which contains a FLAG coding sequence, were provided by Professor Francis Barr. The constructs were transformed into competent XL-1 blue *E.Coli* cells (HA-GLUT4 was cloned by Daniel Fazakerely and full-length FLAG-*Tbc1d1* and FLAG-*As160/Tbc1d4* were cloned by Judith Richardson).

Bacterial cell glycerol stocks were inoculated into luria broth (LB) supplemented with 50 µg/ml ampicillin (SIG) and cultured overnight at 30^{o}C with shaking. Plasmid DNA was purified using Wizard® Plus SV Minipreps purification kit (A1460, PRO), following manufacturer instructions.

2.2.1.3 Agarose Gel Electrophoresis

Agarose gels were used to visualise nucleic acid fragments. 1% agarose (SeaKem Agarose, LON) was prepared in TAE buffer. After boiling, 0.01% Sybr Safe (S33102, LTC) was added. Samples were prepared in a 6X type II gel loading buffer (AB-0594, FIS). DNA fragment size was determined using 100 bp (G2101, PRO) and 1 kb-ladders (G7511, PRO). Electrophoresis was run at 120-150 Volts, for approximately 20 min. After migration the DNA bands were visualised using UV light at wavelength on a trans-illuminator (UVP).

2.2.1.4 Preparation of total RNA from cultured cells

RNA was isolated from differentiating C2C12 myotubes. 600 µl of RLT buffer was added to each 6-Well, pipetted up and down several times and transferred to eppendorf tubes. Total RNA was isolated from samples using the using the RNA Easy Mini Kit (74106, QIA) and processed using an automated QiaCube (9001213, QIA). RNA concentration was determined as detailed in 2.2.1.1. RNA samples were snap frozen on dry ice and stored at -80^{o}C until required.

2.2.1.5 Preparation of RNA from pancreatic Islets

Approximately 100 rat pancreatic islets were lysed in 350 µl RLT buffer then snap frozen and stored at -80^{o}C. Samples were thawed and total RNA was isolated using the RNA Easy Micro Kit (74004, QIA) and processed using an automated QiaCube (9001213, QIA). An on-column digestion of DNA during RNA purification was performed using the RNase-free DNase set (79254, QIA). RNA concentration was determined as detailed in 2.2.1.1. RNA samples were snap frozen on dry ice and stored at -80^{o}C until required.

2.2.1.6 Preparation of total RNA from rat tissue (excluding muscle, adipose)

The homogenisation of rat tissues for the isolation of total RNA was performed using the Precellys Homogeniser Keramik-Kit (91-PCS-CKM, PEQ) following manufacturer's instructions. 60-80 mg of tissue was homogenised in 1.4/2.8 mm tubes, prefilled with ceramic beads, containing 1.4 ml of RLT buffer (79216, QIA). Tissues were homogenised in a Precellys 24 (91-PCS24, PEQ) for three cycles (run time: 30 seconds, pause time: 1.5 min) at 4^{o}C. The homogeniser was pre cooled to 4^{o}C using the Cryolys cooling module (91-PCS-CRYO, PEQ). Total RNA was isolated from homogenised tissue samples using the RNA Easy Mini Kit (74106, QIA) and processed using an automated QiaCube (9001213, QIA) following manufacturer's instructions. An on-column digestion of DNA was performed using the RNase-free DNase set (79254.QIA). RNA concentration was determined as detailed in 2.2.1.1. RNA samples were snap frozen on dry ice and stored at -80^{o}C until required.

2.2.1.7 Preparation of RNA from adipose and muscle tissue

RNA was isolated from adipose and muscle tissue using Trizol® method. 100mg of adipose tissue or 30-60 mg of muscle tissue was homogenised in 1.4/2.8 mm tubes, prefilled with ceramic beads, containing 1.4 ml of Trizol® (15596-026, Invitrogen, LTC). Tissues were homogenised in a Precellys 24 (91-PCS24, PEQ) as previously described. The samples were incubated at room temperature for 5 min and then centrifuged at 10,000 rpm for 10 min at 4^{o}C. The aqueous phase was transferred to new eppendorf tubes. Chloroform was added at one fifth of the sample volume and the suspension was vigorously shaken for 15 sec and incubated at room temperature for a further three min. The samples were phase-separated using centrifugation at 10,000 rpm for 15 min at 4^{o}C. Following centrifugation, 500 µl of the colourless aqueous phase was transferred to new eppendorf tubes. Total RNA was isolated from samples using the RNA easy Mini Kit (74106, QIA) and processed using an automated QiaCube (9001213, QIA).

2.2.1.8 DNase-Treatment

Total RNA samples extracted using the Trizol® method were subjected to DNase-treatment to remove genomic contamination. The digestion of DNA was performed using the Turbo DNA-*free*^{TM} kit (AM1907, LTC), following manufacturer's instructions. 10 µg of total RNA, 1 µl of TURBO DNase and 0.1x volume of TURBO DNase buffer (10X) were added together and made up to 50 µl with DEPC-treated ddH2O. The reactions were incubated at 37^{o}C for 30 min. 10 µl of DNase Inactivation Reagent was added and incubated for 2 min with agitation. The samples were centrifuged for 2 min at 10,000 rpm and the supernatant was transferred to new eppendorf tubes. RNA samples were snap frozen on dry ice and stored at -80^{o}C until required.

2.2.1.9 Reverse-Transcription; CDNA Synthesis

cDNA was synthesised from RNA using the Applied Biosystems® TaqMan® Reverse Transcription Kit (N808 0234, LTC), following manufacturer's instructions.

2.2.1.10 Reverse-Transcription Polymerase Chain Reaction

Qualitative reverse-transcription Polymerase Chain Reaction (RT-PCR) was used to determine the expression pattern of *Tbc1d1* splice variants within primary rat tissues and cultured cells. Reverse transcription of RNA to cDNA was performed as described in 2.2.1.9. Two sets of exon-splicing primers which flank the predicted insertion exons 11 and 12 of the long variant of *Tbc1d1* were designed (EUR) (Table 2.6, 2.1.3.1). Exon-flanking primers bind to the template cDNA and PCR was used to amplify the DNA sequences. PCR was performed using the ThermoPrime Plus *Taq* DNA Polymerase within a ReddyMix™ PCR Master Mix (AB-0575/LD/B, FIS), following manufacturer's instructions (Table 2.9). Final 1x reaction contains 1 U *Taq* DNA Polymerase and 200 µM of each dNTP. DNA amplification was conducted using the following reaction conditions.

Table 2.9: PCR reaction conditions.

Step	Temperature	Time	Number of cycles
Initial Denaturation	95°C	2 min	1 cycle
Denaturation	95°C	25	35 cycles
Annealing	55°C	35	35 cycles
Extension	72°C	65	35 cycles
Final Extension	72°C	5 min	1 cycle

The resulting PCR products were visualised using agarose gel electrophoresis as described in 2.2.1.3.

2.2.1.11 Taqman two-step real-time qPCR

A broad-coverage panel of 26 human tissue cDNAs was purchased from Clontech. 31 separate mouse tissue cDNAs were kindly pre-made by Alison Davies (CVGI group, Astra Zeneca, Macclesfield, UK). cDNA was prepared from C2C12 cells as detailed in (2.2.1.4 and 2.2.1.9). 20 ng of each cDNA sample was plated in triplicate in to wells of a 384-well plate. Pre-designed Taqman® gene expression assay kits were purchased from Applied Biosystems (Table 2.8, 2.1.3.3) Samples were processed using the Absolute qPCR Mix (AB1138/B, FIS) following manufacturer's instructions. Briefly, qPCR was performed using the Thermo-Start DNA Polymerase within a master mix reaction buffer (Table 2.10). Gene expression analysis was performed using an

Applied Biosystems 7900HT real-time PCR system (QIA). The relative gene expression levels for each tissue were calculated using the ΔCT method by normalising data to a geometric mean from three independent reference genes.

Table 2.10: Preparation of two-step qPCR reaction per well of 384-well plate.

Component	Volume (µl)
cDNA	2
Primer/probe (20X)	0.5
Master mix	5
RNase free ddH_2O	2.5
Total Volume (µl)	10

2.2.1.12 Taqman one-step real-time qPCR

RNA samples were diluted to 10 ng/µl with DEPC-treated water (LTC46-2224, Invitrogen, LTC) and plated in 96-well plates. 20 ng of each RNA sample was plated in triplicate in to wells of a 384-well plate. Pre-designed Taqman® gene expression assay kits were purchased from Applied Biosystems (Table 2.8, 2.1.3.3). Samples were processed using the Quantitect Probe RT-PCR kit (204445/3, QIA) following manufacturer's instructions. Briefly, qRT-PCR was performed using the omniscript and sensiscript reverse transcriptases and HotStar*Taq* DNA Polymerase within a RT-PCR reaction buffer (Table 2.11). Gene expression analysis was performed using an Applied Biosystems 7900HT real-time PCR system (QIA). The relative gene expression levels for each tissue were calculated using the ΔCT method by normalising data to a geometric mean from three independent reference genes.

Table 2.11: Preparation of one-step qPCR reaction per well of 384-well plate.

Component	Volume (µl)
RNA	2
Primer/probe (20X)	0.5
RT-PCR buffer	5
RT enzyme	0.1
RNase free ddH_2O	2.4
Total Volume (µl)	10

2.2.2 Cell Culture Methods

2.2.2.1 Cell line Sources

The C2C12 muscle skeletal muscle cell line and the 3T3-L1 adipocyte cell line and the HEK-293 cell line were purchased from the American Type Culture Collection (ATCC). HL1 mouse heart cells (CC) were kindly provided by Dr William.C Claycomb (LSU, New Orleans, LA, USA). Platinum-E (Plat-E) cells (modified HEK 293 cells) and L6 rat skeletal muscle cells (L6 Bath) were provided by Professor David James (Garvan Institute, Sydney, AUS). L6 rat skeletal muscle cells (L6 AZ) were a sub-clone of ECACC 83011421 provided by and cultured at Astra Zeneca (Astra Zeneca, Alderley Park, Macclesfield, UK).

All cell lines were stored in cryovials and kept in liquid nitrogen tanks. Cells were maintained in freeze down medium, normal growth medium supplemented with 10% dimethyl sulfoxide (DMSO) (D2650, SIG) with an extra 10% heat inactivated FBS (SIG).

2.2.2.2 HEK-293 cell culture

Human Embryonic Kidney 293 cells (HEK 293) cells were routinely cultured in growth media (Dulbecco Modified Essential Medium (DMEM) (D6546, SIG) supplemented with 10% (v/v) heat inactivated FBS (SIG), 50 units/ml penicillin, 50 µg/ml streptomycin (P4458, SIG) and 2 mM L-glutamine (G7313, SIG) at 37^{o}C in 10% CO_2. HEK 293 cells were grown to 90% confluence and passaged every 3-4 days.

2.2.2.3 Expression of full-length FLAG-tagged TBC1D1 and TBC1D4 in HEK 293 cells

HEK 293 cells were seeded in 90 mm dish (TKT-110-070A, Nunclon, FIS) in growth media minus antibiotics and grown overnight to 60% confluence. The next day cells were transfected with full-length 1XFLAG-tagged *Tbc1d1* or 3XFLAG-tagged *As160/Tbc1d4* using Lipofectamine® LTX reagent (18324-012, Invitrogen, LTC). Transfection was performed following manufacturer's instructions. Recombinant proteins were expressed in HEK 293 cells for 18 to 24 hours at 37^{o}C in 5% CO_2. One hour prior to cell lysis the culture media was

replenished. Cells were lysed in 2% Sodium Dodecyl Sulphate (SDS) supplemented with protease inhibitors (Halt Protease Inhibitor Cocktail, 78430, Pierce, FIS). Lysates were pipetted up and down several times, transferred to eppendorf tubes and rotated at room temperature for 15 min. Samples were briefly sonicated (6 x 1 second at amplitude 10 microns) using a sonicator and centrifuged at 14,000 x *g* for 30 min at 16^{o}C. The cleared supernatant was transferred to new eppendorf tubes. Protein concentration was determined as detailed in 2.2.3.3. 50 µg of protein lysate was subjected to SDS-PAGE as described in 2.2.3.4. All 10 TBC1D1 antibodies (Table 2.3, 2.1.2) were analysed for specificity against 1XFLAG-tagged TBC1D1 using western blotting as detailed in 2.2.3.5. Preference for TBC1D1 over TBC1D4 was also compared.

2.2.2.4 Calcium phosphate transfection of HEK 293 cells

HEK 293 cells were seeded at 2 x 10^{6} cells per 90 mm dish (TKT-110-070A, Nuclon, FIS) in growth media minus antibiotics. The next day, three hours prior to transfection the media was replenished. For each plate, 20 µg of full-length 3XFLAG-tagged *Tbc1d1* or 3XFLAG-tagged *As160/Tbc1d4* DNA were mixed with 250 mM $CaCl_2$. The $CaCl_2$/DNA mix was added drop wise to a 2 x HBS solution and allowed to stand at room temperature for 30 min until the precipitate was formed. The transfection mix was added drop wise to the cells and incubated for 16 to 24 hours at 37^{o}C in 10% CO_2. The following day the media was replenished and incubated for a further 24 hours. Cells were harvested 40-48 hours after transfection.

2.2.2.5 Purification of FLAG-tagged TBC1D1 and TBC1D4 proteins from HEK 293 cells

HEK 293 cells were recovered in PBS and pelleted at room temperature at 400 x *g* for 5 min. The cells were washed with PBS and centrifugation was repeated. The supernatant was removed and the cells were lysed in HEK 293 cell lysis buffer supplemented with protease inhibitors (Halt Protease Inhibitor Cocktail, 78430, Pierce, FIS). Lysates were pipetted up and down several times, transferred to eppendorf tubes and rotated for 1 hour at 4^{o}C. The samples were centrifuged at 14,000 rpm for 20 min at 4^{o}C. The cleared supernatant was transferred to new eppendorf tubes and incubated with pre-washed anti-FLAG

M2 beads (A2220, SIG) and rotated for two hours at 4^{o}C. The unbound fraction was removed and the beads were washed three times with cell lysis buffer and a further three times with TBS. FLAG-tagged proteins were eluted from the beads with 100 µl 200 µg/ml of FLAG-peptide in TBS. A volume of the eluted fraction was resolved by SDS-PAGE as described in 2.2.3.4. The concentration of recovered purified protein was quantified as detailed in 2.2.3.3. Purified proteins were aliquoted and stored at -80^{o}C until required.

2.2.2.6 C2C12 mouse skeletal muscle cell culture

The C2C12 mouse myoblast cell line, are a skeletal muscle cell model produced by (Blau, et al., 1985). C2C12 cells are a sub-clone of the myogenic cell line derived from adult dystrophic mouse muscle (Yaffe & Saxel, 1977).

Table 2.12: Standardised C2C12 cell culture conditions.

C2C12 methodology	Standardised Condition
Seeding cell density of myoblasts	2.0 x10^{5} / T75 2.0 x 10^{5} / 6 well 5 x 10^{3} / 96 well
Passaging of myoblasts	Every 2-3 days
Seeding cell density for differentiation	4.0 * 10^{3} / 96 well
Myotubes used for experiments	6-8 days post differentiation
Number of days recovery post infection	~ 10days before seeding

C2C12 myoblasts were cultured in normal growth media, Dulbecco's Modified Essential Medium (DMEM) (D6546, SIG) supplemented with 10% (v/v) foetal bovine serum (FBS), antibiotic-antimycotic (AA) solution (S5955, SIG) (containing 100 units/ml penicillin, 100 µg/ml streptomycin 250 ng/ml amphotericin), 2 mM L-Glutamine (G7313, SIG) at 37^{o}C in 10% CO_2. Myoblasts were seeded at a density of approximately 2 x 10^{5} cells per T75 flat bottom flasks (GRE). The cells have a fast doubling time therefore they were routinely passaged every 2 to 3 days. In order to maintain a proliferative phenotype, cell cultures were not allowed to reach confluence. Important C2C12 cell culture conditions can be found in Table 2.12.

2.2.2.7 Pre coating of 96 well micro titre plates

96-well black micro titre plate with µClear base (655090, GRE) were coated with sterile 1% gelatin (214340, Difco, BD) (100 µl/well) for one hour at room temperature. Excess gelatin was removed by tipping and wells were fixed with 0.5% glutaraldehyde (16220, EMS) for 10 min. Plates were washed once with PBS then incubated for 5 min with quench solution. Subsequently the plates were washed two times with DMEM (200 µl/well) and stored in DMEM at 37^{o}C until required.

2.2.2.8 Differentiation of C2C12 myoblasts to myotubes

Myoblasts were seeded in pre coated 96-well plates at 5 x 10^3 cells per well. The next day, differentiation was induced by culturing cells in differentiation media, DMEM supplemented with 5% horse serum (H1270, SIG), antibiotic antimycotic (AA) solution (SIG) and 2 mM L-Glutamine (SIG) at 37^{o}C in 10% CO_2. The media was replenished every two days. Experiments were conducted using myotubes 6-8 days post differentiation. Light microscopy images were obtained of C2C12 cell during differentiation using a 4 x objective and were documented using digital camera (Motic) (Figure 3.1, 3.4.1). Florescence microscopy images were captured using the IN Cell Analyzer system 200 (GE Healthvare) confocal imaging plate reader (Figures A1-5, Appendix).

2.2.2.10 Plat-E cell culture

Platinum-E (Plat-E) cells are a modified HEK 293T cell line (Morita & Kitamura. 2000). These were used for efficient and stable packaging of retrovirus. Cells were cultured in Plat-E growth media, Dulbecco Modified Essential Medium (DMEM) supplemented with 10% (v/v) heat inactivated FBS (SIG), 50 units/ml penicillin, 50 µg/ml streptomycin (P4458, SIG), 2 mM L-glutamine (G7313, SIG), 10 µg/ml blastocidin (15205, SIG) and 1 µg/ml puromycin (540411, Calbiochem, MIL) at 37^{o}C in 10% CO_2. Cells were grown to 90% confluence and passaged every 3-4 days.

2.2.2.11 Generation of the HA-GLUT4 retrovirus

The HA-GLUT4 retrovirus was produced in the Plat E cell line as previously outlined (Shewan, et al., 2003). Cells were transfected with the pBABE HA-

GLUT4 construct using Lipofectamine® 2000 reagent (11668-027, Invitrogen, LTC) following manufacturer instructions. The transfected cells were incubated for 48 hours at 37^{o}C and then transferred to 30^{o}C for a further 24 hours. The supernatant (which contains the retrovirus) was collected and filtered. The virus was aliquoted and immediately frozen at -80^{o}C.

2.2.2.12 Stable expression of HA-GLUT4 in C2C12 muscle cells

C2C12 myoblasts were seeded at 1 x 10^5 per 90 mm dish (TKT-110-070A, Nuclon, FIS) in normal growth media overnight. The next day, cell cultures at ~30% confluence were infected with 25 µl of HA-GLUT4 retrovirus or 200 µl of Empty Vector virus in the presence of 8 µg/ml polybrene (H9268, SIG) for 5 hours at 37^{o}C in 10% CO2. The amount of virus was determined by performing viral titre experiments. The culture media was replenished with normal growth media and the cells were left to recover overnight at 37^{o}C in 10% CO_2. The following day, infected myoblasts were selected for by culturing in normal growth media supplemented with 2 µg/ml puromycin (540411, Calbiochem, MIL) (HA-GLUT4 growth media). A considerable amount of cell death was noted for the HA-GLUT4 cells due to the low viral titre used. The growth media (HA-GLUT4) was replenished every day to remove dead cells from the cultures. The cells were allowed to recover prior to passaging. Once normal growth of the cells resumed, myoblasts were seeded and differentiated into myotubes as described in 2.2.2.8.

2.2.2.13 Phosphorylation of AMPK and Akt

C2C12 myotubes were serum-starved in C2C12 serum free media, DMEM (SIG), 0.2% (w/v) BSA (Probumin COHN 5.2 (T) 3220, CEL) and 2 mM L-glutamine (SIG) overnight at 37^{o}C. The following day, the media was replaced with C2C12 serum free media without bicarbonate (11 mg/ml GIBCO® DMEM (119 00-073, Invitrogen, FIS), 0.2 % (w/v) BSA (CEL) and 20 mM (w/v) HEPES) for two hours before the experiment and were maintained in this throughout incubations. Cells were incubated in a water bath at 37^{o}C. Myotubes were stimulated with insulin (NOV) at 200 nM, AICAR (A9978, SIG) at 2 mM, A769662 (provided by Dr Kei Sakamoto) at 100 µM for indicated times at 37^{o}C.

Protein lysates were prepared as described in 2.2.2.14, or cells were used for GLUT4 translocation experiments as detailed in 2.2.2.16 and 2.2.2.17.

2.2.2.14 Preparation of protein lysates from cultured C2C12 cells

Cells were washed with ice cold PBS, and lysed (15 µl/well) with cell lysis buffer supplemented with protease inhibitors (Halt Protease Inhibitor Cocktail, 78430, Pierce, FIS) and phosphatase inhibitors (Table 2.13). Lysates were pipetted up and down several times and transferred to eppendorf tubes. Samples were briefly sonicated (6 x 1 second at amplitude 10 microns) using a sonicator () and rotated for 1 hour at 4^{o}C. The samples were centrifuged at 14,000 rpm for 20 min at 4^{o}C and the cleared supernatant was transferred to new eppendorf tubes. The protein concentration was determined by BCA protein assay as described in 2.2.3.2. 40 µg of protein lysates were resolved by SDS-PAGE (2.2.3.4) and analysed by western blotting (2.2.3.5).

Table 2.13: List of phosphatase inhibitors.

Phosphatase Inhibitor		**Target**	**Final concentration**
Sodium molybdate	NaM	Acid phosphatases	
Sodium orthovanadate	NaV	Protein tyrosine phosphatases	
Sodium fluoride	NaF	Protein phosphoseryl and phosphothreonyl phosphatases (PSPs)	
Okadaic acid	OA	Protein phosphatase 1 (PP1) and 2A (PP2A)	
Phosphatidic acid	PA	**Protein phosphatase 1 (PP1)**	
Nuclear inhibitor of protein phosphatase 1	Nipp1	Protein phosphatase 1 (PP1)	
Cypermethrin	Cyp	Protein phosphatase 2B (Calcineurin PP2A)	
Dephostatin	Dep	Protein tyrosine phosphatases	

2.2.2.15 siRNA-mediated knock down

C2C12 myotubes at day 2-3 of differentiation were transfected with siRNA oligonucleotides. One day prior to transfection C2C12 differentiation media was replaced with differentiation media minus antibiotics. The following day, the media was replenished prior to transfection. Differentiating C2C12 cells were either transfected with *Tbc1d1*-siRNA, *As160/Tbc1d4*-siRNA or with control non-targeting siRNA (Table 2.7, 2.1.3.2) using DharmaFECT 1® transfection

reagent (T-2001-02, Dharmacon, FIS). Transfections were performed following manufacturer's instructions. Transfection mix preparation for 20 x wells of 96-well micro titre plate detailed in Table 2.14. siRNA oligonucleotides were prepared at 2 µM in PBS (RNase-free and sterile) and diluted to 1 µM in OptiMEM® reduced serum media (31985-062, Invitrogen, FIS), denoted tube 1. In a separate tube, DharmaFECT 1® transfection reagent was prepared in OptiMEM® reduced serum media to the same final volume as tube 1. This was denoted tube 2. The solutions were mixed well and incubated for 5 min at room temperature. The contents of both tubes were combined and incubated for 20 min at room temperature. The mix was diluted with four parts differentiation media minus antibiotics. The final siRNA concentration was 100 nM. The transfection mix was added to the cells (100 µl/96-well) and incubated at 37^{o}C for 24 hours in 10% CO_2. The following day the media was replenished. Cells were used for experiments at day 7 or 8. Protein lysates were prepared as described in 2.2.2.14 and the cells were used for GLUT4 translocation experiments as detailed in 2.2.2.16 and 2.2.2.17

Table 2.14: Preparation of transfection mix for 20x wells of 96-well micro titre plate.

Contents of Tube 1	**Volume (200 µl)**	**Contents of Tube 2**	**Volume (200 µl)**
2 µM siRNA	100 µl	DharmaFECT 1	4 µl
OptiMEM	100 µl	OptiMEM	198 µl

Final Transfection mix	**Volume (2000 µl)**	**Transfection per well**
Tube 1 + Tube 2	400 µl	100 nM siRNA
Culture media (minus antibiotics)	1600 µl	0.4 µl DharmaFECT 1

2.2.2.16 HA-GLUT4 translocation assays; transition experiments

The level of HA-GLUT4 at the plasma membrane in C2C12 myotubes was measured as a percentage of the total expressed HA-GLUT4 described previously (Govers, et al., 2004) (Fazakerely, et al., 2009).

The experiments were conducted using myotubes 6-8 days post differentiation. Myotubes were serum starved overnight and the next day stimulated with agonist as described in 2.2.2.13. After treatment the cells were immediately moved to ice to stop the trafficking. The cells were washed three times in ice-

cold PBS and fixed with 3% paraformaldehyde for 15 min on ice and for a further 30 min at room temperature. The cells were quenched with glycine for 5 min and washed once more with PBS. All residual PBS was removed from cells by dipping. Cells were blocked for 20 min with blocking buffer (those wells used to calculate total cellular HA-GLUT4 were made permeable by blocking with the addition of 0.2 % Saponin). All cells were incubated with primary anti-HA antibody at a 1:500 dilution for 45 min. Cells were washed thoroughly in PBS (3x 5 min) before re-blocking. Cells were incubated with Alexa 488-conjugated goat anti-mouse secondary antibody at 1:100 a dilution for 45 min. Myotubes were once again washed thoroughly in PBS. The fluorescence was measured at the wavelength 485/520 nm using the bottom reading optics on the pheraSTAR micro titre plate reader (BMG).

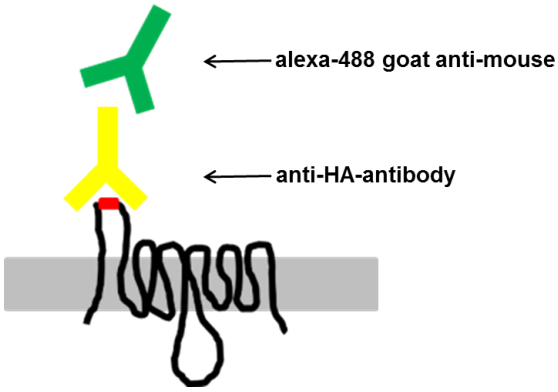

Figure 2.1: Schematic diagram of HA-epitope tagged GLUT4. HA-GLUT4 inserted in to the plasma membrane is detected using anti-HA antibodies and alexa-488 goat anti-mouse. The fluorescence is measured at the wavelength 485/520 nm using the bottom reading optics on the pheraSTAR micro titre plate reader (BMG).

The data (transition from the basal to the stimulated steady-state) can be fitted to a single-exponential function:

$$L(t) = (Y0 - Plateau)e^{-kt} + Plateau$$

The accumulation of GLUT4 at the cell surface over time is denoted by L (t). Y0 is the initial amount of GLUT4 at the plasma membrane in non-stimulated (basal) cells. The amount of GLUT4 at the plasma membrane after long agonist treatment (steady-state level) is the plateau. The rate constant for the transition

from Y0 to the plateau is k. The half time for the transition ($t_{1/2}$) can be determined using $t_{1/2} = \ln 2/k$.

2.2.1.17 Anti-HA antibody uptake assays; GLUT4 recycling experiments

The amount of HA-GLUT4 which recycles with the plasma membrane was measured in basal cells or those stimulated with insulin or AICAR. Myotubes were serum starved overnight and the next day stimulated with agonist as described in 2.2.2.13. After agonist treatment, intact live cells were labelled with a saturating concentration of purified anti-HA antibody (50 µg/ml) for 5 to 300 min at 37^{o}C in the continued presence of agonist. Some cells were kept un-labelled and these were used to measure total cellular HA-GLUT4. After antibody incubations the cells were moved to ice to stop the trafficking and washed thoroughly with PBS. Cells were fixed with 3% paraformaldehyde for 15 min on ice and for a further 30 min at room temperature. Subsequently, cells were quenched with glycine for 5 min and washed once more with PBS. All cells were incubated with blocking buffer (plus saponin) for 20 min. Cells used to calculate total cellular HA-GLUT4 were incubated with anti-HA antibody at a 1:500 dilution for 45 min at room temperature and washed 3 times in PBS. All other pre-labelled cells were maintained in antibody buffer minus antibodies. All cells were incubated with Alexa 488-conjugated goat anti-mouse secondary antibody at a 1:100 dilution for 45 min and again washed thoroughly in PBS. The fluorescence was measured at the wavelength 485/520 nm using the bottom reading optics on the pheraSTAR micro titre plate reader (BMG). HA-GLUT4 labelled with antibody over time was measured in permeabilised cells and calculated as a percentage of the total cellular immuno-reactive GLUT4.

The data (steady-state GLUT4 recycling) can be fitted to a one-phase non-linear regression (single-exponential equation):

$$L(t) = (P - T)e^{-k_{ex}t} + T$$

The accumulation of labelled GLUT4 over time is denoted by L (t). P is the initial plasma membrane level of GLUT4 at Y0. The total amount of the GLUT4 pool which is actively recycling with the plasma membrane is T. The rate constant for

GLUT4 exocytosis at steady-state is k_{ex}. The transition from Y0 to the plateau is k. The half time ($t_{1/2}$) can be determined using $t_{1/2} = \ln 2/k$.

2.2.3 Biochemical Methods

2.2.3.1 Preparation of total protein lysates from mouse tissues

Adult male mice (g) were used for the isolation of tissue samples. Mice were sacrificed by cervical dislocation. Tissues were immediately dissected, wrapped into aluminium foil and snap frozen in liquid nitrogen. The heart was washed in ice-cold PBS prior to freezing to reduce blood from the cleared lysate. Four different skeletal muscles were dissected based on fibre type composition tibialis anterior (TA), extensor digitorum longus (EDL), gastrocnemius (GN) and soleus (SOL) muscles. The anatomical localisation of mouse hind limb muscles are depicted (Figure 2.2). All tissues were stored at -80^{o}C until required.

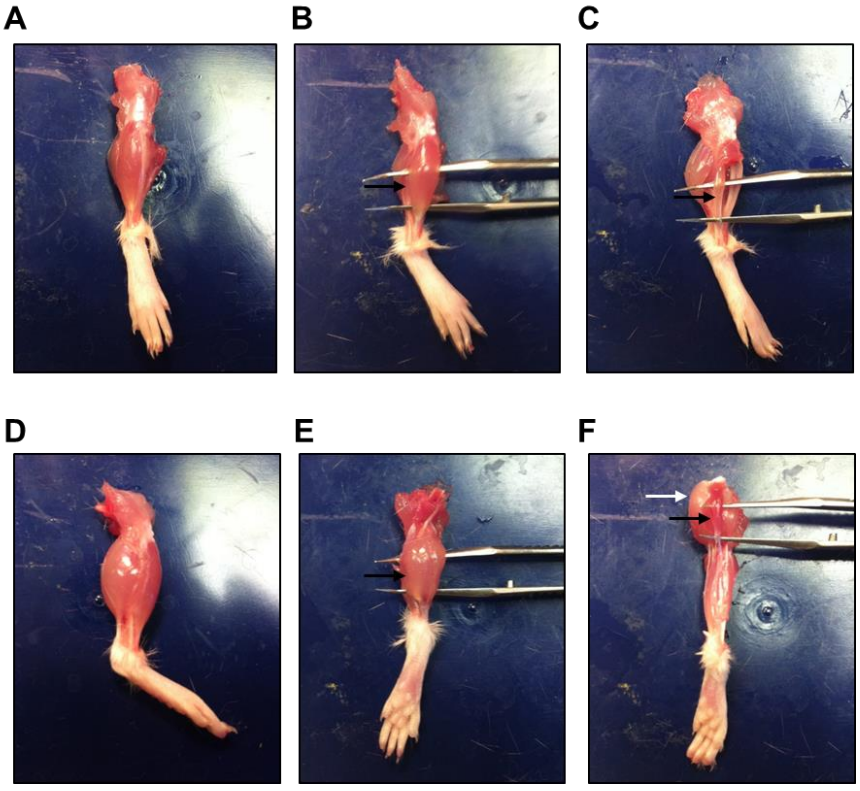

Figure 2.2: Gross anatomical presentation of mouse hind limb muscles after removal of the skin. (A) Anterior view of intact hind limb. (B) Anterior/lateral view, (*black arrow* indicates the Tibialis Anterior (TA) muscle). (C) Anterior/lateral view, (*black arrow* indicates the Extensor Digitorum Longus (EDL) muscle. (D) Medial view. (E) Posterior view, (*black arrow* indicates the calf muscle (Gastrocnemius (GN) and Soleus). (F) Excision of the calf muscle at the calcaneal tendon, (*black arrow* indicates the Soleus muscle; *white arrow* indicates the GN muscle. Images were obtained using digital camera.

Mouse tissues were removed from -80^{o}C and immediately transferred into a glass potter containing ice-cold cell lysis buffer (Table 2.15) and kept on ice. Tissues were quickly homogenised (3 x 10 strokes) using a bench top homogeniser. Tissue homogenates were transferred to eppendorf tubes and further lysed for 30 min on ice. Samples were centrifuged at 13,000 rpm for 20 min at 4^{o}C and cleared supernatants were transferred in to new eppendorf tubes. The protein concentration was determined by BCA protein assay as described in 2.2.3.2. 40 µg of protein lysates were resolved by SDS-Page (2.2.3.4) and analysed by western blotting (2.2.3.5).

Tibialis Anterior muscle from recombinant congenic strain (RCS) B6.SJL-Nob1.10 and transgenic strain FVB/N Tg (MCK-Tbc1d1) were used in order to validate the specificity of our TBC1D1 antibodies. These tissues were provided by Professor Hadi Al-Hasani (Deutsches Diabetes Zentrum (DDZ), Duesseldorf, Germany) (Chadt, et al., 2008).

Table 2.15: Preparation of mouse tissue lysates.

Mouse tissue	
Heart	1 x heart per ml
Brain	1 x brain per ml
Epididymal Fat	1 x fat pad per ml
Tibialis anterior (TA)	1 x muscle per ml
Gastrocnemius (GN)	1/2 muscle per ml
Extensor digitorum longus (EDL)	2 x muscles per ml
Soleus (SOL)	2 x muscle per ml

2.2.3.2 Determining protein concentration

The concentration of total protein within cell or tissue lysate was determined by the BCA (BiCinchoninic Acid) colorimetric protein assay. BCA reagent A (23277, Pierce, FIS) was mixed with BCA reagent B (50:1) following manufacturer instructions. 2 mg/ml Bovine Serum Albumin (BSA) (A9418, SIG) was used for the generation of a protein standard curve. Samples and standards were read in duplicate. The BCA assay was measured at wavelength 565nm.

2.2.3.3 Determining protein concentration using coomassie Blue Staining SDS-PAGE gels

2 mg/ml Bovine Serum Albumin (A9418, SIG) was used for the generation of a standard curve. Protein standard samples and a volume of purified protein were processed using SDS-PAGE as described in 2.2.3.4. After electrophoresis, the SDS-PAGE gel was rinsed once with ddH_2O and stained with coomassie dye (1610436, BIO) at room temperature for 2-24 hours. The coomassie stain was removed and the gel was de-stained in ddH_2O. The protein bands were visualised using a trans-illuminator (UVP) and documented (camera). A standard curve was plotted and the sample protein concentration was estimated.

2.2.3.4 SDS-Polyacrylamide gel electrophoresis SDS-PAGE

Samples were analysed using the standard method of Laemmli Tris-Glycine Sodium Dodecyl Sulphate-Polyacrylamide Gel Electrophoresis (SDS-PAGE) discontinuous buffer system (Laemmli, 1970).1.5 mm thick SDS-PAGE gels were prepared using the Mini protean II system apparatus (BIO) or the Mini vertical apparatus (CBS). Gels were composed of acrylamide/bis acrylamide (30% (w/v) acrylamide) with resolving or stacking gel buffers. The percentage of acrylamide used was determined for each experiment based on the protein of interest. Gel polymerisation was initiated by the addition of % (v/v) N,N,N,N'-tetramethylethylenediamine (TEMED) (T9281, SIG) and 10% (w/v) ammonia persulphate (APS) (AP470, FIS). An appropriate amount of protein lysate was solubilised in 3X sample buffer. The total sample volume was adjusted with 1X sample buffer. Dithiothreitol (DTT) (BP172-5, FIS) was added to the sample at a final concentration of 100 mM (w/v). Samples were vortexed and heated for 5 min at 95^{o}C. Samples were centrifuged at 13,000 rpm for 5 min and loaded onto the SDS-PAGE gels. These were run in electrophoresis buffer at 200 Volts for approximately 1 hour. The molecular weight of the proteins within samples was determined using Novex® Sharp pre-stained protein standards (LC5800, Invitrogen, FIS).

2.2.3.5 Western Blotting

Gels were transferred to nitrocellulose using the Trans-Blot® SD Semi-dry Electrophoretic Transfer Cell Apparatus (170-3940, BIO). Gels were removed from the tanks and immediately placed in transfer buffer. Extra-thick blot absorbent filter paper (170-36-69, BIO) and nitrocellulose membrane (P/N 66485, PAL, VWR) were pre-cut to the dimensions of the gel and allowed to soak in transfer buffer for 20 min. One piece of nitrocellulose membrane followed by the gel, were sandwiched between sheets of buffer soaked blot paper and assembled on to the platinum anode. Air bubbles were removed to ensure contact between the layers for a decent transfer. Any excess buffer was minimised from around the transfer assembly. Finally, the cathode was fitted on top of the stack and secured in place with a lid. The transfer was run at constant milliamps (mA) (which was calculated by the area of gel (cm^2) X 0.8) for 1 hour 50 min or for 2 hours 30 min (when studying large proteins of >150 kDa). After the transfer was complete, the nitrocellulose was removed, briefly washed in ddH_2O and stained with ponceau S stain. Excess ponceau stain was removed by washing with ddH_2O. The molecular weight standards were clearly marked on with pencil. The membrane was either processed immediately of left to air dry.

2.2.3.6 Immuno-blotting and Detection

The nitrocellulose membrane was briefly washed in tris buffered saline containing tween-20 (TBS-T) to remove ponceau S stain. Subsequently, membranes were blocked by submerging in TBST containing 5% (w/v) Marvel milk powder or 5% (v/v) BSA (CEL) (when studying phosphorylated proteins) before appropriate primary antibody incubation (Table 2.3, 2.1.2). Primary antibodies were incubated overnight at 4^oC with continual rocking. Membranes were washed 6 times (over the course of one hour) in TBST. The relevant secondary antibodies coupled to Horse Radish Peroxidase (HRP) were prepared at a 1:4000 dilution in TBST containing 5% Marvel milk powder (Table 2.4, 2.1.2). Membranes were incubated with secondary antibodies at room temperature for 1 hour and then further washed thoroughly 6 times (over the course of one hour) in TBST. Bound secondary antibody conjugated to HRP was detected using enhanced chemi-luminescence reagent (ECL) which utilises

peroxidise catalysed luminal detection method. A working solution of ECL was prepared by mixing equal volumes of ECL A and ECL B. Membranes were incubated at room temperature for 1 minute. Subsequently, membranes were placed between acetate sheets and chemi-luminescence was detected at wavelength using a Hamamatsu camera attached on an EpiChemi II Imager (UVP) for between 1-5 minutes. If more sensitive detection was required the membranes were washed and incubated with Super Signal Dura (34076, Pierce, FIS) or Advance ECL (Amersham, GE) for 5 minutes and imaged as before.

3 Characterising TBC1D1 antibodies and investigating the expression of TBC1D1 and TBC1D4 in muscle

3.1 Introduction

The Rab-GAP proteins TBC1D1 and TBC1D4 have been identified as potential downstream signalling intermediates which regulate GLUT4 translocation (Roach, et al., 2007). They are proposed to function as negative regulators of GLUT4 trafficking through maintaining an un-specified rab protein in its in-active GDP-bound state. Several studies have demonstrated that TBC1D4 and TBC1D1 are phosphorylated in response to insulin and contraction stimulation in skeletal muscle (Kramer, et al., 2006) (Bruss, et al., 2005) (Funai & Cartee, 2008) (Funai & Cartee, 2009) (Vichaiwong, et al., 2010) (Pehmoller, et al., 2009).

TBC1D4 and TBC1D1 contain multiple Akt phosphorylation motifs. To date, several AMPK phosphorylation sites have been identified in TBC1D1. The most well studied site is the consensus AMPK-phosphorylation motif surrounding serine 231 on mouse TBC1D1 (Peck, et al., 2009) (Taylor, et al., 2008) (Chen, et al., 2008) (Roach, et al., 2007). Studies on TBC1D1 function have led to its emergence as a potential signalling protein in regulating GLUT4 trafficking in response to contraction and/or AMPK activation (Chavez, et al., 2008)

At the time this project commenced there were no commercial antibodies available against TBC1D1 protein or TBC1D1 phosphorylated at serine 237, so specific anti-serum was generated against rat TBC1D1 (AGG Astra Zeneca, Macclesfield, UK). The development of TBC1D1 phospho-specific antibodies is important as these are key tools for studying phosphorylation events and can be used to track the activity of the protein.

The objectives of this chapter were to analyse the specificity of the TBC1D1 antibodies for recombinant and endogenous TBC1D1 proteins using western blotting. Furthermore, in order to study the importance of TBC1D1 and TBC1D4 proteins in muscle, we have investigated the relationship between muscle fibre-

type and TBC1D1/TBC1D4 expression. Lastly, to analyse the usefulness of the C2C12 skeletal muscle cell line as a model

3.2 Characterisation of TBC1D1 specific antibodies

3.2.1 Development of TBC1D1 specific antibodies

Three different peptides of rat TBC1D1 were used to generate TBC1D1-specific antibodies (Table 2.5, 2.1.2.2) (Figure 3.1). Three or four rabbits were injected with each peptide and affinity purified anti-serum from terminal bleeds were analysed for specificity against TBC1D1 using western blotting. While this study was in progress, another group had developed their own TBC1D1 specific antibody in order to functionally characterise TBC1D1 in glucose and fatty acid metabolism, this was published in 2008 (Chadt, et al., 2008). This affinity-purified polyclonal antiserum was raised towards an N-terminal peptide of mouse TBC1D1, TBC1D1 H-AH (Figure 3.1). More recently commercial antibodies have become available, we have tested TBC1D1 #4629 (Cell Signalling Technologies) (Figure 3.1).

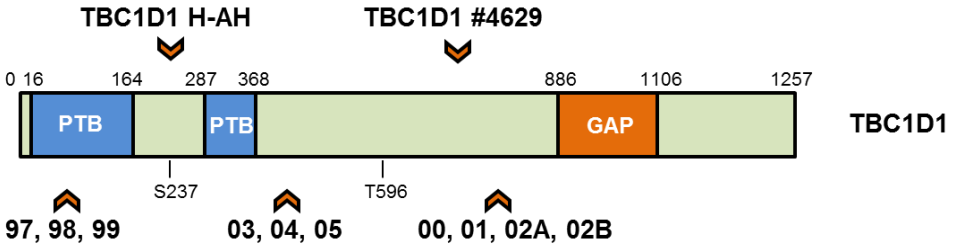

Figure: 3.1: Location of antibody recognition epitopes in rat TBC1D1. 10 purified polyclonal antisera were raised against three epitopes of rat TBC1D1. Epitope ID AZ 3001724 produced antibodies 97, 98 and 99, epitope ID AZ 3001725 for antibodies 00, 01, 02A, 02B and epitope ID AZ 3001726 generated antibodies 03, 04 and 05. N-Terminal epitope polyclonal anti - TBC1D1 H-AH (Prof. Hadi Al-Hasani) was raised towards Try-Gly-Gln-Pro-Ser-A-Pro-Gly-Pro- Arg- Pro-Met-Arg-Lys-SerTGQPSAPGPRPMRKS-CONH2 of mouse TBC1D1. Commercial cell signalling anti-TBC1D1 #4629 was raised toward a peptide sequence around Val 796 of mouse TBC1D1.

A phospho-peptide matching the sequence around serine 237 was used to generate antibodies which would specifically recognise phosphorylated TBC1D1 (Table 2.5, 2.1.2.2). Terminal bleeds were purified using a non-phosphorylated peptide column and examined for specificity in western blots.

3.2.2 TBC1D1 antibodies specifically recognise recombinant TBC1D1 protein over TBC1D4

An initial characterisation screen was performed to examine antibody specificity for recombinant full-length FLAG-tagged TBC1D1 expressed in HEK cells. Preference for TBC1D1 over TBC1D4 was also compared. All 10 generated antibodies were tested using western blotting (Figure 3.2). FLAG-tagged TBC1D1 and TBC1D4 proteins were both detected at approximately 160 kDa by blotting with anti-FLAG antibody. The expression of FLAG-tagged TBC1D1 was higher than that of TBC1D4; however, it was still possible to determine specific immune reactivity against TBC1D1 over TBC1D4.

Antibodies 03, 04, 05 and 00, 01, 02A and 02B specifically recognise FLAG-tagged TBC1D1 over TBC1D4. In particular antibodies 04, 05 and 00 strongly recognise TBC1D1 and display minimal non-specific immune reactivity with other proteins within the HEK cell lysate. 01, 02A and 02B, even though they show preferential recognition of TBC1D1 over TBC1D4, they also recognise multiple non-specific bands throughout the HEK cell lysate. In contrast, antibodies 97, 98 and 99 which are generated against an N-terminal peptide of the protein show little specificity for TBC1D1 and strongly recognise numerous other bands within the HEK cells lysate.

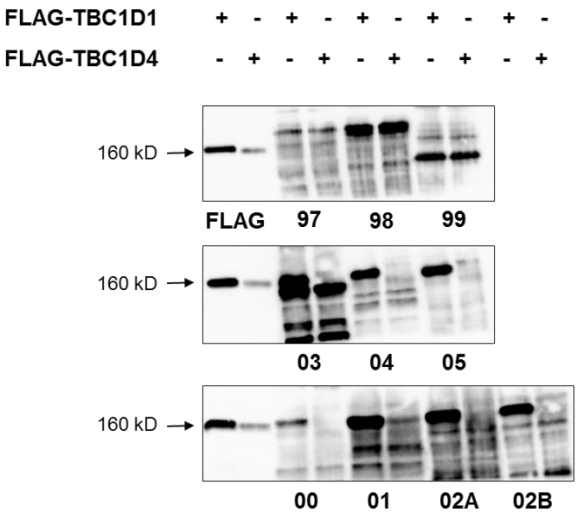

Figure 3.2: Selectivity of TBC1D1 antibody for recombinant TBC1D1. 10antibodies generated against three different peptides were screened against recombinant FLAG-tagged TBC1D1 and FLAG-tagged TBC1D4 expressed in HEK 293 cells. Astra Zeneca polyclonal affinity purified antibodies generated against three peptides of rat TBC1D1. Antibodies 97, 98 and 99 were raised against Glu-Pro-Asp-Leu-Arg-Lys-Ser-Gln-Pro-Trp, ID AZ 3001724. Antibodies 00, 01, 02A, 02B were raised towards Asp-Ser-Pro-Ser-Arg-Tyr-Glu-Asp-Tyr-Ser-Glu, ID AZ 3001725 and antibodies 03, 04 and 05 were raised against Gln-Lys-Leu-Arg-Pro-Arg-Asn-Glu-Gln-Arg-Glu-Asn, ID AZ 3001726. Protein load: 50 µg.

3.2.3 Specificity of TBC1D1 antibodies in muscle

We further characterised the specificity of the TBC1D1 antibodies by western blotting of fast-twitch tibialis anterior (TA) muscle lysates generated from four different mouse strains (Hadi Al-Hasani, German Institute Human Nutrition, Potsdam-Rahbreuche). The recombinant congenic mouse strain (RCS) B6.SJL-Nob1.10 represents a knock-out model for TBC1D1. TBC1D1 was found to be down regulated in skeletal muscle of the Nob1$^{SJL/SJL}$ mouse strain. This was the result of a 7bp deletion in exon 18 which resulted in a frame shift mutation and premature termination of the protein (Chadt, et al., 2008). The transgenic mouse strain, FVB/N-Tg (MCK-*Tbc1d1*), selectively over-express FLAG-*Tbc1d1* in skeletal muscle and heart. Frozen TA muscle from RCS B6.SJL-Nob1.10, wild-type (B6/B6) and mutant (SJL/SJL) and FVB/N-Tg (MCK-*Tbc1d1*) wild-type (Wt) and transgenic (Tg) were directly homogenised and lysates were resolved by SDS-PAGE. 9 antibodies were directly compared with an already characterised polyclonal antibody raised towards an N-terminal peptide of mouse TBC1D1, TBC1D1 H-AH (Hadi Al-Hasani) using western blot techniques (Figure 3.3). Purified antibody TBC1D1 H-AH is specific for TBC1D1 protein as

it recognised two distinct protein bands within B6/B6, Wt and Tg muscle samples at approximately 150 kDa and 160 kDa. The slightly reduced electrophoretic mobility of the 160 kDa band detected in the Tg muscle sample is due to the presence of over-expressed 3XFLAG-TBC1D1. As expected, TBC1D1 protein was not detected in muscle lysate from SJL mice. TBC1D1 was also detected in C2C12 myotube cell lysate but was not detected in TA or cardiomyocyte rat muscle lysates.

Similar western blot profiles were observed with antibodies 00, 01 and 02A, which recognised a distinct full-length TBC1D1 protein band at approximately 160 kDa which was absent from muscle lysate of SJL mice and rat muscle lysates. In addition, western blotting with antibody 02A led to the detection of a band at 150 kDa. Antibodies 97, 98 and 99 show no specificity for endogenous mouse TBC1D1 protein this further confirmed the lack of specificity of these antibodies.

Interestingly, antibodies 04 and 05 which strongly recognised FLAG-tagged rat TBC1D1 detected a distinct but faint protein band of 160 kDa in Tg muscle lysate but did not specifically recognise the endogenous TBC1D1 protein in B6/B6 or Wt mouse muscle lysates. However, antibody 04 faintly detected a band at approximately 160 kDa, which is absent from SJL mice. Intriguingly, antibody 04 strongly identified a protein band of 150 kDa in differentiated C2C12 cells and rat muscle lysates. This was the approximate molecular weight of the smaller TBC1D1 protein band detected in mouse muscle lysates with TBC1D1 02A and H-AH antibodies. An amino acid sequence alignment between rat and mouse TBC1D1 was performed. As detailed in Table 2.5 (2.1.2.2), there were no sequence differences between the two rodents within the antibody recognition epitopes. This cannot therefore explain the different protein band pattern detected by immuno-blotting with TBC1D1 04. The antibody TBC1D1 02A (AZ 3001725) that was generated (AGG, Astrazeneca, Macclesfield, UK), specifically recognises TBC1D1. It was therefore selected and used in all further experiments.

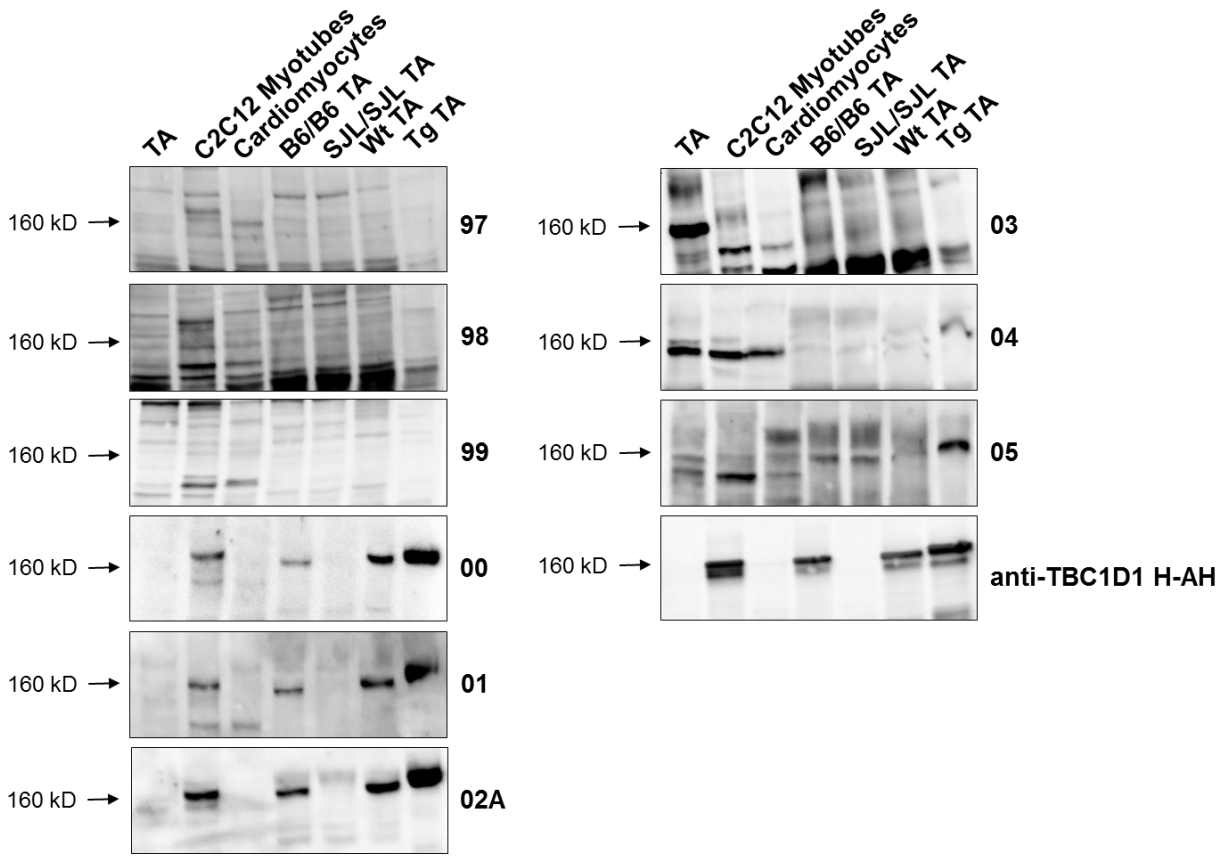

Figure 3.3: Screening of TBC1D1 antibodies using lysates from tibalis anterior (TA) muscle from different mouse strains. C2C12 myotubes, cardiomyocyte and TA muscle from rat. Nine polyclonal TBC1D1 antibodies generated against three peptides of rat TBC1D1. Antibodies 97, 98 and 99, ID AZ 3001724, Antibodies 00, 01, 02A, ID AZ 3001725 and antibodies 03, 04 and 05 ID AZ 3001726 were screened against TA muscle from recombinant congenic mouse B6.SJL-Nob1.10, and muscle specific transgenic mouse FVB/N-Tg(MCK-*Tbc1d1*). Astra Zeneca generated antibodies were directly compared with a polyclonal anti -TBC1D1 H-AH antibody raised towards Try-Gly-Gln-Pro-Ser-A-Pro-Gly-Pro-Arg-Pro-Met-Arg-Lys-Ser-TGQPSAPGPRPMRKS-CONH2 of mouse TBC1D1. Protein load: 30 µg.

3.2.4 Characterising the specificity of TBC1D1 antibody 02A in insulin-responsive cells

The TBC1D1 antibody 02A was further tested for specificity by western blotting cell lysates prepared from a selection of insulin-responsive cell models. These included L6 myotubes, C2C12 myotubes, HL1 cells, 3T3 adipocytes and flexor digitus brevis (FDB) muscle cells. The results shown in Figure 3.4 are representative western blots derived from different experiments.

As shown in Figure 3.4A, blotting with antibody 02A led to the detection of a distinct protein band which migrated at approximately 140 kDa in L6 myotubes. It is apparent that the protein band detected in L6 myotubes does not correspond to the protein bands at 150 kDa and 160 kDa in C2C12 myotubes (Figure 3A).

HL1 cells are a clonal cell line derived from AT-1 mouse atrial cardiomyocyte tumour cells. HL1 cells retain a differentiated adult cardiomyocyte phenotype when cultures are grown to confluence (Claycomb, et al., 1998). Cell lysates were prepared from both confluent (HL1 Heart cells CC) and sub-confluent (HL1 Heart cells) cultures and immuno-blotted with TBC1D1 antibody 02A (Figure 3.4B). Two proteins bands are detected in both HL1 heart cell lysates. These bands migrate at the expected molecular weights of 150 kDa and 160 kDa. Interestingly, in cells maintained at high confluence, the higher molecular weight protein was more abundant than the lower molecular weight protein. In comparison, this was not the case for HL1 cells grown to sub-confluence. In sub confluent cultures the smaller TBC1D1 protein band was most abundant (Figure 3.4B).

In addition, western blotting with antibody 02A led to the detection of a faint protein at approximately 150 kDa in differentiated 3T3-L1 adipocytes (Figure 3.4B). Furthermore, as shown in Figure 3.4C, a single TBC1D1 protein band at 160 kDa is detected in rat FDB muscle cells.

It is important to note that blotting with antibody 02A led to the detection of a protein band at ~260 kDa in HL1 cell lysates and 3T3-L1 adipocytes. Based on the known molecular weight of TBC1D1 it is likely that this protein band is non-specific, despite this protein band being the most intense within these cell types.

.

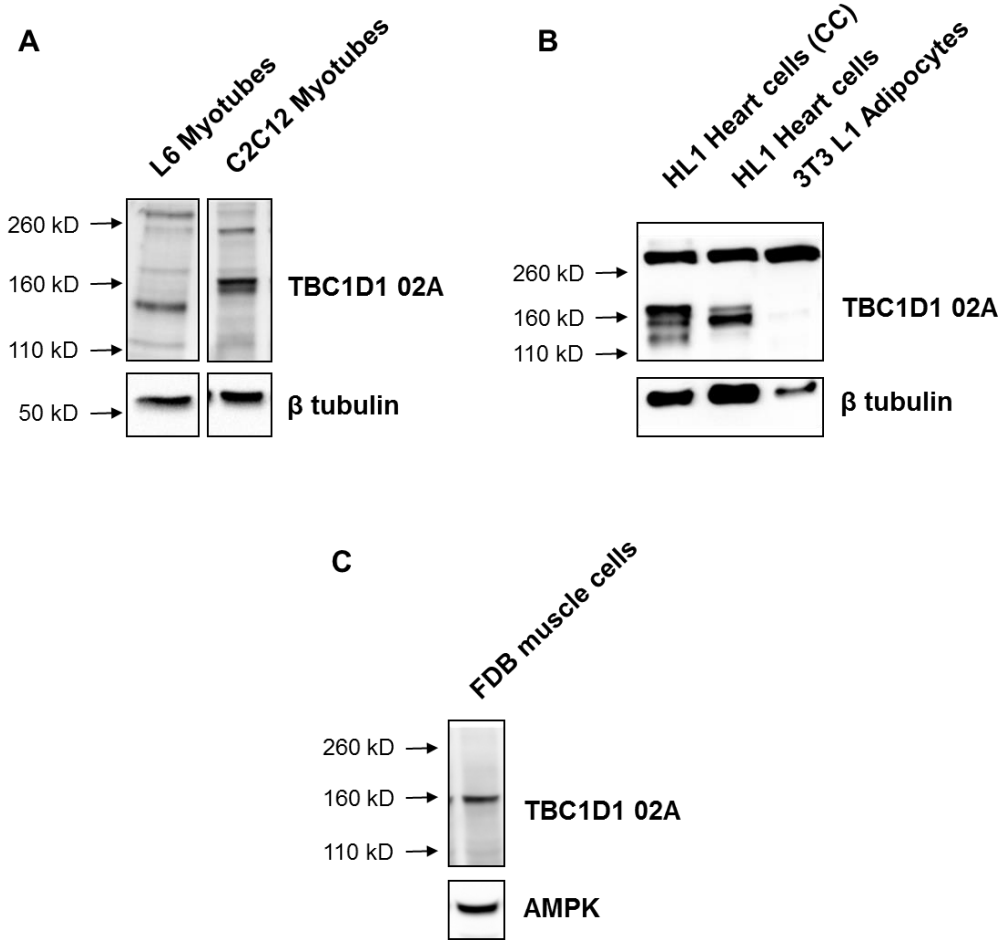

Figure 3.4: Western blot analysis of TBC1D1 across a selection of insulin-responsive cells derived from rodent using total TBC1D1-specific antibody 02A. (A) Protein lysates from transformed cell lines L6 rat myotubes load: 15 µg, Day 7 C2C12 mouse myotubes load: 25 µg - loading control: anti-β tubulin. (B) HL1 mouse heart cells (CC-Batch of cells direct from Claycomb) and 3T3-L1 mouse adipocytes load 20 µg - loading control: anti-β tubulin. (C) Flexor digitus brevis (FDB) muscle cells from rat load: 50 µg - loading control: anti-AMPK. (A-C) All cell lysates were immuno-blotted with anti-TBC1D1 02A. The western blots are derived from different experiments.

3.2.5 Phospho-specific TBC1D1 antibody recognises TBC1D1 phosphorylated at serine 231

Three antibodies were generated against TBC1D1 phosphorylated at serine 237. Terminal bleeds of different rabbits injected with a phospho-peptide the sequence is detailed in Table 2.5 (2.1.2.2). These antibodies have been shown to display specificity by western blotting towards an *in vitro* phosphorylated recombinant TBC1D1 N-terminal construct containing the two PTB domains of the protein (Fazakerely, 2010). Following on from this the specificity of phospho-TBC1D1 91p antibody for endogenous phosphorylated TBC1D1 was assessed in the C2C12 skeletal muscle cell model. These cells were subjected to AMPK activation (Figure 3.5). Stimulation of C2C12 myotubes with AMPK activators AICAR or oligomycin resulted in a marked increased phosphorylation of TBC1D1 at serine 231. Western blotting with phospho-TBC1D1 91p antibody led to the detection of two distinct protein bands of TBC1D1 at approximately 150 and 160 kDa. AMPK activation was assessed by confirming AMPK phosphorylation at threonine 172 and ACC phosphorylation at serine 79 by western blotting.

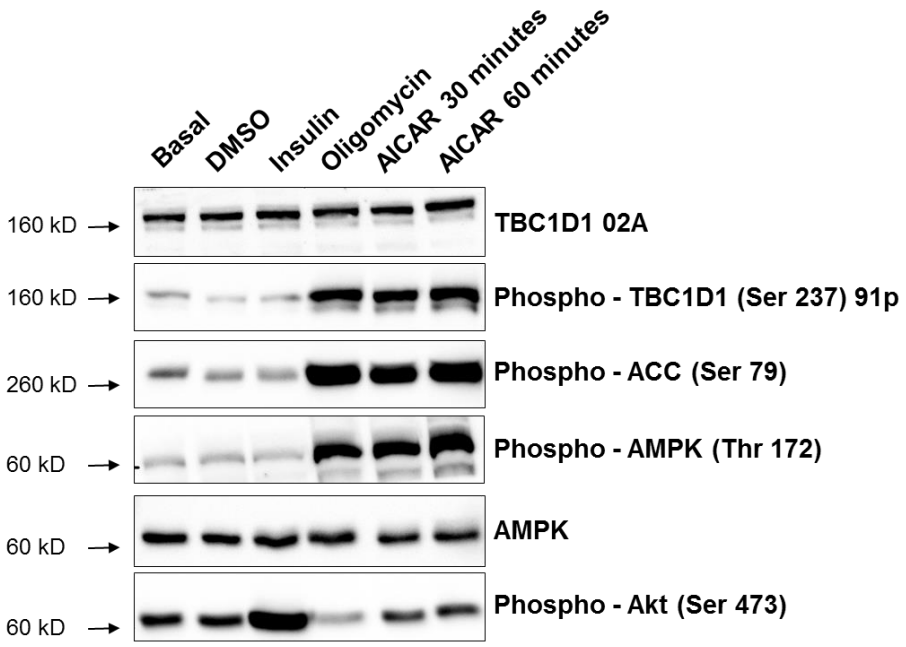

Figure 3.5: Antibody recognition of phosphorylated TBC1D1 by phospho-TBC1D1 (serine 237) 91p antibody in lysates following AMPK activation in C2C12 cells. C2C12 myotubes were maintained under basal conditions or stimulated with AMPK activators Oligomycin at 5 mg/ml for 60 min, 2 mM AICAR for indicated times or Insulin at 200 nM for 5 min. AMPK activation was assessed by immuno-blotting for anti-phospho-AMPK (threonine 172), and down-stream signalling proteins anti-phospho-ACC (serine 79) and anti-phospho-TBC1D1 (serine 237) 91p. AKT activation by insulin stimulation was confirmed by blotting with anti-phospho-AKT (serine 473). Cell lysates were immuno-blotted with anti-TBC1D1 02A, anti-AMPK. AMPK was used as a loading control. Protein load: 30 µg.

3.3 Tissue-specific expression pattern of TBC1D1 and TBC1D4

3.3.1 Relative *Tbc1d1* and *Tbc1d4* mRNA expression by quantitative real-time PCR

In order to characterise the importance of Rab-GAPs TBC1D1 and TBC1D4, the pattern of gene expression across a panel of tissues was determined by Taqman® quantitative real-time PCR. *Tbc1d1* and *Tbc1d4* gene expression profiles were generated for rat, mouse and human tissues. Absolute quantification was not performed; therefore only the relative expression levels between the tissues for each gene could be determined separately. All Taqman® probes used are detailed in Table 2.8 (2.1.3.3). Relative gene expression levels were normalised against a calculated genomic mean of three reference genes (Vandesompele, et al., 2002). The ΔC_t method was implemented to express normalised relative expression levels. C_t values relate to the real-time PCR signal and determine the amount of a target that is present in the sample. PCR efficiency was evaluated by performing template dilution series experiments for all Taqman® expression assays.

3.3.1.1 *TBC1D1* and *TBC1D4* expression in human tissues

A broad-coverage panel of 26 human tissue cDNAs was purchased from Clontech. Pre-designed gene expression assay kits were purchased from Applied Biosystems and were used to amplify *TBC1D1* and *TBC1D4* by two-step real-time qPCR. The relative gene expression levels for each tissue were calculated by normalising data to three independent reference genes, cyclophilin A (*CypA*), β2 microglobulin (*B2m*) and beta-glucuronidase (*Gusβ*). The expression profile for human *TBC1D1* is depicted in Figure 3.6 (top panel) and human *TBC1D4* Figure 3.6 (bottom panel). *TBC1D4* was most highly expressed in skeletal muscle, with distinguishable levels detected in the heart and brain. The expression of *TBC1D1* was significantly pronounced in muscular tissues, including, skeletal muscle, heart, uterus and colon. The data revealed that both genes were ubiquitously expressed in most of the other tissues analysed, however, *TBC1D4* expression was primarily within insulin-responsive tissues. The identification of the skeletal muscle is not known.

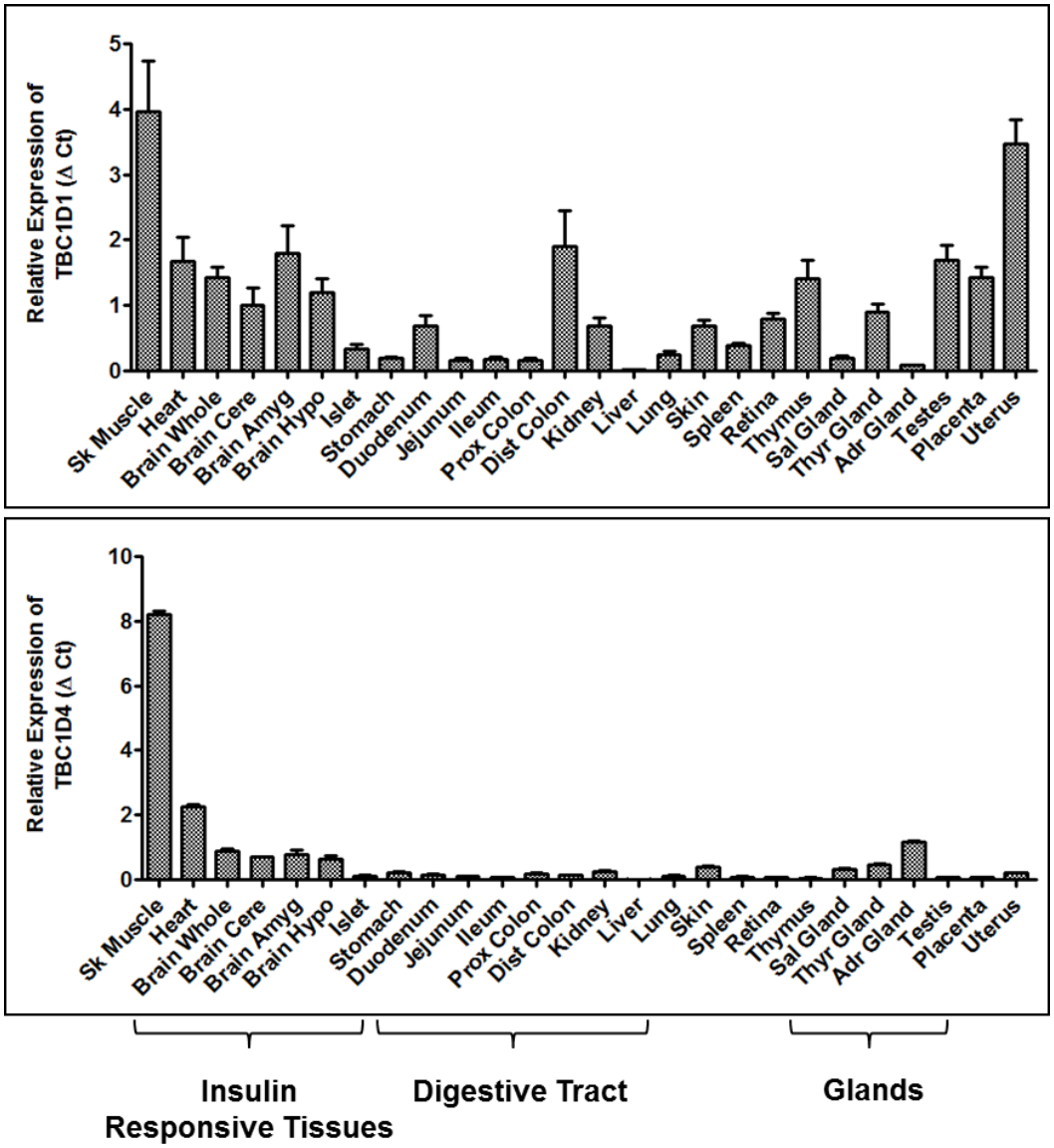

Figure 3.6: Relative *TBC1D1* and *TBC1D4* mRNA expression across a panel of human tissues-using real-time quantitative PCR. A selection of human tissue cDNAs were purchased from Clontech. *TBC1D1* and *TBC1D4* cDNAs were amplified by two-step Taqman® real-time PCR using gene expression kits purchased from Applied Biosystems. Relative expression was calculated using the delta ΔC_t method by normalising the data to three reference genes by geometric averaging of three internal control genes *GUS B, B2M, CYPA.* Top panel: The expression of *TBC1D1.* Bottom panel: the expression of *TBC1D4.*

3.3.1.2 *Tbc1d1* and *Tbc1d4* gene expression in mouse and rat tissues

A gene expression analysis of mouse tissues was performed. 31 separate tissue cDNAs were analysed for the expression of *Tbc1d1* and *Tbc1d4* (these were kindly pre-made by Alison Davies, CVGI group, Astra Zeneca, Macclesfield, UK) using two-step real-time PCR. Relative gene expression

levels were normalised against a calculated genomic mean of three reference genes, hypoxanthine phosphoribosyltransferase (*Hprt*), TATA-binding protein (*Tbp*) and beta-glucuronidase (*Gusβ*). The expression profiles for mouse *Tbc1d1* and *Tbc1d4* are displayed in Figure 3.7A. As shown in Figure 3.7A (top panel), *Tbc1d1* was prominently expressed in the testes, muscle and brown adipose tissue (BAT). Notable expression of *Tbc1d1* was found in many of the tissues analysed, in particular tissues within the gastro-intestinal tract. The expression of *Tbc1d4* was most highly expressed in BAT, skeletal muscle and heart (Figure 3.7A, bottom panel). Interestingly, the expression of *Tbc1d4* in skeletal muscle was approximately three to four-fold greater than that expressed in mature epididymal adipose tissue (Epi mature fat). The type of the mouse skeletal muscle and muscle is not known.

At the time this project commenced, the relative expression of *Tbc1d1* and *Tbc1d4* mRNA within different muscles had not been determined. Therefore, the expression of *Tbc1d1* and *Tbc1d4* was determined in five rat skeletal muscles which were chosen due to their fibre-type composition. tibialis anterior (TA) and extensor digitorum longus (EDL) and gastrocnemius (GN) are fast-twitch oxidative/glycolytic muscles which contain type IIA/IIX/IIB fibres. Flexor digitus brevis (FDB) is a fast-twitch oxidative muscle which contains 90% type IIA fibres. The soleus is a slow-twitch oxidative skeletal muscle which expresses ~90% type I fibres (Bloemberg & Quadrilatero, 2012). Total RNA was isolated from a panel of 26 rat tissues including the five different skeletal muscles. *Tbc1d1* and *Tbc1d4* mRNA expression levels within these tissues were analysed using Taqman® one-step quantitect probe real-time qPCR. The relative gene expression levels were calculated for each tissue by normalising the data to three reference genes hypoxanthine phosphoribosyltransferase (*Hprt*), β2 microglobulin (*B2m*) and beta glucuronidase (*Gus β*). The expression results for *Tbc1d1* and *Tbc1d4* are presented in Figure 3.7B. *Tbc1d1* shows the highest level of expression in skeletal muscle. The expression of *Tbc1d1* in FDB muscle was approximately 2-fold higher than that detected in TA, EDL, GN or soleus muscles (Figure 3.7B top panel). In contrast, *Tbc1d4* was most highly expressed in the TA, EDL and GN muscles (Figure 3.7B bottom panel). The expression of *Tbc1d4* in these muscles was greater than that expressed in the

soleus or FDB muscles. The data revealed that both genes were ubiquitously expressed in most of the other tissues analysed.

A

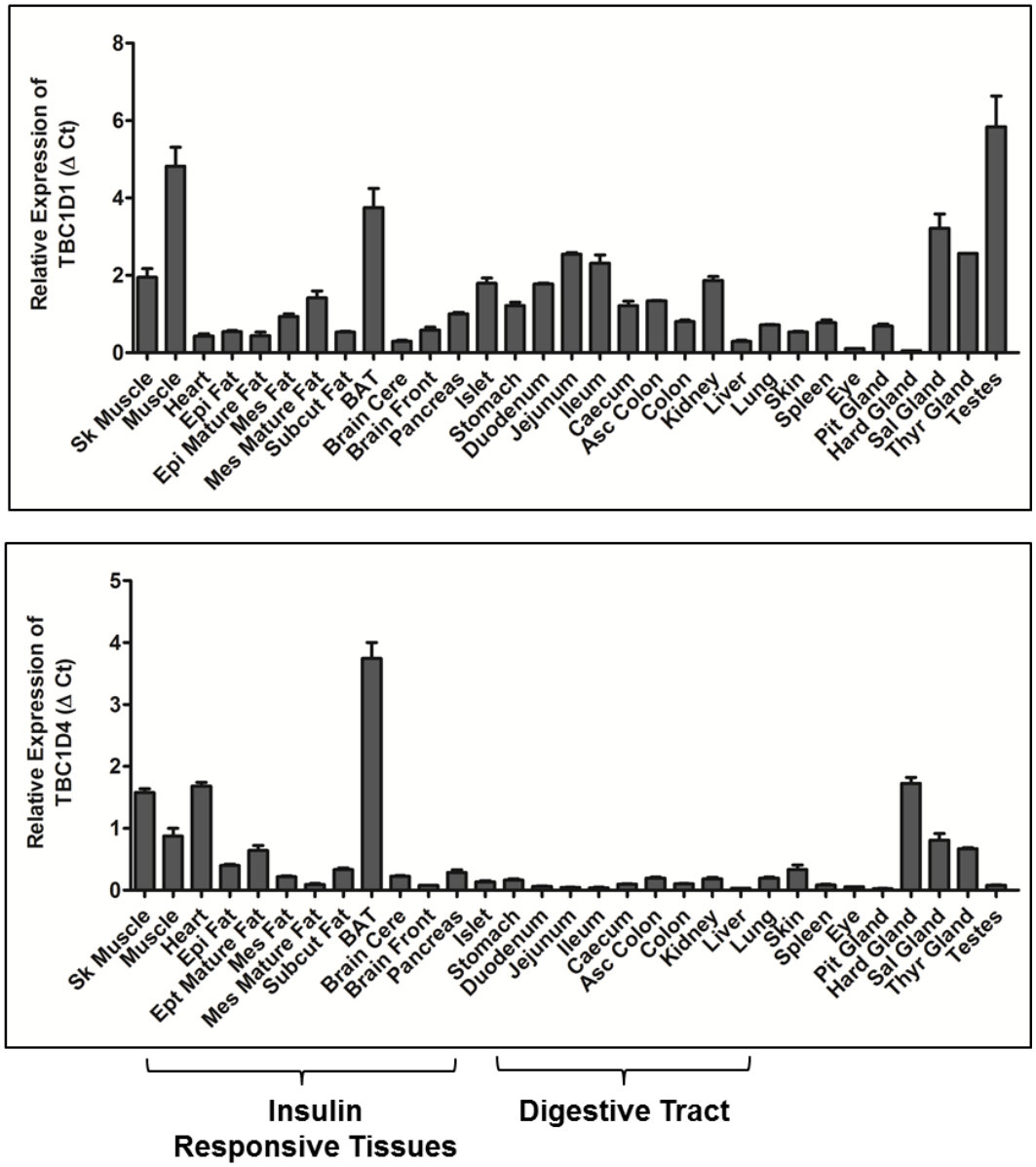

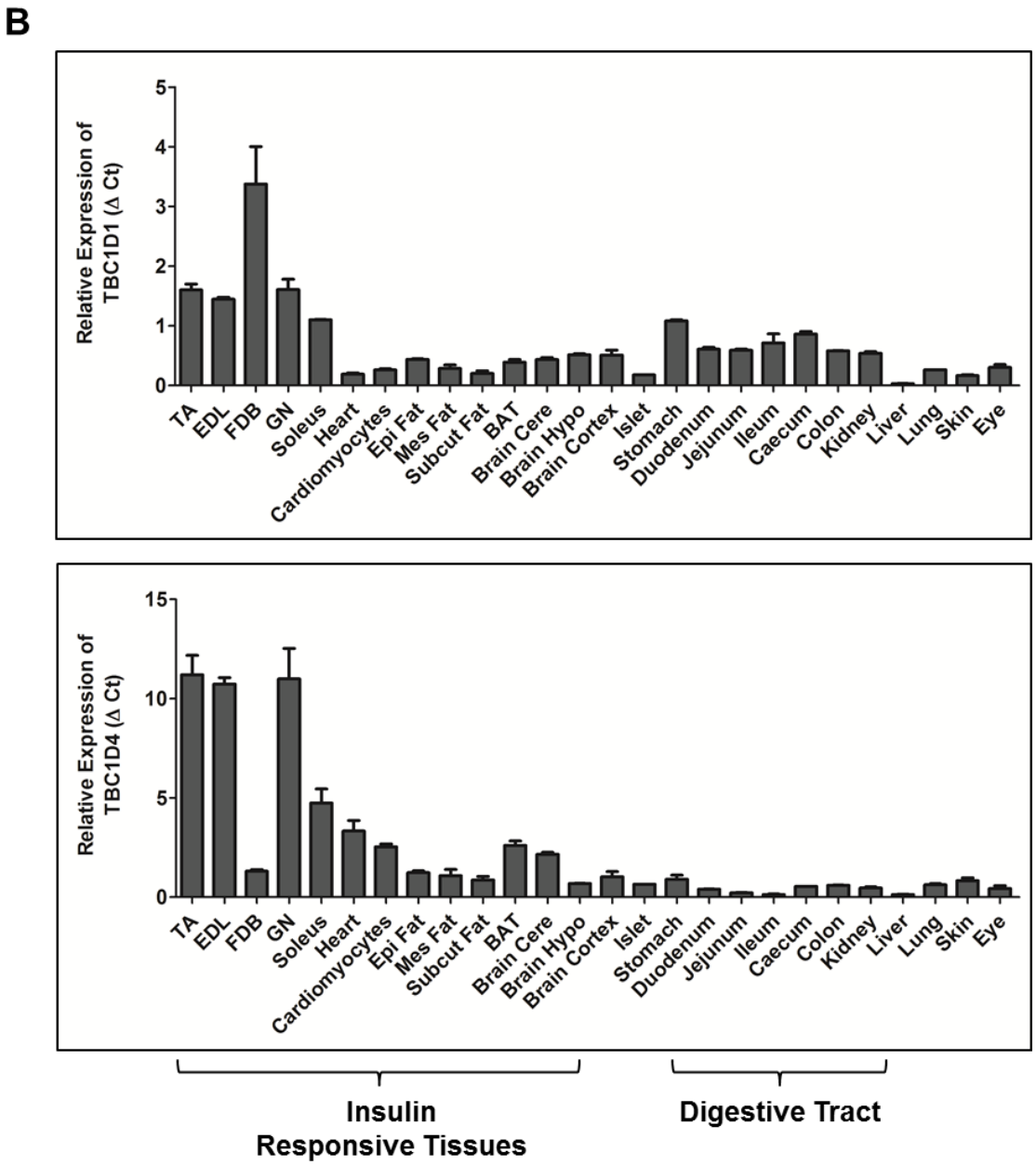

Figure 3.7: Determination of relative *Tbc1d1* and *Tbc1d4* mRNA expression levels in rodent tissues-using real-time quantitative PCR. (A) Expression levels were compared across a panel of mus musculus (Mu) tissues. The selection of cDNAs analysed were kindly donated by Allison (Research Scientist, Astra Zeneca, Alderley Park). *Tbc1d1* and *Tbc1d4* cDNAs were amplified by two-step Taqman® real-time PCR using gene expression assays purchased from Applied Biosystems. Relative expression was calculated based on delta ΔC_t method by normalising the data to three reference genes by geometric averaging of three internal control genes, *Hprt, Tbp and Gus B* (B) mRNA abundances were compared across a panel of rattus norvegicus (Rn) tissues. Total RNA was extracted from tissue homogenates (except muscle and adipose) using the RNA Easy Mini Kit (QIA). Muscle and adipose homogenates were subjected to phenol-based RNA extraction to maximise RNA yield. RNAs were processed using one-step quantitect probe real-time PCR. Gene expression assays kits were purchased from Applied Biosystems. *Hprt, B2m and Gus B* were used as reference genes

3.3.2 Quantification of TBC1D1 and TBC1D4 protein levels in insulin-responsive tissues

To further understand the role of TBC1D1 and TBC1D4 within skeletal muscle, the pattern of protein expression was analysed by western blotting. Absolute protein expression of both TBC1D1 and TBC1D4 was compared within different skeletal muscle tissues and other insulin-responsive tissues (Figure 3.8). Tissues were dissected from mice, homogenised and protein lysates were resolved by SDS-PAGE. Skeletal muscle tissues were selected based on fibre-type composition. tibialis anterior (TA), extensor digitorum longus (EDL) and gastrocnemius (GN) are fast-twitch glycolytic muscles which contain predominately type IIX/IIB. The soleus is a slow-twitch oxidative skeletal muscle which expresses ~80% type I/IIA fibres. Anatomical localisation of mouse hind limb muscles are depicted in Figure 2.2 (2.2.3.1). Expression levels were obtained by extrapolating against the standard curves of purified rat FLAG-tagged TBC1D1 and FLAG-tagged TBC1D4 recombinant proteins. Estimated protein levels were expressed in terms of femto-moles of protein per microgram of tissue lysate.

Quantitative immuno-blot analysis of three independent experiments revealed that all skeletal muscle tissues analysed as well as differentiated C2C12 myotubes expressed the highest levels TBC1D1 protein. EDL muscle (24.8 ± 1.2 femto-moles) and TA muscle (22.9 ± 3.3 femto-moles) expressed slightly higher levels of TBC1D1 compared with GN (17.4 ± 2.0) and soleus muscle (18.6 ± 1.3 femto-moles). Heart tissue expressed significantly lower levels of TBC1D1 (8.1 ± 0.5 femto-moles) compared with skeletal muscle, approximately three-fold lower than EDL muscle. TBC1D4 was most highly expressed in adipose tissue, brain, heart muscle and the soleus muscle. The expression of TBC1D4 in the soleus muscle (2.7 ± 0.6 femto-moles) was significantly more than that detected in the TA, EDL and GN muscles. Quantitative western blotting allows us to directly compare the levels of different proteins expressed within the same tissue sample. Our data revealed that within all types of skeletal muscle analysed and in heart the level of TBC1D1 protein expressed was significantly higher than the level of TBC1D4 protein (Figure 3.8A). We were unable to detect any defined TBC1D1 protein bands in epididymal adipose (epi

fat) tissue and the amount detected in brain tissue by western blotting was very low under the conditions tested (Figure 3.8B). Even though we were unable to accurately quantify the expression of TBC1D1 in these tissues, it is reasonable to conclude that TBC1D4 is more highly expressed in brain and adipose than TBC1D1.

3.3.3 Expression analysis of *Tbc1d1* and *Tbc1d4* splice variants

There appears to be two major splicing variants of *Tbc1d1* and *Tbc1d4* that can be determined from the online sequencing database ENSEMBL. Comparative intron-exon distribution data for *Tbc1d1* and *Tbc1d4* have been extracted for rat, mouse and human and these are depicted in Appendix, Figure 1A, B.

Rat and mouse online sequencing data indicated that a short variant of *Tbc1d1* exists as well as a longer form. These two splice variants translate in to proteins with estimated molecular weights of 132 kDa and 142-143 kDa. Alignments clearly indicate that the long variant of the *Tbc1d1* gene codes for an additional segment (which corresponds to exon 11 and 12) within the center of the protein (Figure 1A, Appendix). Interestingly, *Tbc1d4* also has two alternative splice variants. These correspond to proteins with estimated molecular weights of 139-140 kDa and 146-147 kDa. The longer splice variant occurs because of the inclusion of two addition exons 10 and 11 (Figure 1B, Appendix).

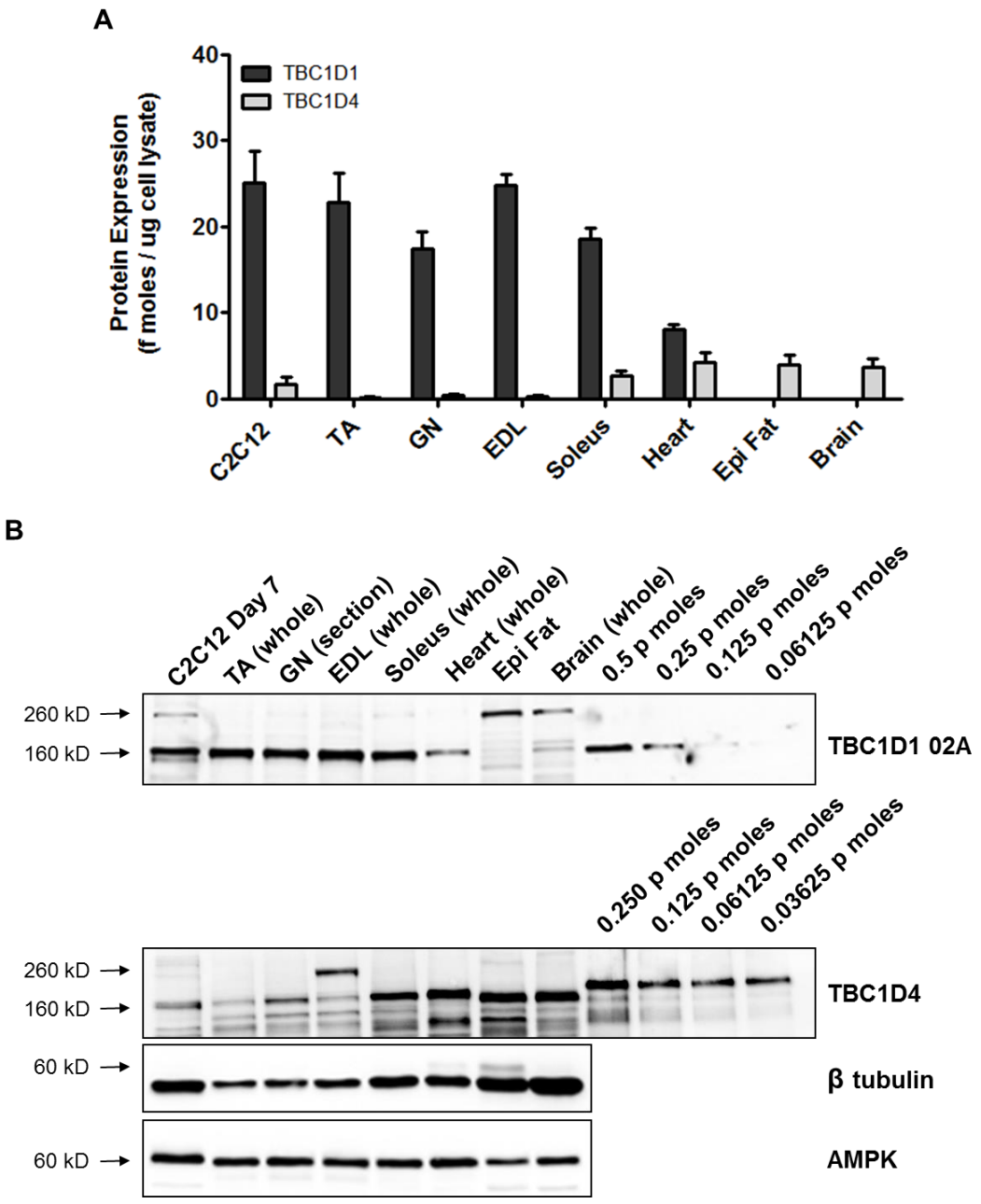

Figure 3.8: Quantification of TBC1D1 and TBC1D4 protein within insulin-responsive tissues as determined by quantitative western blotting. Known amounts of recombinant FLAG-tagged TBC1D1 or FLAG-tagged TBC1D4 that had been expressed in HEK 293 cells were western blotted and probed with anti-TBC1D1 02A or anti-AS160 antibodies to generate calibration curves. Tibialis anterior (TA), gastrocnemius (GN), extensor digitorum longus (EDL) and Soleus muscles, Heart, Epididymal adipose (Epi Fat) and Brain tissue from mouse were excised and homogenised. Tissue protein lysates were western blotted and relative expression of TBC1D1 and TBC1D4 was quantified. (A) Data are expressed as the means ± SE of n = 3 experiments. (B) Representative western blot is shown.

In order to understand more about the expression pattern of *Tbc1d1* splice variants within skeletal muscle and other insulin-responsive tissues, we performed qualitative RT-PCR analysis. Exon-splicing primers which flank the predicted insertion exons 11 and 12 of the long variant of *Tbc1d1* were designed (Table 2.6, 2.1.3.1) (Figure 3.9). To determine the tissue specific distribution of splice variants within skeletal muscles and other tissues, two different sets of primers (primers 1 and primers 2) were used to amplify *Tbc1d1* by PCR. The resulting PCR products were resolved using gel electrophoresis and visualised (Figure 3.10).

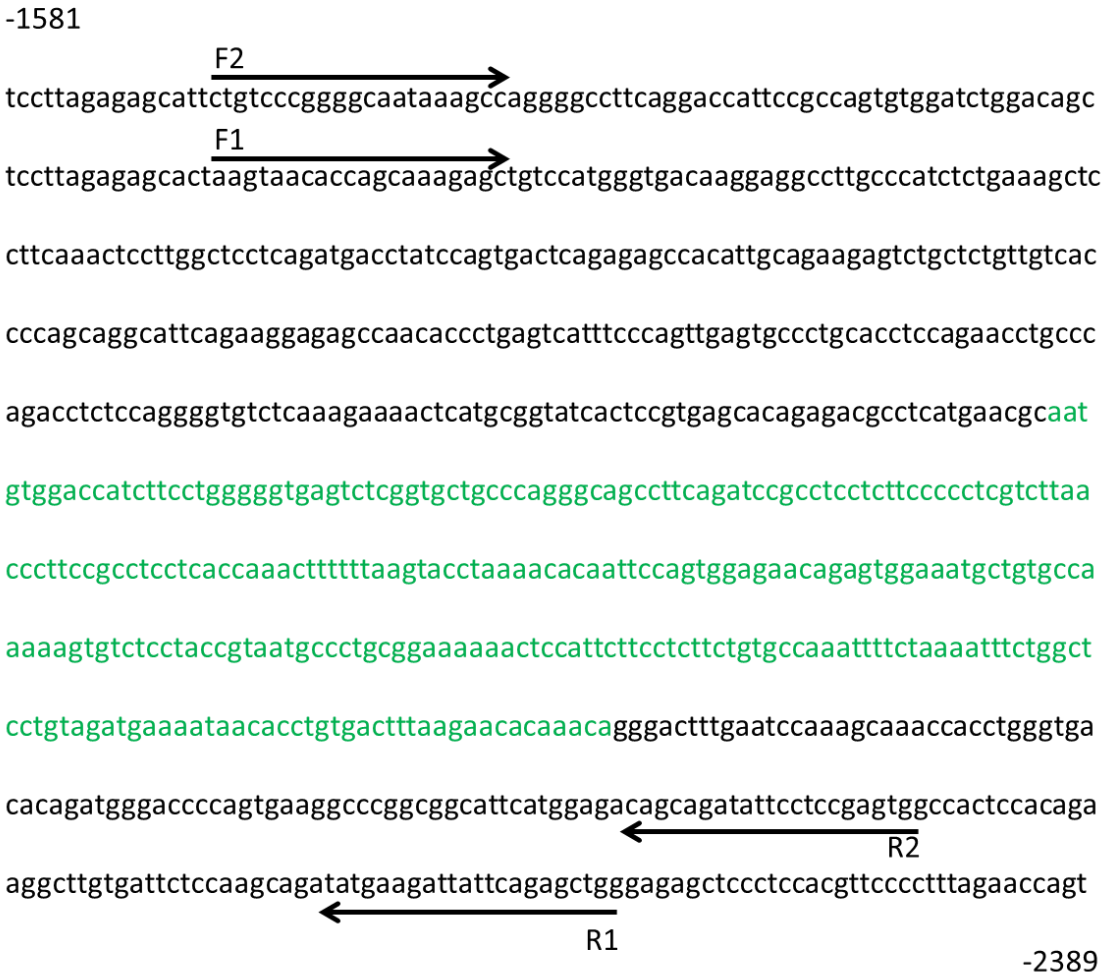

Figure 3.9: Exon flanking *Tbc1d1* PCR primers for qualitative reverse transcription (RT)-PCR experiments. Regions of the rat *Tbc1d1* sequence containing the exon-splicing primer sequences. Two sets of primers were designed against the regions flanking exons 11-12 (highlighted in green) Exon flanking primers 1 (F1-R1) and primers 2 (F2-R2); forward (F) and reverse (R) primer sequences are underlined with arrowhead for orientation. A PCR product containing an extra 286-bp would indicate the presence of exons 11-12 and therefore the expression of the longer splice variant.

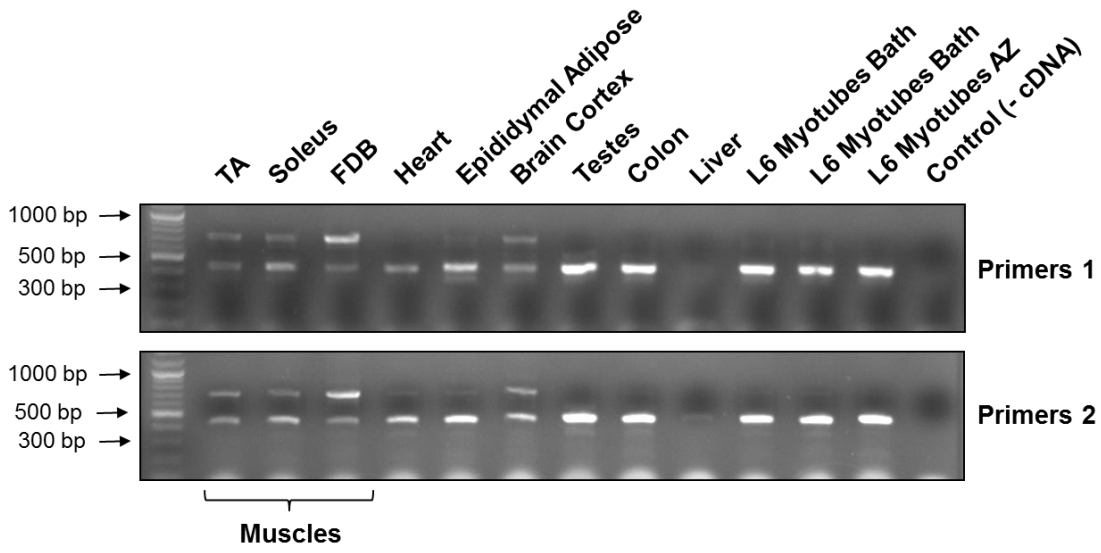

Figure 3.10: Relative distribution of *Tbc1d1* splice variants within a selection of rat tissues. Expression of *Tbc1d1* splice variants within tibialis anterior (TA), soleus, flexor digitus brevis (FDB) muscles, Heart, Epididymal adipose, Brain Cortex, Testes, Colon and Liver, along with the relative distribution in differentiated L6 Myotubes. RNA was isolated and reverse transcribed to cDNA. *Tbc1d1* cDNA was amplified by PCR using exon-flanking PCR primers. Resulting products were resolved by agarose gel electrophoresis and imaged by SYBR safe staining. PCR fragment size was quantified against a 100bp ladder, (PRO).

The skeletal muscles were selected based on differences in their muscle fibre-type composition. Tibialis anterior (TA) muscle is a fast-twitch oxidative/glycolytic muscle that contains predominately type II fibres, soleus is a slow-twitch oxidative type I skeletal muscle and flexor digitus brevis (FDB) is a fast-twitch oxidative skeletal muscle and so contains predominately type IIA fibres. TA, soleus and FDB muscles and brain from rat expressed two defined PCR products, indicating the expression of both isoforms of *Tbc1d1.* Only one shorter PCR product was expressed in heart, epididymal adipose, testes and colon. A *Tbc1d1* PCR product could not be detected within the liver. These data together with the quantitative real time PCR data confirms that *Tbc1d1* is not expressed in the liver (Figure 3.7B, top panel). We also investigated the expression of the two splice variants in the L6 rat muscle cell line. One PCR was detected in differentiated L6 myotubes. This corresponded to the short splice variant of *Tbc1d1*.

The two PCR fragments were calculated as 730 bp and 445 bp (Figure 3.10, primers 1, top panel). The difference calculated between these fragments is 285

bp, which is approximately 10 kDa. These PCR based data correspond with the size difference between the splice variants of *Tbc1d1* from online sequencing databases (Figure 3.9A) and also to the difference between two distinct TBC1D1 protein bands detected within mouse TA muscle by western blotting with TBC1D1 Antibody 02A (Figure 3.3).

3.4 C2C12 skeletal muscle cells as a model for studying the function of TBC1D1

The C2C12 mouse myoblast cell line, are a skeletal muscle cell model produced by Blau et al., 1985. They are a sub-clone of the myogenic cell line derived from adult dystrophic mouse muscle (Yaffe & Saxel, 1977). C2C12 cells can be differentiated for 6-8 days in culture by the addition of horse serum. Myoblasts fuse to form a heterogeneous population of multi-nucleated tubes with distinct morphology (Yoshida, et al., 1998). Light microscopy images of un-differentiated C2C12 cells (Day 0) and differentiating cells at various time points are shown in Figure 3.11. After 48 hours of differentiation, many of the cells began to elongate. By Day 4, there are greater numbers of elongated cells as myoblasts fuse to become multi nucleated myotubes. After Day 4, C2C12 myotubes became larger and more pronounced. However, not all of the cells within the population will differentiate to form myotubes. Some remain in a quiescent state and have been designated 'reserve cells' (Yoshida, et al., 1998).

3.4.1 *Tbc1d1* and *Tbc1d4* mRNA expression in C2C12 cells

The relative *Tbc1d1* and *Tbc1d4* gene expression levels were analysed in C2C12 cells during differentiation using Taqman® real-time quantitative PCR. The expression of *Myod* was also analysed. *Myod* is a transcription factor that activates muscle-specific genes and regulates myogenic differentiation The Taqman® probes used are detailed in Table 2.8 (2.1.3.3). Gene expression levels were normalised against a calculated genomic mean of three reference genes, *Hprt, Tbp, Gus β*. The fold change in gene expression during C2C12 differentiation was determined using the $\Delta\Delta C_t$ method.

As shown in Figure 3.12A, *Tbc1d1* mRNA expression is up-regulated in C2C12 cells during differentiation. *Tbc1d1* mRNA levels were approximately three-fold higher in myotubes on day 7 than in myoblasts on day 0 (Figure 3.12A). The expression of TBC1D4 did not change (Figure 3.12B). The up-regulation of *Tbc1d1* during myotube formation correlates with the increased expression of *Myod* (Figure 3.12C).

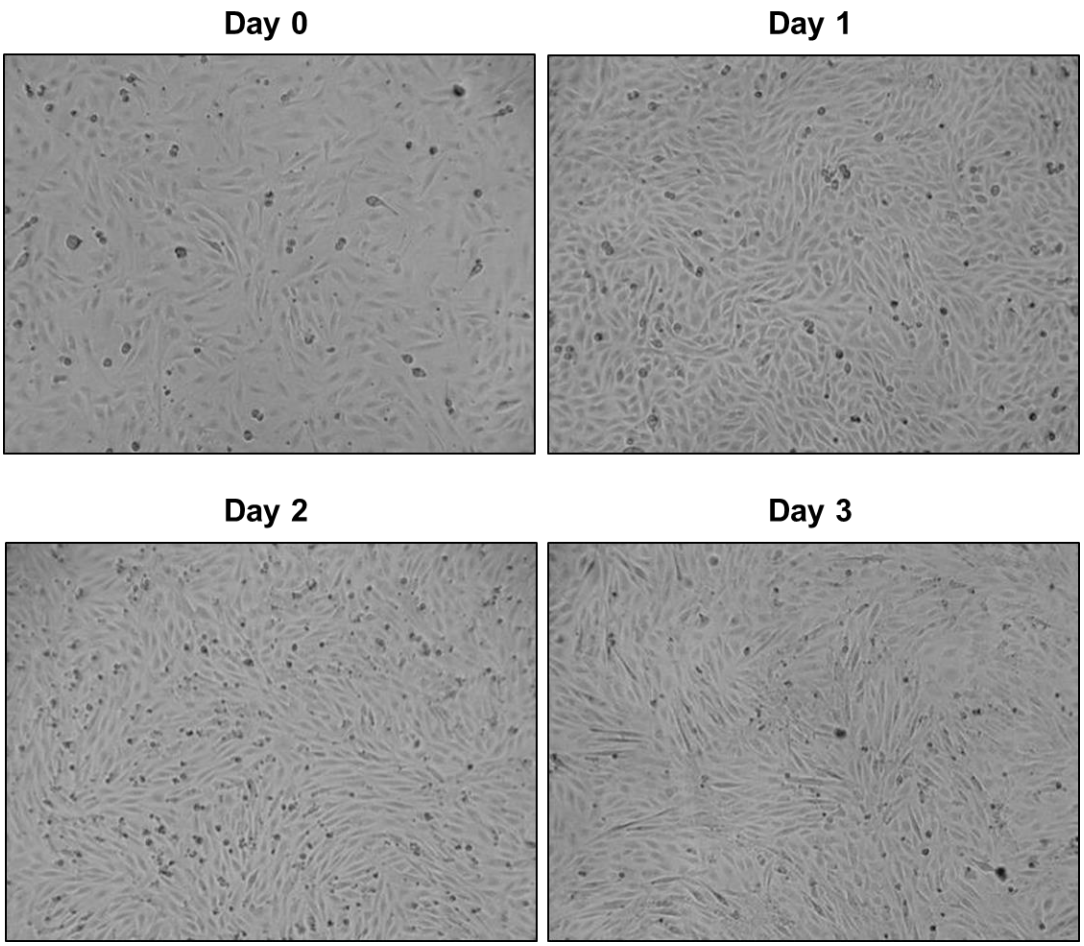
Day 0
Day 1
Day 2
Day 3

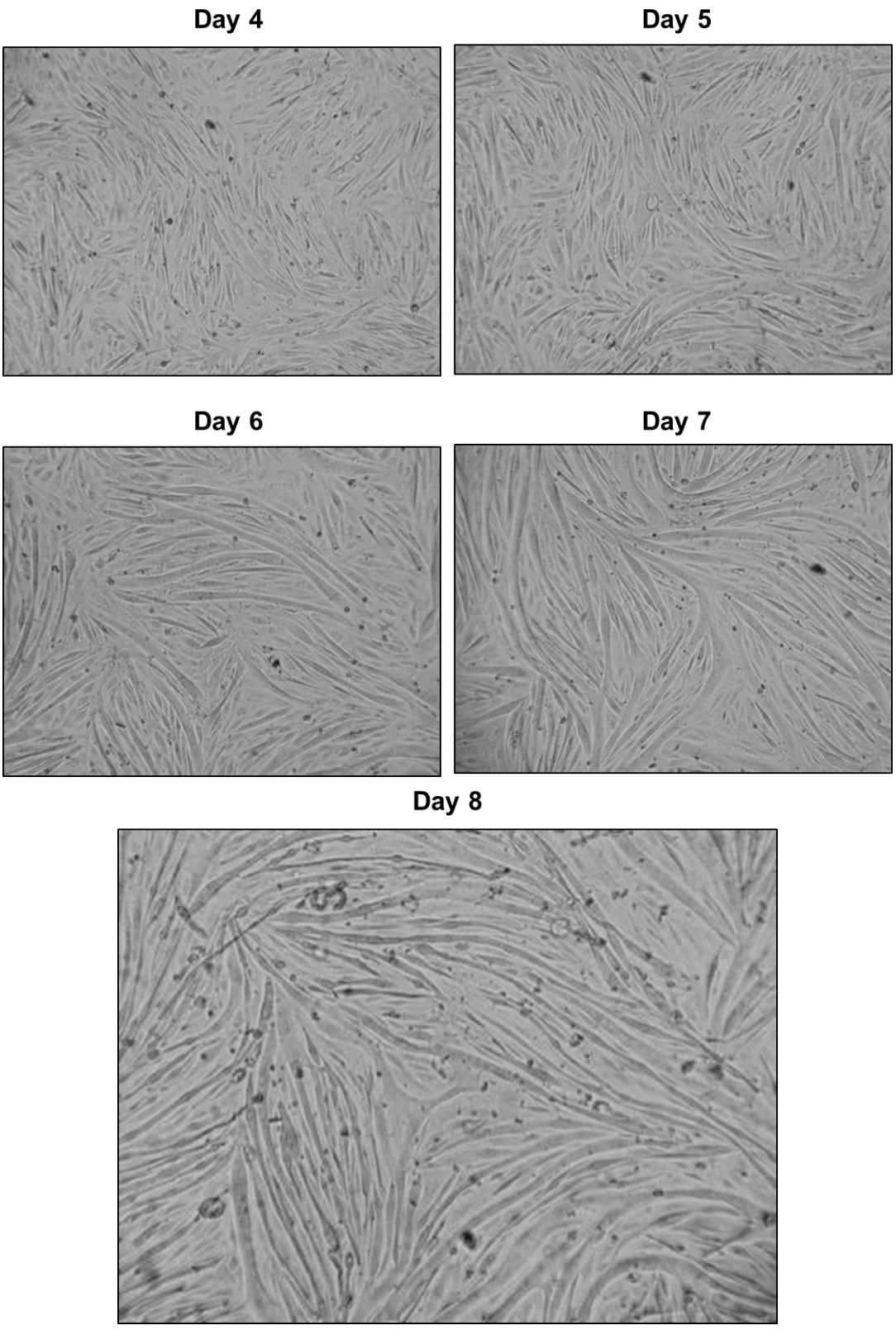

Figure 3.11: Morphology of C2C12 cells during differentiation. Light microscopy images were obtained using a 4x objective and were documented using digital camera (Motic). The images represent C2C12 cells at Day 0 and during differentiation at day 1, 2, 3, 4, 5, 6, 7 and 8.

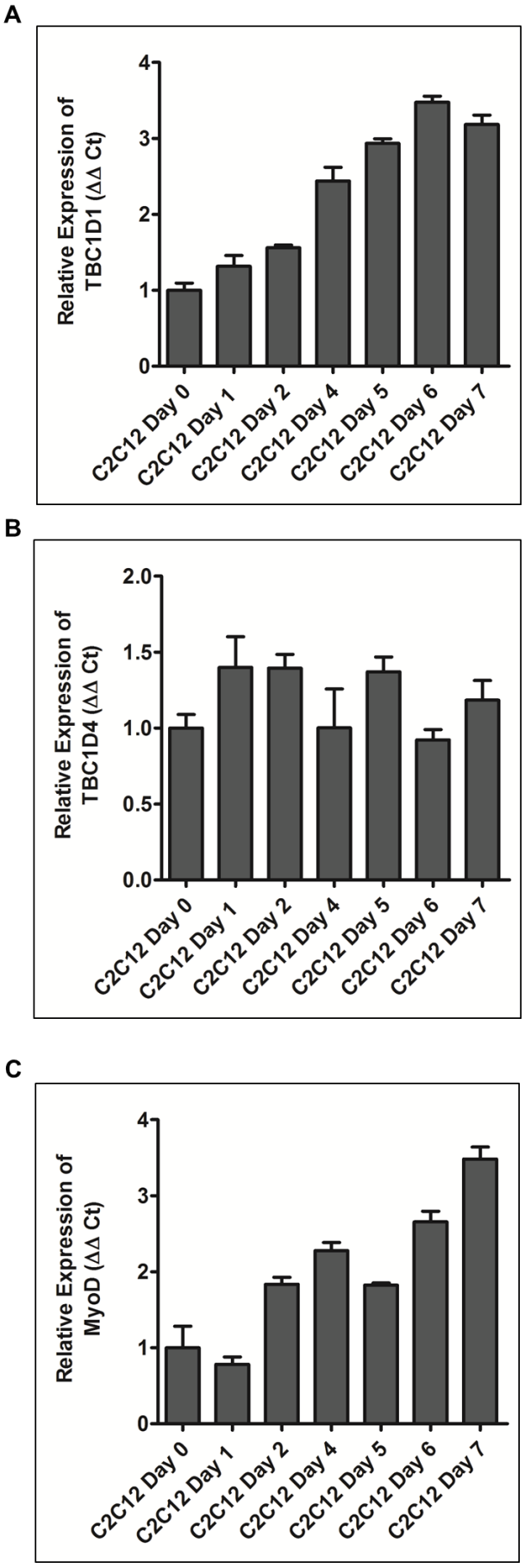
A
Relative Expression of TBC1D1 (ΔΔ Ct)
4
3
2
1
0
C2C12 Day 0
C2C12 Day 1
C2C12 Day 2
C2C12 Day 4
C2C12 Day 5
C2C12 Day 6
C2C12 Day 7
B
Relative Expression of TBC1D4 (ΔΔ Ct)
2.0
1.5
1.0
0.5
0.0
C2C12 Day 0
C2C12 Day 1
C2C12 Day 2
C2C12 Day 4
C2C12 Day 5
C2C12 Day 6
C2C12 Day 7
C
Relative Expression of MyoD (ΔΔ Ct)
4
3
2
1
0
C2C12 Day 0
C2C12 Day 1
C2C12 Day 2
C2C12 Day 4
C2C12 Day 5
C2C12 Day 6
C2C12 Day 7

Figure 3.12: Relative *Tbc1d1*, *Tbc1d4 and Myod* mRNA expression levels in C2C12 cells during differentiation as determined using real-time quantitative PCR. Expression levels were compared in C2C12 cells at day 0 and during differentiation at day 1, 2, 4, 5, 6 and 7. Total RNA was extracted using the RNA Easy Micro Kit (QIA) and reverse transcribed to cDNA. *Tbc1d1*, *Tbc1d4* and *MyoD* cDNAs were amplified by two-step Taqman® real-time PCR using gene expression kits (purchased from Applied Biosystems). Relative expression was calculated based on the delta $\Delta\Delta C_t$ method. The data was normalised to three reference genes by geometric averaging of three internal control genes, *Hprt, Tbp and Gus B.* The expression units are relative to C2C12 Day 0 reference sample. (A) Gene expression of *Tbc1d1* (B) Gene expression of *Tbc1d4* (C) Gene expression of *Myod.* Data are expressed as the means ± SE (intra-assay) of n=1 experiment.

3.4.2 Quantification of TBC1D1 and TBC1D4 protein in C2C12 cells during differentiation in C2C12 cells

The protein expression levels of both TBC1D1 and TBC1D4 were estimated in C2C12 myoblasts and in myotubes during differentiation. Expression levels were calculated within protein lysates by extrapolating against the standard curves of purified rat FLAG-tagged TBC1D1 and FLAG-tagged TBC1D4 recombinant proteins. Estimated protein levels were expressed in terms of femto-moles of protein per microgram of tissue lysate.

Quantitative immuno-blot analysis of three independent experiments revealed that TBC1D1 protein levels were approximately three-fold greater in fully differentiated myotubes (Day 7) (28.7 ± 13.7) compared to myoblasts (Day 0) (7.7 ± 0.6). This appeared to correspond with the up-regulation of the longer splice variant of TBC1D1 of 160 kDa (Figure 3.13A). Conversely, TBC1D4 protein levels were slightly down-regulated in C2C12 myotubes during differentiation. Quantitative western blotting allows us to directly compare the levels of different proteins expressed within the same sample. Our data revealed the level of TBC1D1 protein in myoblasts was higher than the level of TBC1D4 protein in either C2C12 myoblasts (3.6 ± 0.5 femto-moles) or myotubes (2.6 ± 0.2 femto-moles) (Figure 3.13).

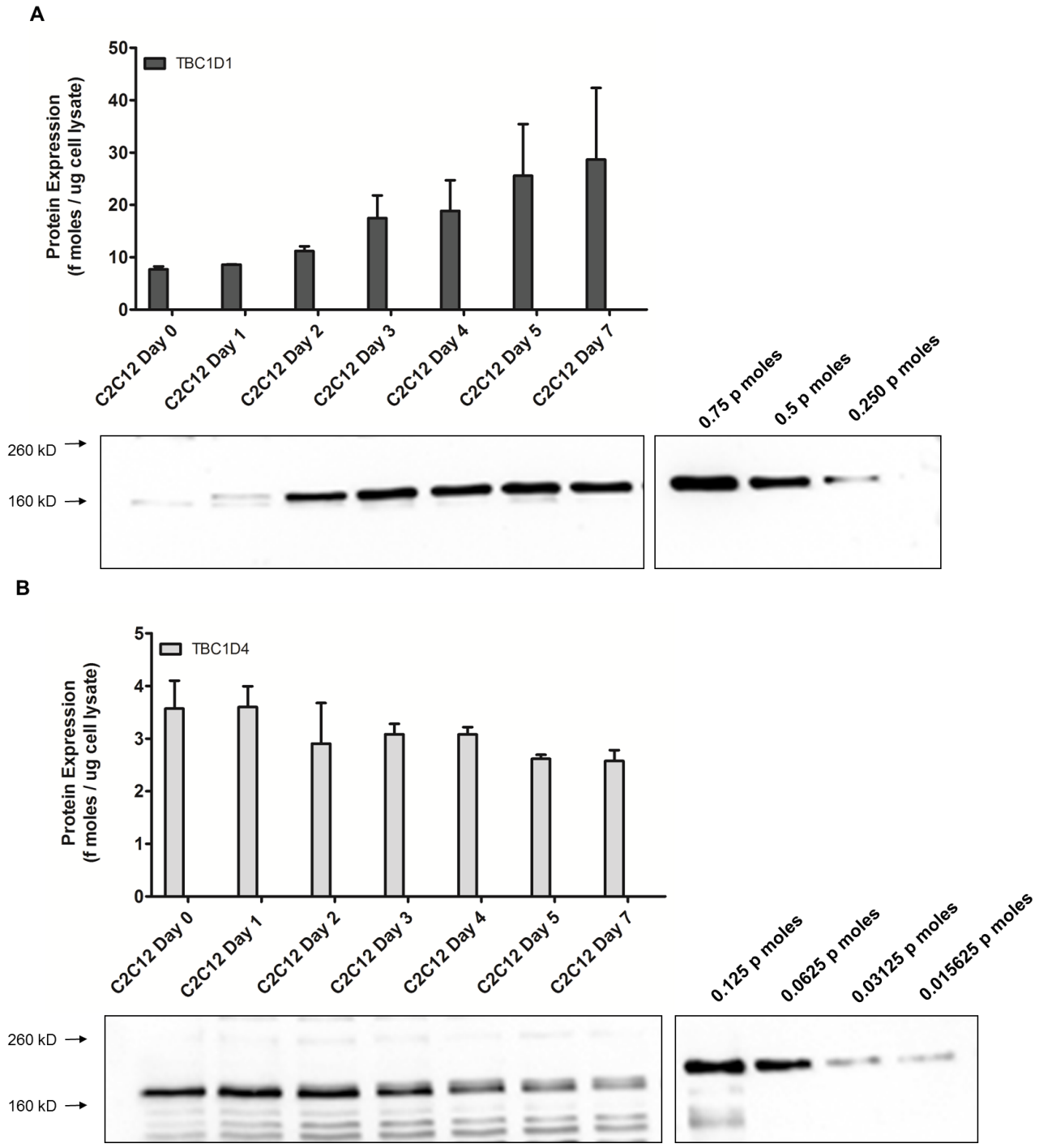

Figure 3.13: Quantification of TBC1D1 and TBC1D4 protein in C2C12 cells during differentiation as determined using quantitative western-blotting. Known amounts of recombinant FLAG-tagged TBC1D1 or FLAG-tagged TBC1D4 that had been expressed in HEK 293 cells were western blotted and probed with anti-TBC1D1 02A or anti-AS160 antibodies to generate calibration curves. C2C12 cells were differentiated and protein lysates were extracted at day 0 and during differentiation at day 1, 2, 4, 5 and 7. Protein lysates were western blotted and relative expression of TBC1D1 and TBC1D4 was quantified. Data are expressed as the means ± SE of n=3 experiments. (A) Expression of TBC1D1. (B) Expression of TBC1D4.

3.4.3 Distribution of *Tbc1d1* splice variants

Further characterisation of the C2C12 cell line was performed to determine whether these cells can represent a useful model for studying the function of TBC1D1 in skeletal muscle. It was therefore necessary to determine by qualitative RT-PCR the relative expression of *Tbc1d1* splice variants within C2C12 cells. Exon-splicing primers were used to amplify *Tbc1d1* by PCR (Figure 3.9), the resulting products were separated by agarose gel electrophoresis and visualised. The relative levels of the splice variants were determined in C2C12 myoblasts (day 0) and during differentiation at days 1-2, 4-7.

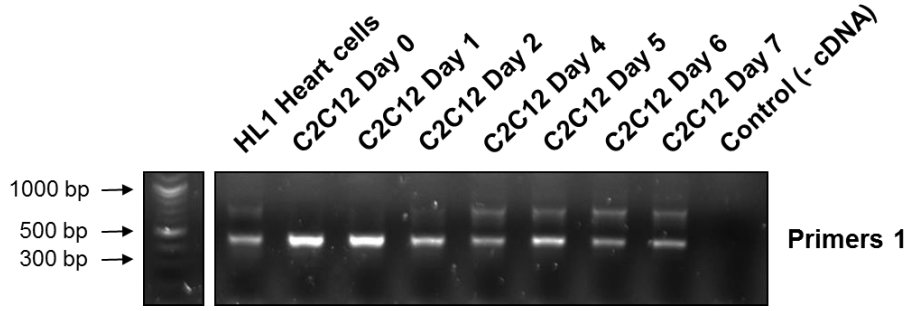

Figure 3.14: Relative distribution of *Tbc1d1* splice variants within C2C12 cells during differentiation as determined by using qualitative RT–PCR. Expression of *Tbc1d1* splice variants in HL1 Heart cells and in C2C12 cells at day 0 and during differentiation at day 1, 2, 4, 5, 6 and 7. RNA was isolated and reverse transcribed to cDNA. *Tbc1d1* cDNA was amplified by PCR using exon-flanking PCR primers. Resulting products were resolved by agarose gel electrophoresis and imaged by SYBR safe staining. PCR fragment sizes were quantified against 100bp ladder (PRO),

Differentiation of C2C12 myoblasts to myotubes led to the induction of the expression of the long splice variant form of *Tbc1d1* (Figure 3.14). This form of *Tbc1d1* was first expressed at day 4 of differentiation and coincides with a distinct morphological change which occurs within the cell culture at around day 4 (Figure 3.14, Figure 3.11). On day 4 there appears to be a greater number of elongated and fused myoblasts. This seems to be associated with the initiation of a rapid differentiation process and distinct morphological changes leading to a myotube population at around day 7. The shorter transcript was highly expressed in C2C12 myoblasts and remains present in the myotubes. The increased abundance of *Tbc1d1* mRNA determined by quantitative real-time

PCR could be due to the up regulation of the long splice variant. Differentiated C2C12 myotubes display a *Tbc1d1* splice variant expression pattern similar to that of primary rat muscle. HL1 heart cells also express both splice variant forms of *Tbc1d1* as determined by RT-PCR analysis.

3.5 Discussion

It is not fully understood whether TBC1D1 and TBC1D4 are both essential in muscle. In order to address this question we have investigated the tissue-specific expression pattern of TBC1D1 and TBC1D4 within different tissues using quantitative real-time PCR and western blotting techniques. We have found that both *Tbc1d1* and *Tbc1d4* were highly expressed in skeletal muscle and heart. In addition, we have shown that TBC1D1 protein is more highly expressed than TBC1D4 in all types of skeletal muscle analysed (TA, EDL, GN and soleus muscles). Finally, we have reported that two distinct TBC1D1 protein bands were detected in primary muscle and C2C12 mouse myotubes at approximately 160 kDa and 150 kDa. Interestingly, the longer variant of TBC1D1 is predominately expressed in muscle and this is up-regulated during C2C12 differentiation. In comparison to L6 muscle cells, C2C12 myotubes display a TBC1D1 splice variant expression pattern which is similar to that of primary muscle. Therefore, C2C12 myotubes may represent a useful muscle-like model to further investigate GLUT4 trafficking in response to insulin stimulation and contraction-mediated signalling.

TBC1D1 (tre-2/USP6, BUB2, cdc16 domain family member 1) and TBC1D4 belong to the TBC Rab-GTPase (Rab-GAP) domain family of proteins. The two proteins are 47% identical and share similar protein domains. These include two N-Terminal phospho-tyrosine binding (PTB) domains and a $Ca^{2+/}$calmodulin binding domain (CBD) situated adjacent to the C-terminal GAP domain. It is well established that TBC1D4 is phosphorylated in response to insulin stimulation and this is important for the regulation of GLUT4 translocation and glucose uptake (Sano, et al., 2003) (Zeigerer, et al., 2004) (Eguez, et al., 2005) (Ramm, et al., 2006) (Thong et al., 2007) (Ishikura, et al., 2007) (Ishikura & Klip, 2008). In addition, several studies have demonstrated that TBC1D1 and TBC1D4 are phosphorylated in response to insulin- and contraction-mediated stimuli in skeletal muscle (Kramer, et al., 2006) (Bruss, et al., 2005) (Funai & Cartee, 2008) (Funai & Cartee, 2009). It has been recently proposed that TBC1D1 could be primarily responsible for regulating contraction-mediated glucose uptake in muscle (Funai & Cartee, 2009) (An, et al., 2010) (Pehmoller, et al.,

2009) (Vichaiwong, et al., 2010). However, whether TBC1D1 and TBC1D4 are both essential in muscle it is not yet fully understood. Furthermore, studies using TBC1D1 deficient mice (B6.SJL-Nob1.10) have demonstrated TBC1D1 is involved in the regulation of both glucose and fatty acid metabolism (Chadt, et al., 2008). In addition, TBC1D1 has been identified as a candidate gene for obesity predisposition (Stone, et al., 2006). Therefore, a key issue which remains to be addressed is the role and the importance of TBC1D1 and TBC1D4 in skeletal muscle function.

To address this issue, we first examined the tissue-specific mRNA expression of *Tbc1d1* and *Tbc1d4* genes using quantitative real-time RT-PCR. We analysed tissue-specific gene expression profiles in human, mouse and rat systems (Figures 3.6 and 3.7). We have found that *Tbc1d1* and *Tbc1d4* were highly expressed in skeletal muscle and heart. This is in support of previous studies (Stone, et al., 2006) (Nagase, et al., 1998). However, we observed a broad rather than tissue-specific expression pattern of *Tbc1d1.* There was notable gene expression in uterus, colon and brown adipose tissue. In contrast, *Tbc1d4* was primarily expressed in insulin-responsive tissues. However, the mRNA expression of *Tbc1d4* was relatively low in adipose tissue (Figure 3.7A, B bottom panels).

In this present study we observed that the individual gene expression profiles for *Tbc1d1* and *Tbc1d4 were* similar in rat, mouse and human. This suggests that there may be evolutionary conservation of *Tbc1d1* and *Tbc1d4* expression in mammals. Phylogenetic data has indicated that *Tbc1d4* emerged after *Tbc1d1* in evolution during vertebrate development (Chen, et al., 2008). The expression of *Tbc1d4* presumably reflects the acquisition of new genes to increase the complexity among vertebrate species.

It has been reported that two protein coding splice variants of the *Tbc1d1* and *Tbc1d4* genes exist (Taylor, et al., 2008). Sequence alignments clearly indicate that the long variant codes for an additional segment within the center of the protein (Figure 3.9). The additional exons translate to an extra ~10 kDa in TBC1D1 and ~7 kDa in TBC1D4.

In this current study we have analysed the distribution of *Tbc1d1* splice variants in several tissues and insulin-responsive cell lines using qualitative RT-PCR (Figure 3.10). Taylor et al., 2008 reported that both isoforms were expressed in skeletal muscle and white adipose tissue. We have shown here that the short splice variant of *Tbc1d1* was expressed in the majority of tissues analysed. In addition, the long splice variant was strongly detected in skeletal muscle and brain. The long variant was expressed at low levels in white epididymal adipose tissue.

In this present study we have shown that the relative expression of the long splice variant of TBC1D1 was increased in HL1 cardiac mouse cells cultured in high cell-density conditions compared to cells grown in low density cultures (Figure 3.4). Confluent HL1 cells maintain a differentiated cardiac phenotype in culture. The cells express the genes for cardiac alpha-myosin heavy chain (α-MHC) and atrial natriuretic factor (ANF) which are expressed in adult heart (Claycomb, et al., 1998). Another important observation in this present study is that the differentiation of C2C12 myoblasts to myotubes led to the up-regulation of the long splice variant form of TBC1D1 (Figure 3.13A) (Figure 3.14). This finding is in support of those of Peck et al., 2009. Interestingly, the expression of the long isoform in C2C12 myotubes is concurrent with the development of sarcomere structure and contractile activity (Nedachi & Kanzaki, 2006). These findings support the hypothesis that the long splice variant may be important for the regulation of TBC1D1 function in muscle.

Similarly to *Tbc1d1*, there is a long and short (AS160_V2) splice variant of *Tbc1d4* (Baus, et al., 2008). The expression of both variants in human tissues has been analysed by quantitative RT-PCR (Baus, et al., 2008). Interestingly, the full-length transcript of *Tbc1d4* is predominately expressed in human skeletal muscle and heart. By contrast, the short splice variant of the *Tbc1d4* gene (transcript variant 2 (AS160_v2)) is ubiquitously expressed in most human tissues (Baus, et al., 2008). Both TBC1D1 and TBC1D4 Rab-GAPs contain a $Ca^{2+/}$calmodulin binding domain (CBD). There is growing evidence implicating Ca^{2+}/calmodulin in the regulation of contraction-mediated glucose uptake into skeletal muscle (Kramer, et al., 2007) (Funai & Cartee, 2009) (Witczak, et al.,

2010). The CBD is not affected by the lack of exons 11 and 12 in the short splice variant. However, it cannot be ruled out that this region may be required for Ca^{2+}/calmodulin binding to the CBD. Furthermore, the splice region may also be important for the potentiation of contraction-mediated responses. The protein region corresponding to the splice region of *Tbc1d1* contains two AMPK consensus motifs (serine 660 and serine 700). These have been shown to be phosphorylated in response to AICAR-treatment in skeletal muscle (Frosig, et al., 2010) (Taylor, et al., 2008). Therefore, it is likely that the long splice variants of TBC1D1 and TBC1D4 are the forms that may act as points of convergence between the insulin and contraction signalling pathways leading to GLUT4 translocation and glucose uptake in skeletal muscle.

The mRNA expression level of a gene is thought to provide a rough estimate about the relative abundance within a tissue. However, with no information about mRNA stability or mRNA translation efficiency, it is more reliable to determine protein expression.

At the time this project commenced there were no commercial antibodies available against TBC1D1. Therefore, specific anti-serum against TBC1D1 and TBC1D1 phosphorylated at serine 237 were generated as part of the CASE studentship with Astra Zeneca (AGG Astra Zeneca, Macclesfield, UK) (Figure 3.1). Subsequently, a number of research groups have reported on the generation and use of anti-TBC1D1 antibodies (Chen, et al., 2008) (Chadt, et al., 2008) (Chavez, et al., 2008) (Taylor, et al., 2008).

In our preliminary antibody characterisation studies, we have shown that the antibody 02A (which has been raised against the rat peptide Asp-Ser-Pro-Ser-Arg-Thr-Glu-Asp-Tyr-Ser-Glu corresponding with TBC1D1 amino acids 766-776), specifically recognises endogenous TBC1D1 (Figure 3.3). We have shown that use of these antibodies led to the detection of a distinct protein band with the expected molecular weight of ~160 kDa in mouse skeletal muscle and heart (Figure 3.3, 3.4 and 3.8). A number of previous studies have reported that the long isoform of TBC1D1 in mouse and human skeletal muscle lysates migrates at an apparent molecular mass of 150~160 kDa (Taylor, et al., 2008)

(Pehmoller, et al., 2009) (Frosig, et al., 2010) (Jessen, et al., 2011). We could not detect TBC1D1 in rat TA muscle lysates when immuno-blotted using TBC1D1 02A antibody (Figure 3.3). This was surprising because the polyclonal antibodies were raised against synthetic peptides of rat TBC1D1 protein. It is possible that the level of TBC1D1 protein is relatively low compared with the abundance of connective tissue and contractile proteins within muscle tissue. In support of this, we could detect TBC1D1 in isolated rat FDB muscle cells. Further work is required to establish this. Furthermore, we have reported that two distinct protein bands were detected in C2C12 mouse myotubes at approximately 160 kDa and 150 kDa (Figures 3.3 and 3.4A). In addition, we have shown that identical protein bands are detected in C2C12 myotubes lysates immuno-blotted with two other primary antibodies raised towards different epitopes in TBC1D1 (Figure 3.3 and data not shown). TBC1D1 H-AH is previously described in (Chadt, et al., 2008), TBC1D1 #4629 (Cell Signalling Technologies) is previously described in (Taylor, et al., 2008). The presence of the higher molecular weight band of 160 kDa detected in muscle corresponded with the expression of the long splice variant (Figure 3.3 and 3.4).

The phosphorylation of TBC1D1 at serine 231 in C2C12 myotubes occurs in response to AMPK activation. Western blotting with phospho-specific TBC1D1 antibody led to the detection of two distinct protein bands at approximately 150 and 160 kDa. Therefore, it is reasonable to conclude that both bands correspond to the major isoforms of TBC1D1.

In contrast to earlier findings by Taylor et al., 2008, we could not detect a distinct TBC1D1 protein band in white epididymal adipose tissue. A possible explanation could be that the polyclonal antibody TBC1D1 02A preferentially detects the long TBC1D1 isoform. In this current study we found that epididymal adipose tissue predominately expressed the short splice variant of the *Tbc1d1* gene (Figure 3.10). However, the antibody 02A recognition epitope corresponds to amino acids 764-774 of the mouse TBC1D1. This region is located close to the C-terminal region of the splice site (amino-acids 631-723 of TBC1D1). In addition, two isoforms are detected in C2C12 myotubes and HL1 cardiac muscle cells. Furthermore, a faint band corresponding to the shorter isoform of

TBC1D1 was detected in 3T3-L1 mouse adipocytes (Figure 3.4B). Another more plausible explanation is that the western blot technique is not sensitive enough to detect the level of TBC1D1 protein expressed in adipose tissue. RT-PCR is a very sensitive technique in which low numbers of RNA transcripts can be detected.

In this study we have used quantitative western blotting to estimate the amount of TBC1D1 and TBC1D4 in different types of mouse muscle. This is in contrast to several studies which have investigated the relationship between the expression levels of TBC1D1 and TBC1D4 with respect to muscle type using relative quantification techniques (Taylor, et al., 2008) (Szekeres, et al., 2012). Relative quantification is limited as it only allows the expression levels of TBC1D1 and TBC1D4 to be determined between the tissues separately. Using a quantitative approach in this study, we have shown here that within all types of skeletal muscle analysed (TA, EDL, GN and soleus muscles) the amount of TBC1D1 protein expressed (femto-moles of protein per microgram of tissue lysate) was significantly more than the level of TBC1D4 protein. In addition, the amount of TBC1D1 in TA and EDL muscles (which consist of >60% type IIB/IIX fast-twitch glycolytic muscle fibres (Bloemberg & Quadrilatero, 2012)) was slightly higher than that in GN muscle (mixed fibre-type) or in soleus muscle (which consists of ~80% type I/IIA oxidative muscle fibres (Bloemberg & Quadrilatero, 2012)).The results reported by Taylor et al., 2008, are in accordance with ours since they observed a higher expression of TBC1D1 in TA muscle compared with in the soleus muscle. In addition, we have found that the expression of TBC1D4 was significantly higher in the soleus muscle compared with the other muscle types. TBC1D4 protein expression was similar in the soleus muscle, heart, adipose tissue and brain. Furthermore, TBC1D4 expression in the soleus, GN, EDL and TA is positively correlated with the skeletal muscle content of oxidative fibres (Type I and IIA). Henriksen et al., 1990, reported that insulin-stimulated glucose transport was higher in the rat soleus muscle compared with the EDL muscle and this was correlated with the increased expression of GLUT4 protein in the soleus muscle (Henriksen, et al., 1990). Therefore, the larger insulin-responsive pool of GLUT4 in the soleus muscle could to be associated with the increased level of TBC1D4. However, it

is important to note that in contrast to mouse soleus muscle, the rat soleus muscle has been shown to consist of predominately type I slow twitch fibres (Bloemberg & Quadrilatero, 2012).

Finally, C2C12 myotubes display a TBC1D1 splice variant expression pattern which is similar to that of primary muscle. This is in contrast to what we have found for the L6 muscle cell model (Figure 3.4A and Figure 3.10). However, several studies have reported the expression the both the long and short splice variants of TBC1D1 in L6 myotubes (Chen, et al., 2008).

It has been reported that C2C12 cells can be classified as 'hybrid' muscle cells. This is because they express both fast and slow MHC isoforms (Zebedin, et al., 2004). In support a 'hybrid' phenotype, our data has revealed that C2C12 myotubes express both TBC1D1 and TBC1D4 proteins. Interestingly, the amount of TBC1D1 and TBC1D4 proteins expressed (femto-moles of protein per microgram of cell lysate) demonstrated that cultured C2C12 myotubes do not represent either fast or slow twitch muscle types but are a hybrid type of muscle cell. Therefore, C2C12 myotubes could represent a unique model for investigation of the importance of TBC1D1 and TBC1D4 for the regulation of GLUT4 trafficking in response to insulin stimulation and contraction-mediated signalling in muscle in general.

In conclusion, the development of TBC1D1 specific antibodies especially the phospho-specific antibody provide useful tools for investigating TBC1D1 leading to GLUT4 trafficking. In this study we have highlighted the importance for extensive antibody characterisation studies. By evaluating cross-species reactivity of the antibodies in both rat and mouse tissue lysates and analysing the validity of antibodies using knockout mice. Our data support that there are variations between the expression levels of TBC1D1 and TBC1D4 within different fibre-type muscles. Furthermore, that the longer variant of TBC1D1 is predominately expressed in muscle and that this is up-regulated during C2C12 differentiation. However, to what reason and extent these differences affect insulin- and contraction-mediated glucose uptake in muscle is still unknown. Further work is required to determine the roles for TBC1D4 and TBC1D1 in

GLUT4 trafficking. Considering that most skeletal muscles are composed of a mixture of muscle fibres, it will be of importance for future studies to investigate GLUT4 trafficking with respect to muscle fibre-type. Furthermore, there may be slight differences in the fibre-type composition of the same muscle from different rodent species and so this will have to be considered.

4 Characterising GLUT4 trafficking in the C2C12 muscle cell culture model

4.1 Introduction

Glucose transport into adipose and muscle cells is controlled through processes which regulate the rate at which GLUT4 is trafficked and inserted in to the plasma membrane and the rate GLUT4 is retrieved from the cell surface. In the absence of insulin stimulation, GLUT4 is rapidly removed from the cell surface and slowly recycled. Thus, the net effect is that the majority of GLUT4 transporters are actively retained within intracellular compartments and absent from the plasma membrane pool.

The intracellular trafficking route for GLUT4 can be simplified into discrete trafficking steps (Figure 1.3, 1.3.2.6). These are the biogenesis of GSV (this includes the release of GSV from sequestration mechanisms), the translocation of GSVs to the cell surface, tethering, docking, fusion events and GLUT4 endocytosis (Larance, et al., 2008). However, the question is which of these steps of GLUT4 trafficking are the major sites of insulin action. Furthermore, the dysregulation of insulin-stimulated glucose uptake into peripheral tissues is a major feature of T2DM. However, exercise-mediated GLUT4 translocation and glucose disposal appears to be normal in insulin-resistant individuals. Therefore, it is of importance also to understand the effects of contraction-mediated signalling on GLUT4 trafficking.

The development of exofacial epitope-tagged GLUT4 fusion proteins have been important for studies of GLUT4 trafficking in both adipose and muscle cells. These GLUT4 reporter constructs contain a hemagglutinin (HA) or Myc tag in the first exofacial loop (which enables the rapid detection of GLUT4 which has been inserted into the plasma membrane) and can also have a C-Terminal GFP tag (HA/Myc-GLUT4-GFP). Using these reporter proteins the rate at which GLUT4 arrives at the cell surface can be measured as a function of time (transition kinetics). Secondly, several studies have used these reporter proteins to study the effect of insulin on GLUT4 exocytic pathways at steady-

state (Martin, et al., 2006) (Karylowski, et al., 2004) (Govers, et al., 2004) (Fazakerely, et al., 2009). For these studies intact live cells are labelled with a saturating concentration of purified anti-HA antibody. The concentration of antibody used is sufficient to label all HA-GLUT4 that appears at the cell surface. Thus, anti-HA accumulation (uptake) over time is a function of the rate of GLUT4 exocytosis (k_{ex}). In addition, the size of the GLUT4 actively cycling pool can be determined. Therefore, the effect of insulin on the release of GLUT4 from an intracellular storage compartment can be resolved.

Two different models of GLUT4 retention have been proposed. These models are illustrated in Figure 1.4 (1.3.2.6). The first model details that intracellular GLUT4 traffic is governed by a dynamic system (Figure 1.4B, 1.3.2.6). In this 'dynamic equilibrium retention' model the actively cycling GLUT4 pool is regulated by a very slow cycling rate under basal conditions. Importantly, this model states that GSVs are in continual exchange with the endosomal compartment and so the entire insulin-responsive GLUT4 pool can eventually recycle with the plasma membrane in basal cells. Stimulation with insulin concurrently increases the rate of GLUT4 exocytosis (k_{ex}) and decreases GLUT4 endocytosis (k_{en}), thus redistributing GLUT4 to the cell surface (Martin, et al., 2006) (Karylowski, et al., 2004).

The second model is known as the 'static retention model' (Figure 1.4C, 1.3.2.6). GLUT4 is stored within specialised non-cycling GSVs sequestered away from the ERC (Govers, et al., 2004) (Coster, et al., 2004) (Muretta, et al., 2008) (Fujita, et al., 2010). Insulin stimulates the release of GLUT4 from a 'static retention mechanism to the plasma membrane and thus increasing the size of the GLUT4 cycling pool. Furthermore, insulin stimulation increases the exocytic rate (k_{ex}) of this pool at steady-state. No effect on k_{en} was observed. The actual mechanism for how insulin regulates GLUT4 recycling is still disputed. However, it is likely that a combination of both 'static retention' and 'dynamic recycling' mechanisms will contribute to the regulation of GLUT4 trafficking (Muretta, et al., 2008) (Xu, et al., 2011).

There are only a few studies which address this question in muscle cells. Further support for the ‘dynamic recycling’ model comes from experimental studies carried out in L6 myoblasts stably expressing Myc-tagged GLUT4 (Foster, et al., 2001). Additionally, partial GLUT4 static retention has been proposed for L6 skeletal muscle cells expressing HA-GLUT4 (Fazakerely, et al., 2009).

The aim of these investigations is to address whether immortal muscle cell lines can provide an alternative *in vitro* model system for accurately measuring the kinetics of GLUT4 trafficking. These muscle cell lines are advantageous to use as they can be readily sourced and cultured. and so have great potential for industry applications. For these studies we have chosen to utilise the C2C12 skeletal muscle cell model. In comparison to L6 cells, C2C12 develop partially formed transverse (T) -tubules (which is an important site for glucose uptake in muscle) (Rudich & Klip, 2003). Furthermore, we have shown that C2C12 myotubes display a TBC1D1 splice variant expression pattern which is similar to that of primary muscle. Therefore, C2C12 myotubes may represent a useful muscle-like model to further investigate GLUT4 trafficking in response to insulin stimulation and contraction-mediated signalling.

4.2 Establishing the model for studying GLUT4 trafficking

For these studies an immortal myoblast cell line was used. Myoblasts can be readily differentiated in culture and in contrast to primary muscle cells they can be efficiently infected and transfected. We have employed the C2C12 skeletal cell culture model to study GLUT4 trafficking. The main focus of this research was to understand the importance of TBC1D1 and TBC1D4 in muscle cells. As discussed above (3.4.3), and in contrast to L6 cells, C2C12 myotubes display a TBC1D1 splice variant expression pattern similar to that of primary muscle.

Two major problems are faced when using C2C12 or L6 muscle cells. Firstly, the differentiated cell phenotype is highly dependent on the differentiation conditions and culture conditions used. It was necessary to standardise C2C12 culture conditions for both growth and differentiation of the cells. This is documented in Table 2.12 (2.2.2.6). It was important to grow these cells in sub-confluent cultures, in order to maintain a proliferative phenotype. Secondly, C2C12 cells express low levels of endogenous GLUT4 and therefore biotinylated photolabels (which have been developed to monitor GLUT4 trafficking events) cannot be used with these cells. Instead, myoblasts are infected with a GLUT4 reporter construct containing a HA epitope tag inserted within the first exofacial loop of the protein. HA-GLUT4 can be stably expressed within C2C12 myoblasts using this retroviral expression system. Cell surface GLUT4 can then be detected by labelling with cell impermeant anti-HA antibodies. The methods developed for studies of GLUT4 trafficking using the C2C12 muscle cell model were based on previous experiments carried out within our group in L6 skeletal muscle cells (Fazakerely, et al., 2009). Experiments using epitope-tagged GLUT4 reporter proteins were adapted from initial studies developed to observe GLUT4 trafficking in 3T3-L1 adipocytes (Govers, et al., 2004) (Muretta, et al., 2008) (Martin, et al., 2006) (Karylowski, et al., 2004).

4.2.1 Retroviral expression of HA-GLUT4

It has been reported that over expression of GLUT4 in adipose cells interferes with insulin-stimulated GLUT4 translocation to the plasma membrane (Al Hasani, et al., 1999). C2C12 cells express low levels endogenous GLUT4, so over-expression could over load the trafficking machinery. It was therefore important to consider whether the expression of HA-GLUT4 in C2C12 cells would affect GLUT4 trafficking.

C2C12 myoblasts were infected with either increasing concentrations of pBABE-puro HA-GLUT4 retrovirus (HAG4 0.025-0.2 ml) or the corresponding pBABE-puro empty vector control virus (EV). A viral concentration-dependant increase in the expression of HA-GLUT4 was observed by western blotting of protein lysates with anti-GLUT4 and -HA antibodies (Figure 4.1A). Expression of GLUT4 reporter protein was substantially higher than the endogenous levels of GLUT4 within these cells. Endogenous GLUT4 could be faintly detected in EV cells by a longer western blot exposure.

A sample of rat adipose cell, low-density microsomal (LDM) (containing a known amount of GLUT4) was used as a standard to quantify the expression of GLUT4 in C2C12 cells that were infected with increasing volumes of HA-GLUT4 virus. The mean results are depicted in Figure 4.1B. Cells infected with 0.1 or 0.2 ml of virus expressed significantly more GLUT4 compared with cells infected with 0.025 ml (Figure 4.1B). This over-expression resulted in an increased level of GLUT4 at the cell surface in basal cells and affected insulin-stimulated GLUT4 translocation (Figure 4.1C).

The lowest amount of retrovirus (0.025ml) was used to infect C2C12 cells for all subsequent experiments. The amount of GLUT4 expressed was calculated to be 6.6 ± 1.4 femto-moles per microgram of cell lysate (Figure 4.1B). The amount of GLUT4 expressed in non-infected myotubes was calculated to be 0.017 ± 0.003 femto-moles per microgram (Figure 4.1D). Therefore, the level of over-expression was calculated to be approximately 400 times greater than the amount of GLUT4 expressed in non-infected differentiated C2C12 myotubes (Figure 4.1D).

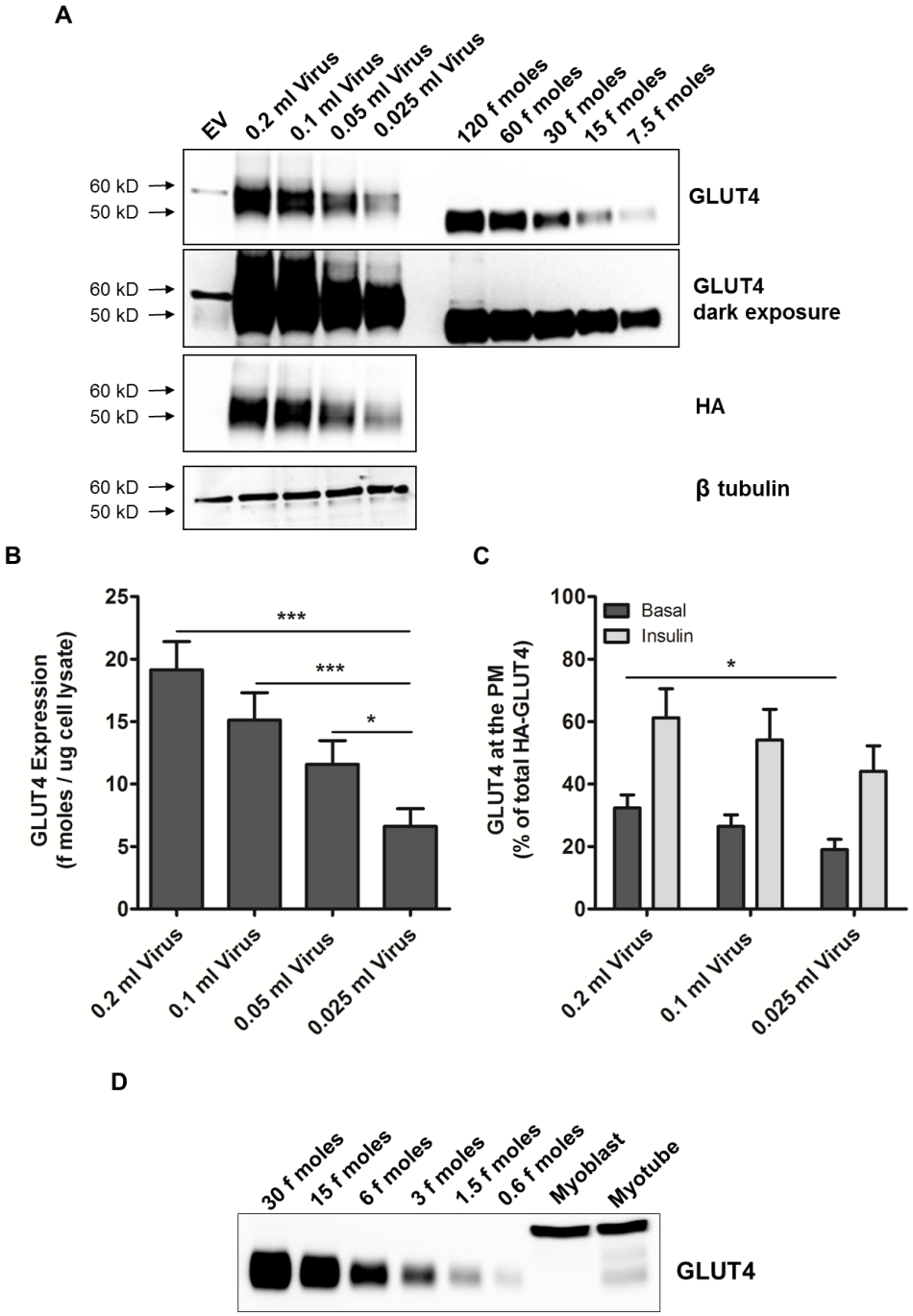

Figure 4.1: Increasing HA-GLUT4 viral titre on cell and plasma membrane GLUT4 expression levels. (A) C2C12 myoblasts were infected with increasing volumes of HA-GLUT4 retro-virus (0.025 - 0.2 ml) or empty vector (EV) virus as a control. HA-GLUT4 expression levels were determined compared to EV cells by western blotting with anti-GLUT4, HA and β –Tubulin antibodies. Expression of GLUT4 was quantified by western blotting against a calibration curve generated using known amounts of rat adipocyte low density microsome (LDM) fraction. (1µg of LDM is equivalent to 60 femto-moles of GLUT4) Protein load: 10 µg. (B) Quantification of HA-GLUT4 in C2C12 myoblasts was determined by densitometry analysis of five experiments. (C) C2C12 myotubes were maintained under basal conditions (dark grey bars) or stimulated with insulin at 200 nM for 5 min (light grey bars), The plasma membrane levels of GLUT4 were determined by incubating fixed cells with anti-HA primary antibodies and anti-mouse Alexa 488 secondary antibodies. The results are expressed as a percentage

of total HA-GLUT4 in permeabilised cells. (D) The expression of endogenous GLUT4 in C2C12 myoblasts and C2C12 myotubes. Repeated measures analysis of variance (ANOVA) test was used with Tukey multiple comparison test at p=0.05. * p≤0.05, ** p≤0.01, *** p≤0.005.

4.2.2 Investigating the change in phosphorylation of TBC1D1 in response to AMPK activation of C2C12 cells

Several studies have demonstrated that AMPK is a key mediator of contraction-stimulated signalling responses that regulate glucose uptake in muscle (Mu, et al., 2001) (Wright, et al., 2005) (Jessen, et al., 2002) (Jensen, et al., 2008). Therefore, to investigate the regulation of GLUT4 trafficking with respect to AMPK-activation we have utilised the AMP-mimetic, 5-Aminoimidazole-4-carboxamide 1-β-D-ribofuranoside (AICAR). AICAR is a cell-permeable adenosine analogue that can be phosphorylated to ZMP (an AMP analogue) in the target cell. In muscle, treatment with AICAR has been shown to activate AMPK-α_2 which increases cell surface levels of GLUT4 transporters and enhances glucose transport (Koistinen, et al., 2003) (Hayashi, et al., 1998) (Sajan, et al., 2010). We also examined the response to direct AMPK activator, A-769662. A-769662 is a small-molecule thienopyridone which was identified by Abbott laboratories (Cool, et al., 2006). A-769662 has been reported to stimulate glucose uptake and GLUT4 translocation in L6 myotubes (Guigas, et al., 2009) (Fazakerely, et al., 2009). A-769662 lacks the off-target effects described for AICAR as it is not an AMP-analog (Viollet, et al., 2009). Further, use of this compound is discussed in (Goransson, et al., 2007).

Under serum starvation conditions, C2C12 myotubes were treated either with AICAR, or insulin-stimulated or stimulated with both in combination. C2C12 cell lysates were prepared and immuno-blotted with phospho-specific antibodies. Changes in the phosphorylation status of AMP-activated protein kinase (AMPK), its down-stream targets acetyl-CoA carboxylase (ACC) and TBC1D1 and Akt all were assessed. The basal phosphorylation levels of signalling proteins varied between experiments, even though optimised serum-starvation conditions were followed. This affected the calculated fold-change above the basal phosphorylation and induced large un-avoidable error in this ratio. The expression of AMPK was also assessed using western blotting. In addition, the

specificity of antibodies towards Rab-GAPs TBC1D1 and TBC1D4 were also evaluated (Figure 4.2).

We first determined the expression of TBC1D1 and TBC1D4 in C2C12 mouse myotubes. Western blotting with TBC1D1 02A antibody led to the detection of two distinct protein bands in C2C12 mouse myotubes at approximately 150 and 160 kDa (Figure 4.2A) (Figure 3.3, 3.2.3; Figure 3.4A, 3.2.4). Furthermore, TBC1D4 was detected in C2C12 cells migrating at the expected molecular weight ~160 kDa.

AICAR-treatment alone or in combination with insulin resulted in a marked increase in phosphorylation of AMPK at threonine 172 and the downstream kinase ACC at serine 79 (Figure 4.2A, C, D). AMPK activation resulted in an increase in the phosphorylation of TBC1D1 at serine 237 (Figure 4.2A, B). We compared the effect of a short-time exposure of AICAR for 5 min with a longer treatment for 45 min on the activation of AMPK in C2C12 cells. We did not observe a time-dependant increase in the relative phosphorylation of AMPK threonine 172, ACC serine 79 and TBC1D1 serine 237. As expected, AICAR-treatment did not increase the phosphorylation of Akt at serine 473 (Figure 4.2A, E).

Interestingly, treatment with the direct AMPK activator A-769662 did not activate AMPK in C2C12 cells. There were no detectable increases in the phosphorylation of AMPK at threonine 172, ACC at serine 79 or TBC1D1 at serine 237 over basal phosphorylation levels (Figure 4.2A). As expected, treatment with A-769662 did not increase the phosphorylation of Akt at serine 473. Recently, it has been reported that A-769662 exclusively activates β1-subunit containing AMPK hetero-trimeric complexes (Scott, et al., 2008) (Treebak, et al., 2009). Therefore it is likely that C2C12 myotubes lack or express a very low proportion of β1-containing AMPK complexes. In support of this, it has been reported that mouse skeletal muscle expresses predominately α2β2γ3 hetero-trimeric complexes (O'Neill, et al., 2011). Furthermore, no β1-containing complexes have been reported to be present in human skeletal muscle (Wojtaszewski, et al., 2005).

Insulin stimulation induced the phosphorylation of Akt at serine 473 in C2C12 cells. Furthermore, C2C12 cells stimulated with insulin and AICAR in combination did not further enhance the phosphorylation status of either AMPK or Akt (Figure 4.2).

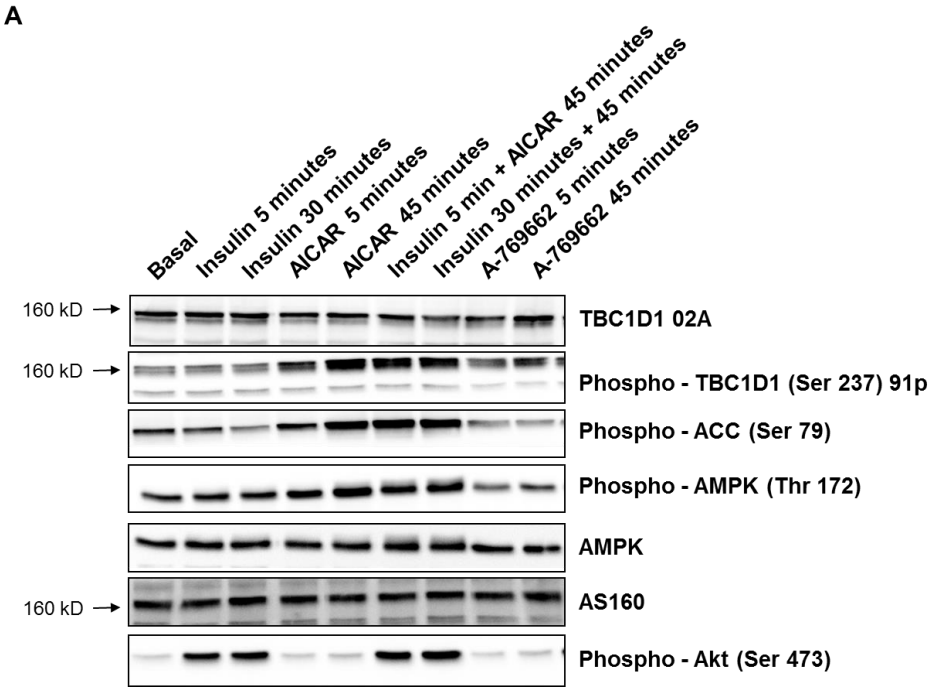

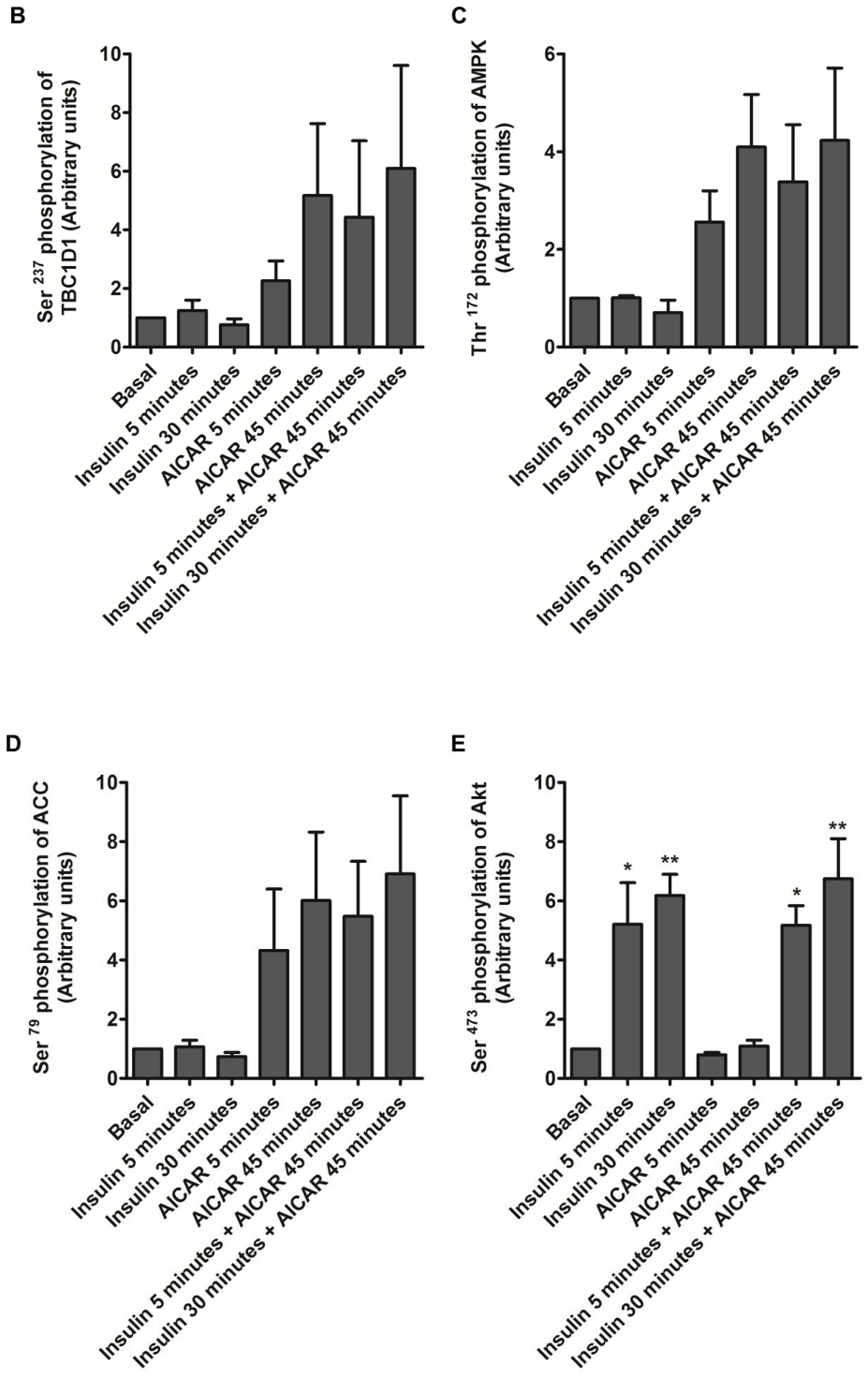

Figure 4.2: Characterisation of the signalling responses in C2C12 myotubes following insulin stimulation and/or treatment with AICAR. C2C12 myotubes were maintained under basal conditions or stimulated with insulin at 200 nM and/or treated with AICAR at 2 mM or A-769662 at 100 µM for the indicated times. (A) Representative western-blot analysis. Insulin-stimulated Akt activation was detected by blotting with anti-phospho-Akt (serine 473). AMPK-activation was assessed by immuno-blotting with anti-phospho-AMPK (threonine 172), anti-phospho-ACC (serine 79) and anti-phospho-TBC1D1 91p (serine 237). Cell lysates were immuno-blotted with anti-TBC1D1 02A, anti-AMPK and anti-AS160. Protein load: 30 µg. (B-E) Quantification analysis of phosphorylated TBC1D1 at serine 237 p=3147, AMPK at

threonine 172 p=0.0361, ACC at serine 79 p=0.0798 and Akt at serine 473 p=0.0002 respectively. Repeated measures analysis of variance (ANOVA) test was used with Tukey multiple comparison at p=0.05. * p≤0.05, ** p≤0.01.

4.2.3 Investigating the insulin-stimulated phosphorylation of Akt and TBC1D4 in C2C12 cells

C2C12 cells were serum starved and incubated in the absence or presence of insulin (200 nM) for 2 to 60 min. Cell lysates were then prepared and immuno-blotted with phospho-specific antibodies towards Akt and TBC1D4. The relative phosphorylation levels of Akt and TBC1D4 proteins were normalised to total Akt. The results were then expressed as a fold-change above basal phosphorylation levels.

Insulin increased the phosphorylation of Akt at serine 473 and TBC1D4 at threonine 642. The pattern of insulin-induced phosphorylation of Akt and TBC1D4 were similar. Peak Akt phosphorylation was reached after 5 min (26.2 ± 5.6 fold) of insulin stimulation (Figure 4.3A, B). The phosphorylation of Akt was sustained throughout the 60 min time course. Insulin induced a rapid and transient phosphorylation of TBC1D4/AS160 at threonine 642 (2-15 min), although this did not reach statistical significance. The phosphorylation of TBC1D4 returned to near basal levels within 30 min of insulin stimulation (Figure 4.3A, C).

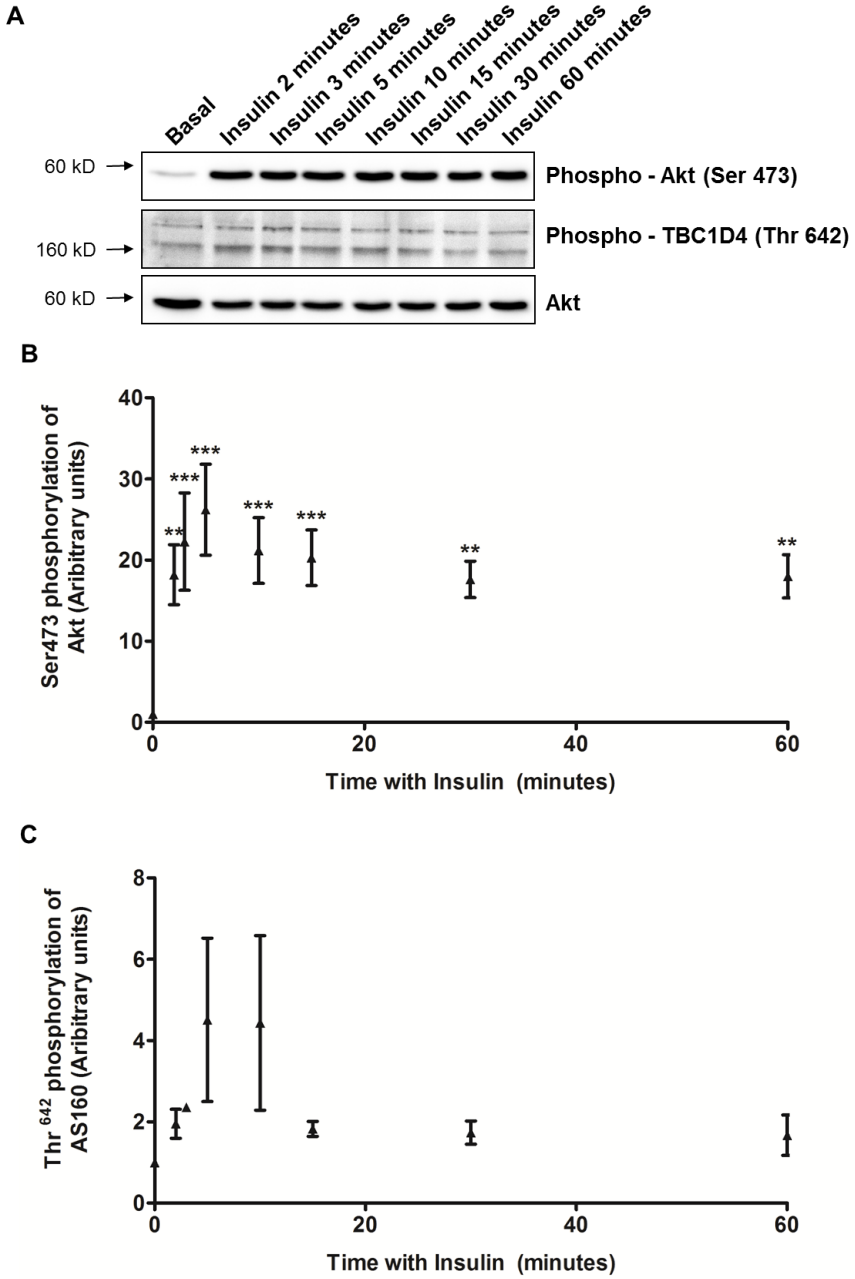

Figure 4.3: Activation of Akt and Rab-GAP TBC1D4 after insulin stimulation in C2C12 myotubes. C2C12 myotubes were maintained under basal conditions (t=0) or stimulated with Insulin at 200 nM for 2, 3, 5, 10, 15, 30 and 60 min. (A) Representative western-blot showing the time course of Akt and TBC1D4 phosphorylation using anti-phospho-Akt (serine 473) and anti-phosho-AS160 (threonine 642) antibodies respectively. (B, C) Densitometry units were normalised to total Akt protein in the sample by immuno-blotting with an anti-Akt antibody. Results are expressed relative to the basal value. Results represent the mean ± SE of 3 experiments. (B) Time course of serine 473 Akt phosphorylation. (C) Time course of threonine 642 TBC1D4 phosphorylation. Repeated measures analysis of variance (ANOVA) test was used with Tukey multiple comparison at p=0.05. ** p≤0.01, *** p≤0.005.

4.3 HA-GLUT4 trafficking assays in C2C12 myotubes

The methods developed for the studies of GLUT4 trafficking using the C2C12 muscle cell model were based on previous experiments carried out within our group in L6 muscle cells (Fazakerely, et al., 2009). The assay which were implemented are based on those developed by Govers et al, for the studies of GLUT4 trafficking in 3T3-L1 adipocytes. The aim of these studies was to analyse the trafficking kinetics of HA-tagged GLUT4 in C2C12 cells in response to insulin or AMPK activation.

C2C12 myoblasts were infected with either HA-GLUT4 (GLUT4 reporter construct containing a HA epitope tag) retrovirus (0.025 ml) or the corresponding empty vector (EV) control virus. Infected myoblasts were seeded in 96-Well plates and then differentiated for 6-8 days. C2C12 myoblasts fuse to form a heterogeneous population of multi-nucleated myotubes (Figure 3.11, 3.4.1).

In this study, AICAR was used to activate AMPK. Treatment of C2C12 cells with the direct AMPK-activator A-769662 did not induce AMPK activation (Figure 4.2A). Or increase the cell surface levels of GLUT4 above basal levels (data not shown).

4.3.1 Insulin stimulation and AMPK-activation increase cell surface GLUT4 levels; Transition experiments

C2C12 myotubes were serum-starved and incubated with either insulin (200 nM) or AICAR (2 mM) or stimulated with both in combination for 2 to 60 min. The time-dependant accumulation of GLUT4 (HA-GLUT4) at the plasma membrane was measured. HA-GLUT4 at the cell surface was determined by immuno-labelling with anti-HA antibodies. HA-GLUT4 at the cell surface was calculated as a percentage of total cellular GLUT4. Total cellular immuno-reactive GLUT4 was measured in permeabalised cells. The results were normalised to cells infected with the pBABE-puro empty vector control virus. For each experiment a minimum of three intra-assay replicates for at each time point were analysed.

The transition from the basal to the stimulated steady-state data can be fitted to a single-exponential function:

$$L(t) = (Y0 - Plateau)e^{(-kt)} + Plateau$$

The accumulation of GLUT4 at the cells surface over time is denoted by L (t). Y0 is the initial amount of GLUT4 at the plasma membrane in non-stimulated (basal) cells. The amount of GLUT4 at the plasma membrane after long agonist treatment (steady-state level) is the plateau. The rate constant for the transition from Y0 to the plateau is k. The half time for the transition ($t_{1/2}$) can be determined using $t_{1/2} = ln2/k$. The observed rate constant (k) for the transition is a function of the initial translocation of GLUT4 to the plasma membrane (k_{out}) and the rate constant for GLUT4 endocytosis (k_{en}) (Brewer et al., 2012).

In non-stimulated C2C12 myotubes, approximately 15% of the total cellular GLUT4 was present at the cell surface. Treatment with AICAR (which activates AMPK) increased the plasma membrane levels of GLUT4 in a time-dependant manner. AICAR stimulated a 2- to 3-fold increase in the level of GLUT4 transporters at the cell surface. Within 30 min a new steady-state was reached and this was maintained for at least a further 30 min (Figure 4.4A, B). AICAR stimulated the accumulation of HA-GLUT4 at the cells surface with a $t_{1/2}$ of ~7 min ($k = 0.099 \pm 0.035$ min^{-1}), fitting the transition data to a single exponential association (r^2 value: 0.610) (Figure 4.4C). The transition from basal to AICAR-stimulated steady-state was significantly slower than that measured from basal to insulin-stimulated steady-states (p=0.0068).

Insulin stimulation resulted in a rapid and transient accumulation of GLUT4 at the plasma membrane. The maximum level of cell surface GLUT4 was reached after 5 min (2- to 3-fold increase) (Figure 4.4A-C). This returned to near basal levels within 60 min after insulin stimulation. As expected, the time-course could not be accurately fitted to a one-phase association curve (r^2 value: 0.240). Therefore, just the data representing the transition from the basal steady-state to the maximum insulin-stimulated state were used, fitting a one-phase

exponential curve (r^2 value: 0.847) (Figure 4.4C). This transition occurred with a $t_{1/2}$ of ~1.24 min (k=0.559 ± 0.110 min^{-1}) (Figure 4.4D).

Finally, we investigated whether insulin and AICAR had an additive effect on GLUT4 translocation. In C2C12 myotubes, stimulation with insulin and AICAR in combination resulted in a 5-fold increase in cell surface GLUT4. The combination of insulin plus AICAR significantly increased the steady-state GLUT4 level compared with AICAR treatment alone. A new steady-state level was reached within 20 min and this remained for at least 60 min (Figure 4.4A, B). The transition from basal steady-state plasma membrane GLUT4 levels occurred with a $t_{1/2}$ of 4.7 min (k=0.148 ± 0.021 min^{-1}), fitting a single exponential curve (r^2 value: 0.899) (Figure 4.4C, D). The synergistic effect of insulin and AICAR to increase GLUT4 at the cell surface was not due to enhanced Akt or AMPK activity (Figure 4.2).

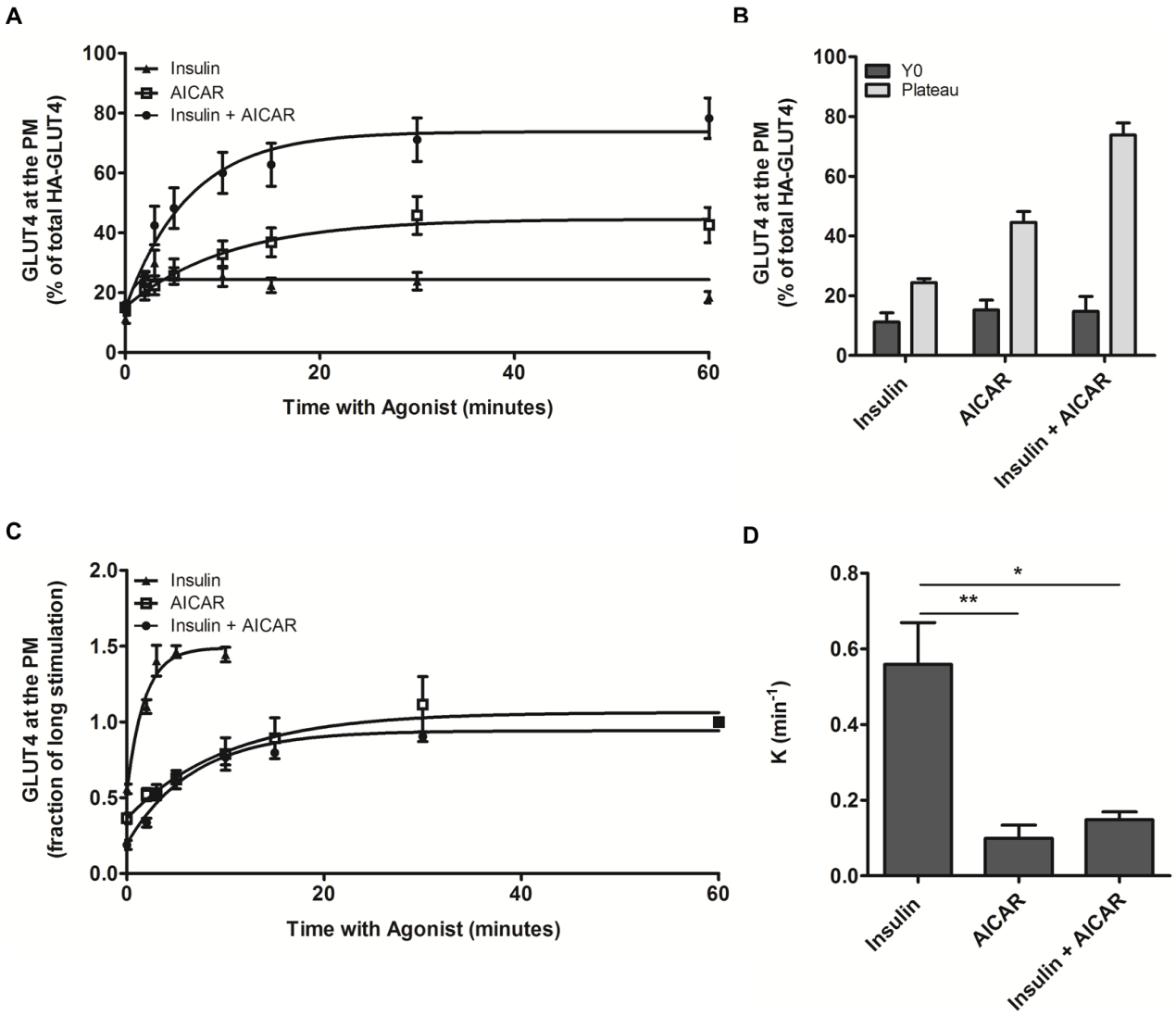

Figure 4.4: The transition of HA-GLUT4 levels from the basal to the stimulated state in C2C12 myotubes. C2C12 myotubes were maintained under basal conditions (t=0) or stimulated with insulin at 200 nM (solid triangles), AICAR at 2 mM (open squares) or insulin plus AICAR (solid circles) for 2 to 60 min. (A) The plasma membrane levels of GLUT4 were determined by incubating fixed cells with anti-HA primary antibodies and anti-mouse Alexa 488 secondary antibodies. The results are expressed as a percentage of total HA-GLUT4 in permeabilised cells. The results represent the mean + SE from 5-7 experiments. The data was fitted to a single-exponential function. (B) Cell surface levels of GLUT4 at t=0 (Y0) (dark grey bars) and at t=∞ **(**plateau) (light grey bars) were calculated from curve fitting. (C) Cell surface levels of GLUT4 were expressed as a fraction of long-time agonist stimulation. Curve fitting was performed through indicated data points. (D) Transition rate constant were determined for Insulin, AICAR and with Insulin plus AICAR in combination. Un-paired student t-test was used at p=0.05. * p≤0.05, ** p≤0.01.

4.3.2 Measuring GLUT4 recycling in C2C12 myotubes; Anti-HA antibody uptake assays.

When the transition phase from basal steady-state is over a new steady-state level of GLUT4 at the cell surface is reached, as discussed in 4.3.1. GLUT4 levels at the plasma membrane remain unchanged when the system is in steady-state. As this is a dynamic system GLUT4 at the cell surface is continually exchanging with GLUT4 within intracellular compartments. The rates at which GLUT4 moves into and out of the plasma membrane are equal. Therefore, steady-state GLUT4 trafficking kinetics can be investigated in cells stimulated with agonists. Anti-HA antibody uptake assays were developed by Govers et al, to measure the rate of HA-GLUT4 exocytosis (k_{ex}) and the size of the GLUT4 cycling pool (T) in 3T3-L1 adipocytes (Govers, et al., 2004). These were further developed to study GLUT4 traffic in L6 myotubes (Fazakerely, et al., 2009). Both of these studies used a saturating concentration of anti-HA antibodies at 50 µg/ml in order to accurately determine the GLUT4 cycling pool. To validate that this is a saturating antibody concentration in our system, anti-HA uptake assays were performed in non-stimulated C2C12 myotubes. Cells were labelled with increasing concentrations of anti-HA antibody (5-120 µg/ml) for 180 min. The labelling of HA-GLUT4 saturated at approximately 40 µg/ml of antibody. Therefore, all anti-HA antibody uptake assays were performed using a final anti-HA antibody concentration of 50 µg/ml.

Anti-HA antibody uptake assays were based on the assumption that antibody binding is instantaneous. Thus, anti-HA accumulation (uptake) over time would be a function of the rate of the exchange of GLUT4 between intracellular compartments and the plasma membrane (k_{ex}).

4.3.2.1 Analysis of anti-HA uptake curve fits

For these studies, C2C12 myotubes were serum-starved and either insulin-stimulated or treated with AICAR or treated with both in combination. In addition, some cells remained un-stimulated (basal). Subsequently, intact live cells were labelled with a saturating concentration of purified anti-HA antibody for 5 to 300 min in the continued presence of agonist. HA-GLUT4 labelled with

antibody over time was measured in permeabilised cells and calculated as a percentage of the total cellular immuno-reactive GLUT4 (Figure 4.5).

Anti-HA antibody uptake data can be fitted to a one-phase non-linear regression (single-exponential equation):

$$L(t) = (P - T)e^{-k_{ex}t} + T$$

This model is based on the assumption that GLUT4 is trafficked to the plasma membrane from one intracellular compartment. This is an over-simplification as many GLUT4 compartments are likely to contribute to the overall GLUT4 trafficking rates. However, we can use this model to estimate several steady-state kinetic parameters.

The accumulation of labelled GLUT4 over time is denoted by L (t). P is the initial plasma membrane level of GLUT4 at Y0. The total amount of the GLUT4 pool which is actively recycling with the plasma membrane is T. The rate constant for GLUT4 exocytosis at steady-state is k_{ex}. The half time ($t_{1/2}$) can be determined using $t_{1/2} = ln2/k_{ex}$.

The analysis of P values from the one-phase non-linear regression analysis of anti-HA uptake data revealed that approximately 10% of the total cellular GLUT4 was present at the cell surface in non-stimulated C2C12 myotubes (Figure 4.5C). This result was consistent with the result measured from the transition experiments (Figure 4.4A, B). However, in cells treated with insulin or AICAR the P fit parameter values inferred from these curve-fits were not significantly different to non-stimulated cells (Figure 4.5C). This is in contrast to the transition data analysis which revealed that stimulation with insulin or AICAR resulted in a ~2- to 3-fold increase in GLUT4 at the plasma membrane. In addition, a ~5 fold increase of cell surface levels of GLUT4 was observed in cells stimulated with insulin and AICAR in combination (Figure 4.4A, B).

The standard error (SE) values for the P and k_{ex} fit parameters were >20% of the predicted values, indicating large variation within the data sets. In addition, the r^2 of the fits were low which suggested that a single exponential function

may not be the most appropriate. However, the data could not be fitted to a two-phase non-linear regression (multiple exponential treatments). Conversely, the SE values for the T fit parameter were less than 5 % of the predicted values.

4.3.2.2 Insulin stimulation and AICAR-treatment increase the size of the GLUT4 cycling pool

In non-stimulated (basal) C2C12 myotubes, 64% of the total cellular GLUT4 is actively recycling with the plasma membrane within 300 min (Figure 4.5A, B). This was increased with insulin stimulation and AICAR-treatment to 75% and 78%, respectively. In C2C12 cells, stimulation with insulin and AICAR in combination further increased the amount of GLUT4 recycling with the cell surface to 85%. However, insulin and AICAR treated in combination did not significantly increase the amount of GLUT4 that is actively recycling compared with AICAR-treatment alone. In addition, the estimated values indicated that not all of the GLUT4 available actively recycles with the plasma membrane. There appears to be a residual ‘latent GLUT4 pool’ that remains within intracellular compartments, which is not mobilised in response to insulin stimulation or treatment with AICAR.

In cells stimulated with insulin, the total amount of GLUT4 in the recycling system reached maximum levels within 150 min. Conversely, in non-stimulated cells or cells treated with AICAR alone, the maximum level of GLUT4 in the recycling system was reached within approximately 200 min.

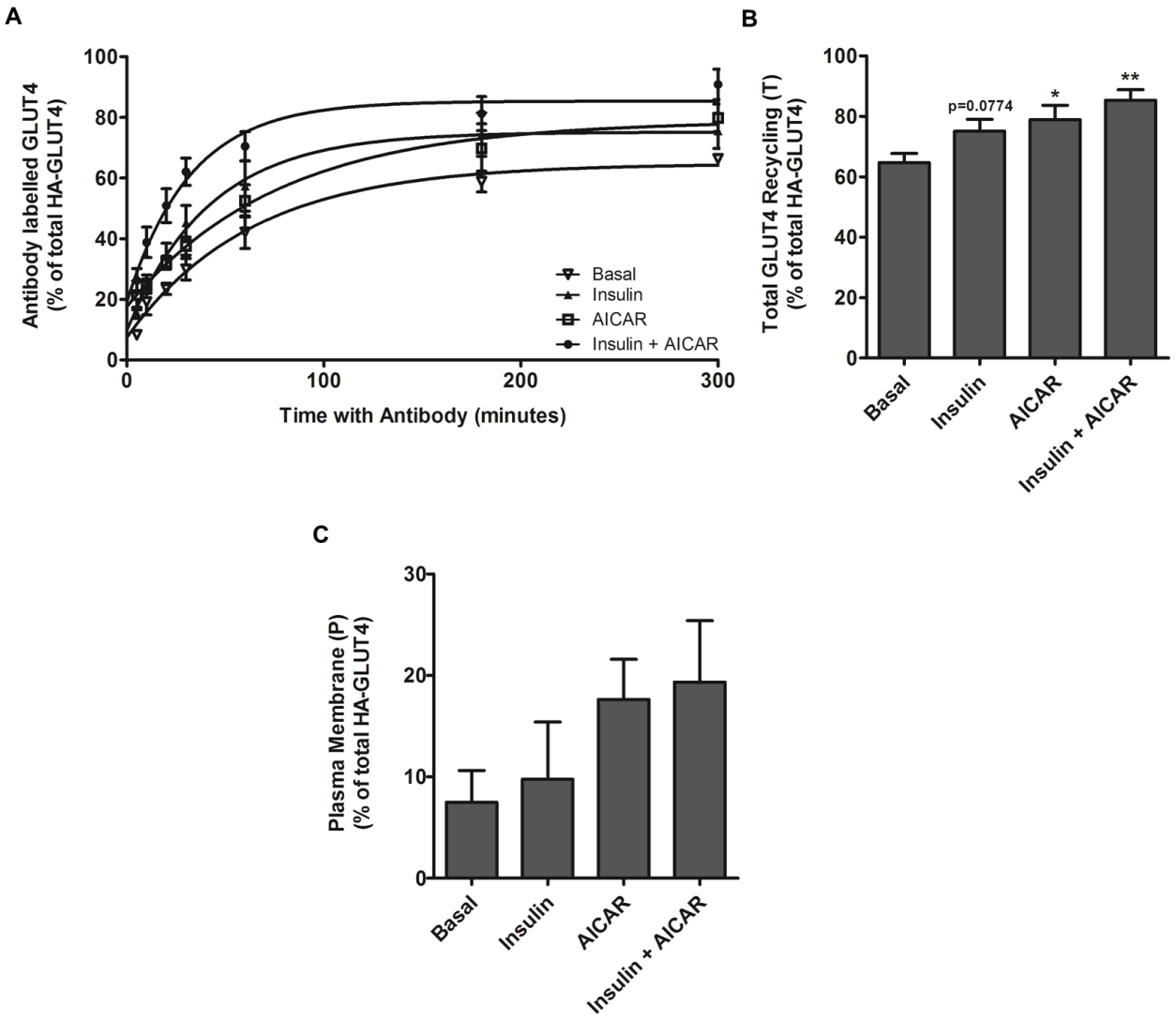

Figure 4.5: Time courses of anti-HA antibody labelling of the actively recycling GLUT4 pool in live C2C12 myotubes. C2C12 myotubes expressing HA-GLUT4 were maintained in basal conditions (open inverted triangles) or either stimulated with insulin at 200 nM (solid triangles) or AICAR at 2 mM (open squares) or insulin plus AICAR in combination (solid circles) for indicated times to reach maximum GLUT4 cell surface levels, then incubated with 50 µg/ml of anti-HA antibody for 5-300 min at 37°C, in the continued presence of agonist. The cells were fixed, permeabilised and incubated with anti-mouse Alexa 488 secondary antibody. (A) Results are calculated as a percentage of the total cellular immuno-reactive HA-GLUT4. Results represent the mean + SE of four non-paired experiments. A one-phase non-linear regression curve was fitted to determine kinetic parameters. (B) The total amount of the GLUT4 pool which is actively recycling with the plasma membrane (T) (C) The initial plasma membrane level of GLUT4 at Y0 (P). Un-paired student t-test was used at p=0.05. * p≤0.05 ** p≤0.01.

4.3.2.3 Insulin stimulates GLUT4 exocytosis

Anti-HA antibody data for each condition was expressed as a fraction of the maximum amount of GLUT4 labelled within 300 min in order to infer a more accurate estimation of the rate of GLUT4 exocytosis (k_{ex}) at steady-state (Figure 4.6A). The SE values for the k_{ex} parameter were <15% of the predicted value and the r^2 for the curve-fits were improved to >0.90 in all cases.

In basal C2C12 myotubes, we observed an exocytosis rate constant (k_{ex}) of 0.016 ± 0.003 for GLUT4 ($t_{1/2}$ of ~40 min) (Figure 4.6B). Insulin stimulates a relatively small increase in the k_{ex} for GLUT4 to 0.023 ± 0.003 ($t_{1/2}$ of ~30 min). In contrast, AICAR slightly decreased k_{ex} for GLUT4 to 0.013 ± 0.002 ($t_{1/2}$ of ~50 min). Interestingly, the exocytosis rate constant (k_{ex}) for GLUT4 was 2-fold higher in cells treated with insulin and AICAR in combination (k_{ex} 0.031 + 0.005, $t_{1/2}$ ~20 min) compared with basal cells (Figure 4.6A).

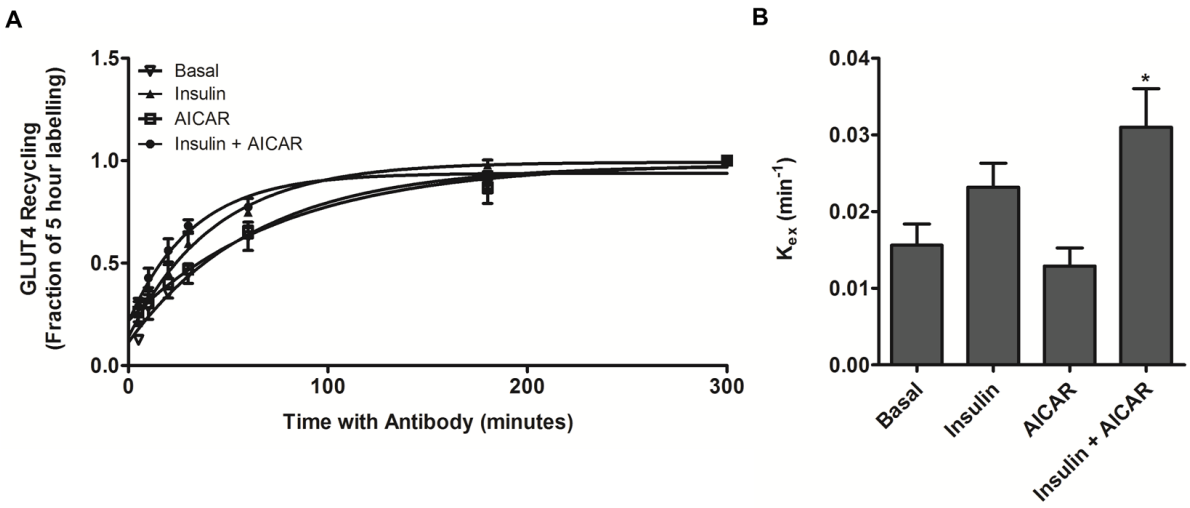

Figure 4.6: Kinetic parameters of anti-HA antibody labelling surface GLUT4 in C2C12 myotubes. C2C12 myotubes expressing HA-GLUT4 were maintained in basal conditions (open inverted triangles) or either stimulated with insulin at 200 nM (solid triangles), AICAR at 2 mM (open squares) or insulin plus AICAR in combination (solid circles) for indicated times to reach maximum surface GLUT4 levels, then incubated with anti-HA antibody (final concentration of 50 µg/ml) for 5-300 min at 37°C in the continued presence of agonist. The cells were fixed, permeabilised and incubated with anti-mouse Alexa 488 secondary antibody. (A) Results are calculated as a percentage of the total cellular immuno-reactive HA-GLUT4. Results represent the mean + SE from four experiments. A one-phase non-linear regression curve was fitted to determine kinetic parameters. (B) The exocytosis rate constant (k_{ex}) for GLUT4 was measured. Un-paired student t-test was used at p=0.05. * p≤0.05.

4.3.2.4 AMPK-activation inhibits GLUT4 endocytosis

In the current study the effect of agonist treatment on the rate of GLUT4 endocytosis at steady-state was not directly measured. However, as the system is in steady-state, the rate at which GLUT4 appears at and is retrieved from the plasma membrane is balanced. Therefore, the rate constant for GLUT4 endocytosis (k_{en}) can be estimated using parameters derived from the uptake data.

$$k_{en} = \frac{k_{ex}\,(T - P)}{P} \qquad or \qquad k_{en} = \frac{k_{ex}}{P}$$

Where (T-P) is the proportion of cycling GLUT4 pool in intracellular compartments and P is the proportion of GLUT4 at the plasma membrane and k_{ex} is the rate constant for exocytosis at steady-state (Coster, et al., 2004). This can be simplified and written where *P* which equals the partitioning co-efficient. *P*=(P/(P-T))

Using this model we found that insulin stimulation alone increased the endocytic rate constant (k_{en}) for GLUT4 (k_{en} ~0.112 min^{-1} for basal to ~0.150 min^{-1} for insulin-stimulated cells). In contrast, AICAR-treatment alone led to a reduction in k_{en} to ~0.047 min^{-1}. However, the k_{en} for GLUT4 was only slightly reduced in cells treated with insulin and AICAR in combination compared to basal cells (~0.106 min^{-1}).

The SE values for the P fit parameter derived from the anti-HA uptake data indicated that there were large variations within the data sets at early time points. Furthermore, the most striking observation was the amount of GLUT4 at the cell surface (P) in cells treated with either insulin or AICAR derived from the curve fits, were not significantly different to basal cells. Therefore, we are underestimating the proportion of GLUT4 at the plasma membrane and subsequently underestimating *P*. Therefore leading to an over estimation for $k_{en.}$

4.3.2.5 The labelling efficiency of anti-HA antibody

When anti-HA antibody uptake data was expressed as a percentage of total cellular immuno-reactive GLUT4, large variability was observed between the repeated data-sets, this was particularly evident within the early time points (Figure 4.5A, C). The accuracy and reliability of kinetic parameter estimations depends on the curve-fits to the data especially within the early time points, which is further discussed in 4.3.2.1.

All uptake assays were carried out using a final concentration of anti-HA antibody at 50 µg/ml. This was determined experimentally as a saturating antibody concentration required to label the entire GLUT4 cycling pool within 180 min.

Anti-HA antibody uptake assays are based on the assumption that antibody binding is instantaneous. Thus, the concentration of antibody is sufficient to label all of the GLUT4 at the plasma membrane. We therefore wanted to test this to determine whether the entire plasma membrane pool can be labelled at shorter incubation times with a final concentration of anti-HA antibody at 50 µg/ml.

C2C12 myotubes were serum starved and then either maintained under basal conditions or insulin-stimulated. Subsequently, intact live cells were labelled with increasing concentrations of purified anti-HA antibody (36-120 µg/ml) for 5 and 180 min in the continued presence of agonist. The results are represented as a percentage of the GLUT4 labelled with maximum antibody concentration tested.

Our data confirmed that the minimum concentration of purified anti-HA antibody required to saturate the labelling of surface GLUT4 was between 36-50 µg/ml during 180 min of labelling (Figure 4.7). This was observed for cells maintained in basal conditions or cells stimulated with insulin. However, incubating cells for just 5 min with saturating concentration of antibody, only labelled a fraction of the GLUT4 present at the cell surface. Antibody concentrations below 120 µg/ml

(maximum tested), labelled significantly lower levels of GLUT4. Similar antibody dose response values were observed in basal and insulin-stimulated cells.

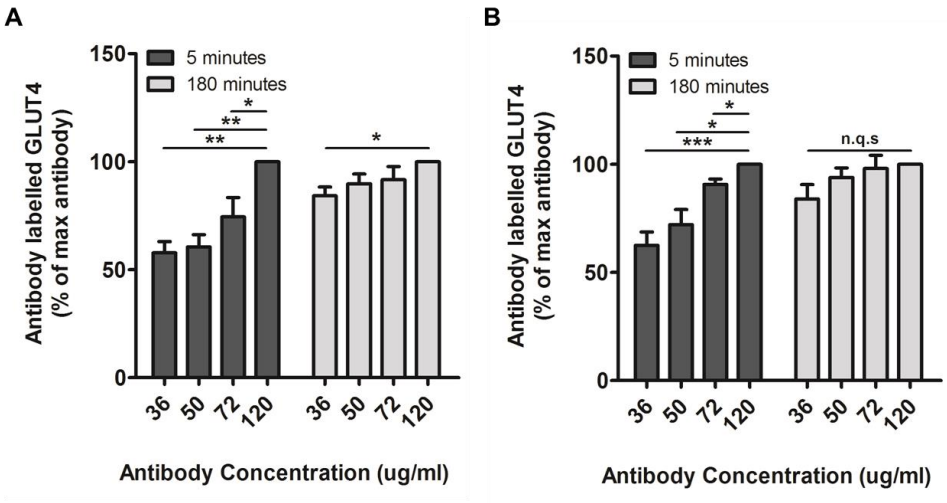

Figure 4.7: Labelling efficiency of cell surface HA-GLUT4 at short incubation time points is dependent on anti-HA antibody concentration. C2C12 myotubes were maintained in basal conditions (A) or stimulated with Insulin at 200 nM for 5 min (B). Cells were incubated with increasing concentrations of anti-HA antibodies (36-120 µg/ml) for 5 (dark grey bars) or 180 min (light grey bars) at 37°C. Cells were then fixed, permeabilised and incubated with anti-mouse Alexa 488 secondary antibody. Results are calculated as a percentage of the total HA-GLUT4 available and expressed as a percentage of the 120 µg/ml values. Results represent the mean ± SE from 3-4 experiments. Repeated measures analysis of variance (ANOVA) test was used with Tukey multiple comparison at p=0.05. * p≤0.05, ** p≤0.01. *** p≤0.005.

4.4 Discussion

There have been many technical challenges which have impeded the detailed kinetic analysis of endogenous GLUT4 trafficking in primary skeletal muscle. Therefore, the C2C12 cell culture model provides an alternative *in vitro* model system. These cells can be readily sourced and easily manipulated and so have great potential for industry applications. In this chapter we have optimised a 96-Well plate assay to investigate GLUT4 trafficking in C2C12 myotubes. We provide evidence for the use of C2C12 myotubes as a model system to measure the kinetics of GLUT4 trafficking in response to insulin and contraction-mediated signalling. Our findings support current concepts that insulin stimulates the rapid release of GLUT4 to the plasma membrane. Interestingly, the effect of insulin alone to increase cell surface GLUT4 levels was transient. In addition, treatment with the AMPK-activator, AICAR stimulates the slow accumulation of GLUT4 at the cell surface through the inhibition of GLUT4 endocytosis. Of importance, we have shown that the combination of AICAR and insulin treatments was synergistic to increase GLUT4 at the plasma membrane and the combined treatment significantly increases the rate of GLUT4 exocytosis (k_{ex}) at steady state. These findings support the presence of more than one distinct intracellular GLUT4 pool and provides evidence that multiple and complex mechanisms exist to enhance glucose disposal in muscle cells.

In the basal to agonist transition experiments, the exponential rise of cell surface GLUT4 can be measured over time. In C2C12 myotubes, insulin stimulation resulted in a rapid and transient 2- to 3–fold accumulation of GLUT4 at the plasma membrane (k ~0.559, $t_{1/2}$ ~1.2 min) (Figure 4.4). Subsequently, cell surface GLUT4 levels rapidly declined and returned to near steady-state basal levels within 15 to 30 min after insulin stimulation. Similarly, insulin has been found to stimulate a rapid 2- to 3-fold increase in GLUT4 at the cell surface in L6 myotubes expressing HA-GLUT4 ($t_{1/2}$ ~1.2 min) (Fazakerely, et al., 2009). Furthermore, comparable transition response kinetics, have been observed in L6 myotubes stably expressing Myc-tagged GLUT4 ($t_{1/2}$ ~2.5 min)

(Somwar, et al., 2001). However in contrast to C2C12 cells, within 10 min a new steady-state level of cell surface GLUT4 is reached.

A similar insulin-stimulated 'overshoot' of cell surface GLUT4 expression has been reported in several studies in both 3T3-L1 fibroblasts (Govers, et al., 2004) (Bogan, et al., 2001) and 3T3-L1 adipocytes (Zeigerer, et al., 2002) (Bogan, et al., 2001) (Huang, et al., 2005). However, in 3T3-L1 cells an insulin-dependent biphasic response is observed. Generally, studies in 3T3-L1 cells report that insulin stimulates a pronounced 5- to 12-fold increase in GLUT4 at the plasma membrane. After the initial transient peak in cell surface GLUT4 over basal levels, cell surface levels reduce (approximately 30-40%) and a new insulin-stimulated steady-state level is reached. It has been proposed that this 'transient overshoot' corresponds with the mobilisation of GLUT4 from highly insulin-responsive vesicles which are rapidly depleted upon insulin addition (Bogan, et al., 2001). The initial GLUT4 exocytosis rate during the transition is greater than the rate of GLUT4 exocytosis at steady-state. GLUT4 exocytosis at steady-state is rate-limited at steps during its trafficking through endosomal recycling compartments. This mechanism of action is similar to one that has been proposed to describe first-phase insulin secretion from pancreatic β-cells. This results from the rapid fusion of insulin granules present in a readily releasable pool (RRP) that are pre-docked at the cell surface (Wang & Thurmond, 2009). Recently, TIRF-imaging of HA-GLUT4-GFP has been used to characterise the dynamics of GLUT4 trafficking in live muscle fibres from transgenic mice. Interestingly, it was discovered that the majority of GLUT4 exocytic events at the plasma membrane in response to insulin stimulation in muscle were from the fusion of pre-tethered GLUT4 vesicles rather than the recruitment and tethering of GLUT4 vesicles from intracellular cell depots (Lizunov, et al., 2012). Therefore, from our present results it seems reasonable to conclude that C2C12 myotubes appear to possess a small insulin-responsive GLUT4 compartment. In support of this, the insulin-regulated amino peptidase (IRAP) is up-regulated during differentiation of C2C12 myotubes. IRAP is a major constituent of GLUT4 storage vesicles (Malide, et al., 1997) (Kandror, et al., 1995). The insulin-stimulated transient accumulation of GLUT4 at the cell surface in C2C12 myotubes could be the result of the rapid exocytosis of a pool

of fusion-ready GLUT4 vesicles. However, C2C12 cells lack other mechanisms which regulate the robust insulin-stimulated increase in cell surface GLUT4 levels as demonstrated in 3T3-L1 cells. Additionally, C2C12 cells appear to lack efficient pathways which control the steady-state level of cell surface GLUT4 present in other insulin-responsive cells.

Our present findings are in contrast to an earlier study which reported that GLUT4 is not targeted to an insulin-sensitive compartment in C2C12 myotubes (Tortorella & Pilch, 2002). For this study the investigators treated C2C12 cells with dexamethasone to induce GLUT4 gene expression. Sub-fractionation based experiments were used to determine GLUT4 translocation from a low-density microsomal fraction (LDM) to a plasma membrane fraction upon insulin stimulation. However, only a single time-point measurement for insulin (15 min) was analysed. Based on our data, insulin stimulation for 15 min would be too long and the initial peak in insulin-stimulated cell surface GLUT4 would have been overlooked.

Several studies have reported that insulin stimulation results in only a small increase in glucose uptake in C2C12 cells (1.2- to 1.5-fold) (Kumar & Dey, 2002) (Niu, et al., 2010) (Tortorella & Pilch, 2002). The lack of insulin-stimulated glucose uptake could be due to a deficiency of endogenous GLUT4 expression or the transient presence of GLUT4 at the cell surface. It has been reported that there is a time delay between the presence of GLUT4 at the cell surface and 2-deoxyglucose uptake in L6 muscle cells (Somwar, et al., 2001). The transient (2- to 3-fold) increase in cell surface GLUT4 would be too rapid and as a consequence a similar increase in glucose transport would not be measured. Conversely, a possible explanation could be that the presence of GLUT4 at the cell surface is masked by the action of other glucose transporters. For example, GLUT1 and GLUT3 are expressed at different stages of muscle cell differentiation (Yamamoto, et al., 2008).

Using anti-HA antibody uptake assays, the GLUT4 steady-state recycling kinetics can be measured. By using this experimental method two separate effects on GLUT4 exocytosis (the size of the actively recycling GLUT4 pool and

the intrinsic rate of cycling (k_{ex})) can be determined (Brewer, et al., 2011). We found that ~85% of the insulin-stimulated steady-state pool (64% of the total GLUT4 pool) is actively recycling with the plasma membrane in non-stimulated C2C12 myotubes (Figure 4.5). This result is in agreement with previous data described in L6 myotubes expressing HA-GLUT4 (Fazakerely, et al., 2009). Together these findings suggest that differentiated muscles cells possess a small GLUT4 pool ~15% of the insulin-stimulated GLUT4 pool (~21% of the total pool) that is statically retained/sequestered away from the general endosomal recycling pathway (ERC) in the absence of insulin.

The concept of GLUT4 'static retention' was first reported in studies using confluent quiescent 3T3-L1 adipocytes (Govers, et al., 2004) (Coster, et al., 2004) (Muretta, et al., 2008). However, in 3T3-L1 cells only ~15-25% of the insulin-stimulated GLUT4 recycling pool (~10-15% of the total GLUT4 pool) is actively engaged in recycling with the plasma membrane in adipocytes under basal conditions. The majority of GLUT4 is sequestered within specialised 'non-cycling/slow cycling' GLUT4 storage vesicles (GSVs). This retention mechanism in part is responsible for maintaining the low cell surface GLUT4 levels in the absence of insulin. Conversely, McGraw and colleagues have shown that GLUT4 retention is exclusively regulated by a 'dynamic-recycling' mechanism in 3T3-L1 adipocytes (Martin, et al., 2006) (Karylowski, et al., 2004). These studies have observed that over-time the total 'insulin-responsive' GLUT4 pool can access the plasma membrane in the absence of insulin. The GLUT4 storage compartment is continually recycling with the general ERC, albeit very slowly. However, Muretta et al., discovered that the lifting and re-plating of confluent differentiated 3T3-L1 adipocytes (as performed in Martin et al, for microscopy based studies) has been shown to increase the size of the basal GLUT4 recycling pool (Muretta, et al., 2008). The exact mechanism for this dramatic effect on GLUT4 recycling is yet to be determined. However, it is possible that re-plating of 3T3-L1 cells affects adipogenic differentiation. In support of this, Govers et al. observed that the 'static retention' mechanism is acquired during adipocyte differentiation. Furthermore, direct analysis of GLUT4 dynamics using quantum dot technology has revealed that the majority of GLUT4 (64%) is present within a stationary GLUT4 compartment in

differentiated 3T3-L1 basal cells and this is absent in fibroblasts (Fujita, et al., 2010). Although, this study revealed that 'replating' 3T3-L1 adipocytes did not affect GLUT4 stationary behaviour. Further support for the 'dynamic recycling' model comes from experimental studies carried out in L6 myoblasts stably expressing Myc-tagged GLUT4 (Foster, et al., 2001). These findings suggest that un-differentiated myoblasts may not possess a 'statically retained' GLUT4 compartment that has been proposed here for differentiated muscle cells.

Fundamental differences between adipose and muscle may explain the substantial; GLUT4 'static retention' in 3T3-L1 adipocytes compared with in muscle cell lines. However, it is more likely that L6 and C2C12 myotubes do not recapitulate the complex mechanisms which regulate GLUT4 trafficking as L6 and C2C12 muscle cells do not fully differentiate. Compared to mature muscle fibres, skeletal muscle cell lines do not develop mature sub-cellular compartments or establish full contractile activity. Mature transverse (T) - tubules (an important site for glucose uptake in muscle) are only partially formed in differentiated C2C12 cells and are deficient in L6 myotubes (Rudich & Klip, 2003). Furthermore, both L6 and C2C12 skeletal muscle cell lines express low endogenous levels of GLUT4 and exhibit reduced insulin-responsive glucose uptake compared to primary muscle (1.5- to 2-fold in muscle cells compared with 3- to 9-fold in primary muscle) (Kramer, et al., 2006) (Karlsson, et al., 2009).

In this study we have highlighted an important technical issue associated with the anti-HA antibody uptake assay as a model for studying GLUT4 recycling. The model assumes that antibody binding is instantaneous. Therefore, anti-HA accumulation (uptake) over time would be a function of GLUT4 exocytosis (k_{ex}). However, this can only true if antibody accumulation is not dependent on antibody concentration. We report here that an antibody concentration of 50 µg/µl (which is a saturating antibody concentration required to label the entire GLUT4 cycling pool within 180 min) is insufficient to label the entire GLUT4 pool at the plasma membrane in 5 min. Therefore, it appears that antibody accumulation is a function of both antibody binding and the rate for GLUT4 exocytosis (k_{ex}). As a consequence, it is important to note that this model may

not accurately determine the true exocytosis rate constant for GLUT4 at steady-state. However, we did not directly measure whether the rate of antibody accumulation was dependant on antibody concentration. Furthermore, the accuracy of the curve-fits to the data especially within the early time points is required for the correct estimation of P (the initial plasma membrane level of GLUT4 at Y0). The correct value for P is necessary for calculating the partitioning coefficient (*P).* This is a ratio between GLUT4 at the cell surface and GLUT4 within intracellular pools at steady-state. Therefore, a correct partitioning coefficient (*P*) is required for the accurate estimation of the rate for GLUT4 endocytosis (k_{en}).

In C2C12 cells, we have found that in addition to increasing the size of the GLUT4 recycling pool (64% to 75%), insulin-stimulated a slight increase in the steady-state exocytic rate constant (k_{ex}) ~1.5-fold, from 0.016 to 0.023 min^{-1} (half-time ~30 min) (Figure 4.6). However, the effect of insulin on steady-state GLUT4 recycling kinetics was unable to sustain plasma membrane GLUT4 levels. In 3T3-L1 adipocytes expressing HA-GLUT4, insulin has been shown to stimulate a similar modest increase in k_{ex} for GLUT4 from 0.014min^{-1} to 0.03 min^{-1} (Govers, et al., 2004) (Coster, et al., 2004). This is further supported by Mastick and colleagues who have observed a similar effect of insulin on the rate of anti-HA antibody uptake (k_{obs}) (0.012 min^{-1} basal to 0.036 min^{-1} insulin-stimulated) (Muretta, et al., 2008). However, in these studies insulin was found to regulate the release of a large pool of GLUT4 from a ‘static’ storage compartment in to the general recycling pathway, thus, substantially increasing cell surface GLUT4 levels. It has been proposed that the release of GLUT4 from a retention compartment is the major rate-limiting step for GSV translocation in 3T3-L1 adipocytes (Brewer, et al., 2011) (Xu, et al., 2011). Therefore, the lack of a substantial GLUT4 storage compartment may account for the inadequate transition from basal to insulin-stimulated steady-states in C2C12 myotubes. Conversely, in other studies insulin elicits a greater fold increase in the intrinsic steady-state GLUT4 exocytic rate (k_{ex}). In 3T3-L1 adipocytes, Mcgraw and colleagues have shown that insulin markedly increases k_{ex} for GLUT4 ~7-13 fold from 0.006-0.007 min^{-1} to 0.05-0.08 min^{-1}. Furthermore, insulin significantly inhibited k_{en} (Karylowski, et al., 2004) (Martin, et al., 2006). In this ‘dynamic

retention' model, insulin solely regulates the rate of GLUT4 movement between the intracellular compartments and the plasma membrane. The action of insulin to stimulate GLUT4 exocytic pathways is consistent with earlier studies in both primary muscle and adipose cells. In rat muscle, insulin stimulation has been shown to markedly increase GLUT4 exocytosis rate (k_{ex} 0.01 to 0.067 min^{-1}) (Karlsson, et al., 2009). Similarly, insulin stimulates an increase in k_{ex} (0.01 to 0.086 min^{-1}) in primary adipocytes (Jhun, et al., 1992). However, in these systems the effect of insulin on the release of GLUT4 from storage compartment to increase the total amount of GLUT4 which is able to recycle with the cell surface could not be measured.

In this study the observed rate constant that is calculated from the single exponential fitting of anti-HA antibody uptake data is assumed to be a measure of k_{ex}. This is interpreted based on a 'two pool' model (Holman, et al., 1994) (Figure 1.4, 1.3.2.6). This model assumes that GLUT4 is trafficked between an intracellular compartment and the plasma membrane as one kinetic pool. However, it is likely that multiple pools contribute to the overall GLUT4 trafficking kinetics. For instance the rapid transition kinetics in response to insulin stimulation and the slower recycling kinetics at steady-state can only be explained based on a multiple-pool model (Muretta, et al., 2008). Furthermore, the current intracellular retention models propose that there at least two intracellular pools of GLUT4 (Figure 1.4, 1.3.2.6). In support of this, it has been recently observed that after acute insulin stimulation (3-6 min), GLUT4 is predominately carried on smaller vesicles (50 nm) (GSVs) which translocate to the cell surface in 3T3-L1 adipocytes. Insulin stimulates the release of specialised GSVs which are sequestered in basal cells. In addition, insulin promotes the exocytosis of a pool of fusion-competent vesicles at the cell surface. However, during continued insulin stimulation typically larger GLUT4 vesicles (150 nm) translocate to the plasma membrane. These vesicles are identical to those which transport TfR (Xu, et al., 2011). Therefore, it has been proposed that insulin also functions to switch GLUT4 traffic between two distinct circuits. This model for insulin-stimulated GLUT4 translocation has been named the dual brake-accelerator model and is depicted in Figure 4.8 (Xu, et al., 2011).

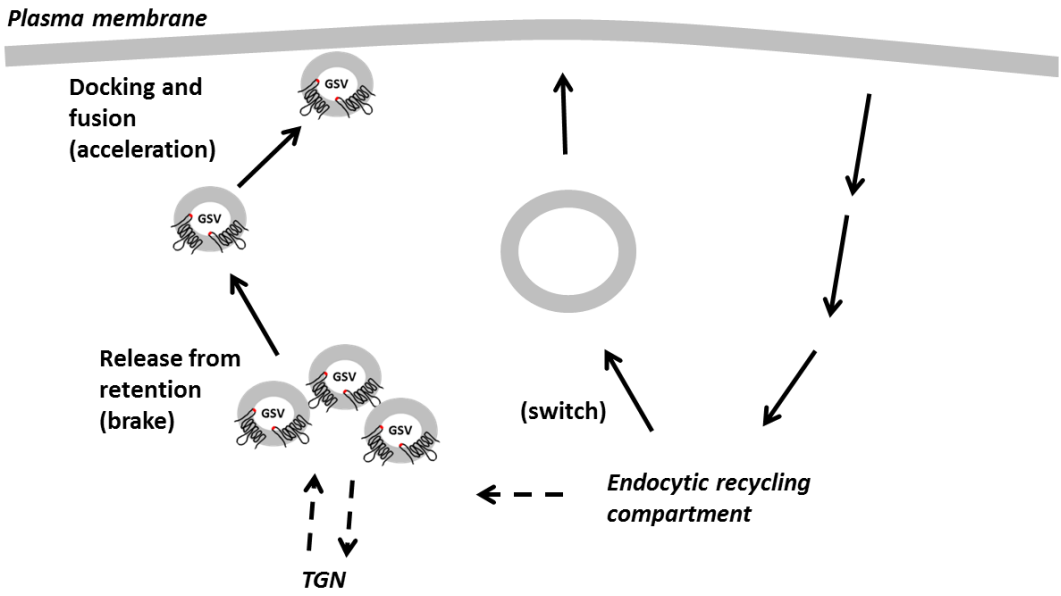

Figure 4.8: The dual brake-accelerator model for insulin-stimulated GLUT4 translocation. This schematic has been adapted from (Xu, et al., 2011). Insulin mediates the release of GLUT4 from an intracellular retention pool (brake) and stimulates the exocytosis of a fusion-ready pool of GSVs at the cell surface (acceleration). During continual insulin stimulation GLUT4 is trafficked to the plasma membrane on larger vesicles which bypass the GSV compartment. Insulin regulates the switching of GLUT4 traffic between two cycles.

The dual brake-accelerator model unites the static retention and dynamic recycling models which describe basal intracellular GLUT4 retention. Our experimental data support the presence of a small insulin-responsive GSV compartment in C2C12 myotubes. Therefore are consistent with an accelerator mode of insulin action. However, our results revealed that C2C12 cells lack a substantial GSV retention compartment. The release of an intracellular brake is essential for a robust insulin-stimulated response in 3T3-L1 adipocytes. Interestingly, the removal of this brake through the knockdown of TUG (a protein which is required for GSV intracellular retention) resulted in only a transient 2-fold pulse of GLUT4 exocytosis in 3T3-L1 adipocytes in response to insulin stimulation (Xu, et al., 2011). These results were remarkably similar to what we have reported here in C2C12 myotubes.

In the current study the effect of insulin stimulation on the rate of GLUT4 endocytosis (k_{en}) was not determined experimentally. However, we cannot rule out this as a site of insulin action. Several reports in 3T3-L1 adipocytes (Martin, et al., 2006) (Yang & Holman, 1993) and rat adipocytes (Jhun, et al., 1992)

have reported that insulin reduces the rate constant for GLUT4 endocytosis (k_{en}). In L6 myotubes it has been reported that the predominant effect of insulin was on the inhibition of GLUT4 endocytosis (k_{en} ~0.4 min^{-1} to 0.2 min^{-1}) as opposed to stimulating GLUT4 exocytosis (k_{ex} ~0.06 min^{-1} to 0.07 min^{-1}) (Fazakerely, et al., 2009). Although, in contrast to other kinetic studies in this L6 cell system the rate for GLUT4 recycling was very fast under basal conditions. Conversely, studies in 3T3 L1 adipocytes (Govers, et al., 2004). L6 myoblasts (Foster, et al., 2001) and rat cardiomyocytes (Yang & Holman, 2005) have observed that insulin has little effect on the rate of GLUT4 internalisation.

It is well established that exercise is important and beneficial for overall fitness, body weight and for the management of T2DM, in part through the activation of metabolic processes which increase glucose uptake into skeletal muscle (Defronzo, et al., 1981). Importantly, exercise-mediated GLUT4 translocation appears normal in people with type II diabetes despite impaired insulin responses (Zierath, et al., 1997). Therefore, it is of importance to investigate the effect of contraction-mediated stimuli in the regulation of GLUT4 trafficking in muscle. Although the AMP-mimetic (AICAR) activates AMPK, it is important to note that AICAR does not recapitulate the full extent of contraction-induced responses. AICAR-mediated glucose uptake is impaired in skeletal muscle from AMPK-α_2 knockout (AMPK-α_2 KO) although contraction-stimulated glucose uptake is not affected (Jorgensen, et al., 2004). However, AICAR is a useful tool to study the role of AMPK-signalling in regulating GLUT4 trafficking. Furthermore, numerous studies have reported additive effects of both AMPK-activators and insulin on glucose uptake and/or GLUT4 translocation in to muscle (Hayashi, et al., 1998) (Yang & Holman, 2005) (Yang & Holman, 2006) (Bergeron, et al., 1999).

In this present study, we find that AICAR stimulates a maximal 2- to 3-fold increase in the level of GLUT4 transporters at the cell surface in C2C12 cells (basal to AICAR steady-state transition rate k ~0.099 min^{-1}, $t_{1/2}$ ~7 min) (Figure 4.4). The magnitude of the effect of AICAR treatment on cell surface GLUT4 levels is comparable with data previously reported for C2C12 myotubes (Niu, et al., 2010), L6 myotubes (Fazakerely, et al., 2009) (Sajan, et al., 2010) and in

isolated primary skeletal muscle (Koistinen, et al., 2003). Furthermore, the accumulation of cell surface GLUT4 is slow and reaches maximum levels 30 min after AICAR-treatment. This is in contrast to when cells are stimulated with insulin (insulin stimulates a rapid and transient increase in GLUT4 at the cell surface). The increase in AMPK-phosphorylation in response to AICAR treatment is comparable at 5 and 45 min. Therefore, the slow response is not due to a slow onset of AMPK activation. We find that the exocytic rate constant for GLUT4 does not increase above basal levels following treatment with AICAR (k_{ex} ~0.016 min^{-1} for basal versus ~0.013 min^{-1} for AICAR) (Figure 4.6). These values are surprisingly similar to those reported for the exocytosis of GP15-labelled GLUT4 in rat skeletal muscle (Karlsson, et al., 2009). Treatment with AICAR increases the size of the GLUT4 cycling pool compared to basal cells (64% to 78%) (Figure 4.5). This data suggests that AMPK-activation may regulate the mobilisation of an intracellular GLUT4 pool. We cannot therefore, exclude the possibility that AICAR stimulates exocytosis directly. However, this may be just a transient pulse release of GLUT4 that occurs shortly after treatment with AICAR. It is unlikely that these responses alone are sufficient to account for the sustained increase of cell surface GLUT4 levels observed. In cardiomyocytes, AMPK-activation following metformin treatment (Yang & Holman, 2006), hypoxia or the inhibition of mitochondrial H+-ATP synthase using oligomycin (Yang & Holman, 2005) led to the inhibition of endocytosis. Furthermore, exposing L6 myotubes to 2, 4 dinitrophenol (DNP) which simultaneously activates both AMPK and PKC reduces GLUT4 internalisation. Additionally, AICAR or direct AMPK activator A-769662 treatment alone, have been shown to reduce endocytosis in L6 myotubes (Fazakerely, et al., 2009). Here, we find treatment with AICAR reduced the rate constant for GLUT4 endocytosis (k_{en} ~0.112 min^{-1} basal versus ~0.043 min^{-1} AICAR). However, a degree of caution must be applied as this parameter was estimated from the uptake data and has not been determined experimentally. Alternatively, the rate for GLUT4 endocytosis can be directly measured using internalisation assay

Interestingly, we find that insulin and AICAR when added simultaneously result in a 4- to 5-fold increase of cell surface GLUT4 levels over basal levels (basal to Insulin + AICAR steady-state transition rate k ~0.148 min^{-1}, $t_{1/2}$ ~4.7 min)

(Figure 4.4). This data revealed that the combined effect of insulin stimulation and AMPK-activation was synergistic to increase GLUT4 cell surface levels. This finding supports that at least two distinct mechanisms may regulate GLUT4 accumulation at the cell surface. In support of this, we report that treatment with insulin and AICAR resulted in a partially additive effect on the size of the actively recycling GLUT4 pool compared to basal cells (64% to 85%) (Figure 4.5). These findings support the existence of distinct pools of GLUT4 in muscle (Douen, et al., 1990) (Fazakerely, et al., 2009). Furthermore, the results support the concept that insulin stimulation and contraction-mediated signalling promote the release of GLUT4 into the actively recycling pool through distinct signalling mechanisms. Intriguingly, we observed that 15% of the total GLUT4 pool is not mobilised in response to combined treatment with insulin and AICAR, similar to what has been reported in L6 myotubes (Fazakerely, et al., 2009). In support of this, a comparable sized non-cycling pool has been observed in 3T3 adipocytes. Here, it has been speculated that this small 'latent GLUT4 pool' represents GLUT4 transporters that are synthesised early which are not mobilised in response to insulin stimulation (Coster, et al., 2004) (Govers, et al., 2004).

In addition, we have found that co-stimulation with insulin and AICAR increase the steady-state rate constant for exocytosis (k_{ex}) ~2-fold, from 0.016 to 0.031 min^{-1} (half-time ~20 min) (Figure 4.6). This effect is more pronounced compared with the measured rate constant for insulin-stimulated GLUT4 exocytosis (k_{ex}). Thus, it is conceivable that the activation of both AMPK and Akt signalling pathways simultaneous may converge on a single signalling intermediate to enhance GLUT4 exocytosis. Furthermore, the concurrent slowing of GLUT4 internalisation in response to AMPK-activation is likely to contribute to the sustained cell surface levels of GLUT4. However in this current study the effect of insulin and AICAR treatment in combination on the rate of GLUT4 endocytosis could not be accurately determined. Together, these findings suggest that multiple and complex mechanisms may exist in muscle cells in response to different agonist treatment to regulate GLUT4 trafficking.

In conclusion, we have optimised a 96-Well plate assay for the study of GLUT4 trafficking in C2C12 myotubes. In these studies our data revealed that insulin-stimulation and treatment with the AMPK-activator (AICAR) increased the levels of GLUT4 at the plasma membrane by two-fold. Insulin-stimulation and activation of AMPK mobilised GLUT4 from a non-cycling compartment in to the actively cycling pool. Furthermore, insulin increased GLUT4 exocytosis (k_{ex}) of this cycling pool. By contrast activation of AMPK inhibited GLUT4 internalisation (k_{en}). The combined effect of insulin-stimulation and AMPK-activation was synergistic and led to increased GLUT4 cell surface levels above those obtained with either treatment alone. Furthermore, Insulin-stimulation and AMPK activation in combination resulted in a partially additive effect on the size of the actively recycling GLUT4 pool and further enhanced k_{ex} of this cycling pool. These results provide evidence to further enhance our understanding of how GLUT4 trafficking is regulated in response to insulin and AMPK-activation.

5 Role of TBC1D1 and TBC1D4 in the regulation of GLUT4 trafficking in muscle cells

5.1 Introduction

TBC1D1 and TBC1D4 are related Rab-GTPase activating proteins (Rab-GAP). The two proteins are 47% identical and share similar protein domains including a TBC domain at the C-Terminus along with two N-Terminal phosphotyrosine binding (PTB) domains (Roach, et al., 2007). TBC1D4 is highly expressed in insulin-responsive tissues which include adipose tissue, brain and heart and in oxidative soleus muscle. In contrast, TBC1D1 is primarily expressed in skeletal muscle (Taylor, et al., 2008) (Szekeres, et al., 2012) (Figure 3.8, 3.3.2). They exhibit similar catalytic activity towards the rab proteins 2A, 8, 10 and 14 (Roach, et al., 2007). TBC1D4 has been found to regulate rab proteins involved in the mobilisation of GLUT4 to the plasma membrane (Miinea, et al., 2005) (Sano, et al., 2007) (Ishikura, et al., 2007). They are proposed to function as negative regulators of GLUT4 trafficking through maintaining an un-specified rab proteins in its in-active GDP-bound state.

TBC1D4 and TBC1D1 contain multiple Akt phosphorylation motifs. Two Akt phosphorylation motifs in mouse TBC1D1 threonine 590 (596) and serine 501 (507) are conserved phosphorylation sites on TBC1D4 threonine 642 (649) and serine 570 (577) (Peck, et al., 2009) (Taylor, et al., 2008) (rat sequences are displayed in brackets). The phosphorylation of TBC1D4 in response to insulin stimulation is important for the regulation of GLUT4 translocation and glucose uptake (Sano, et al., 2003) (Zeigerer, et al., 2004) (Roach, et al., 2007) (Eguez, et al., 2005) (Ramm, et al., 2006) (Thong et al., 2007) (Ishikura, et al., 2007) (Ishikura & Klip, 2008). TBC1D4 phosphorylation leads to the in-activation of its GAP activity and therefore allows the rab to switch to an activate GTP bound state.

Several studies have demonstrated that TBC1D4 and TBC1D1 are phosphorylated in response to insulin and contraction stimulation in skeletal muscle (Kramer, et al., 2006) (Bruss, et al., 2005) (Funai & Cartee, 2008)

(Funai & Cartee, 2009) (Vichaiwong, et al., 2010) (Pehmoller, et al., 2009). Therefore they may be important downstream intermediates regulating glucose transport in response to both insulin and contraction signalling. The over-expression of TBC1D4 4P (TBC1D4 mutated to alanine at four phosphorylation sites serine 318, serine 588, threonine 642 and serine 751, therefore removing its capacity to undergo phosphorylation) in TA muscle inhibited insulin- and contraction-stimulated glucose uptake (Kramer, et al., 2006). The inhibition was reversed when GAP activity was simultaneous disrupted with the R/K mutation. Although, the over expression of wild-type TBC1D4 also reduced contraction-mediated glucose uptake. TA muscle expresses a very low level of endogenous TBC1D4 protein and so the over-expression may result in some aberrant effects.

Multiple AMPK phosphorylation sites have been identified in TBC1D1. These are serine 231, serine 660, serine 700 and threonine 499 (Peck, et al., 2009) (Taylor, et al., 2008) (Chen, et al., 2008) (Roach, et al., 2007). The identification of TBC1D1 as an AMPK substrate supports a role for TBC1D1 as a downstream signalling intermediate of contraction. Moreover, AMPK-dependent signaling mechanisms are essential for contraction-mediated glucose transport and phosphorylation of TBC1D1 in type II glycolytic skeletal muscles (EDL and EPI) (Funai & Cartee, 2009) (Pehmoller, et al., 2009). In contrast, one predicted AMPK site has been identified in TBC1D4 at serine 711 and this site is phosphorylated in response to AICAR and contraction in mouse muscle. However, mutation of this site to alanine does not affect glucose uptake.

The over expression of TBC1D1 4P (mutation to alanine at four Akt/AMPK phosphorylation sites serine 231, serine 499, threonine 590, serine 621) in TA muscle decreased contraction and not insulin-stimulated glucose transport (An, et al., 2010). Therefore, it has been proposed that TBC1D1 could be primarily responsible for regulating contraction-mediated glucose uptake in muscle (Funai & Cartee, 2009) (An, et al., 2010) (Vichaiwong, et al., 2010) (Pehmoller, et al., 2009). However, the over expression of a TBC1D1 R125W mutant protein has been found to impair insulin-induced glucose transport in TA muscle (An, et al., 2010). This mutation tryptophan at arginine 125 in TBC1D1 has been

identified as a candidate causing severe familial obesity predisposition in humans (Stone, et al., 2006) (Meyre, et al., 2008). Therefore, it has been suggested that the presence of TBC1D1 R125W could affect insulin-responsive glucose disposal in skeletal muscle and thus consequently lead to the associated manifestation of obesity. The exact mechanism for how this mutation affects TBC1D1 function is unknown. Furthermore, precisely how TBC1D1 is involved in insulin-regulated GLUT4 trafficking is still to be determined.

The objective of these studies was to investigate the importance of TBC1D1 and TBC1D4 for the regulation of GLUT4 trafficking in response to insulin and AMPK-activation in muscle. To investigate this, we have performed siRNA-mediated knockdown of *Tbc1d1* and *Tbc1d4* in C2C12 myotubes expressing HA-GLUT4. Using these cell models we were able to directly monitor the transition kinetics for HA-GLUT4 translocation. Furthermore, in the previous chapter of this thesis, our data support the existence for distinct pools of GLUT4 in muscle cells. We have observed that insulin and AICAR regulate the release of GLUT4 in to the actively recycling pool. Therefore, utilising these knockdown cell models we can examine the effect of silencing TBC1D1 and TBC1D4 on the GLUT4 recycling pool.

5.2 siRNA-mediated knockdown of *Tbc1d1* and *Tbc1d4* in C2C12 myotubes

5.2.1 Characterisation

C2C12 myoblasts were seeded in 96-well plates and differentiation was induced the following day. Two days post differentiation; the cells were transfected with *Tbc1d1*-specific, *Tbc1d4*-specific or non-targeting control siRNA oligonucleotides (Dharmacon 'SMARTpool' or individual oligonucleotides as indicated in Table 2.7, 2.1.3.2). Six days after transfection, the transfection efficiency was directly assessed using western blotting techniques to measure the protein expression level of TBC1D1 and TBC1D4 within a population of transfected cells. As illustrated in Figure 5.1, lipid-based transfection of C2C12 cells with *Tbc1d1*-specific siRNA resulted in a ~75% knockdown of TBC1D1 protein compared with non-targeting control siRNA treated cells. In addition, TBC1D4 protein was reduced ~50% in cells transfected with *Tbc1d4*-specific siRNA. Importantly, *Tbc1d1*-specific siRNA did not reduce the protein expression of closely related Rab-GAP TBC1D4 or vice versa. These results demonstrate that endogenous TBC1D1 and TBC1D4 can be knocked down in differentiated C2C12 myotubes using siRNA. Of note, the efficiency of TBC1D1 knockdown was reduced (~50%) when cells were transfected with *Tbc1d1*-specific siRNA and *Tbc1d4*-specific siRNA simultaneously compared to the single targeting of TBC1D1 alone. In contrast, the level of TBC1D4 protein knockdown was the same or slightly improved in TBC1D4/TBC1D1 double knockdown cells compared with TBC1D4 single knockdown cells.

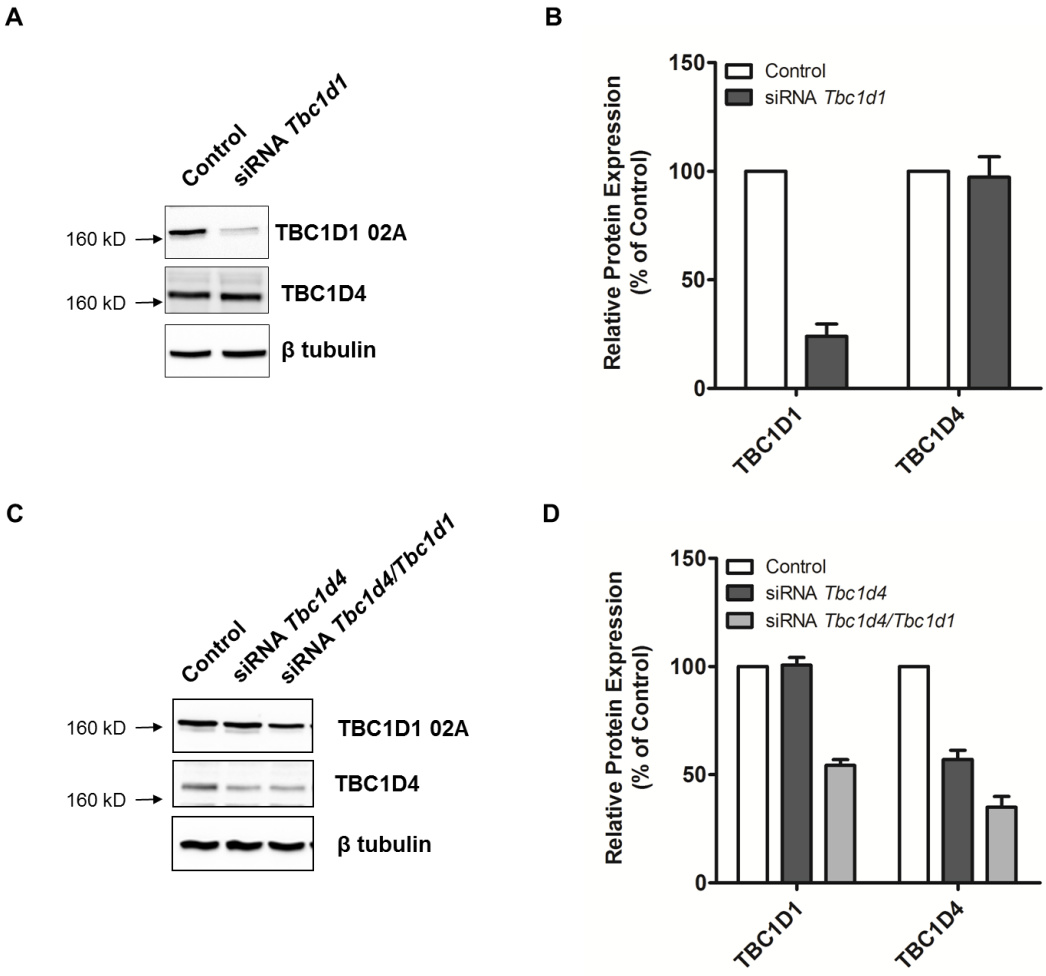

Figure 5.1: Efficiency of knockdown by siRNA *Tbc1d1* (single oligo) and *Tbc1d4* (SMARTpool). HA-GLUT4 expressing C2C12 cells were transfected with 100 nM siRNA specific for *Tbc1d1* or 50 nM *Tbc1d4* siRNA or non-targeting siRNA (control) on day 2. Cells were cultured for a further 6 days. TBC1D1 and TBC1D4 protein expression was analysed by western blotting with anti-TBC1D1 02A and anti-TBC1D4. β tubulin was used as a control. Protein load: 30µg. (A) Representative western-blot (B) TBC1D1 and TBC1D4 protein levels were quantified in TBC1D1 depleted cells (dark grey bars) compared to control cells (open bars); results represent the mean ± SE from 6 experiments. (C) Representative western blot (D) TBC1D1 and TBC1D4 protein levels were quantified in TBC1D4 depleted cells (dark grey bars) and TBC1D4/TBC1D1 double knockdown cells (light grey bars) compared to control cells (open bars); results represent the mean ± SE from 3 experiments

The differentiated C2C12 myotube phenotype is highly dependent on the culture conditions for both growth and differentiation of the cells, as outlined previously (4.2). Therefore, it was important to assess transfection toxicity. Cell viability and morphology was assessed in transfected cultures compared to non-transfected control cells. Furthermore, it was essential to investigate whether the specific knockdown of TBC1D1 or TBC1D4 in C2C12 myotubes would affect myotube differentiation. siRNA transfected and non-transfected control cells were cultured in 96-well plates. Light microscopy images were taken at various time points during differentiation to myotubes. Several wells for each cell type were tracked throughout differentiation. Representative images are depicted in Figure 5.2. We found that lipid-transfection in C2C12 cells on day 2 of differentiation did not affect the ability of cells to differentiate. In all cases, cells had formed distinct multi-nucleated myotubes by day 6. However, on day 4, transfected wells did appear to contain a greater number of rounded cells. This indicated a level of transfection toxicity. In addition, transfected myotubes appeared to be more defined, slightly longer and developed a ‘stringy’ appearance compared to non-transfected control cells. Furthermore, we find that the specific knockdown of TBC1D1 or TBC1D4 in C2C12 myotubes did not appear to affect cell morphology compared to cells transfected with non-targeting control siRNA.

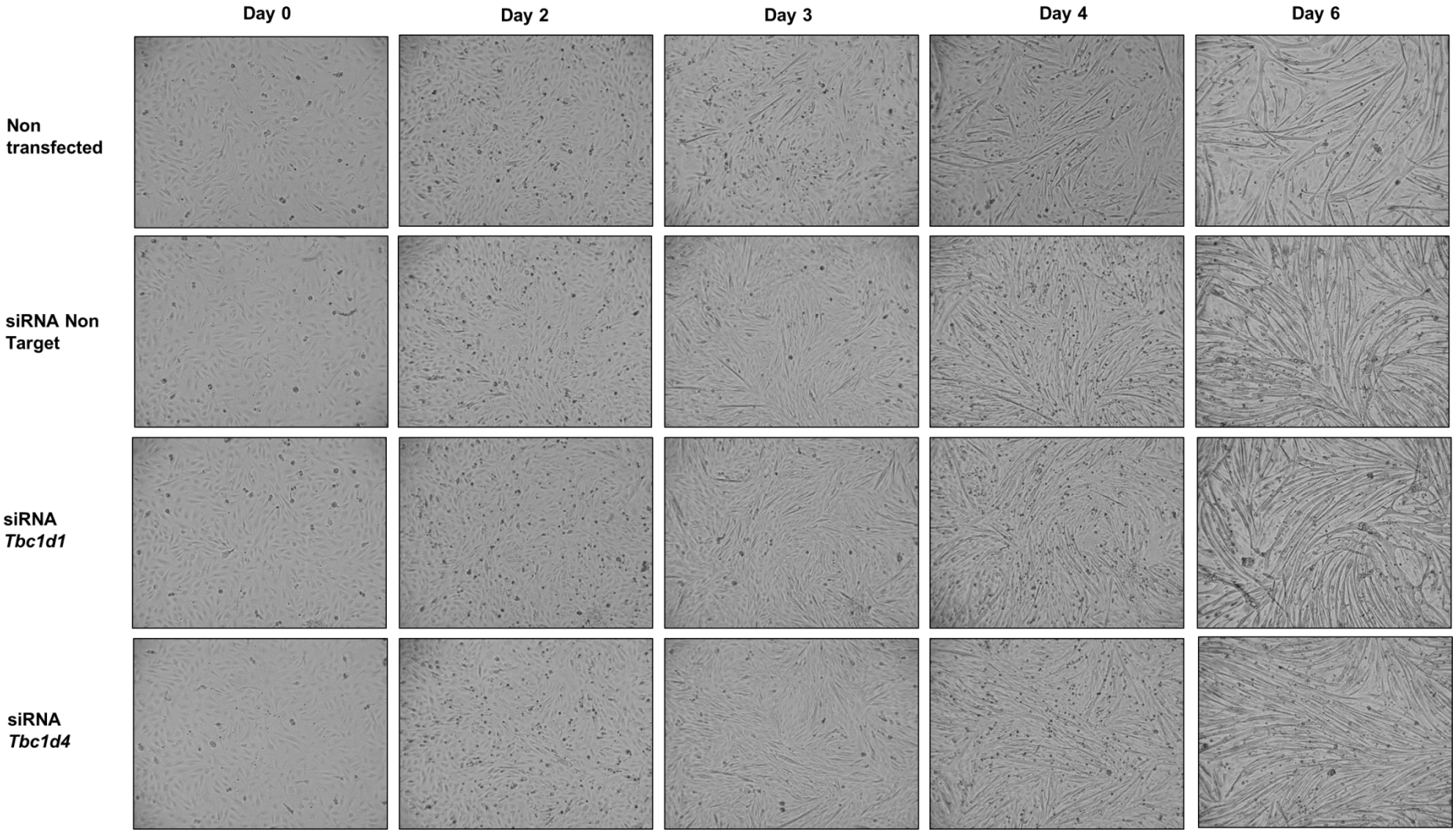
Day 0
Day 2
Day 3
Day 4
Day 6
Non transfected
siRNA Non Target
siRNA Tbc1d1
siRNA Tbc1d4

Figure 5.2: Morphology of TBC1D1-depleted, TBC1D4-depleted and control C2C12 cells during differentiation. C2C12 myotubes were lipid-transfected with *Tbc1d1*-specific or *Tbc1d4*-specific or non-targeting control siRNA. Cells were cultured for a further 3 days. Light microscopy images were obtained using a 4x objective and were documented using a digital camera (Motic). The images represent C2C12 cell morphology at day 0 and during differentiation at day 2, 3, 4 and 6. Several wells of a 96-well plate were tracked throughout myotube differentiation for each condition. Representative images from one well are depicted.

5.2.2 siRNA-mediated knockdown of *Tbc1d1* increases cell surface GLUT4 levels in non-stimulated C2C12 myotubes but does not affect insulin-induced GLUT4 translocation

In this study we examined the effect of knockdown of TBC1D1 on the relative amount of GLUT4 at the cell surface in C2C12 myotubes. C2C12 myotubes were serum starved and incubated with either insulin (200 nM) or AICAR (2 mM) for 2 to 60 min. We investigated the time-dependant accumulation of GLUT4 (HA epitope-tagged GLUT4) at the plasma membrane. HA-GLUT4 at the cell surface was determined by immuno-labelling with anti-HA antibodies. HA-GLUT4 at the cell surface was calculated as a percentage of total cellular immuno-reactive GLUT4. To note, TBC1D1 knockdown did not affect the level of expression of the HA-tagged GLUT4.

The results were normalised to cells infected with the pBABE-puro empty vector control virus. For each experiment three intra-assay replicates for at each time point and condition were analysed. Knockdown of TBC1D1 protein expression was determined for each experiment using western blot analysis of C2C12 myotubes cell lysates. We observed a consistent ~75% knockdown of TBC1D1 protein in a population of cells transfected with *Tbc1d1*-specific siRNA compared with cells transfected with non-targeting control siRNA (Figure 5.1A, B). Importantly, knockdown of TBC1D1 in C2C12 myotubes did not affect TBC1D4 protein levels.

The basal cell surface level of HA-GLUT4 was increased in TBC1D1 knockdown cells compared with control siRNA treated cells (Figure 5.3A-C) (Figure 5.4A-C). The cell surface GLUT4 levels in basal TBC1D1 knockdown cells were between 30-60% higher compared with basal control cells.

The depletion of TBC1D1 had little effect on the maximum level of GLUT4 transporters at the cell surface in the presence of AICAR (~32.5 ± 2.1, siRNA

Tbc1d1 versus ~34.4 ± 7.8, Control) (Figure 5.3A, B). Therefore, there was a reduction in the net gain of cell surface HA-GLUT4 above basal levels in TBC1D1 knockdown cells compared with control cells. The knockdown of TBC1D1 was only partially AICAR-mimetic. Treatment with AICAR promoted the time-dependant elevation in cell surface GLUT4 levels in both knockdown and control cells. By fitting the transition data to a single-exponential function, the observed rate constant and $t_{1/2}$ for the transition from the basal to the AICAR steady-state was determined. The r^2 goodness-of-fit measure indicated that a single-exponential curve does not fit well the data obtained in TBC1D1 knockdown cells (r^2 values: control, 0.933; siRNA *Tbc1d1*, 0.679). The basal to AICAR transition appreared to be slower in the TBC1D1 knockdown cells (k ~0.031 ± 0.022 min^{-1}, $t_{1/2}$ ~22 min) than in the control cells (k ~0.055 ± 0.010 min^{-1}, $t_{1/2}$ ~13 min) although the were not significantly different p = 0.3769. (Figure 5.3C, D).

We next investigated whether TBC1D1 was involved in the regulation of insulin-stimulated GLUT4 translocation in C2C12 myotubes. In insulin-stimulated TBC1D1 knockdown cells the level of cell surface HA-GLUT4 reached a slightly higher level compared with insulin-stimulated control cells. Therefore, the net gains in cell surface HA-GLUT4 above basal levels were unaffected by TBC1D1 knockdown in C2C12 myotubes. Insulin promoted a rapid and transient 2-fold accumulation of GLUT4 at the cell surface in TBC1D1 knockdown cell similar to control cells (Figure 5.4A). The observed transition rate constant (k) from basal steady-state to maximal insulin-stimulated level in TBC1D1 knockdown cells was not significantly different compared with control cells (k = 0.537 ± 0.342 min^{-1}, $t_{1/2}$ ~1.29 min, siRNA *Tbc1d1* versus k ~0.379 ± 0.276 min^{-1}, $t_{1/2}$ ~1.82 min, Control) (Figure 5.4C, D). However, there was substantial variation in the level of HA-GLUT4 at the surface over time. This is reflected in the low r^2 values for both curves (r^2 values: control, 0.569; siRNA *Tbc1d1*, 0.494). In both cell types, GLUT4 at the cell surface rapidly declined and returned to their respective basal levels within 60 min after insulin stimulation. Accordingly, cell surface GLUT4 levels were significantly elevated in TBC1D1 knockdown cells compared to control cells, 60 min after insulin addition (Figure 5.4B).

The magnitude of the knockdown effect (evaluated using the plate-based assay result) could not be correlated with the level of protein knockdown. Both results represent an average from a population of cells. Furthermore, we did not directly determine the number of transfection positive cells within a population. Therefore, we could not directly normalise results for each condition to the level of knockdown.

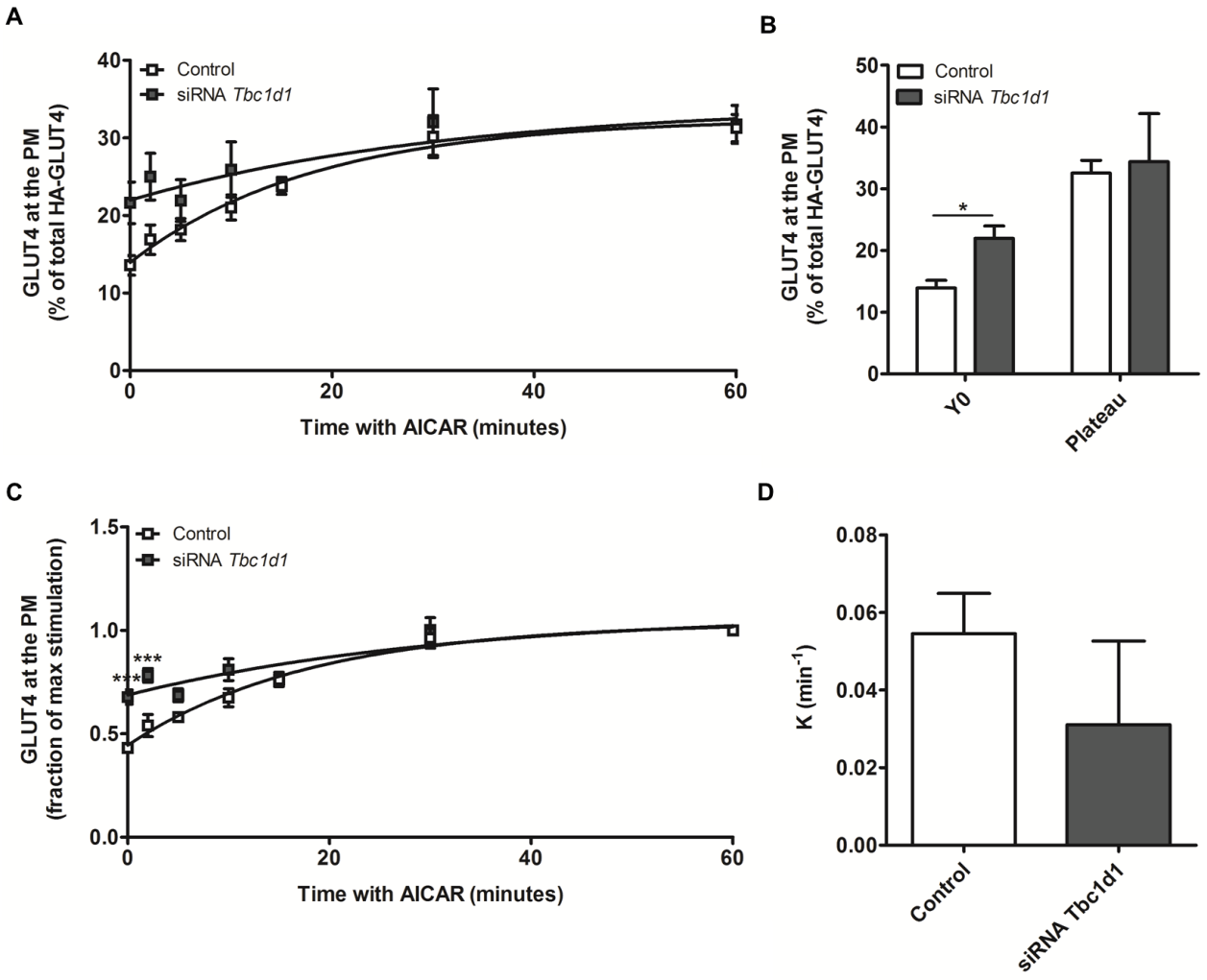

Figure 5.3: Knockdown of TBC1D1 increases cell surface levels of GLUT4 in basal C2C12 myotubes. C2C12 cells were transfected with 100nM siRNA specific for *Tbc1d1* (siRNA *Tbc1d1*) or non-targeting control siRNA (control) 2 days after the initiation of differentiation. Cells were cultured for a further 6 days. C2C12 myotubes were maintained under basal conditions (t=0) or stimulated with AICAR at 2 mM for 2 to 60 min. (A) The cell surface levels of HA-GLUT4 in control (open squares) and TBC1D1 knockdown cells (solid squares) was determined by incubating fixed cells with anti-HA primary antibodies and anti–mouse Alexa 488 secondary antibody. The results are expressed as a percentage of total immuno-reactive HA-GLUT4 within in permeablised cells. Results represent the mean + SE from 3 experiments. An unpaired t-test was performed at p=0.05. * p≤0.05 (B) The cell surface levels of GLUT4 at t=0 (Y0) and at t=∞ (plateau) were calculated from the data sets. (C) The cell surface levels of GLUT4 were expressed as a fraction of maximum AICAR (long-time) stimulation. A single-exponential function was fitted to determine the observed rate constant (k_{obs}) for the transition. Two-way analysis of variance (ANOVA) test was used with Bonferroni post test at p=0.05. *** p≤0.001 (D) The observed rate constant (k_{obs}) for the transition from the basal to the AICAR stimulated steady-state were determined for TBC1D1 knockdown *(*siRNA *Tbc1d1) and* control cells.

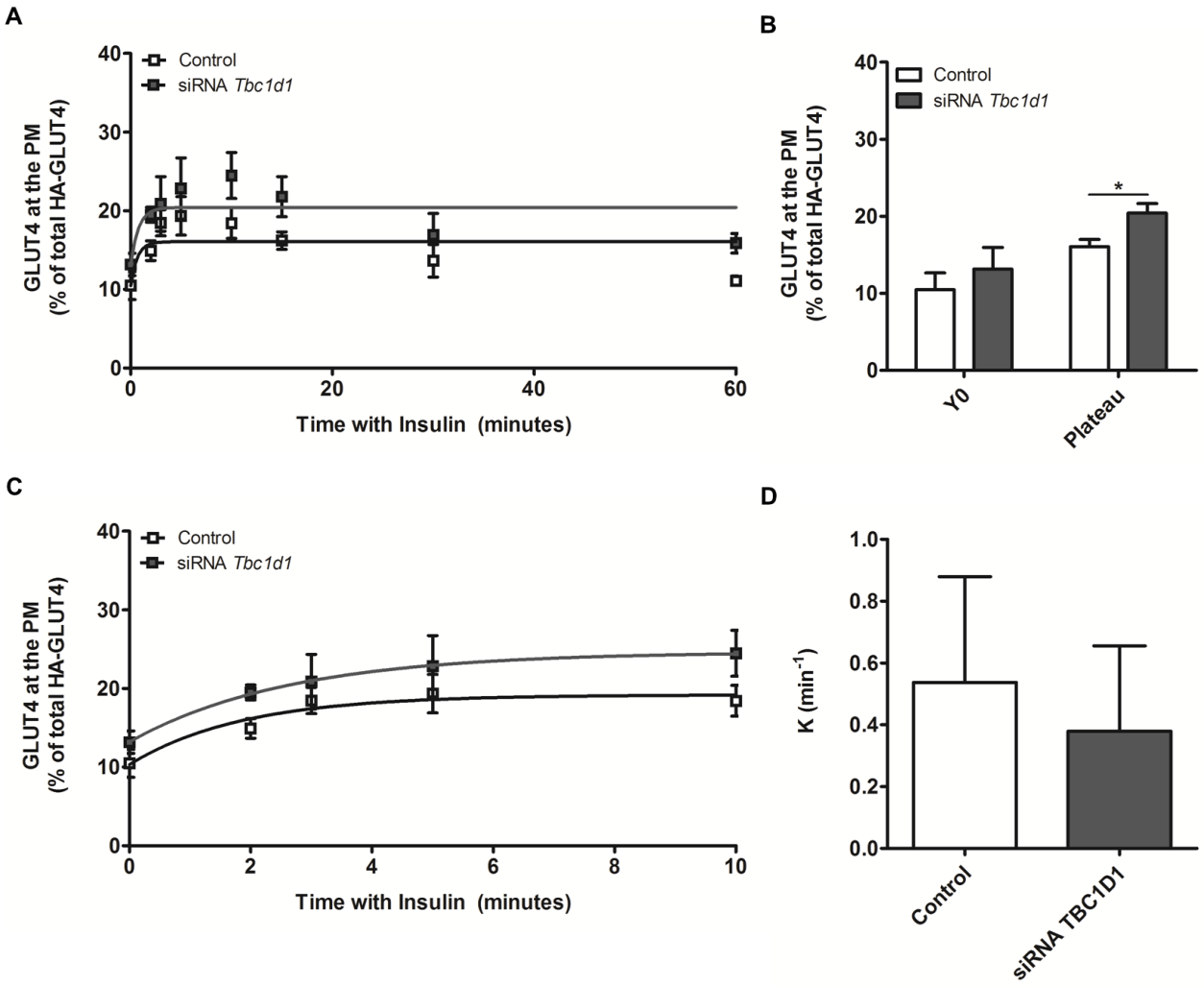

Figure 5.4: TBC1D1 knockdown affects cell surface levels of GLUT4 in basal and insulin-stimulated C2C12 myotubes. C2C12 cells were transfected with 100nM siRNA specific for *Tbc1d1* or non-targeting siRNA (control) on day 2 of differentiation. The cells were cultured for a further 6 days. C2C12 myotubes were maintained under basal conditions (t=0) or stimulated with insulin at 100 nM for 2 to 60 min. (A) The cell surface levels of HA-GLUT4 in control (open squares) and TBC1D1 knockdown cells (solid squares) were determined in fixed cells using anti-HA primary antibodies and anti–mouse Alexa 488 secondary antibody. The results are expressed as a percentage of total immuno-reactive HA-GLUT4 within permeabilised cells. Results represent the mean + SE from 3 experiments. (B) The cell surface levels of GLUT4 at t=0 (Y0) and at t=∞ (plateau) were calculated from the data sets. An unpaired t-test was performed at p=0.05. * p≤0.05 (C) The cell surface levels of GLUT4 were expressed as a fraction of maximum insulin (long-time) stimulation. A single-exponential function was fitted to determine the observed rate constant (k_{obs}) for the transition. (D) The observed rate constant (k_{obs}) for the transition from the basal to the insulin-stimulated state were determined for TBC1D1 knockdown *(*siRNA *Tbc1d1) and* control cells

5.2.3 siRNA-mediated knockdown of *Tbc1d4* does not affect basal cell surface levels of GLUT4 in C2C12 myotubes

In this next study we examined the effect of knockdown of TBC1D4 on the relative amount of GLUT4 at the cell surface in C2C12 myotubes. Endogenous TBC1D4 protein expression was reduced ~50% in myotubes transfected with siRNA-*Tbc1d4* compared with cells transfected with non-targeting control siRNA (Figure 5.1C, D).

C2C12 myotubes were serum starved and either kept under basal conditions or incubated with AICAR (2 mM) for 2 to 60 min. We investigated the time-dependant accumulation of GLUT4 (HA epitope-tagged GLUT4) at the plasma membrane. HA-GLUT4 at the cell surface was calculated as a percentage of total cellular immuno-reactive GLUT4. Importantly, the depletion of TBC1D4 did not affect total cell expression of HA-GLUT4.

Knockdown of TBC1D4 did not affect the basal levels of cell surface HA-GLUT4 compared with basal control cells. Thus, in contrast to TBC1D1, TBC1D4 is not required for regulating GLUT4 retention in basal C2C12 myotubes (Figure 5.5A, B). Furthermore, the depletion of TBC1D4 did not prevent the elevation of GLUT4 transporters at the cell surface following AICAR-treatment. However, it is important to note that knockdown of TBC1D4 was not highly efficient. Therefore, residual protein levels of TBC1D4 may be enough for normal function.

Additionally, we examined the effect of TBC1D4/TBC1D1 double knockdown cells. Surprisingly, the double knockdown of TBC1D1 and TBC1D4 did not result in an elevation of basal cell surface GLUT4 expression compared to control cells (Figure 5.5A, B). This may have been due to the reduced efficiency of TBC1D1 knockdown in siRNA *Tbc1d4/Tbc1d1* double knockdown cells compared with the single targeting of TBC1D1 alone. The difference may be due to residual levels of TBC1D1 protein persisting which prevented a noticeable reduction in TBC1D1 function.

It was apparent from the r^2 goodness-of-fit measures that the data obtained in control non-targeting siRNA cells did not fit a single-exponential curve (r^2 values: control, 0.29; siRNA *Tbc1d4*, 0.81; siRNA *Tbc1d4/Tbc1d1,* 0.74) (Figure 5.5C). Therefore, this ambiguous control data has made the results from these experiments difficult to interpret. The transition rate constant from basal to AICAR steady-state in the TBC1D4 knockdown cells was seemingly slow (k ~0.02 ± 0.01 min^{-1}, $t_{1/2}$ ~33 min). Whereas, a more normal transition response curve was observed in the TBC1D4/TBC1D1 double knockdown cells (k ~0.06 ± 0.02 min^{-1}, $t_{1/2}$ ~12 min). These interpretations have been made in comparison to cells transfected with non-targeting control siRNA from the previous set of experiments (Figure 5.3). Therefore such assumptions must be treated with caution.

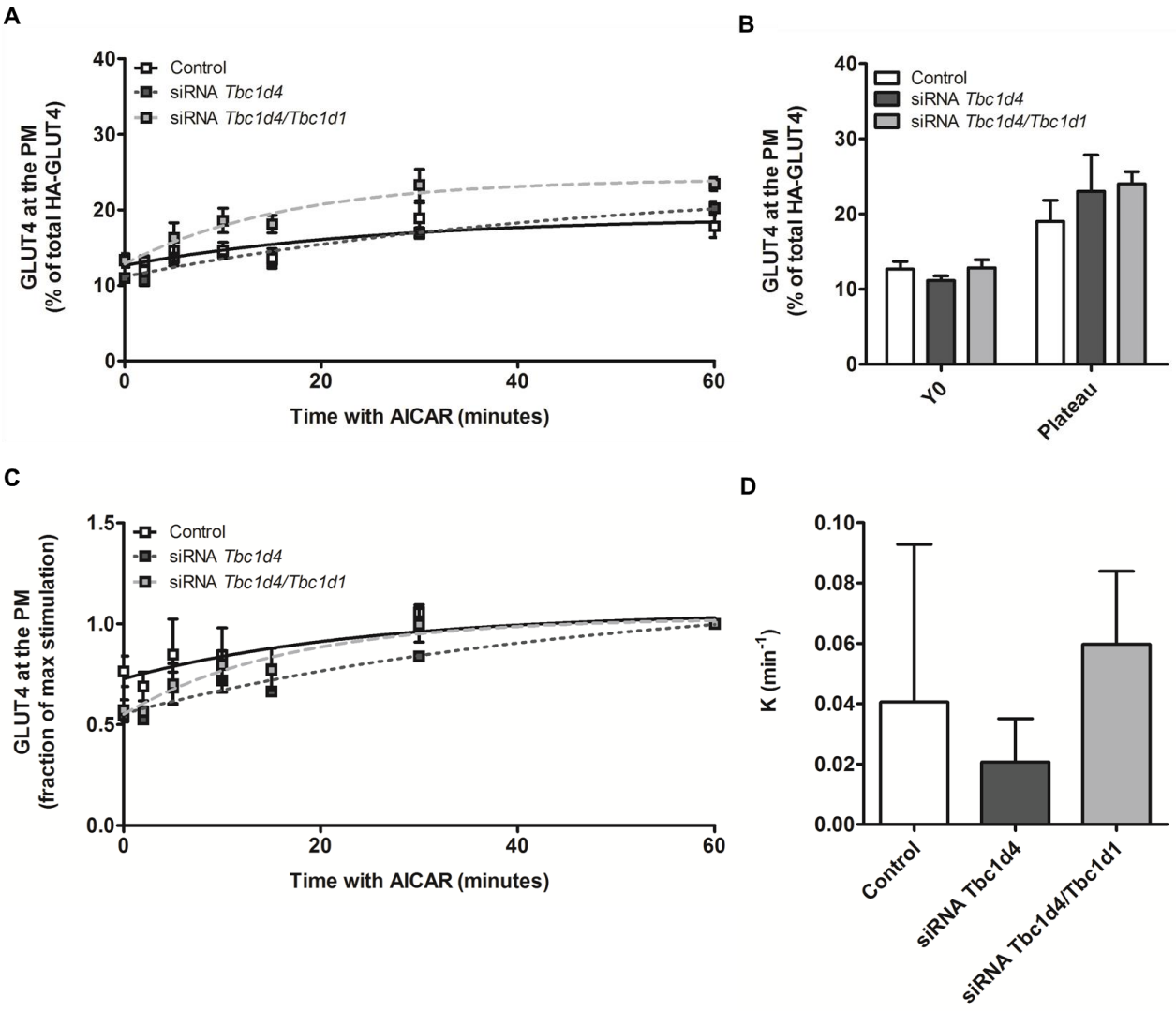

Figure 5.5: Knockdown of TBC1D4 does not affect cell surface levels of GLUT4 in basal C2C12 myotubes. C2C12 cells were transfected with 50 nM siRNA specific for *Tbc1d4* (siRNA *Tbc1d4*) or with 50 nM siRNA specific for *Tbc1d4* and 100 nM of siRNA specific for *Tbc1d1* (siRNA *Tbc1d4/Tbc1d1*) or non-targeting control siRNA (control) on day 2 of muscle cell differentiation. Cells were cultured for a further five days. C2C12 myotubes were maintained under basal conditions (t=0) or stimulated with AICAR at 2 mM for 2 to 60 min. (A) The cell surface levels of HA-GLUT4 in control (open squares), TBC1D4 knockdown cells (solid squares) and TBC1D4/TBC1D1-knockdown cells (grey squares) were determined by incubating fixed cells by with anti-HA primary antibodies and anti–mouse Alexa 488 secondary antibody. The results are expressed as a percentage of total immuno-reactive HA-GLUT4 within in permeabilised cells. Results represent the mean + SE from 3 experiments. (B) The cell surface levels of GLUT4 at t=0 (Y0) and at t=∞ (plateau) were calculated from the data sets. (C) The cell surface levels of GLUT4 were expressed as a fraction of maximum AICAR (long-time) stimulation. A single-exponential function was fitted to determine the observed rate constant (k) for the transition. (D) The observed rate constant (k) for the transition from the basal to the AICAR stimulated steady-state were determined for knockdown *(*siRNA *Tbc1d4 and* siRNA *Tbc1d4/Tbc1d1) and* control cells.

5.2.4 TBC1D1 regulates the release of GLUT4 from a non-cycling/slow cycling pool in to the actively recycling pool

C2C12 myotubes were serum starved and stimulated with insulin at 200 nM or maintained in basal conditions. Subsequently, live cells were incubated at 37^{o}C in the presence of anti-HA antibody for 300 min to measure the amount of HA-GLUT4 actively recycling with the plasma membrane. The amount of GLUT4 actively recycling within 300 min was calculated as a percentage of total cellular immuno-reactive GLUT4. The results were expressed as a percentage of the maximum amount of GLUT4 labelled within 300 min in insulin-stimulated control cells (Figure 5.6C).

In C2C12 myotubes, knockdown of TBC1D1 increased the size of the actively-cycling GLUT4 pool in both basal and insulin-stimulated cells compared with control cells, although this did not reach statistical significance (Basal, p=1366; Insulin, p=1872) (Figure 5.6C). Conversely, knockdown of TBC1D4 did not affect the amount of GLUT4 in the cell surface recycling pool in basal or insulin-stimulated C2C12 myotubes.

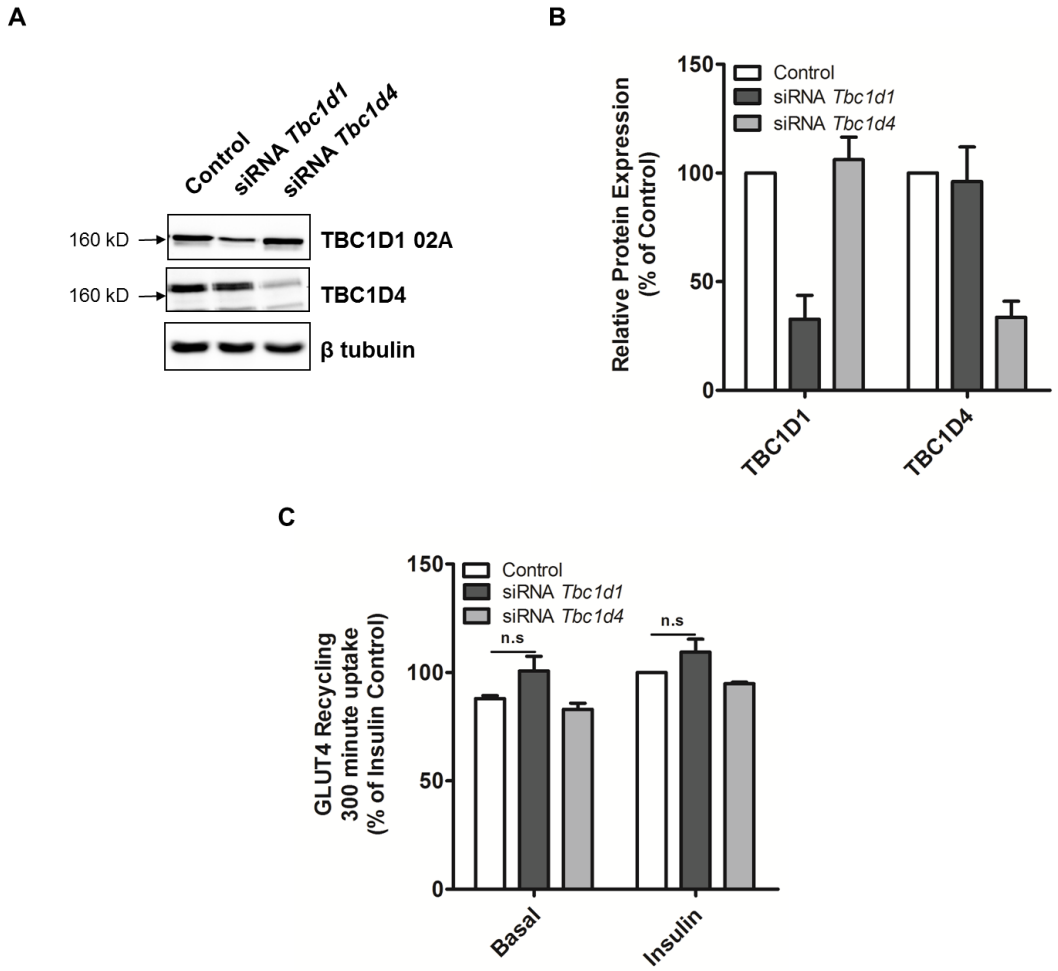

Figure 5.6: Knockdown of TBC1D1 increases the size of the actively cycling GLUT4 pool in basal and insulin-stimulated C2C12 myotubes. HA-GLUT4 expressing C2C12 cells were transfected with 100 nM siRNA specific for *Tbc1d1* or 50 nM siRNA specific for *Tbc1d4* or non-targeting siRNA (control) on day 2. Cells were cultured for a further 5 days. (A) TBC1D1 and TBC1D4 protein expression was analysed by western blotting with anti-TBC1D1 02A and anti-TBC1D4. β tubulin was used as a control. A representative western blot is shown. (B) TBC1D1 and TBC1D4 protein levels were quantified in TBC1D1 knockdown cells (dark grey bars) and TBC1D4 knockdown cells (light grey bars) compared to control cells (open bars); results represent the mean ± SE from 3 experiments. (C) siRNA transfected C2C12 myotubes were maintained in basal conditions or stimulated with Insulin at 200 nM for 5 min. Cells were incubated with agonist + 50 µg/ml of anti-HA antibody for 300 min at 37^{o}C, then fixed, permeabilised and incubated with anti–mouse Alexa 488 secondary antibody. Results are calculated as a percentage of the GLUT4 labelled in insulin-stimulated control cells. Results represent the mean ± SE from 3 experiments. An unpaired t-test was performed at p=0.05.

5.3 Discussion

Cell culture models provide alternative *in vitro* model systems to study. In contrast to primary muscle cells, these cells can be readily sourced, cultured and large populations of cells can be obtained for robust investigations and so have great potential for industry applications. In this chapter we have established a lipid-transfection based protocol for siRNA-mediated knockdown of *Tbc1d1* and *Tbc1d4* in differentiated C2C12 myotubes. Using these knockdown muscle cell models we were able to investigate the role for Rab-GAPs in the regulation of GLUT4 trafficking. We have shown that knockdown of TBC1D1 increases GLUT4 at the plasma membrane in basal cells therefore may play an important role in regulating GLUT4 intracellular retention mechanisms. Interestingly, TBC1D1 depleted cells remain insulin responsive. Insulin stimulates the rapid and transient accumulation of GLUT4 at the cell surface. This suggests that TBC1D1 may not be directly regulated by insulin alone. The experimental data presented here supports the effect of knockdown on the release of GLUT4 from storage compartments. However, due to experimental constraints, time course recycling data could not be investigated and so the effect of TBC1D1 and TBC1D4 knockdown on the intrinsic rate of GLUT4 recycling (k_{ex}) could not be distinguished.

Here, we show that siRNA mediated knockdown of TBC1D1 increased basal cell surface levels of HA-GLUT4 in C2C12 myotubes (Figure 5.3 and Figure 5.4) (Figure 5.7A,B). This is similar to observations made in L6 myotubes, where silencing TBC1D1 significantly elevated basal cell surface levels (50%) of GLUT4myc (Ishikura & Klip, 2008). Together these results suggest that endogenous TBC1D1 is required for basal GLUT4 intracellular retention. TBC1D1 has been found to be more effective at regulating GLUT4 retention in L6 myotubes compared to myoblasts (Ishikura & Klip, 2008). Consistent with this, the expression of TBC1D1 is up-regulated during differentiation of L6 (Chavez, et al., 2008) and C2C12 muscle cells (Peck, et al., 2009) (3.4.3).

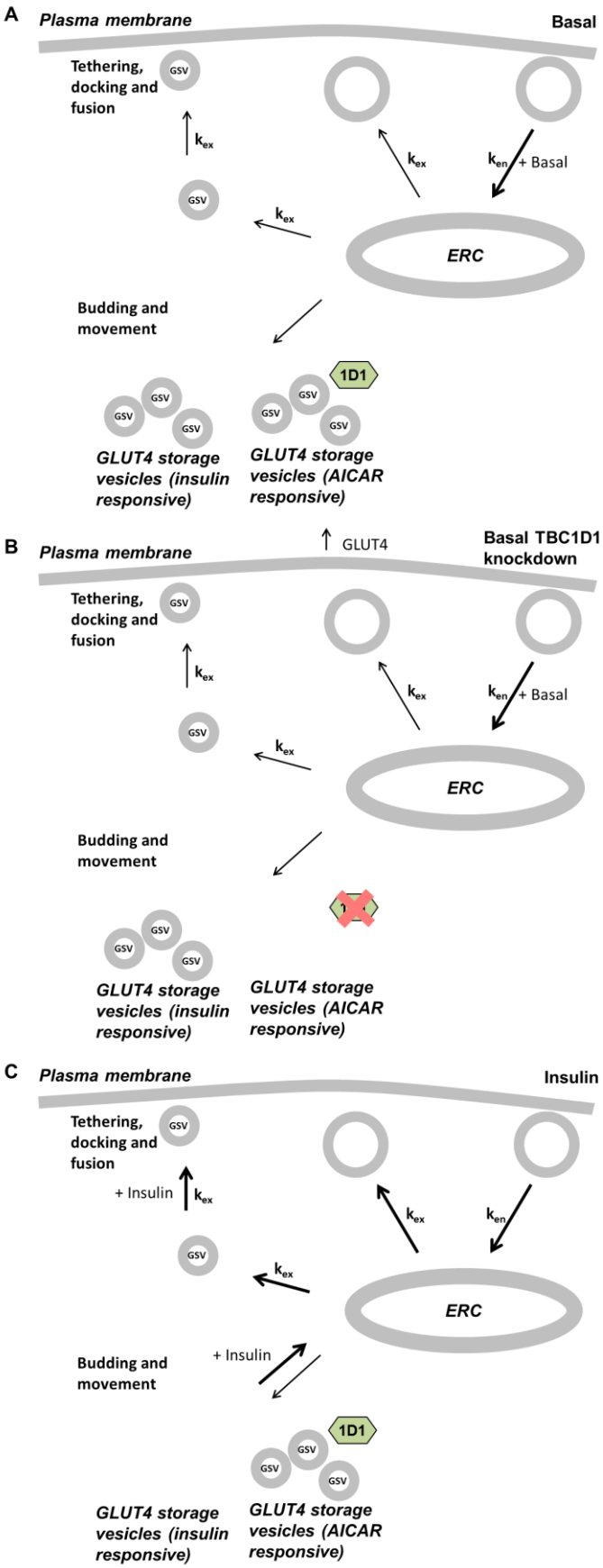
A
Plasma membrane
Basal
Tethering, docking and fusion
GSV
k_{ex}
k_{en} + Basal
ERC
Budding and movement
1D1
GLUT4 storage vesicles (insulin responsive)
GLUT4 storage vesicles (AICAR responsive)
B
Plasma membrane
GLUT4
Basal TBC1D1 knockdown
Tethering, docking and fusion
k_{ex}
k_{en} + Basal
ERC
Budding and movement
GLUT4 storage vesicles (insulin responsive)
GLUT4 storage vesicles (AICAR responsive)
C
Plasma membrane
Insulin
Tethering, docking and fusion
+ Insulin
k_{ex}
k_{en}
ERC
Budding and movement
+ Insulin
1D1
GLUT4 storage vesicles (insulin responsive)
GLUT4 storage vesicles (AICAR responsive)

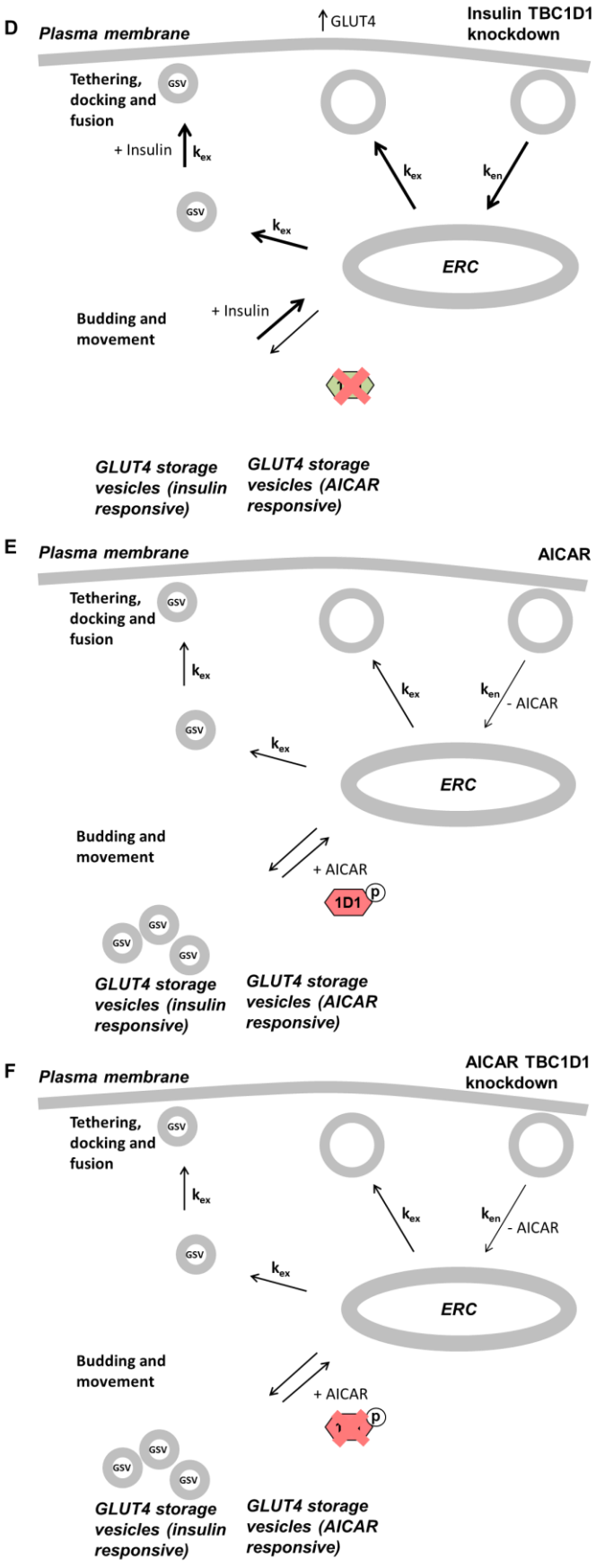
D
Plasma membrane
GLUT4
Insulin TBC1D1 knockdown
Tethering, docking and fusion
GSV
+ Insulin
k_{ex}
k_{en}
ERC
Budding and movement
GLUT4 storage vesicles (insulin responsive)
GLUT4 storage vesicles (AICAR responsive)
E
Plasma membrane
AICAR
- AICAR
+ AICAR
1D1
P
GLUT4 storage vesicles (insulin responsive)
GLUT4 storage vesicles (AICAR responsive)
F
Plasma membrane
AICAR TBC1D1 knockdown
GLUT4 storage vesicles (insulin responsive)
GLUT4 storage vesicles (AICAR responsive)

Figure 5.7: A role for TBC1D1 in GLUT4 trafficking in C2C12 myotubes. In the three-pool model GLUT4 recycles through two intracellular compartments (endosomal recycling compartment (ERC) and GLUT4 storage vesicular compartment (GSV)) and the plasma membrane. The additional pool can account for the initial rapid stimulation of GLUT4 translocation to the plasma membrane following insulin stimulation and the slower steady-state $t_{1/2}$ value for GLUT4 exocytosis in the continued presence of insulin. (A) In the basal state, cell surface levels of GLUT4 are kept low from the slow movement of GLUT4 to the plasma membrane and the rapid retrieval back to endosomal recycling compartment (ERC). A small fraction of GLUT4 transporters are sequestered to a stationary non-cycling GSV compartment. A pool of GSVs are retained through the action of TBC1D1. (B) Knockdown of TBC1D1 removes this retention and releases GLUT4 stored in static storage vesicles (GSVs) in to the endosomal recycling compartment and increases cell surface levels. (C, D) Insulin simulates the release of a GSV pool to the plasma membrane in control and TBC1D1 knockdown cells. This pool is not retained through the action of TBC1D1. (E) Treatment with AICAR leads to the phosphorylation of TBC1D1 and releases a GSV pool in to the endosomal recycling compartment and increases cell surface levels. (F) Knockdown of TBC1D1 in addition to AICAR treatment has no further effect on the cell surface levels of GLUT4. Key: *Arrows*– indicate the movement of GLUT4 between compartments. Heavy weighted arrows indicate increased movement. *Green 1D1*: TBC1D1 with active GAP domain, *Red 1D1:* TBC1D1 with inactive GAP domain, *Red crosses*: Indicate the knockdown of TBC1D1.

The silencing of TBC1D1 in C2C12 myotubes acts as a partial AICAR-mimetic. However, the depletion of TBC1D1 alone does not completely prevent AICAR-mediated responses. Interestingly, siRNA-mediated knockdown of TBC1D1 did not affect the maximum cell surface levels of GLUT4 attained following AICAR-treatment. However, the basal to AICAR transition rate appeared to be slightly slower in the TBC1D1 knockdown cells (k ~0.03 ± 0.02 min^{-1}, $t_{1/2}$ ~22 min) than in the control cells (k ~0.06 ± 0.01 min^{-1}, $t_{1/2}$ ~13 min) (Figure 5.3). It is likely that the retention mechanism governed by TBC1D1 is released upon phosphorylation by AMPK. This is illustrated in Figure 5.7. In support of this, we have shown here that TBC1D1 is phosphorylated on serine 237 in response to AMPK-activation. This is in support of data presented in other studies (Peck, et al., 2009) (Pehmoller, et al., 2009) (Roach, et al., 2007) (Chen, et al., 2008) (Taylor, et al., 2008). In 3T3-L1 adipocytes an insulin-dependent association between 14-3-3 and phosphorylated TBC1D4 plays an important role in the inactivation of TBC1D4 Rab-GAP activity and the regulation of GLUT4 trafficking (Ramm, et al., 2006) (Koumanov, et al., 2011). In contrast, the phosphorylation of TBC1D1 on threonine 596 in response to insulin stimulation is insufficient to induce 14-3-3 binding in muscle (Chen, et al., 2008) (Pehmoller, et al., 2009). Instead, the binding of TBC1D1 to 14-3-3 is regulated through the phosphorylation of TBC1D1 on serine 237 in response to AMPK-activation (Chen, et al., 2008) (Pehmoller, et al., 2009).

We have shown here that TBC1D1 knockdown increased the level of GLUT4 at the plasma membrane in basal C2C12 myotubes did not affect insulin-stimulated GLUT4 translocation to the plasma membrane. The insulin-stimulated net gains in cell surface HA-GLUT4 above respective basal levels were unaffected by TBC1D1 knockdown (Figure 5.4). The proposed mechanism for this finding is illustrated in Figure 5.7C, D. These results are consistent with those described for L6 myotubes and support the concept that endogenous TBC1D1 may also function to restrict insulin-stimulated responses (Ishikura & Klip, 2008). The over expression of wild-type TBC1D1 or the dominant-negative mutant TBC1D1 4P (TBC1D1 mutated to alanine at four Akt/AMPK phosphorylation sites serine 231, threonine 499, threonine 590 and serine 621, therefore removing its capacity to undergo phosphorylation) in mouse tibialis anterior muscle does not abrogate normal insulin-stimulated glucose transport (An, et al., 2010). The authors speculated that either TBC1D1 is not required for insulin-stimulated glucose transport or that other Akt phosphorylation sites on TBC1D1 are critical for insulin-induced responses. Our results support the former, as insulin-stimulated net gains in cell surface HA-GLUT4 were un-affected following depletion of TBC1D1 from C2C12 myotubes. Taken together, these findings may suggest that the expression of endogenous TBC1D1 may function to constrain the extent to which insulin alone can induce the release of GLUT4 to the cell surface in muscle. In contrast, the ectopic expression of wild-type TBC1D1 (active GAP) in 3T3 L1 adipocytes had an inhibitory effect on insulin-stimulated GLUT4 at the plasma membrane. This was rescued completely when TBC1D1 was simultaneously mutated to lysine at arginine 941, which inactivated GAP activity (Peck, et al., 2009) (Chavez, et al., 2008). Interestingly, the inhibitory effect of wild-type TBC1D1 on insulin-stimulated responses in 3T3-L1 adipocytes was partially rescued when cells were treated with AICAR (Peck, et al., 2009). Therefore, it is reasonable to conclude that the ectopic expression of TBC1D1 in fat cells may lead to aberrant effects in part due to the absence of signalling pathways regulating TBC1D1 activity. A role for AMPK under basal conditions has been suggested. In muscle-specific α_2-inactive AMPK transgenic (AMPKα2iTG), α_2AMPK kinase dead (α_2AMPK KD) and β1β2 knockout (AMPKβ1β2KO) mice basal phosphorylation of TBC1D1 was significantly reduced (Vichaiwong, et al., 2010) (Pehmoller, et al., 2009)

(O'Neill, et al., 2011). Furthermore, in α_2AMPK KD mice TBC1D1 association with 14-3-3 is impaired (Pehmoller, et al., 2009). Thus, the regulation of TBC1D1 by AMPK in basal muscle cells could somehow regulate insulin-responsiveness. In support of this, AMPK is required for insulin-stimulated phosphorylation of TBC1D1 at threonine 596 (Pehmoller, et al., 2009). Although signalling via PI 3-kinse is important for mediating insulin-stimulated TBC1D1 phosphorylation. However, full alleviation of TBC1D1-induced retention (through in-activation of TBC1D1 GAP activity) could be dependent on other factors specific in muscle. Conversely, the expression of TBC1D1 may dominantly inhibit the endogenous proteins and interfere with insulin-induced responses which would normally function in adipose cells.

Additionally, we have shown here that silencing TBC1D1 does not significantly affect the observed transition rate constant (k) from basal steady-state to a maximal insulin-stimulated state compared with control cells (k = 0.537 ± 0.342 min^{-1}, $t_{1/2}$ ~1.29 min, siRNA *Tbc1d1* versus k ~0.379 ± 0.276 min^{-1}, $t_{1/2}$ ~1.82 min, Control) (Figure 5.4). In view of a concept first proposed by Bogan et al, this ‘transient overshoot’ of cell surface GLUT4 levels observed following acute insulin stimulation corresponds with the rapid mobilisation of GLUT4 from a highly insulin-responsive GSV compartment (Bogan, et al., 2001) (4.4). These insulin-regulated exocytic events occur independently of TBC1D1 in C2C12 myotubes. Furthermore, TBC1D1 does not appear to regulate the rate of release of these vesicles towards the plasma membrane. It is plausible that endogenous TBC1D1 may restrict insulin-stimulated responses through regulating the formation or size of this insulin-responsive vesicular compartment in C2C12 myotubes.

The proposed mechanisms by which GLUT4 is trafficked within intracellular compartments to regulate GLUT4 sequestration in fat and muscle cells are controversial. In more recent years, two distinctly different but plausible models have been supported primarily based on experimental studies carried out in 3T3-L1 adipocytes. The first model proposes ‘GLUT4 static retention’ which was pioneered by James and colleagues (Govers, et al., 2004) (Coster, et al., 2004) and which has been robustly supported (Muretta, et al., 2008) (Brewer, et al.,

2011) (Fujita, et al., 2010) (1.3.2.6 Figure 1.4C). Conversely, model 2 proposed by McGraw and colleagues details that intracellular GLUT4 traffic is governed by a dynamic system where the entire insulin-responsive GLUT4 pool can eventually recycle with the plasma membrane in basal cells (Martin, et al., 2006) (Karylowski, et al., 2004) (1.3.2.6 Figure 1.4D). These models have directly led to further controversies over the most important site for insulin action. For the static GLUT4 compartment model, insulin functions to release GLUT4 from an intracellular stored compartment 'prefusion steps'. Conversely, a direct effect on vesicle docking/fusion at the plasma membrane in response to insulin stimulation fits with the dynamic recycling model (Dugani & Klip, 2005) (Leney & Tavare, 2009).

In differentiated muscle cells, GLUT4 intracellular sequestration is regulated both by dynamic cycling and static retention mechanisms (Fazakerely, et al., 2009) (4.3.2). In cultured skeletal muscles cells we and others have shown that they possess small statically retained GLUT4 pools (~10% of total GLUT4 pool) that are mobilised in to the actively cycling pool in response to insulin stimulation or AICAR-treatment. Furthermore, treatment with insulin and AICAR in combination result in a partially additive effect on the size of the actively recycling GLUT4 pool compared to basal cells (64% of the total GLUT4 pool, basal-state versus 85%, agonist-stimulated) (Figure 20, 4.3.2.2). Here we have shown that TBC1D1 knockdown increased the actively recycling GLUT4 pool in non-stimulated C2C12 myotubes (Figure 5.6). Although this observed trend did not reach statistical significance. Importantly, this mobilised GLUT4 pool appeared additive to the GLUT4 pool that is mobilised in response to insulin. These results are consistent with TBC1D1 functioning as a retention signal that is relieved upon phosphorylation by AMPK in response to AICAR treatment (Figure 5.7C, D). In a recent study the phosphorylation of ectopically expressed TBC1D1 at serine 237 has emerged as being vital to facilitate AICAR-responsive GLUT4 liberation from a 'statically retained' compartment. This was established in a 3T3-L1-based GLUT4-retention 'experimental reconstitution model'. (Hatakeyama & Kanzaki, 2013).

Through limitations of these experiments we were unable to investigate further the effect of TBC1D1 knockdown on GLUT4 exocytosis and endocytosis. It will be of importance to examine whether silencing TBC1D1 affects the rate for basal GLUT4 recycling (k_{ex}) at steady-state, in addition to regulating the release of GLUT4 from a storage compartment. Furthermore, it will be of interest to evaluate the effects of TBC1D1 knockdown on insulin-stimulated GLUT4 exocytosis. Multiple insulin and AMPK-regulated phosphorylation sites have been identified in TBC1D1 (Peck, et al., 2009) (Chen, et al., 2008) (Taylor, et al., 2008) (Roach, et al., 2007). Furthermore, numerous studies have reported additive effects of both AMPK-activators and insulin on glucose uptake and/or GLUT4 translocation in to muscle (Bergeron, et al., 1999) (Yang & Holman, 2005) (Yang & Holman, 2006) (Hayashi, et al., 1998) (Fazakerely, et al., 2009). In support of this, we have observed that the combined effect of insulin stimulation and AMPK-activation was synergistic to increase GLUT4 cell surface levels in C2C12 myotubes. Additionally, we have found that co-stimulation with insulin and AICAR resulted in a greater increase in the steady-state rate constant for HA-GLUT4 exocytosis (k_{ex}) compared to insulin stimulation alone (0.016 min^{-1} , basal state, 0.023 min^{-1}, insulin-stimulated, 0.031 min^{-1}, insulin plus AICAR) (Figure 4.6, 4.3.2.3). Therefore, it may be that insulin and AICAR-mediated signalling pathways directly converge and phosphorylate TBC1D1 to regulate the release GLUT4 from a dynamic retention mechanism. Alternatively, AMPK-mediated phosphorylation of TBC1D1 (at serine 237) and subsequent binding to 14-3-3 proteins could liberate GLUT4 in to an insulin-responsive GSV compartment. Consistent with this, a unique ‘regulatory mode shift’ mechanism of TBC1D1 has been recently described. TBC1D1 develops the capacity for insulin-responsive GLUT4 liberation and phosphorylation at threonine 596 only after pre-treatment with AICAR. Furthermore an intact PTB1 domain is essential for this (Hatakeyama & Kanzaki, 2013).

In this present study we have found that siRNA-mediated knockdown of TBC1D4 did not affect basal cell surface levels of GLUT4 compared to control cells. These results indicated that in comparison to TBC1D1, endogenous TBC1D4 may not be required for basal retention in C2C12 myotubes.

Consistent with this, silencing TBC1D4 did not affect the size of the actively cycling GLUT4 pool in basal cells or in response to insulin. Thus, the mobilisation of a small statically retained GLUT4 pool in response to insulin stimulation occurs independently of TBC1D4. These results are in contrast to studies in basal L6 muscle cells where depletion of TBC1D4 elevated GLUT4 at the plasma membrane (Ishikura & Klip, 2008). However, notably, this increase was more marked in L6 myoblasts compared to differentiated myotubes.

In cultured 3T3-L1 adipocytes TBC1D4 is essential for basal GLUT4 intracellular retention and regulating the release of GLUT4 in to the plasma membrane (Larance, et al., 2005) (Eguez, et al., 2005) (Brewer, et al., 2011). shRNA-mediated knockdown of TBC1D4 increased GLUT4 at the cell surface in 3T3-L1 adipocytes under basal conditions (Eguez, et al., 2005) (Brewer, et al., 2011). Importantly, silencing TBC1D4 does not completely inhibit insulin-induced gain of GLUT4 at the cell surface. Similarly, we have shown here that C2C12 myotubes are still insulin-responsive following the depletion of TBC1D4. Interestingly, shRNA mediated knockdown of TBC1D4 reduced the insulin response in 3T3-L1 adipocytes (Eguez, et al., 2005) (Brewer, et al., 2011). Whilst, the depletion of TBC1D4 did not affect insulin-induced cell surface levels of GLUT4 in L6 cells (Ishikura & Klip, 2008). These dissimilar results may be explained simply by the fact that TBC1D4 knockdown efficiency is reduced in L6 cells compared to 3T3-L1 adipocytes. Alternatively, TBC1D4 may have another role in insulin-stimulated responses in 3T3-L1 adipocytes.

As two different models have been proposed to explain how GLUT4 is trafficked within intracellular compartments to regulate basal retention, this has have led to debate over how TBC1D4 regulates GLUT4 retention. More specifically, how insulin regulates the mobilisation of GLUT4 to directly increase cell surface levels. It is now well supported that this retention mechanism governed by TBC1D4 GAP activity is released upon phosphorylation by Akt following insulin stimulation. In support of this, the over expression of the mutant TBC1D4 4P (TBC1D4 mutated to alanine at four phosphorylation sites serine 318, serine 588, threonine 642, serine, removing its capacity to undergo phosphorylation) in 3T3-L1 adipocytes acts as a dominant-negative mutant and results in the partial

inhibition of insulin-stimulated cell surface GLUT4 levels (Zeigerer, et al., 2004) (Sano, et al., 2003). Similar effects have been observed in L6 cells (Stockli, et al., 2008) (Thong, et al., 2007). In addition, the over-expression of TBC1D4 4P inhibited insulin-stimulated glucose uptake in tibialis anterior muscle (Kramer, et al., 2006).The effect of the dominant interfering mutant was subsequently rescued by the concurrent disruption of Rab-GAP activity. It is likely that TBC1D4 is required for the pre-fusion events involving the recruitment/docking of GLUT4 containing vesicles to the plasma membrane. In support of this the over expression of TBC1D4 4P has been shown to inhibit the insulin-induced recruitment/docking of GLUT4 towards the plasma membrane in 3T3-L1 adipocytes (Zeigerer, et al., 2004). This was determined using total internal reflection microscopy (TIRF) which detects HA-GLUT4-GFP fluorescence within an evanescent excitation field (250nm from the membrane). However, it is still not clear as yet to which specific pre-fusion step is regulated by TBC1D4. Additionally, Bai et al. have demonstrated that TBC1D4 is likely to be involved in regulating the docking of GSVs at the plasma membrane (Bai, et al., 2007). In support of this, Brewer et al. have shown that knockdown of TBC1D4 mobilises GLUT4 from a static compartment to increase the size of a primed pre-fusion vesicular compartment (Brewer, et al., 2011). Interestingly, the transition from basal to insulin-stimulated steady-state was faster in TBC1D4 knockdown cells compared with control cells. However, TBC1D4 depletion did not affect the rate constant for exocytosis (k_{ex}) for the actively cycling pool of GLUT4 under basal conditions or following insulin stimulation. It was therefore deduced that TBC1D4 is regulating a rate-limiting step (pre-fusion) in the transition from basal to an insulin-stimulated steady-state in control cells. Conversely, in the basal state the rate limiting step is situated downstream of TBC1D4 in the final stages of GLUT4 translocation. In contrast, in a dynamic recycling system it has been observed that the total ‘insulin-responsive’ GLUT4 pool can access the plasma membrane in the absence of insulin. However, the actively cycling GLUT4 pool is governed by a very slow recycling rate under basal conditions. In these studies, shRNA-mediated silencing of *Tbc1d4* increases the basal exocytosis recycling rate constant (k_{ex}) for GLUT4 (0.005 min^{-1} control to 0.02 min^{-1} TBC1D4 knockdown) and does not affect the k_{ex} for

GLUT4 following insulin stimulation (Eguez, et al., 2005). The reason for two very different GLUT4 recycling models is yet to be determined.

Regardless of the exact mechanism, we have shown here that C2C12 myotubes lack a robust 'non-cycling/slow-cycling' GSV compartment (Figure 4.5, 4.3.2.2). Furthermore, on-going insulin stimulation has been found to induce only a minor increase in GLUT4 at the cell surface in C2C12 myotubes. C2C12 myotubes may lack critical components involved in the development and stability of a GLUT4 storage compartment. For instance, in a recent study, shRNA knockdown of TUG (a protein which is required for GSV intracellular retention) resulted in only a transient 2-fold pulse of GLUT4 exocytosis in 3T3-L1 adipocytes in response to insulin stimulation (Xu, et al., 2011). These results are surprisingly similar to what we have observed here in C2C12 myotubes. It is therefore plausible that C2C12 cells may well be deficient in the protein TUG. Alternatively, the protein TUG could be part of a protein complex which is responsible for complete GLUT4 sequestration in basal cells. Therefore, we cannot rule out that other proteins are involved in maintaining an intact GLUT4 retention compartment. This requires further investigation. Recently an 'experimental reconstitution model' for insulin-responsive GLUT4 trafficking has been established by exogenously expressing TBC1D4 and sortilin in 3T3-L1 fibroblasts. Through the direct analysis of GLUT4 dynamics using quantum dot technology it was observed that siRNA-mediated knockdown of sortilin in differentiated 3T3-L1 adipocytes ablated the GLUT4 static behaviour and increased GLUT4 movements (Hatakeyama & Kanzaki, 2011). Alternatively, the lack of an insulin-responsive compartment may be a consequence of reduced expression of endogenous TBC1D4. However, we observed similar protein expression levels of TBC1D4 (femto-moles of protein per microgram of lysate) in C2C12 myotubes to that in adipose tissue and soleus muscle. We may have underestimated intracellular levels of TBC1D4 in adipose and soleus muscle tissues (due to the abundance of extracellular cellular protein components in tissue samples). Furthermore, it has been reported that there are two protein coding splice variants of the *Tbc1d4* gene (Baus, et al., 2008). The full-length transcript of *Tbc1d4* has been found predominately expressed in skeletal muscle. Therefore, it is reasonable to suggest on this basis of our data that the

long variant is expressed in C2C12 muscle cells. Interestingly, the over-expression of the short-variant TBC1D4 protein increased insulin-stimulated GLUT4 translocation and glucose uptake in L6 myotubes (Baus, et al., 2008). Conversely, the over expression of full-length TBC1D4 did not affect insulin-induced cell surface levels of GLUT4 in L6 myotubes (Stockli, et al., 2008). Therefore, the differential expression of TBC1D4 splice variants could confer specific function. The inclusion/exclusion of a specific protein domain could impede protein-protein interactions and directly affect membrane targeting.

Surprisingly, the double knockdown did not increase basal cell surface GLUT4 levels compared to control myotubes. A possible explanation could be that the efficiency of TBC1D1 knockdown in TBC1D4/TBC1D1 double knockdown cells was reduced compared with the single targeting of TBC1D1 alone. A >70% knockdown 'threshold' is deemed by commercial companies as a cut-off for an efficient knockdown assay. In addition, it was apparent that the data obtained in control non-targeting siRNA cells were ambiguous which made the results from these experiments difficult to interpret. It is possible that the increased concentration of siRNA used for these experiments may have caused non-specific silencing effects. It would therefore be important to further optimise these double knockdown experiments to ensure that the lowest effective concentration of siRNA is used.

In conclusion, our results support a model whereby TBC1D1 inactivation by signalling-dependant phosphorylation is required for GLUT4 translocation. Knockdown of TBC1D1 increased cell surface levels of GLUT4 in basal and in insulin-stimulated C2C12 myotubes. Furthermore, TBC1D1 knockdown increased the release of GLUT4 in to the actively recycling pool. By contrast TBC1D1 knockdown did not change the levels of GLUT4 at the plasma membrane that occur in the presence of the AMPK-activator (AICAR). We have also revealed that TBC1D4 does not appear to regulate basal intracellular GLUT4 retention in C2C12 myotubes. This is likely due to the fact that C2C12 myotubes lack a robust 'non-cycling/slow cycling' insulin-responsive GSV compartment. For future investigations it would be of interest to establish whether the formation/stability of a GLUT4 static compartment can be

programmed in C2C12 myotubes. This may help to improve the C2C12 muscle cell line as a model for studying GLUT4 trafficking.

6 Overall Discussion

6.1 General discussion and conclusions

A substantial amount of research has been dedicated to investigate GLUT4 trafficking in primary adipose cells and 3T3-L1 adipocytes and how insulin signalling regulates GLUT4 translocation. Whereas, fewer studies have focused on how this is regulated in skeletal muscle cells. There have been many technical challenges associated with this complex tissue. The abundance of structural proteins in skeletal muscle tissue has made sub-cellular membrane fractionation procedures problematic for the analysis of GLUT4 intracellular distribution. Furthermore, there are difficulties associated with the isolation of single skeletal muscle fibres. This has impeded detailed kinetic analysis of endogenous GLUT4 trafficking using biotinylated photolabelling techniques and morphological analyses of GLUT4 using immunofluorescence microscopy. Alternative methods have been developed utilising the ectopic expression of epitope-tagged GLUT4 (GLUT4-GFP) in primary skeletal muscle tissue. This experimental approach has enabled more detailed investigations of GLUT4 translocation in response to insulin and contraction-mediated signalling *in situ* (Lauritzen, et al., 2008) (Lauritzen, et al., 2006). More recently, the transgenic expression of an exofacial-tagged GLUT4 (HA-GLUT4-GFP) in mice has enabled direct measurements of GLUT4 inserted into the cell membrane of intact single muscle fibres (Lizunov, et al., 2012) (Fazakerely, et al., 2009). Technical problems associated with the preparation of primary muscle have prevented these models from being used more extensively used within the field for the examination of GLUT4 trafficking kinetics. Therefore, immortal skeletal muscle cell lines (L6 cells and C2C12 myotubes) have provided alternative model systems. Clonal skeletal muscle cells can be easily maintained in culture and can be efficiently manipulated through transduction and transfection techniques.

The investigations carried out for this thesis utilised the exofacial-tagged GLUT4 construct (HA-GLUT4) to analyse GLUT4 trafficking following insulin and contraction-mediated signalling in C2C12 skeletal muscle cells. Using this cell

model we were able to use the HA-tag to directly monitor the kinetics of HA-GLUT4 translocation The objective for these current investigations was to examine the role of the Rab-GTPase activating proteins (GAP) TBC1D1 and TBC1D4 with respect to GLUT4 trafficking. In order to investigate this, small interfering RNA (siRNA) constructs were utilised to specifically knockdown TBC1D1 and TBC1D4 in C2C12 myotubes. To date, there is limited and varied information available regarding an efficient transfection system in C2C12 myotubes. Many studies have used electroporation in order to effectively transfect C2C12 myotubes (Chadt, et al., 2008) (Tao, et al., 2011) (Verrier, et al., 2011). However, the high rate of cell death following electroporation has meant that this method is difficult to apply to plate assays where high numbers of cells are required. We have therefore optimised a siRNA gene silencing approach using lipid-based transfection. Un-differentiated C2C12 myoblasts expressing HA-GLUT4 were transfected at an intermediate differentiation stage (Day 2) and experiments were conducted using fully differentiated C2C12 myotubes.

The use of C2C12 myotubes disclosed unique insights into the regulation of GLUT4 trafficking. Our data revealed the activation of insulin or AMPK signalling pathways resulted in distinct effects on GLUT4 trafficking parameters in C2C12 cells. We have determined that insulin initiates an increase of GLUT4 exocytosis and that activation of AMPK inhibited GLUT4 internalisation. The combined effect of insulin stimulation and AMPK-activation was synergistic and led to increased GLUT4 cell surface levels. Insulin stimulation and AICAR-treatment in combination result in the partial additive mobilisation of GLUT4 into the actively recycling pool in C2C12 myotubes. Therefore, these data support the concept that these stimuli promote GLUT4 accumulation at the cell surface via distinct signalling pathways. In addition, GLUT4 exocytosis was enhanced following the co-stimulation with insulin and AICAR. Thus, the activation of both AMPK and Akt signalling pathways may also converge on a single signalling intermediate to enhance GLUT4 exocytosis. Together our results indicate that multiple and complex mechanisms exist in muscle cells to regulate GLUT4 redistribution to the cell surface.

TBC1D1 and TBC1D4 are proposed to function as negative regulators of GLUT4 trafficking which function through maintaining an un-specified rab protein in its in-active GDP-bound state. The phosphorylation of TBC1D1/TBC1D4 leads to the in-activation of its GAP activity and therefore allows the rab to switch to an activate GTP bound state. Current evidence supports the model that the Rab-GAP TBC1D4 is primarily required for basal intracellular retention of GLUT4. This is supported through knockdown studies in 3T3-L1 adipocytes (Eguez, et al., 2005) (Brewer, et al., 2011) and in L6 muscle cells (Ishikura & Klip, 2008). Therefore it was somewhat surprising to find that siRNA-mediated depletion of TBC1D4 did not affect basal cell surface levels of GLUT4 in C2C12 myotubes. However, there are several possible explanations for this result. Firstly, there was a significant amount of residual TBC1D4 protein within cells transfected with *Tbc1d4*-specific siRNA. Therefore, this could be sufficient to carry out a normal function. Further optimisation of knockdown protocols to improve efficiency will be important to test this. Secondly, this result could indicate that there is a limited role for TBC1D4 in C2C12 myotubes. In support of this, we have shown that TBC1D4 protein levels were to some extent down-regulated during C2C12 cell differentiation. TBC1D4 is expressed predominately in oxidative soleus skeletal muscle than in glycolytic muscles such as tibialis anterior and extensor digitorum longus. Therefore it is possible that C2C12 myotubes may represent a characteristic glycolytic muscle type cell and therefore express a reduced level of TBC1D4. Alternatively, TBC1D4 is not able to function correctly in C2C12 myotubes. In support of this, TBC1D4 has been found to restrict the movement of GLUT4 from a 'non-cycling/slow-cycling' GSV compartment into an actively cycling GLUT4 pool in 3T3-L1 adipocytes (Eguez, et al., 2005) (Brewer, et al., 2011). The insulin-mediated phosphorylation of TBC1D4 is required to release this brake through the inactivation of its Rab-GAP activity. Therefore, TBC1D4 is central for regulating the large proportion of insulin-stimulated GLUT4 translocation in adipocytes. Our findings revealed that a robust 'non-cycling/slow-cycling' GSV compartment is deficient in C2C12 myotubes (Figure 6.1). Furthermore, this inadequate basal GLUT4 retention mechanism is likely to be responsible for the lack of a robust insulin-responsive GLUT4 translocation system in C2C12 cells. Additional support for this mechanism has come from studies in L6 myoblasts,

where a slow GLUT4 recycling rate governs basal intracellular retention. Insulin stimulation markedly increases the rate of recycling for GLUT4, thus, redistributing GLUT4 to the cell surface (Foster, et al., 2001).

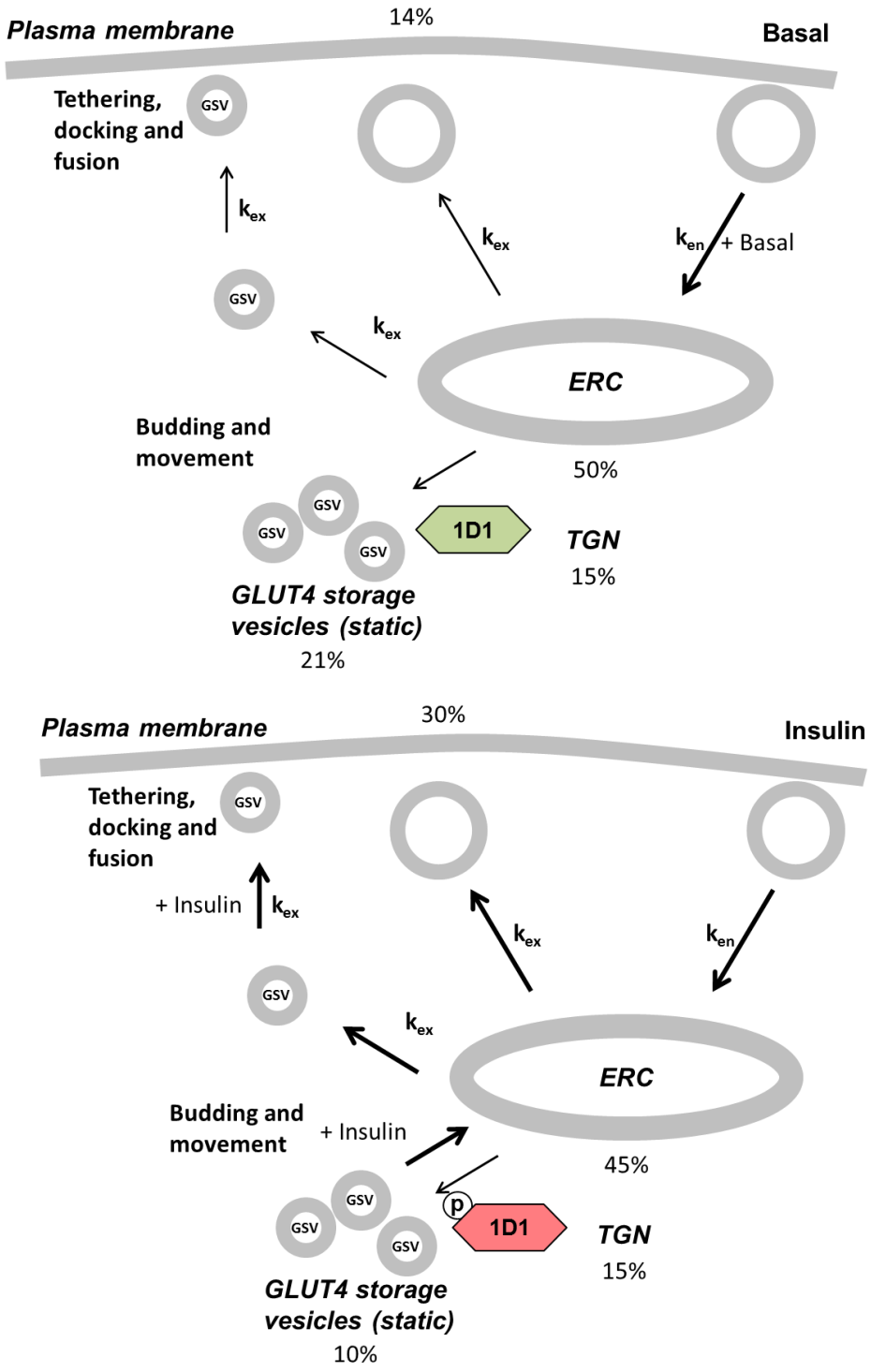

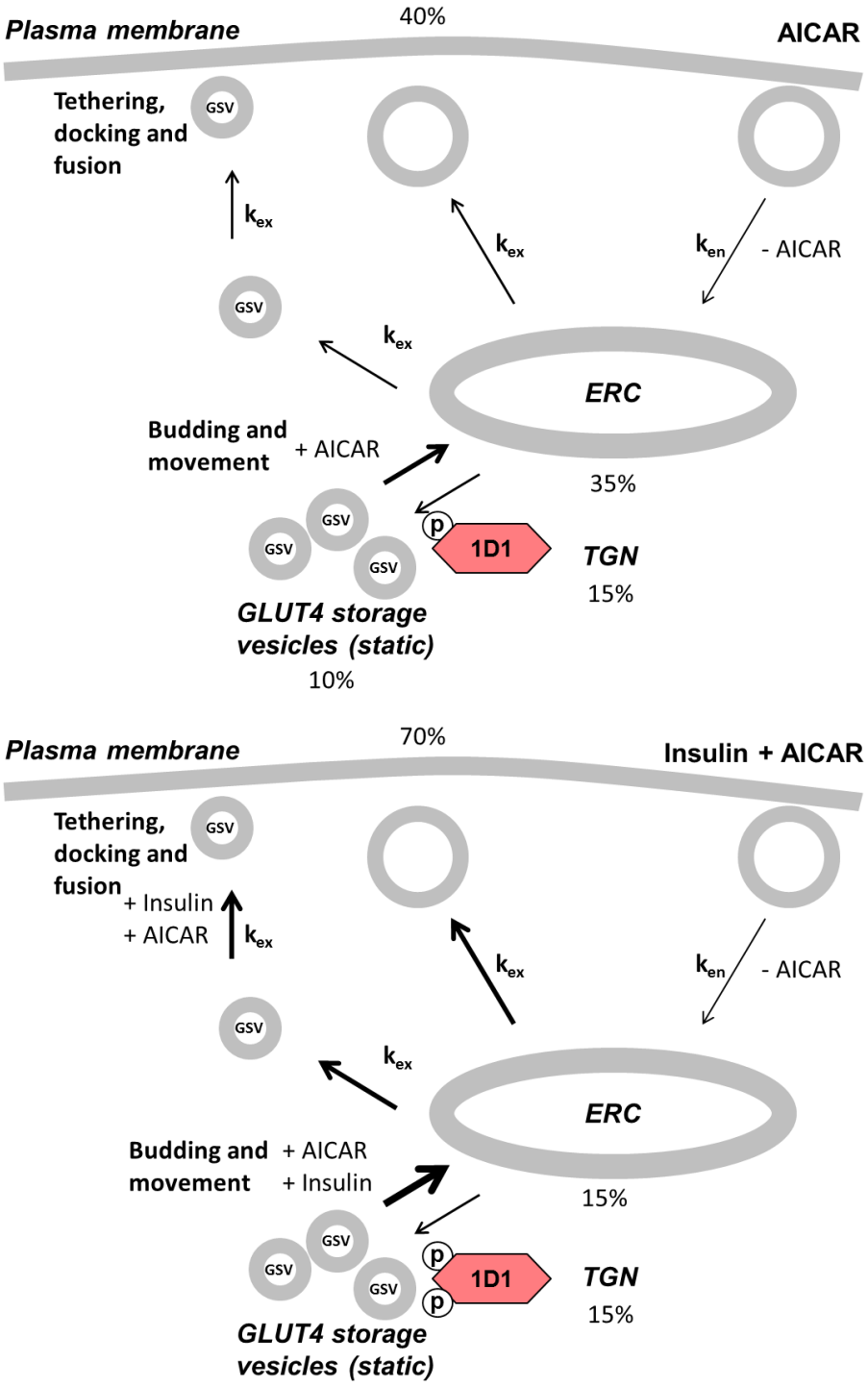
Plasma membrane
40%
AICAR
Tethering, docking and fusion
GSV
k_{ex}
k_{en}
- AICAR
ERC
Budding and movement
+ AICAR
35%
p
1D1
TGN
15%
GLUT4 storage vesicles (static)
10%
Plasma membrane
70%
Insulin + AICAR
Tethering, docking and fusion
+ Insulin
+ AICAR
Budding and movement
+ AICAR
+ Insulin
15%
TGN
15%
GLUT4 storage vesicles (static)

Figure 6.1: Regulation of GLUT4 trafficking in C2C12 myotubes. These models are based on the three-pool for GLUT4 recycling. In the three-pool models, GLUT4 recycles through two intracellular compartments; the endosomal recycling compartment (ERC) and GLUT4 storage vesicles and the plasma membrane. The additional pool can account for the initial rapid stimulation of GLUT4 translocation to the plasma membrane following insulin stimulation and the slower steady-state $t_{1/2}$ value for GLUT4 exocytosis in the continued presence of insulin. In the basal state, cell surface levels of GLUT4 are kept low (14%) from the slow movement of GLUT4 to the plasma membrane and the rapid retrieval back to ERC. A small pool of GLUT4 is sequestered in a static GLUT4 storage compartment (GSV). GLUT4 retention is regulated by active TBC1D1 (1D1 green). Insulin simulates the release of GLUT4 from a static GSV pool in to the ERC to increase cell surface levels to 30%. AICAR inhibits the internalisation of GLUT4 from the plasma membrane and simulates the release of GLUT4 from a static GSV pool in to the recycling compartment to increase cell surface levels (40%). Insulin plus AICAR in combination have additive effects to increase cell surface levels of GLUT4 (70%). The percentage values are measured as a fraction of total cellular GLUT4. A small proportion of GLUT4 is not actively recycling (15%) and is thought to reside in the Trans Golgi Network (TGN). Arrows indicate the movement of GLUT4 between compartments. Heavy weighted arrows indicate increased movement.

Importantly, other retention mechanisms exist in order to maintain low surface levels of GLUT4 in basal C2C12 myotubes. TBC1D1 Rab-GAP activity is proposed to be regulated through phosphorylation in much the same way as TBC1D4. TBC1D1 contains many insulin-regulated phosphorylation sites (Peck, et al., 2009) (Taylor, et al., 2008). Several studies have demonstrated that TBC1D1 is phosphorylated in response to insulin in skeletal muscle (Kramer, et al., 2006) (Bruss, et al., 2005) (Funai & Cartee, 2008) (Funai & Cartee, 2009). However, in contrast to TBC1D4 multiple AMPK phosphorylation sites have been identified in TBC1D1 (Peck, et al., 2009) (Taylor, et al., 2008) (Chen, et al., 2008) (Roach, et al., 2007). The identification of TBC1D1 as an AMPK substrate supports a role for TBC1D1 as a downstream signalling intermediate of contraction. Furthermore, it has been proposed that TBC1D1 could be primarily responsible for regulating contraction-mediated glucose uptake in muscle (Funai & Cartee, 2009) (An, et al., 2010) (Vichaiwong, et al., 2010) (Pehmoller, et al., 2009). Importantly, we have shown here that the amount of TBC1D1 protein expressed (femto-moles of protein per microgram of tissue lysate) is significantly greater than the level of TBC1D4 in all types of skeletal muscle. This finding contradicts our current understanding that the expression of TBC1D1 and TBC1D4 is muscle-type specific (Taylor, et al., 2008) (Szekeres, et al., 2012). However, these assumptions were based on relative quantification experiments. This original hypothesis has led to speculation over the function of TBC1D1 in glycolytic fibre-type muscles (TA, EDL) than in oxidative soleus muscles. Instead, our observations enable us to address

TBC1D1 function as common feature of both oxidative and glycolytic skeletal muscles in general. However, the predominant expression of TBC1D4 in oxidative soleus muscle may indirectly affect the function of TBC1D1 in these muscles.

It is important to note that mouse soleus muscle consists of ~80% type I (slow-twitch) and type IIA (fast-twitch) oxidative muscle fibres. In contrast, rat soleus muscle has been shown to contain predominately type I slow twitch fibres (Bloemberg & Quadrilatero, 2012). This is comparable to human soleus muscle (Gollnick, et al., 1974). It is plausible therefore that the high level of TBC1D1 expression in mouse soleus muscle that we have observed in this present study could be related to its content of type II fibres. Consequently, the relative Rab-GAP expression levels may relate to the metabolic requirements for the individual muscle-fibres. Considering that most skeletal muscles are composed of a mixture of muscle fibres, it will be of great importance for future studies to investigate GLUT4 trafficking with respect to muscle fibre-type.

Through siRNA-mediated silencing of TBC1D1 we show that TBC1D1 is required for basal GLUT4 intracellular retention in C2C12 myotubes. TBC1D1 is required for the sequestration of a ‘statically retained’ pool of GLUT4. We find that the depletion of TBC1D1 was only partially AICAR-mimetic and does not impair the maximum cell surface levels of GLUT4 attained following AICAR-treatment. This supports the concept that TBC1D1 is at least partly required for regulating contraction-mediated GLUT4 translocation. The retention mechanism governed by the activity of Rab-GAP TBC1D1 is likely to be released upon phosphorylation by AMPK which follow AICAR-treatment (Figure 6.1). In support of this, we have shown here that TBC1D1 is phosphorylated on serine 237 in response to AMPK-activation. This is in support of data presented in other studies (Peck, et al., 2009) (Pehmoller, et al., 2009) (Chen, et al., 2008) (Taylor, et al., 2008) (Roach, et al., 2007).

In a recent study a GLUT4-retention ‘experimental reconstitution model’ has been established in 3T3-L1 fibroblasts over-expressing sortilin. The stationary behaviour of GLUT4 was determined through the direct analysis of GLUT4

dynamics using Quantum-dot nanometry. It has been revealed that sortilin is critical for the recruitment of internalised GLUT4 to the specialised sub-domain of the TGN via an endosome to TGN retrieval mechanism. This interaction is crucial for the development of a 'static GLUT4 retention' compartment in 3T3-L1 adipocytes. Furthermore, the TGN-golgin Golgin 97 plays an important role in the recruitment of GLUT4 to the TGN for the development of a stationary GLUT4 compartment. Golgins are required for tethering events in membrane fusion. Additionally, the expression of TBC1D4 within this artificial cell model is essential for insulin-responsive liberation of GLUT4 from this static GLUT4 compartment (Hatakeyama & Kanzaki, 2011). Following on from this study the 'experimental reconstitution model' has been used to examine the functional role for TBC1D1. Interestingly, the phosphorylation of TBC1D1 at Serine 237 has emerged as being critical to facilitate AICAR-responsive GLUT4 liberation from 'static retention' (Hatakeyama & Kanzaki, 2013).

In 3T3-L1 adipocytes an insulin-dependent association between 14-3-3 and TBC1D4 plays an important role in the inactivation of TBC1D4 Rab-GAP activity and the regulation of GLUT4 trafficking (Ramm, et al., 2006) (Koumanov, et al., 2011). In contrast, the binding of TBC1D1 to 14-3-3 is regulated through the phosphorylation of TBC1D1 at serine 237 in L6 myotubes (Chen, et al., 2008). Therefore, the association between TBC1D1 phosphorylated at AMPK sites and 14-3-3 may play an important role in the mobilisation of GLUT4 in C2C12 myotubes.

Interestingly, we have found that TBC1D1 knockdown in C2C12 myotubes did not affect the cell response to insulin. Consistent with this, insulin alone does not liberate GLUT4 from 'static retention' within a cell-based GLUT4-retention 'experimental reconstitution model' despite augmenting the phosphorylation of ectopically expressed TBC1D1 at threonine 596 (Hatakeyama & Kanzaki, 2013). Furthermore, TBC1D1 phosphorylated at threonine 596 in response to insulin appears to be insufficient to induce 14-3-3 binding (Chen, et al., 2008) (Pehmoller, et al., 2009). Instead, we have found that TBC1D1 knockdown potentiated the transient cell surface levels of GLUT4 reached following insulin stimulation in C2C12 myotubes. Therefore, endogenous TBC1D1 appears to be

required to restrict insulin-induced GLUT4 redistribution to the cell surface. The rapid and transient accumulation of GLUT4 at the cell surface is likely to correspond with the early fusion of GLUT4 containing vesicles at the cell surface in response to insulin. It is possible that TBC1D1 could directly regulate the formation of this insulin-responsive GSV compartment. One plausible mechanism is that following TBC1D1 knockdown GLUT4 is liberated from 'static retention' and released directly into the insulin-responsive GSV compartment. Alternatively, TBC1D1 may regulate more than one discrete pathway in muscle cells. TBC1D1 could be differentially localised within the cell and may well be regulated through multiple signalling pathways. For instance, Insulin and AICAR-mediated signalling pathways could converge to phosphorylate TBC1D1 and release GLUT4 from a dynamic retention mechanism. The phosphorylation of TBC1D1 on both putative AMPK and Akt sites could enable TBC1D1 to be differentially regulated. Consistent with the latter, TBC1D1 develops the capacity for insulin-responsive GLUT4 liberation from 'static state' only after pre-treatment with AICAR (Hatakeyama & Kanzaki, 2013). Furthermore, this function of TBC1D1 is dependent on an intact first phosphotyrosine-binding domain (PTB) domain (PTB1) (Hatakeyama & Kanzaki, 2013). A model such as this may explain the enhanced GLUT4 exocytosis following the co-stimulation with insulin and AICAR in C2C12 myotubes. Unfortunately, we were unable to determine whether silencing TBC1D1 affected GLUT4 exocytosis under either basal conditions or following insulin stimulation or AICAR-treatment. Further studies will be required to investigate this.

This current study supports TBC1D1 as a regulator of insulin and AMPK-mediated GLUT4 translocation. However, we find that TBC1D1 is not required for insulin-stimulated GLUT4 redistribution to the plasma membrane in C2C12 myotubes. In support of this the over expression of TBC1D1 4P in TA muscle did not affect insulin-stimulated glucose transport (An, et al., 2010). However, the over expression of TBC1D1 carrying the missense mutation R125W (originally identified as a candidate causing severe familial obesity predisposition in humans (Stone, et al., 2006) (Meyre, et al., 2008) has been found to impair insulin-induced glucose transport in TA muscle. The precise mechanism for how this mutation affects TBC1D1 and its regulation is still

unknown. However, the mutation is found within the PTB1 domain. PTB domains are important for protein-protein interactions. Therefore, it is plausible that the R125W mutation could affect the interaction of TBC1D1 with 14-3-3 or other proteins involved in regulating Rab-GAP activity. Recently, a truncation mutant of TBC1D4 (AS160 R363X) has been described which is involved in acanthosis nigricans and postprandial hyperglycemia in humans. It was found that the mutant TBC1D4 protein interacts with wild-type TBC1D4 and inhibits insulin-stimulated GLUT4 translocation (Dash, et al., 2009). Furthermore, the overexpression of a TBC1D4 PTB tandem construct inhibits 14-3-3 binding to endogenous TBC1D4 and an *in vitro* vesicle fusion reaction which inhibits insulin-stimulated gain of GLUT4 at the cell surface in adipocytes (Koumanov, et al., 2011).

Interestingly, the putative AMPK-phosphorylation motif at serine 237 is located between the two PTB domains of TBC1D1. Surprisingly, the over expression of TBC1D1 R125W in TA muscle did not affect contraction-stimulated glucose transport (An, et al., 2010). Further investigations are required to determine how the R125W mutation in TBC1D1 aberrantly impairs glucose uptake. It will be crucial to determine more specifically how this mutation in TBC1D1 affects GLUT4 trafficking.

It seems plausible that a GLUT4 sorting defect through the absence of sortilin or an underdeveloped TGN could be responsible for the lack of a substantial ‘static GLUT4 compartment’ in C2C12 myotubes. Alternatively, the GSVs may form from the TGN but mechanisms which regulate retention and stability are compromised. For instance, through the lack of protein TUG. This static behaviour of GLUT4 is required for maximal insulin-stimulated cell surface GLUT4 levels. Therefore, for future investigations it would be of interest to establish whether the formation of a GLUT4 static compartment can be artificially programmed in C2C12 myotubes. To improve the C2C12 cell line as a model for studying GLUT4 trafficking in muscle.

Further investigations will be needed to fully characterise the importance and function of TBC1D1 and TBC1D4 splice variants. It is clear that the long

variants of both proteins are primarily expressed in skeletal muscle (Baus, et al., 2008). Furthermore, the long splice-variant of TBC1D1 is up-regulated during the differentiation of C2C12 myotubes. In contrast, the short splice variant of TBC1D4 is up-regulated during differentiation in 3T3-L1 adipocytes (Chavez, et al., 2008). This suggests that these variants may have a particular important role within these tissues.

6.2 Future Directions

Both the transition experiments and anti-HA antibody uptake assays described in this thesis are based on those developed by Govers et al, for the studies of GLUT4 trafficking in 3T3-L1 adipocytes (Govers, et al., 2004) (Coster, et al., 2004). Additionally, these assays have been optimised in our laboratory to study GLUT4 trafficking in L6 myotubes (Fazakerely, et al., 2009). These assays have been developed and optimised in a 96-well plate format which has enabled multiple variables and replicates to be tested and analysed in a single plate experiment. These assays can then be evaluated using a fluorescence-based micro titre plate reader which allows rapid quantitative analysis. Furthermore, plate-readers provide information for a cell-population which avoids any experimental bias through single-cell imaging techniques. However, we have made the assumption that the population average will reflect the most prominent effect within individual cells. During these experimental investigations some issues have emerged potentially regarding the application of investigations using population-based averages in C2C12 myotubes. Firstly, these studies do not provide sufficient information to ascertain whether multiple cell populations respond differently to insulin or contraction-mediated stimuli. Differentiated C2C12 cells form a heterogeneous population of multi-nucleated tubes, even under standardised culture conditions for both growth and differentiation of the cells (Yoshida, et al., 1998). In particular giant rounded multinucleated structures are a common feature in cultures of differentiated C2C12 cells. Furthermore, some cells remain as a myoblastic population. It is possible, therefore, that the error within the experimental results detailed in this thesis may have been affected because of this. Cell population-based analysis has been useful for the studies of GLUT4 trafficking in L6 myotubes (Fazakerely, et al., 2009) (Govers, et al., 2004) (Somwar, et al., 2001) (Foster, et al., 2001). However, this could be explained by the fact that L6 myotubes may form a less heterogeneous population at least morphologically.

Secondly, we did not determine whether the transfection efficiency of siRNA constructs differed across sub-populations of differentiating C2C12 cells. This could heighten the variability in the functional read out of our assays (HA-

GLUT4 at the cell surface) based on an average population of cells. In future investigations it may be more appropriate to develop short hairpin RNA (shRNA) constructs to target and knockdown *Tbc1d1* and *Tbc1d4* in C2C12 myotubes. This approach has been routinely used to silence *Tbc1d1* (Chavez, et al., 2008) and *Tbc1d4* (Eguez, et al., 2005) (Brewer, et al., 2011) (Larance, et al., 2005) in 3T3-L1 adipocytes. These shRNA constructs are introduced using retroviral vectors. Use of this approach would overcome difficulties with transfection techniques and would allow for the selection of stable knockdown cells. Additionally, C2C12 myoblasts cells could be simultaneously co-infected with retroviruses for HA-GLUT4 and shRNA constructs which would prevent the manipulation of cells during the early stages of differentiation. However, even with shRNA-mediated gene silencing there will still be cell-to-cell variation of protein expression levels.

Cell heterogeneity is an important factor and its impact on population based analyses has been recently reviewed (Altschuler & Wu, 2010). In future investigations using C2C12 myotubes it will be of great importance to address this issue. Detailed studies to establish whether the responses of sub populations of cells are different from each other and the population average would be required in order test this. Furthermore, a consistent theme addressed in this thesis is the importance of information obtained from time-course analysis and not just end point results. This is vital in order to understand the dynamic behaviour of a system.

The application of confocal microscopy imaging techniques have been routinely used to study the kinetics of GLUT4 trafficking within populations of single-nucleated 3T3-L1 cells (Karylowski, et al., 2004) (Martin, et al., 2006). However, traditional imaging techniques cannot be as easily applied to study large multi-nucleated C2C12 cells. Furthermore, fluorescence imaging has the disadvantage of being less high-throughput especially when there are multiple sub-populations of cells. More recently, high content analysis (HCA) in cell-based systems has been developed which effectively combines high-throughput automated fluorescence microscopy with quantitative imaging analysis. This technology enables detailed temporal and spatial information to be acquired

along with the capacity to identify and selectively analyse sub populations of cells. In future investigations the development of a high-content cell-based assay will be an extremely valuable tool to measure HA-GLUT4 trafficking in C2C12 myotubes.

Although not presented in the thesis work, a validation experiment has been recently performed to investigate the usefulness of a HCA approach to study HA-GLUT4 translocation in C2C12 myotubes. We conducted a study to measure the time dependant accumulation of GLUT4 (HA-GLUT4) at the cell surface in response to insulin and AICAR using the confocal imaging plate reader, the IN Cell Analyzer system 2000 (GE Healthcare). The nuclei were identified based on DAPI staining. The results represent the fluorescence intensity measured around each nucleus. Representative fluorescence images are presented in an appendix. Further work is required to develop and test custom built protocols to analyse multiple cell populations using the IN Cell Investigator Software. Furthermore, it will be a great advantage to correlate the knockdown of a target with the phenotypic changes and relate this to the different sub populations of cells. HCA systems will be an important and valuable tool for future investigations.

In summary, we have attempted to comprehensively investigate GLUT4 trafficking in the C2C12 skeletal muscle cells as they respond to insulin signalling and AMPK activation. We found that the combined activation of insulin and AMPK-signalling pathways were synergistic to increase GLUT4 at the cell surface. We present evidence that basal GLUT4 retention is regulated through mechanisms involving TBC1D1 in C2C12 myotubes. The results also support a model whereby TBC1D1 inactivation is required for AICAR-induced GLUT4 translocation. This may occur partly through the mobilisation of GLUT4 into the actively recycling pool. Additionally, TBC1D1 may also be important for negatively-regulating insulin-stimulated GLUT4 at the cell surface in muscle cells. The activation of both AMPK and Akt signalling pathways may converge on TBC1D1 to enhance GLUT4 exocytosis. Furthermore, our findings support the concept that insulin can directly stimulate the accumulation of GLUT4 at the

plasma membrane through TBC1D4-independent mechanisms. This is likely to occur through the fusion of highly insulin-responsive GSVs at the cell surface.

Finally, the work presented in this thesis provides evidence to support the involvement of AMP-activated protein kinase and subsequent downstream signalling pathways that lead to GLUT4 translocation. We thereby have added support to the idea that this activation route is an attractive therapeutic target for the treatment of type II diabetes and obesity.

Appendix

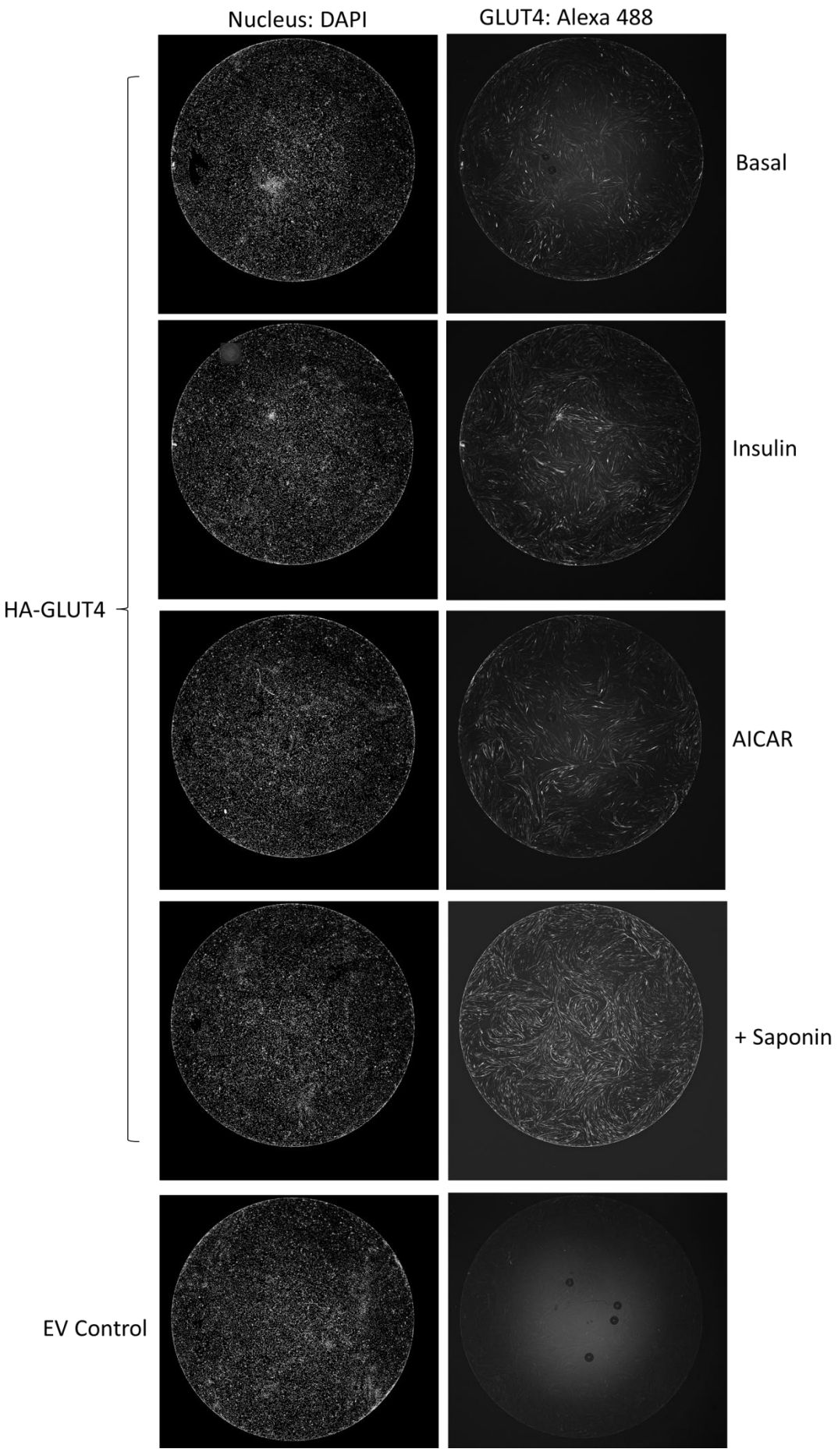
Nucleus: DAPI
GLUT4: Alexa 488
Basal
Insulin
AICAR
+ Saponin
HA-GLUT4
EV Control

Figure A1: Representative fluorescence microscopy images of basal, insulin-stimulated and AICAR-treated C2C12 myotubes expressing HA-GLUT4. C2C12 myoblasts were infected with 0.025ml HA-GLUT4 retro-virus or empty vector (EV) virus as a control. C2C12 myotubes on day 7 post differentiation were maintained under basal conditions, stimulated with insulin at 200 nM for 5 min or treated with AICAR at 2 mM for 45 min. The cell surface levels of GLUT4 was determined by incubating fixed cells with anti-HA primary antibodies and anti-mouse Alexa 488 secondary antibodies. Total cellular GLUT4 was determined in premeabilised cells pre-treated with saponin prior to primary antibody staining. All cells were co-stained with the nuclear stain 4,6-diamidino-2- phenylindole (DAPI). Images were captured using the IN Cell Analyzer system 2000 high content analysis (HCA) confocal imaging plate reader (GE Healthcare). Images were aquired at 2x as a single image field on a 96-Well plate (2x 0.1 NA objective). Images are representative of three intra-assay repeat wells.

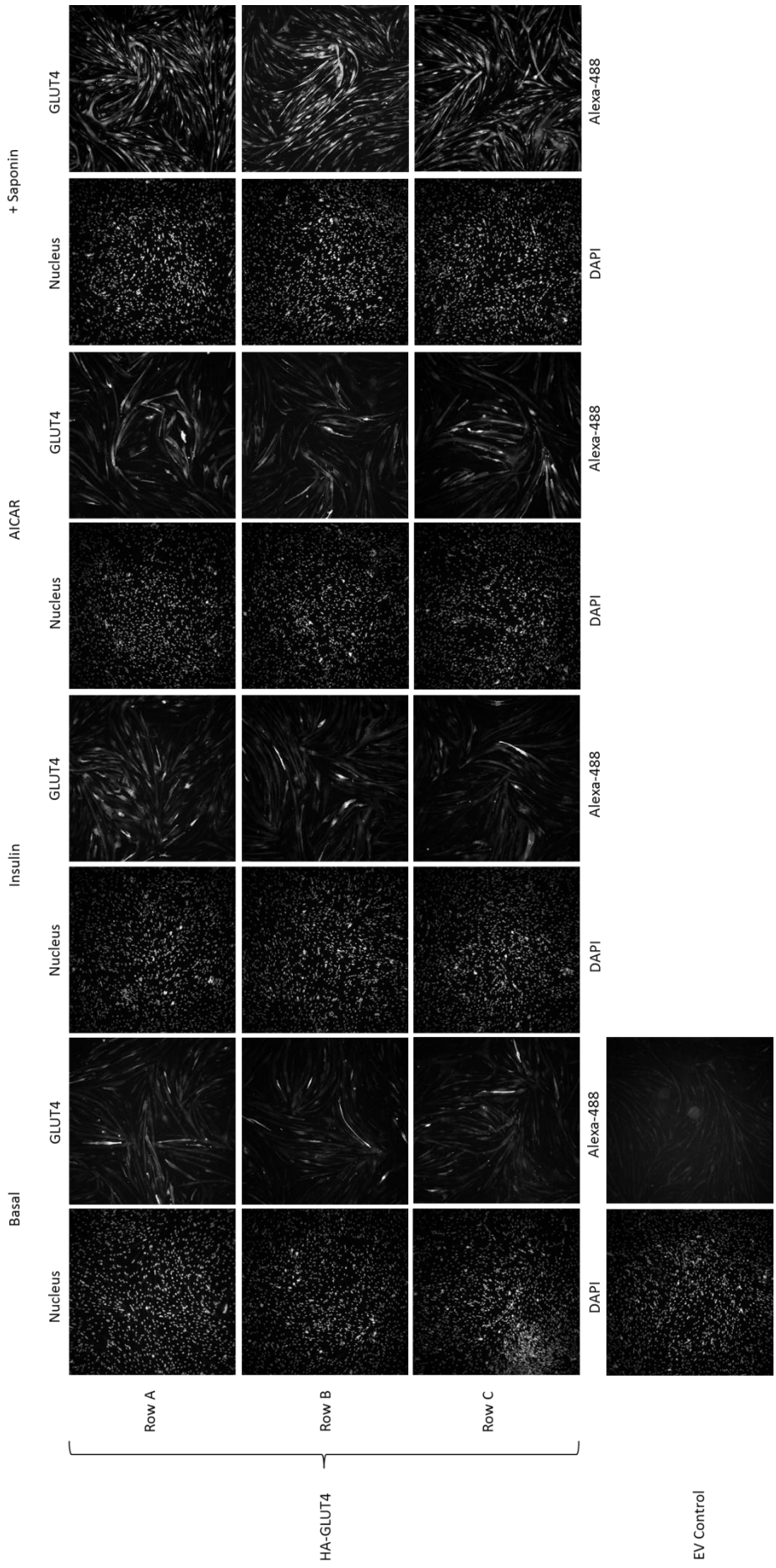
Basal
Insulin
AICAR
+ Saponin
Nucleus
GLUT4
DAPI
Alexa-488
Row A
Row B
Row C
HA-GLUT4
EV Control

Figure A2: Florescence microscopy images of basal, insulin-stimulated and AICAR-treated C2C12 myotubes expressing HA-GLUT4. C2C12 myoblasts were infected with 0.025ml HA-GLUT4 retro-virus or empty vector (EV) virus as a control. C2C12 myotubes on day 7 post differentiation were maintained under basal conditions, stimulated with insulin at 200 nM for 5 min or treated with AICAR at 2 mM for 45 min. The cell surface levels of GLUT4 was determined by incubating fixed cells with anti-HA primary antibodies and anti-mouse Alexa 488 secondary antibodies. Total cellular GLUT4 was determined in premeabilised cells pre-treated with saponin prior to primary antibody staining. All cells were co-stained with the nuclear stain 4,6-diamidino-2- phenylindole (DAPI). Images were captured using the IN Cell Analyzer system 2000 high content analysis (HCA) confocal imaging plate reader (GE Healthcare). One field was captured per well of a 96-Well plate. One field was captured per well of a 96-Well plate. Images were aquired using a 20x 0.75 NA objective lens.

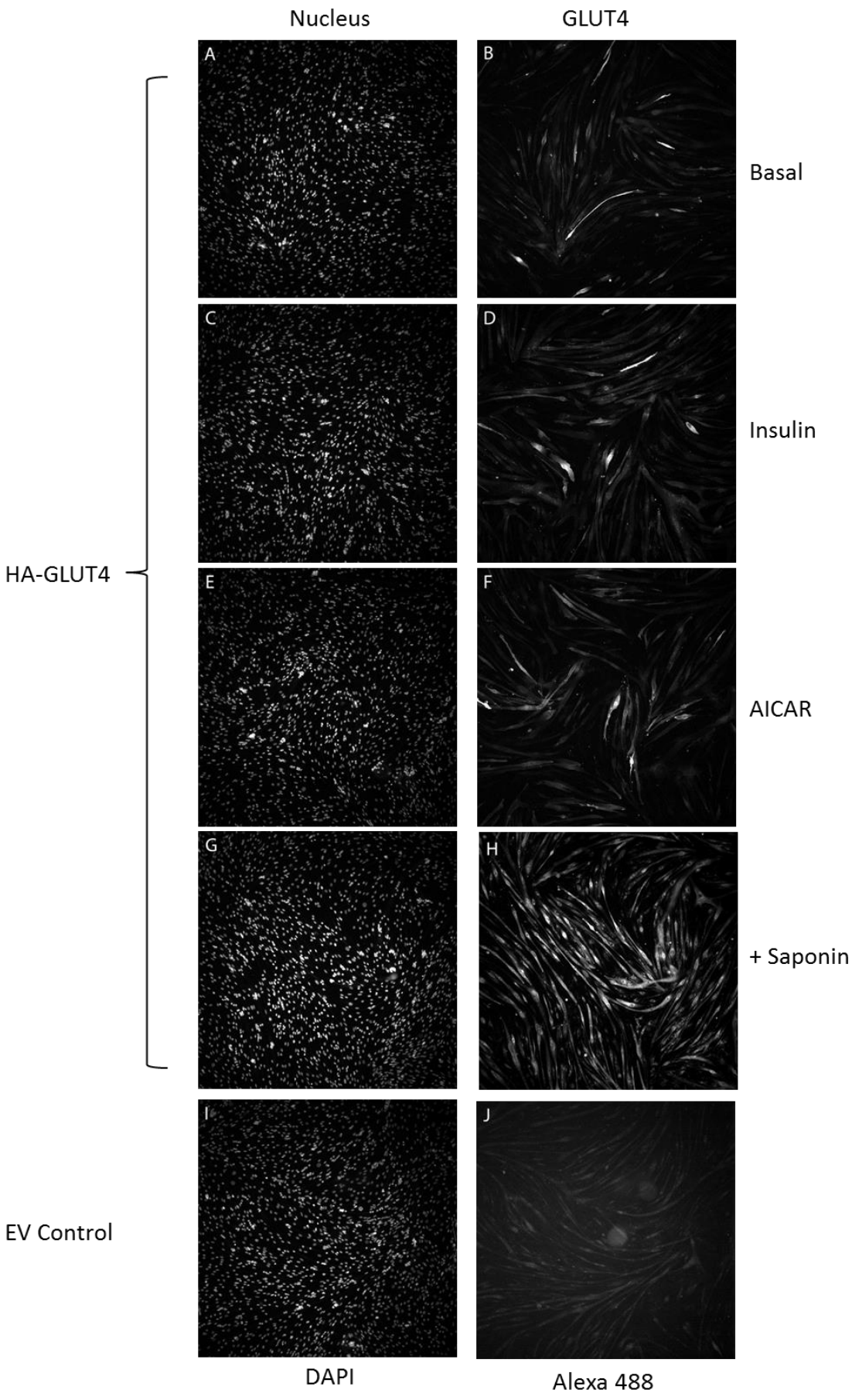
Nucleus
GLUT4
A
B
Basal
C
D
Insulin
HA-GLUT4
E
F
AICAR
G
H
+ Saponin
I
J
EV Control
DAPI
Alexa 488

Figure A3: Representative florescence microscopy images of basal, insulin-stimulated and AICAR-treated C2C12 myotubes expressing HA-GLUT4. C2C12 myoblasts were infected with 0.025ml HA-GLUT4 retro-virus or empty vector (EV) virus as a control. C2C12 myotubes on day 7 post differentiation were maintained under basal conditions, stimulated with insulin at 200 nM for 5 min or treated with AICAR at 2 mM for 45 min. The cell surface levels of GLUT4 was determined by incubating fixed cells with anti-HA primary antibodies and anti-mouse Alexa 488 secondary antibodies. Total cellular GLUT4 was determined in premeabilised cells pre-treated with saponin prior to primary antibody staining. All cells were co-stained with the nuclear stain 4,6-diamidino-2- phenylindole (DAPI). Images were captured using the IN Cell Analyzer system 2000 high content analysis (HCA) confocal imaging plate reader (GE Healthcare). One field was captured per well of a 96-Well plate. Images were aquired using a 20x 0.75 NA objective lens. Images are representative of three intra-assay repeat wells.

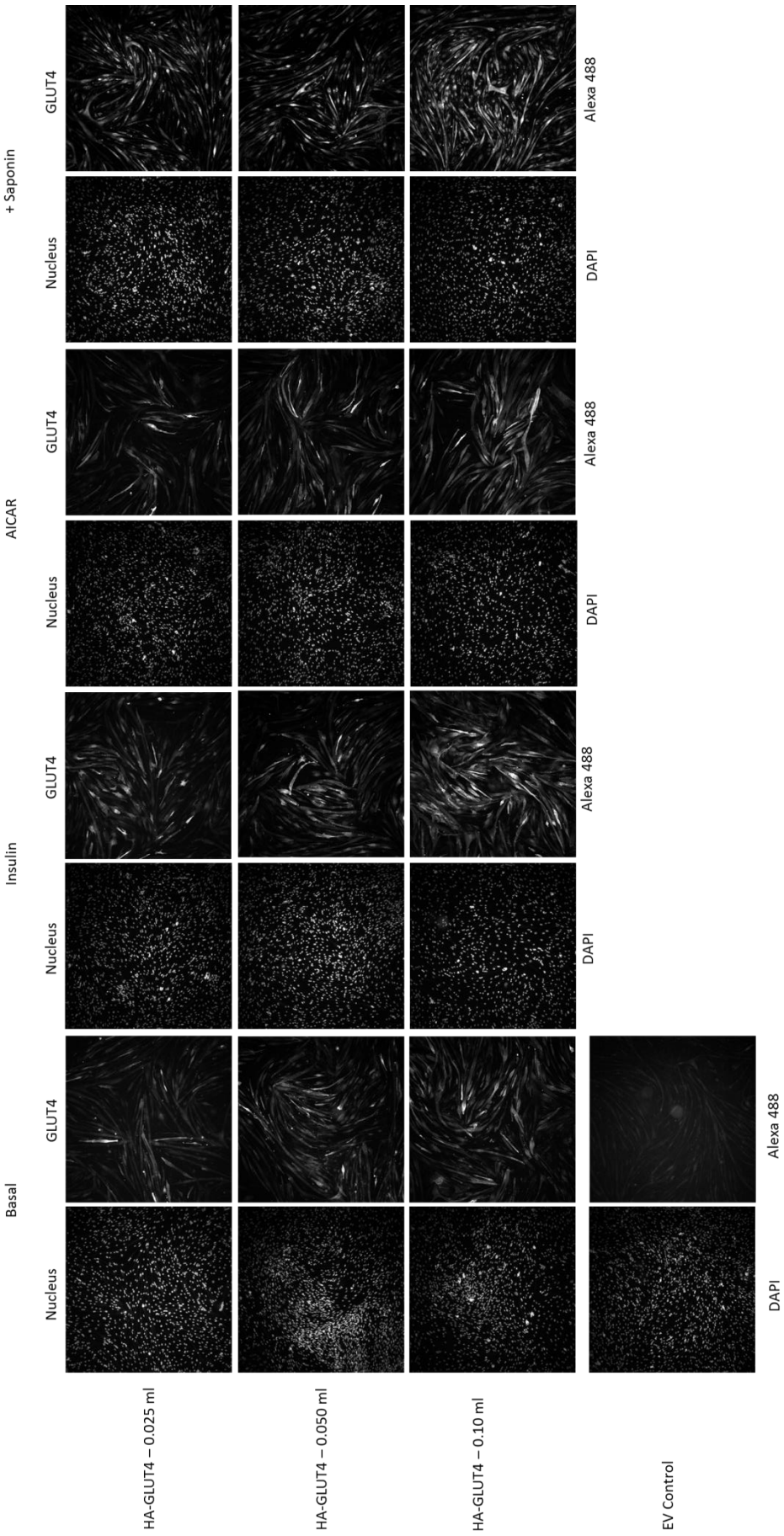
Basal
Insulin
AICAR
+ Saponin
Nucleus
GLUT4
DAPI
Alexa 488
HA-GLUT4 – 0.025 ml
HA-GLUT4 – 0.050 ml
HA-GLUT4 – 0.10 ml
EV Control

Figure A4: Representative fluorescence microscopy images of basal, insulin-stimulated and AICAR-treated C2C12 myotubes expressing HA-GLUT4. C2C12 myoblasts were infected with increasing volumes of HA-GLUT4 retro-virus (0.025 - 0.1 ml) or empty vector (EV) virus as a control. C2C12 myotubes on day 7 post differentiation were maintained under basal conditions, stimulated with insulin at 200 nM for 5 min or treated with AICAR at 2 mM for 45 min. The cell surface levels of GLUT4 was determined by incubating fixed cells with anti-HA primary antibodies and anti-mouse Alexa 488 secondary antibodies. Total cellular GLUT4 was determined in premeabilised cells pre-treated with saponin prior to primary antibody staining. All cells were costained with the nuclear stain 4,6-diamidino-2- phenylindole (DAPI). Images were captured using the high content analysis (HCA) confocal imaging plate reader, the IN Cell Analyzer system 2000 (GE Healthcare). the IN Cell Analyzer system 2000 (GE Healthcare). One field was captured per well of a 96-Well plate. Images were aquired using a 20x 0.75 NA objective lens. Images are representative of three separate wells.

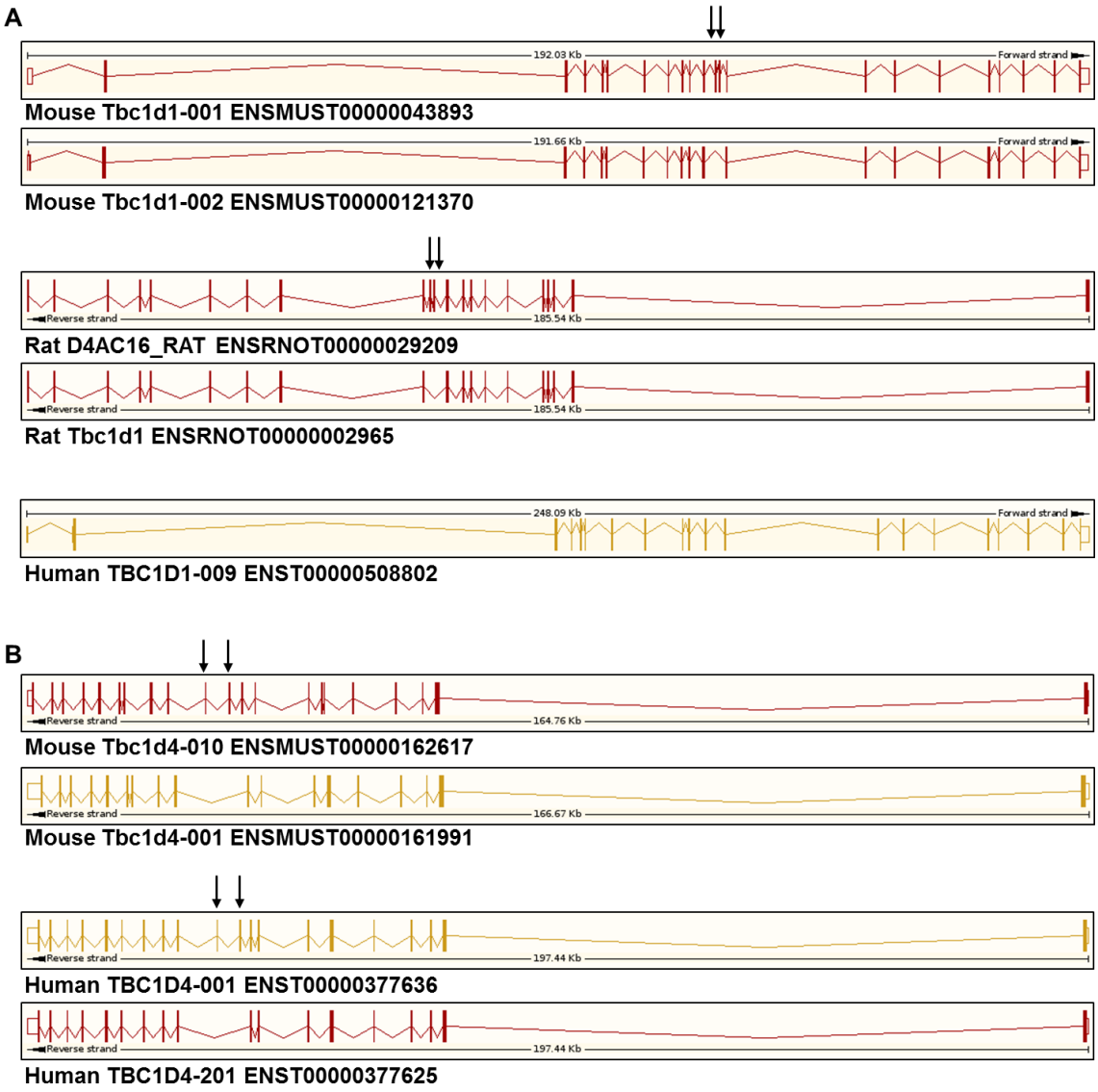

Figure A5: Splice variants of *Tbc1d1* and *Tbc1d4*. (A) Schematic representation of *Tbc1d1* conserved splice variants in mouse (Mus musculus), rat (Rattus norvegicus) and human (Homo sapiens) which have been compiled from Ensembl. There appear to be two splice variants of *Tbc1d1* conserved in rodent (Mu: long isoform: 6465 bp, translation: 1255 aa, molecular weight: 143 kDa and short isoform: 5410 bp, translation: 1162 aa, molecular weight: 132 kDa), (Rn: long isoform: 3867bp translation: 1257 aa 142 kDa and short isoform: 3582 translation: 1162 aa molecular weight: 132 kDa) and only one *TBC1D1* transcript: 5700 bp translation: 1159 aa molecular weight: 131 kDa in human. (B) Schematic representation *Tbc1d4* splice variants in mouse and human compiled from Ensembl. Mouse: long transcript: 4762 bp, translation: 1306 aa, molecular weight: 147 kDa and short transcript: 6483 bp, translation: 1243 aa, molecular weight: 140 kDa. Human: long transcript: 6364 bp, translation: 1298 aa, molecular weight: 146 kDa and short transcript: 6174 bp, translation: 1235 aa, molecular weight: 139 kDa. Appendix 1: Amino acid sequence alignment of TBC1D1 splice isoforms in Mouse, Rat and Human compiled from RefSeq, Ensembl, SWISSPROT and EMBL. Long isoform is denoted as full-length TBC1D1 protein.

References

Abel, E. D. et al., 2001. Adipose-selective Targeting of the GLUT4 Gene Impairs Insulin Action in Muscle and Liver. *Nature,* Volume 409, pp. 729-733.

Al Hasani, H., Yver, D. R. & Cushman, S. W., 1999. Overexpression of the Glucose Transporter GLUT4 in Adipose Cells Interferes With Insulin-stimulated Translocation. *FEBS Letters,* Volume 460, pp. 338-342.

Alessi, D. R., 2001. Discovery of PDK1, One of the Missing Links in Insulin Signal Transduction. *Biochemical Society Transactions,* Volume 29, pp. 1-14.

Alessi, D. R. et al., 1996. Mechanism of Activation of Protein Kinase B by Insulin and IGF-1. *The EMBO Journal,* Volume 15, pp. 6541-6551.

Altschuler, S. J. & Wu, L. F., 2010. Cellular Heterogeneity: Do Differences Make a Difference?. *Cell,* Volume 141, pp. 559-563.

Amati, F. et al., 2011. Skeletal Muscle Triglycerides, Diacylglycerols, and Ceremides in Insulin Resistance. *Diabetes,* Volume 60, pp. 2588-2597.

An, D. et al., 2010. TBC1D1 Regulates Insulin-and Contraction-Induced Glucose Transport in Mouse Skeletal Muscle. *Diabetes,* Volume 59, pp. 1358-1365.

Antonescu, C. N. et al., 2008. Clathrin-Dependent and Independent Endocytosis of Glucse Transporter 4 (GLUT4) in Myoblasts: Regulation of Mitochondrial Upcoupling. *Traffic,* Volume 9, pp. 1173-1190.

Araki, E. et al., 1994. Alternative Pathways of Insulin Signalling in Mice with Targeted Disruption of the IRS-1 Gene. *Nature,* Volume 372, pp. 186-190.

Aucott, L. S., 2008. Influences of Weight Loss on Long-term Diabetes Outcomes. *Proceedings of the Nutrition Society,* Volume 67, pp. 54-59.

Bai, L. et al., 2007. Dissecting Multiple Steps of GLUT4 Trafficking and Identifying the Sites of Insulin Action. *Cell Metabolism,* Volume 5, pp. 47-57.

Baldeweg, S. E. et al., 2000. Insulin-resistance, Lipid and Fatty Acid Concentrations in 867 Healthy Europeans. *European Journal of Clinical Investigation,* Volume 30, pp. 45-52.

Baus, D. et al., 2008. Identification of a Novel AS160 Splice Variant That Regulates GLUT4 Translocation and Glucose Uptake in Rat Muscle Cells. *Cellular Signalling,* Volume 20, pp. 2237-2246.

Bergeron, R. et al., 1999. Effect of AMPK Activation on Muscle Glucose Metabolism in Conscious Rats. *American Journal of Physiology, Endocrinology and Metabolism,* Volume 276, pp. E938-E944.

Bergman, R. N. & Ader, M., 2000. Free Fatty Acids and Pathogenisis of Type Two Diabetes Mellitus. *Trends in Endocrinology and Metabolism,* Volume 11, pp. 351-356.

Birnbaum, M. J., 1989. Identification of a Novel Gene Encoding and Insulin-Responsive Glucose Transporter Protein. *Cell,* Volume 57, pp. 305-315.

Blau, H. M. et al., 1985. Plasticity of the Differentiated State. *Science,* Volume 230, pp. 758-766.

Bloemberg, D. & Quadrilatero, J., 2012. Rapid Determination of Myosin Heavy Chain Expression in Rat, Mouse, and Human Skeletal Muscle Using Multicolor Immunofluorescence Analysis. *PLoS ,* 7(4), pp. 1-11.

Bogan, J. S., McKee, A. E. & Lodish, H. F., 2001. Insulin-Resposive Compartments Containing GLUT4 in 3T3-L1 and CHO Cells: Regulating by Amino Acid Concentrations. Volume 21, pp. 4785-4806.

Bogan, J. S. et al., 2012. Endoproteolytic Cleavage of TUG regulates GLUT4 Glucose Transporter Translocation. *The Journal of Biological Chemistry,* Volume 287, pp. 23932-23947.

Bonen, A. et al., 2000. Acute Regulation of Fatty Acid Uptake Involves the Cellular Redistribution of Fatty Acid Translocase. *The Journal of Biological Chemistry,* Volume 275, pp. 14501-14508.

Bonen, A. et al., 1998. Palmitate Transport and Fatty Acid Transporters in Red and White Muscles. *American Journal of Physiology, Endocrinology and Metabolism,* Volume 275, pp. 471-478.

Boura-Halfon, S. & Zick, Y., 2009. Phosphorylation of IRS Proteins, Insulin Action and Insulin Resistance. *American Journal of Physiology Endocrinology and Metabolism,* Volume 296, pp. E581-E591.

Brewer, P. D., Romenskaia, Kanow, M. A. & Mastick, C. C., 2011. Loss of AS160 Akt Substrate Causes GLUT4 to Accumulate in Compartments That Are Primed for Fusion in Basal Adipocytes. *The Journal of Biological Chemistry,* Volume 286, pp. 26287-26297.

Bruce, C. R. et al., 2006. Endurance Training in Obese Humans Improves Glucose Tolerance and Mitochondrial Fatty Acid Oxidation and Alters Muscle Lipid Content. *American Journal of Physiology, Endocrinology and Metabolism,* Volume 291, pp. E99-E107.

Bruss, M. D., Arias, E. B., Lienhard, G. E. & Cartee, G. D., 2005. Increased Phosphorylation of Akt Substrate of 160 kDa (AS160) in Rat Skeletal Muscle in Response to Insulin or Contractile Activity. *Diabetes,* Volume 54, pp. 42-50.

Bryant, N. J., Govers, R. & James, D. E., 2002. Regulated Transport of the Glucose Transporter GLUT4. *Nature Reviews,* Volume 3, pp. 267-277.

Cantley, L. C., 2002. The Phosphoinositide 3-Kinase Pathway. *Science,* Volume 296, pp. 1655-1657.

Chadt, A., Joost, H.-G. & Al-Hasani, H., 2009. Deletion of the Rab-GAP Protein TBC1D1 Protects From Lipid Induced Insulin Resistance in Skeletal Muscle. *Diabetologia,* Volume 52, pp. 891-900.

Chadt, A. et al., 2008. Tbc1d1 Mutation in Lean Mouse Strain Confers Leaness and Protects from Diet-induced Obesity. *Nature Genetics,* Volume 40, pp. 1354-1359.

Charron, M. J., Brosius III, F. C., Alper, S. L. & Lodish, H. F., 1989. A Glucose Transport Protein Expressed Predominately in Insulin Responsive Tissues. *Proceedings of the National Academy of Sciences,* Volume 86, pp. 2535-2539.

Chavez, J. A. et al., 2003. A Role for Ceramide, but Not Diacylglycerol, in the Antagonism of Insulin Signal Transduction by Saturated Fatty Acids. *The Journal of Biological Chemistry,* Volume 278, pp. 10297-10303.

Chavez, J. A. et al., 2008. Inhibition of GLUT4 Translocation by TBC1D1, a Rab GTPase-activating Protein Abundant in Skeletal Muscle is Partially Relieved by AMP-activated Protein Kinase Activation. *The Journal of Biological Chemistry,* Volume 283, pp. 9187-9195.

Chen, S. et al., 2008. Complemetary Regulation of TBC1D1 and AS160 by Growth Factors, Insulin and AMPK-activators. *Biochemical Journal,* Volume 409, pp. 449-459.

Chen, S., Wasserman, D. H., MacKintosh, C. & Sakamoto, K., 2011. Mice with AS160/TBC1D4-Thr649Ala Knockin Mutation Are Glucose Intolerant with Reduced Insulin Sensitivity and Altered GLUT4 Trafficking. *Cell Metabolism,* Volume 13, pp. 68-79.

Chen, Y. et al., 2012. Rab10 and Myosin-Va Mediate Insulin-stimulated GLUT4 Storage Vesicle Translocation in Adipocytes. *Journal of Biological Chemistry,* Volume 198, pp. 545-560.

Cho, H. et al., 2001. Insulin Resistance and a Diabetes Mellitus-Like Syndrome in Mice Lacking the Protein Kinase Akt2 (PKBb). *Science,* Volume 292, pp. 1728-1731.

Clarke, J. F. et al., 1994. Inhibition of the Translocation of GLUT1 and GLUT4 in 3T3L1 cells by the Phosphatidylinositol 3-Kinase Inhibitor, Wortmannin. *Biochemical Journal,* Volume 300, pp. 631-635.

Claycomb, W. C. et al., 1998. HL-1 Cells: A Cardiac Muscle Cell Line That Contracts and Retains Phenotypic Characteristics of the Adult Cardiomyocyte. *Proceedings of the National Academy of Sciences,* Volume 95, pp. 2979-2984.

Cool, B. et al., 2006. Indentification and Characterisation of a Small Molecule AMPK Activator That Treats Key Components of Type 2 Diabetes and the Metabolic Syndrome. *Cell Metabolism,* Volume 3, pp. 403-416.

Coster, A. C. F., Govers, R. & James, D. E., 2004. Insulin Stimulates the Entry of GLUT4 into the Endosomal Recycling Pathway by a Quantal Mechanism. *Traffic,* Volume 5, pp. 763-771.

Cushman, S. W. & Wardzala, L. J., 1980. Potential Mechanism of Insulin Action on Glucose Transport in the Isolated Rat Adipose Cell. *The Journal of Biological Chemistry,* Volume 255, pp. 4758-4762.

Dash, S. et al., 2009. A Truncation Mutation in TBC1D4 in a Family with Acanthosis Nigricans and Postprandial Hyperinsulinemia. *Proceedings of the National Academy of Sciences,* Volume 106, pp. 9350-9355.

Dawson, K., Aviles-Hernandez, A., Cushman, S. W. & Malide, D., 2001. Insulin-Regulated Trafficking of Dual Labelled Glucose Transporter 4 in Primary Rat Adipose Cells. *Biochemical and Biophysical Research Communications,* Volume 287, pp. 445-454.

Defronzo, R. A., Ferrannini, E., Sato, Y. & Felig, P., 1981. Synergistic Interaction Between Exercise and Insulin and Perpheral Glucose Uptake. *The Journal of Clinical Investigation,* Volume 68, pp. 1468-1474.

Douen, A. G. et al., 1990. Exercise-Induces Recruitment of the 'Insulin-responsive Glucose Transporter. *The Journal of Biological Chemistry,* Volume 265, pp. 13427-13430.

Dube, J. J. et al., 2008. Exercise-induced Alterations in Intramyocellular Lipds and Insulin Resistance: The Althete's Paradox Revisited. *American Journal of Physiology, Endocrinology and Metabolism,* Volume 294, pp. E882-E888.

Dugani, C. B. & Klip, A., 2005. Glucose Transporter 4: Cycling, Compartments and Controversies. *EMBO Reports,* Volume 6, pp. 1137-1142.

Eckel, R. H., Grundy, S. M. & Zimmet, P. Z., 2005. The Metabolic Syndrome. *Lancet,* Volume 365, pp. 1415-1428.

Eguez, L. et al., 2005. Full Intracellular Retention of GLUT4 Requires AS160 Rab GTPase Activating Protein. *Cell Metabolism,* Volume 2, pp. 263-272.

Fazakerely, D. J., 2010. *Investigating GLUT4 Trafficking in Muscle,* Thesis PhD: University of Bath.

Fazakerely, D. J. et al., 2009. Kinetic Evidence for Unique Regulation of GLUT4 Trafficking By Insulin and AMPK Activators in L6 Myotubes. *The Journal of Biological Chemistry,* Volume 285, pp. 1653-1660.

Fernandes, A. B., Patarrao, R. S., Videira, P. A. & Macedo, M. P., 2011. Understanding Postprandial Glucose Clearance by Peripheral Organs: The Role of Hepatic Parasympathetic System. *Journal of Neuroendocrinology,* Volume 23, pp. 1288-1295.

Foster, L. J., Li, D., Randhawa, V. K. & Klip, A., 2001. Insulin Accelerates Inter-endosomal GLUT4 Traffic via Phosphatidylinositol 3-Kinase and Protein Kinase B. *The Journal of Biological Chemistry,* Volume 276, pp. 44212-44221.

Franke, T. F. et al., 1995. The Protein Kinase Encoded by the Akt Proto-Oncogen Is a Target of the PDGF-Activated Phosphatidylinositol 3-Kinase. *Cell,* Volume 81, pp. 727-736.

Froguel, P. & Boutin, P., 2001. Genetics of Pathways Regulating Body weight in the Development of Obesity in Humans. *Experimental Biology and Medicine,* Issue 226, pp. 991-996.

Frosig, C. et al., 2010. Exercise-induced TBC1D1 Ser237 Phosphorylation and 14-3-3 Protein Binding Capacity in Human Skeletal Muscle. *The Journal of Physiology,* Volume 588, pp. 4539-4548.

Fujita, H. et al., 2010. Identification of Three Distinct Functional Sites of Insulin-mediated GLUT4 Trafficking in Adipoyctes Using Quantitative Single Molecular Imaging. *Molecular Biology of the Cell,* Volume 21, pp. 2721-2731.

Fukumoto, H. et al., 1989. Cloning and Characterisation of the Major Insulin-responsive Glucose Transporter Expressed in Human Skeletal Muscle and other Insulin-responsive Tissues. *The Journal of Biological Chemistry,* Volume 264, pp. 7776-7779.

Funai, K. & Cartee, G. D., 2008. Contraction-stimulated Glucose Transport in Rat Skeletal Muscle is Sustained Despite a Reversal of Increased PAS-phosphorylation of AS160 and TBC1D1. *Journal of Applied Physiology,* Volume 105, pp. 1788-1795.

Funai, K. & Cartee, G. D., 2009. Inhibition of Contraction-stimulated AMP-Activated Protein Kinase Inhibits Contraction-Stimulated Increases in PAS-TBC1D1 and Glucose Transport Without Altering PAS-AS160 in Rat Skeletal Muscle. *Diabetes,* Volume 58, pp. 1096-1104.

Funai, K. et al., 2009. Increased AS160 Phosphorylation, but not TBC1D1 Phosphorylation, With Increased Postexercise Insulin Sensitivity in Rat Skeletal Muscle. *American Journal of Physiology, Endocrinology and Metabolism,* Volume 297, pp. E242-E251.

Gollnick, P. D. et al., 1974. Human Soleus Muscle: A Comparison of Fibre Type Composition and Enzyme Activities with Other Leg Muscles. *Pflugers Archiv,* 348(3), pp. 247-255.

Goodpaster, B. H., He, J., Watkins, S. & Kelley, D. E., 2001. Skeletal Muscle Lipid Content and Insulin Resistance: Evidence for a Paradox in Endurance-Trained Athletes. *The Journal of Clinical Endocrinology and Metabolism,* Volume 86, pp. 5755-5761.

Goransson, O. et al., 2007. Mechanism of Action of A-769662, a Valuable Tool for Activation of AMP-activated Protein Kinase. *The Journal of Biological Chemistry,* Volume 282, pp. 32549-32560.

Govers, R., Coster, A. C. F. & James, D. E., 2004. Insulin Increases Cell Surface GLUT4 Levels by Dose Dependently Discharging GLUT4 into a Cell Surface Recylcing Pathway. *Molecular and Cellular Biology,* Volume 24, pp. 6456-6466.

Guigas, B. et al., 2009. Beyond AICA Riboside: In Search of New Specific AMP-activated Protein Kinase Activators. *IUBMB Life,* Volume 61, pp. 18-26.

Hardie, G. D., 2004. The AMP-activated Protein Kinase Pathway - New Players Upstream and Downstream. *Journal of Cell Science,* Volume 117, pp. 5479-5487.

Hashiramoto, M. & James, D. E., 2000. Characterisation of Insulin-Responsive GLUT4 Storage Vesicles Isolated from 3T3-L1 Adipocytes. *Molecular and Cellular Biology,* Volume 20, pp. 416-427.

Hatakeyama, H. & Kanzaki, M., 2011. Molecular Basis of Insulin-Responsive GLUT4 Trafficking Systems Revealed by Single Molecular Imaging. *Traffic,* 12(12), pp. 1-16.

Hatakeyama, H. & Kanzaki, M., 2013. Regulatory Mode Shift of TBC1D1 is Required for Aquisition of Insulin-Responsive GLUT4 Trafficking Activity. *Molecular Biology of the Cell,* 24(6), pp. 809-817.

Hawley, J. A. & Lessard, S. J., 2008. Exercise Training-induced Improvements in Insulin Action. *Acta Physiologica,* Volume 192, pp. 127-135.

Hayashi, T. et al., 1998. Evidence for 5-AMP-Activated Protein Kinase Mediation of the Effect of Muscle Contraction on Glucose Transport. *Diabetes,* Volume 47, pp. 1369-1373.

Henriksen, E. J. et al., 1990. Glucose Transporter Protein Content and Glucose Transport Capacity in Rat Skeletal Muscles. *American Journal of Physiological ,* Volume 259, pp. E593-E598.

Hirabara, S. M., Curi, R. & Maechler, P., 2009. Saturated Fatty-acid Induced Insulin Resistance is Associated With Mitochondrial Dysfunction in Skeletal Muscle Cells. *Journal of Cellular Physiology,* pp. 187-194.

Hoehn, K. L. et al., 2008. IRS1-Independant Defects Define Major Nodes of Insulin Resistance. *Cell Metabolism,* Volume 7, pp. 421-433.

Hoehn, K. L. et al., 2009. Insulin Resistance is a Cellular Antioxidant Defence Mechanism. *PNAS,* Volume 42, pp. 17787-17792.

Holland, W. L. et al., 2007. Inhibition of Ceramide Synthesis Ameliorates Glucocorticoid-, Saturated-Fat-, and Obesity-Induced Insulin Resistance. *Cell Metabolism,* Volume 5, pp. 167-179.

Holland, W. L. et al., 2007. Lipid Mediators of Insulin Resistance. *Nutrition Reviews,* Volume 65, pp. S39-S46.

Holman, G. D. et al., 1990. Cell Surface Labelling of Glucose Transporter Isoform GLUT4 by Bis-mannose Photolabel. *The Journal of Biological Chemistry,* Volume 265, pp. 18172-18179.

Holman, G. D., Leggio, L. L. & Cushman, S. W., 1994. Insulin-stimulated GLUT4 Glucose Transporter Recycling. Volume 269, pp. 17516-17524.

Howlett, K. F., Mathews, A., Garnham, A. & Sakamoto, K., 2007. The Effect of Exercise and Insulin on AS160 Phosphorylation and 14-3-3 Binding Capacity in Human Skeletal Muscle. *American Journal of Physiology, Endocrinology and Metabolism,* Volume 294, pp. E401-E407.

Huang, P., Altshuller, Y. M., Hou, J. C. P. J. E. & Frohman, M. A., 2005. Insulin-stimulated Plasma Membrane Fusion of GLUT4 Glucose Transporter-containing Vesicles is Regulated by Phospholipase D1. *Molecular Biology of the Cell,* Volume 16, pp. 2614-2623.

Hundal, H. S. et al., 1992. Cellular Mechanism of Metformin Action Involves Glucose Transporter Translocation from Intracellular Pool to the Plasma Membrane in L6 Muscle Cells. *Endocrinology,* Volume 131, pp. 1165-1173.

Ishikura, S., Bilan, P. J. & Klip, A., 2007. Rabs 8A and 14 Are Targets of the Insulin-regulated Rab-GTP AS160 Regulating GLUT4 Traffic in Muscle Cells. *Biochemical and Biophysical Research Communications,* Volume 353, pp. 1074-1079.

Ishikura, S. & Klip, A., 2008. Muscle Cells Engage Rab8A and Myosin Vb in Insulin-dependant GLUT4 Translocation. *American Journal of Physiology, Endocrinology and Metabolism,* Volume 295, pp. C1016-C1025.

Jacinto, E. et al., 2006. SIN1/MIP1 Maintains rictor-mTOR Complex Integrity and Regulates Akt Phosphorylation and Substrate Specificity. *Cell,* Volume 127, pp. 125-137.

James, D. E. & Piper, R. C., 1994. Insulin-resistance, Diabetes and the Insulin-regulated Trafficking of GLUT4. *The Journal of Cell Biology,* Volume 126, pp. 1123-1126.

James, D. E., Strube, M. & Mueckler, M., 1989. Molecular Cloning and Characterisation of an Insulin-Regulatable Glucose Transporter. *Nature,* Volume 338, pp. 83-87.

Jedrychowski, M. P. et al., 2010. Proteomic Analysis of GLUT4 Storage Vesicles Reveals LRP1 to Be Important Vesicle Component and Target of Insulin Signalling. *The Journal of Biological Chemistry,* Volume 285, pp. 104-114.

Jensen, T. E. et al., 2008. AMPK a1 Activation is Required for Stimulation of Glucose Uptake by Twitch Contraction, but Not by H2O2, in Mouse Skeletal Muscle. *PLoS,* 3(5), pp. E2102 1-9.

Jessen, N. et al., 2011. Exercise Increases TBC1D1 Phosphorylation in Human Skeletal Muscle. *American Journal of Physiology, Endocrinology and Metabolism,* Volume 301, pp. E164-E171.

Jessen, N. et al., 2002. Effects of AICAR and Exercise on Insulin-stimulated Glucose Uptake, Signalling, and GLUT4 Content in Rat Muscles. *Journal of Applied Physiology,* Volume 94, pp. 1373-1379.

Jhun, B. H. et al., 1992. Effects of Insulin on Steady-state Kinetics of GLUT4 Subcellular Distribution in Rat Adipocytes. *The Journal of Biological Chemistry,* Volume 267, pp. 17710-17715.

Joost, H. G. et al., 2002. Nomenclature of the GLUT/SLC2A Family of Sugar/Polyol Transport Facilitators. *American Journal of Physiology, Endocrinology and Metabolism,* Volume 282, pp. 974-976.

Jorgensen, S. B. et al., 2004. Knockout of the a2 but Not a1 5'-AMP-activated Protein Kinase Isoform Abolishes 5-Aminoimidazole-4-carboxamide-1-b-4-ribofuranoside- but Not Contraction-induced Glucose Uptake in Skeletal Muscle. *The Journal of Biological Chemistry,* Volume 279, pp. 1070-1079.

Kaddai, V. et al., 2009. Rab4b is a Small GTPase Invovled in the Control of the Glucose Transporter GLUT4 Localisation in Adipocytes. *PLoS ONE,* 4(4), pp. E5257 1-15.

Kahn, B. B., 1992. Facililitative Glucose Transporters: Regulatory Mechanisms and Dysregulation in Diabetes. *Journal of Clinical Invesitgation,* Volume 89, pp. 1367-1374.

Kandror, K. V., Coderre, L., Pushkin, A. V. & Pilch, P. F., 1995. Comparison of Glucose-transporter Containing Vesicles from Rat Fat and Muscle Tissues:

Evidence For a Unique Endosomal Compartment. *Biochemical Journal,* Volume 387, pp. 383-390.

Kandror, K. V. & Pilch, P. F., 1996. The Insulin-like Growth Factor II/Mannose 6-Phosphate Receptor Utilises the Same Membrane Compartments as GLUT4 for Insulin-dependant Trafficking to and from the Rat Adipocyte Cell Surface. *The Journal of Biological Chemistry,* Volume 271, pp. 21703-21708.

Kane, S. & Lienhard, G. E., 2005. Calmodulin Binds to the Rab GTPase Activating Protein Required for Insulin-stimulated GLUT4 Translocation. *Biochemical and Biophysical Research Communications,* Volume 335, pp. 175-180.

Kane, S. et al., 2002. A Method to Identify Serine Kinase Substrates. *The Journal of Biological Chemistry,* Volume 227, pp. 22115-22118.

Karlsson, H. K. R. et al., 2009. Kinetics of GLUT4 Trafficking in Rat and Human Skeletal Muscle. *Diabetes,* Volume 58, pp. 847-854.

Karylowski, O., Zeigerer, A., Cohen, A. & McGraw, T., 2004. GLUT4 is Retained by an Intracellular Cycle of Vesicle Formation and Fusion with Endosomes. *Molecular Biology of the Cell,* Volume 15, pp. 870-882.

Keller, S. R., 2003. The Insulin-regulated Aminopeptidase: A Companion and Regulator of GLUT4. *Frontiers in Bioscience,* Volume 8, pp. S410-S420.

Kelley, D. E., 2005. Skeletal Muscle Fat Oxidation: Timing and Flexibility Are Everything. *The Journal of Clinical Investigation,* Volume 115, pp. 1699-1702.

Kim, Y.-B., Peroni, O. D., Franke, T. F. & Kahn, B. B., 2000. Divergent Regulation of Akt1 and Akt2 Isoforms in Insulin Target Tissues of Obese Zucker Rats. *Diabetes,* Volume 49, pp. 847-856.

Kohn, A. D., Summers, S. A., Birnbaum, M. & Roth, R. A., 1996. Expression of a Constitutively Active Akt Ser/Thr Kinase in 3T3-L1 Adipocytes Simulates

Glucose Uptake and Glucose Transporter4 Translocation. *The Journal of Biological Chemistry,* Volume 271, pp. 31372-31378.

Koistinen, H. A. et al., 2003. 5-Amino-Imidazole Carboxamide Riboside Increases Glucose Transport and Cell-Surface GLUT4 Content in Skeletal Muscle from Subjects with Type 2 Diabetes. *Diabetes,* Volume 52, pp. 1066-1072.

Koumanov, F., Richardson, J. D., Murrow, B. A. & Holman, G. D., 2011. AS160 Phosphotyrosine-binding Domain Constructs Inhibit Insulin-stimulated GLUT4 Vesicle Fusion with the Plamsma Membrane. *The Journal of Biological Chemistry,* Volume 286, pp. 16574-16582.

Koumanov, F. et al., 1998. Cell-surface Biotinylation of GLUT4 Using Bis-mannose Photolabels. *Biochemical Journal,* Volume 330, pp. 1209-1215.

Kramer, H. F. et al., 2007. Calmodulin-Binding Domain of AS160 Regulates Contraction-but Not Insulin-Stimulated Glucose Uptake in Skeletal Muscle. *Diabetes,* Volume 56, pp. 2854-2862.

Kramer, H. F. et al., 2006. Distinct Signals Regulate AS160 Phosphorylation in Response to Insulin, AICAR, Contraction in Mouse Skeletal Muscle. *Diabetes,* Volume 55, pp. 2067-2076.

Kramer, H. F. et al., 2006. AS160 Regulates Insulin - and Contraction-stimulated Glucose Uptake in Mouse Skeletal Muscle. *The Journal of Biological Chemistry,* Volume 281, pp. 31478-31485.

Kumar, N. & Dey, C. S., 2002. Metformin Enhances Insulin Signalling in Insulin-dependent and -independant Pathways in Insulin Resistant Muscle Cells. *British Journal of Pharmacology,* Volume 137, pp. 329-336.

Kupriyanova, T. A. & Kandror, K. V., 2000. Cellugyrin is a Marker for a Distinct Population of Intracellular Glut4-containing Vesicles. *The Journal of Biological Chemistry,* Volume 275, pp. 36263-23268.

Kupriyanova, T. A., Kandror, V. & Kandror, K. V., 2002. Isolation and Characterisation of the Two Major Intracellular Glut4 Storage Compartments. *The Journal of Biological Chemistry,* Volume 277, pp. 9133-9138.

Laemmli, U. K., 1970. Clevage of Structural Proteins During the Assembly of the Head of Bacteriophage T4. *Nature,* Volume 227, pp. 680-685.

Lampson, M. A. et al., 2001. Insulin-regulated Release from the Endosomal Recycling Compartment Is Regulated by Budding of Specialised Vesicles. Volume 12, pp. 3489-3501.

Lansey, M. N. et al., 2012. Deletion of Rab GAP AS160 Modifies Glucose Uptake and GLUT4 Translocation in Primary Skeletal Muscles and Adipocytes and Impairs Glucose Homeostatis. *American Journal of Physiology, Endocrinology and Metabolism,* Volume 303, pp. E1273-E1286.

Larance, M., Ramm, G. & James, D. E., 2008. The GLUT4 Code. *Molecular Endocrinology,* 22(2), pp. 226-233.

Larance, M. et al., 2005. Characterisation of the Role of the Rab GTPase-activatiing Protein AS160 in Insulin-regulated GLUT4 Trafficking. *The Journal of Biological Chemistry,* Volume 280, pp. 37803-37813.

Laurie, S. M., Corley Cain, C., Lienhard, G. E. & Castle, J. D., 1993. The Glucose Transporter Glut4 and Secretory Carrier Membrane Proteins (SCAMPs) Colocalise in Rat Adipocytes and Partially Segregateduring Insulin Stimulation. *The Journal of Biological Chemistry,* Volume 268, pp. 19110-19117.

Lauritzen, H. P. M. M. et al., 2008. Large GLUT4 Vesicles Are Stationary While Locally and Reversibly Depleted During Transient Insulin Stimulation of Skeletal Muscle of Living Mice. *Diabetes,* Volume 57, pp. 315-324.

Lauritzen, H. P. P. M., Galbo, H., Toyoda, T. & Goodyear, L. J., 2010. Kinetics of Contraction-Induced GLUT4 Translocation in Skeletal Muscle Fibres in Living Mice. *Diabetes,* Volume 59, pp. 2134-2144.

Lauritzen, H. P. P. M. et al., 2006. Imaging of Insulin Signalling in Skeletal Muscle of Living Mice Shows Major Role of T-Tubules. *Diabetes,* Volume 55, pp. 1300-1306.

Lazar, M. A., 2005. How Obesity Causes Diabetes: Not a Tall Tale. *Science Signalling,* Volume 307, pp. 373-375.

Lee, J. S. et al., 2006. Saturated, But Not n-6 Polyunsaturated, Fatty Acids Induce Insulin Resistance: Role of Intramuscular Accumulation of Lipid Metabolites. *Journal of Applied Physiology,* Volume 100, pp. 1467-1474.

Leney, S. E. & Tavare, J. M., 2009. The Molecular Basis of Insulin-stimulated Glucose Uptake: Signalling, Trafficking and Potential Drug Targets. *Journal of Endocrinology,* Volume 203, pp. 1-18.

Levine, R. & Goldstein, M., 1955. On the Mechanism of Insulin Action. *Recent Progress in Hormone Research,* Volume 11, pp. 343-380.

Liu, L.-B., Omata, W., Kojima, I. & Shibata, H., 2007. The SUMO Conjugating Enzyme Ubc9 is a Regulator of GLUT4 Turnover and Targeting to the Insulin-responsive Storage Compartment in 3T3-L1 Adipocytes. *Diabetes,* Volume 56, pp. 1977-1985.

Lizcano, J. M. et al., 2004. LKB1 is a Master Kinase That Activates 13 Kinases of the AMPK Subfamily, Including MARK/PAR-1. *The EMBO Journal,* Volume 23, pp. 833-843.

Lizunov, V. A. et al., 2012. Insulin Stimulates Fusion, but Not Tethering, of GLUT4 Vesicles in Skeletal Muscle of HA-GLUT4-GFP Transgenic Mice. *American Journal of Physiology Endocrinology and Metabolism,* Volume 302, pp. E950-E960.

Ljubicic, V. & Hood, D. A., 2008. Kinase-specific Responsiveness to Incremental Contractile Activity in Skeletal Muscle with Low and High Mitochonidria Content. *American Journal of Physiology, Endocrinology and Metabolism,* Volume 295, pp. 195-204.

Luiken, J. J. F. P. et al., 2001. Insulin Induces the Translocation of the Fatty Acid Transporter FAT/CD36 to the Plasma Membrane. *American Journal of Physiology, Endocrinology and Metabolism,* Volume 282, pp. 491-495.

Maarbjerg, S. J., Sylow, L. & Richter, E. A., 2011. Current Understanding of Increased Insulin Sensitivity After Exercise: Emerging Candidates. *Acta Physiologica,* Volume 202, pp. 323-335.

Malide, D., Dwyer, N. K., Blanchette-Mackie, J. & Cushman, S. W., 1997. Immunocytochemical Evidence That GLUT4 Resides in a Specialised Translocation Post-endosomal VAMP2- positive Compartment in Rat Adipose Cells in the Absence of Insulin. *Journal of Histochemistry and Cytochemistry,* Volume 45, pp. 1083-1096.

Malide, D., Ramm, G., Cushman, S. W. & Slot, J. W., 2000. Immunoelectron Microscopic Evidence That GLUT4 Translocation Explains the Stimulation of Glucose Transport in Isolated Rat White Adipose Cells. *Journal of Cell Science,* Volume 113, pp. 4203-4210.

Marsh, b. J., Alm, R. A., McIntosh, S. R. & James, D. E., 1995. Molecular Regulation of GLUT-4 Targeting in 3T3-L1 Adipocytes. *The Journal of Cell Biology,* Volume 130, pp. 1081-1091.

Martin, O. J., Lee, A. & McGraw, T. E., 2006. GLUT4 Distribution between the Plasma Membrane and the Intracellular Compartments Is Maintained by an Insulin-moulated Bipartite Dyanmic Mechanism. *The Journal of Biological Chemistry,* Volume 281, pp. 484-490.

Martin, S. et al., 1996. The Glucose Transporter (GLUT4) and Vesicle-associated Membrane Protein-2 (VAMP-2) Are Segregated from Recycling

Endosomes in Insulin-sensitive Cells. *The Journal of Cell Biology,* Volume 124, pp. 625-625.

Meyre, D. et al., 2008. R125W Coding Variant in TBC1D1 Confers Risk For Familial Obesity and Contributes to Linkage on Chromosome 4p14 in the French Population. *Human Molecular Genetics,* Volume 17, pp. 1798-1802.

Miinea, C. P. et al., 2005. AS160, the Akt Substrate Regulating GLUT4 Translocation, has a Functional Rab-GTPase-activating Protein Domain. *Biochemical Journal,* Volume 391, pp. 87-93.

Misra, A. & Khurana, L., 2008. Obesity and the Metabolic Syndrome in Developing Countries. Volume 93, pp. 9-30.

Morris, N. J. et al., 1998. Sortilin is the Major110-kDa Protien in GLUT4 Vesicles from Adipocytes. *The Journal of Biological Chemistry,* Volume 273, pp. 3582-3587.

Mueckler, M. et al., 1985. Sequence and Structure of a Human Glucose Transporter. *Science,* Volume 229, pp. 941-945.

Mu, J. et al., 2001. A Role for AMP-Activated Protein Kinase in Contraction and Hypoxia-Regulated Glucose Transport in Skeletal Muscle. *Molecular Cell,* 7(5), pp. 1085-1094.

Muretta, ,. J. M., Romenskaia, I. & Mastick, C. C., 2008. Insulin Releases GLUT4 from Static Storage Compartments into the Cycling Endosomes and Increases the Rate Constant for GLUT4 Exocytosis. *The Journal of Biological Chemistry,* Volume 283, pp. 311-323.

Musi, N. et al., 2001. AMPK-activated Protein Kinase Activity and Glucose Uptake in Rat Skeletal Muscle. *American Journal of Physiology, Endocrinology and Metabolism,* Volume 280, pp. E677-E684.

Musi, N. et al., 2001. AMP-activated Protein Kinase Activity and Glucose Uptake in Rat Skeletal Muscle. *American journal of Physiology, Endocrinolgy and Metabolism,* Volume 280, pp. E677-E684.

Nagase, T. et al., 1998. Prediction of the Coding Sequences of Unidentified Human Genes. IX. The Complete Sequences of 100 New cDNA Clones from Brain Which Can Code for Large Proteins in vitro. *DNA Research,* Volume 5, pp. 31-39.

Nedachi, T. & Kanzaki, M., 2006. Regulation of Glucose Transporters by Insulin and Extracellular Glucose in C2C12 Myotubes. *American Journal of Physiology, Endocrinology and Metabolism,* Volume 291, pp. E817-E828.

Niu, W. et al., 2010. Contraction-related Stimuli Regulate GLUT4 Traffic in C2C12-GLUT4myc Skeletal Muscle Cells. *American Journal of Physiology, Endocrinology and Metabolism,* Volume 298, pp. E1058-E1071.

Okada, T. et al., 1994. Essential Role of Phosphatidylinositol 3-Kinase in Insulin-induced Glucose Transport and Antilipolysis in Rat Adipocytes. *The Journal of Biological Chemistry,* Volume 269, pp. 3568-3573.

O'Neill, H. M. et al., 2011. AMP-activated Protein Kinase (AMPK) b1b2 Muscle Null Mice Reveal an Essential Rolen for AMPK in Maintaining Mitochondrial Content and Glucose Uptake During Exercise. *Proceedings of the National Academy of Sciences,* Volume 108, pp. 16092-16097.

Pan, X., Eathiraj, S., Munson, M. & Lambright, D. G., 2006. TBC-domain GAPs for Rab GTPases Accelerate GTP Hydrolysis by a Dual-finger Mechanism. *Nature,* Volume 442, pp. 303-306.

Park, S.-Y., Jin, W., Woo, J. R. & Shoelson, S. E., 2011. Crystal Structures of Human TBC1D1 and TBC1D4 (AS160) Rab-GTPase-activating Protein (Rab-GAP) Domains Reveal Critical Elements for GLUT4 Translocation. *The Journal of Biological Chemistry,* Volume 286, pp. 18130-18138.

Peck, G. R. et al., 2009. Insulin-stimulated Phosphorylation of the Rab-GTPase-activating Protein TBC1D1 Regulates GLUT4 Translocation. Volume 284, pp. 30116-30023.

Pehmoller, C. et al., 2009. Genetic Disruption of AMPK Signalling Abolishes Both Contraction- and Insulin-stimulated TBC1D1 Phosphorylation and 14-3-3 Binding in Mouse skeletal Muscle. *American Journal of Physiology, Endocrinology and Metabolism,* Volume 297, pp. E665-E675.

Ploug, T. et al., 1998. Analysis of GLUT4 Distribution in Whole Skeletal Muscle Fibres: Indentification of Distinct Storage Compartments That Are Recruited by Insulin and Muscle Contractions. *The Journal of Cell Biology,* Volume 142, pp. 1429-1446.

Ralston, E. & Ploug, T., 1996. GLUT4 in Cultured Skeletal Muscle Myotubes is Segregated from the Transferrin Receptor and Stored in Vesicles Associated with the TGN. *Journal of Cell Science,* Volume 109, pp. 2967-2978.

Ramm, G., Larance, M., Guilhaus, M. & James, D. E., 2006. A Role for 14-3-3 in Insulin-stimulated GLUT4 Translocation through its Interaction with the Rab-GAP AS160. *The Journal of Biological Chemistry,* Volume 281, pp. 29174-29180.

Ranadive, S. A. & Vaisse, C., 2008. Lessons From Extreme Human Obesity: Mongenic Disorders. *Endocrinology and Metabolism Clinics of North America,* 37(3), pp. 733-751.

Randle, P. J., 1964. The Interrelationships of Hormones, Fatty Acid and Glucose in the Provision of Energy. *Journal of Postgraduate Medicine,* Volume 40, pp. 457-463.

Richardson, P. M. & Li, Z., 1995. Molecular Cloning of a cDNA With a Novel Domain Present in the Tre-2 Oncogene and the Yeast Cell Cycle Regulators BUB2 and cdc16. *Oncogene,* 11(6), pp. 1139-1148.

Roach, W. G., Chavez, J. A., Miinea, C. P. & Lienhard, G. E., 2007. Substrate Specificity and Effect on GLUT4 Translocation of the Rab GTPase-activating Protein TBC1D1. *Biochemical Journal,* Volume 403, pp. 353-358.

Rudich, A. & Klip, A., 2003. Push/pull Mechanisms of GLUT4 Traffic in Muscle Cells. *Acta Physiologica Scandinavica ,* Volume 178, pp. 297-308.

Russell, A. P. et al., 2003. Lipid Peroxidation in Skeletal Muscle of Obese as Compared to Endurance-trained Humans: A Case of Good Versus Bad Lipids?. *FEBS Letters,* Volume 551, pp. 104-106.

Sajan, M. P. et al., 2010. AICAR and Metformin, But Not Exercise, Increase Muscle Glucose Transport Through AMPK-, ERK-, and PDK1-dependant Activation of atypical PKC. *American Journal of Physiology Endocrinology and Metabolism,* Volume 298, pp. E179-E192.

Sajan, M. P. et al., 2006. Repletion of Atypical Protein Kinase C Following RNA Interference-mediated Depletion Restores Insulin-stimulated Glucose Transport. *The Journal of Biological Chemistry,* Volume 281, pp. 17466-17473.

Sakamoto, K. et al., 2006. Role of Akt2 in Contraction-stimulated Cell Signalling and Glucose Uptake in Skeletal Muscle. *American Journal of Physiology Endocrinolgy and Metabolism,* Volume 291, pp. E1031-E1037.

Sakamoto, K., Goransson, O., Hardie, D. G. & Alessi, D. R., 2004. Activity of LKB1 and AMPK-related Kinases in Skeletal Muscle: Effects of Contraction, Phenformin and AICAR. *American Journal of Physiology, Endocrinology and Metabolism,* Volume 287, pp. E310-E317.

Sakamoto, K. & Holman, G. D., 2008. Emerging Role for AS160/TBC1D4 and TBC1D1 in the Regulation of GLUT4 Traffic. *American Journal of Physiology Endocrinology and Metabolism,* Volume 295, pp. E29-E37.

Sano, H. et al., 2007. Rab10, a Target of the AS160 Rab GAP, is Required for Insulin-Stimulated Translocation of GLUT4 to the Adipocyte Plasma Membrane. *Cell Metabolism,* Volume 5, pp. 292-303.

Sano, H. et al., 2003. Insulin-stimulated Phosphorylation of a Rab-GTPase-activating Protein Regulates GLUT4 Translocation. *The Journal of Biological Chemistry,* Volume 278, pp. 14599-14602.

Schiaffino, S. & Reggiani, C., 2011. Fibre Types in Mammalian Skeletal Muscle. *Physiological Reviews,* Volume 91, pp. 1447-1531.

Scott, J. W. et al., 2008. Thienopyridone Drugs Are Selective Activators of AMP-activated Protein Kinase b1-Containing Complexes. *Chemistry and Biology,* Volume 15, pp. 1220-1230.

Shaw, R. J. et al., 2004. The Tumor Supressor LKB1 Kinase Directly Activates AMP-activated Kinase and Regulates Apoptosis in Response to Energy Stress. *PNAS,* Volume 101, pp. 3329-3335.

Shewan, A. M. et al., 2003. GLUT4 Recycles via a trans-Golgi Network (TGN) Subdomain Enriched in Syntaxins 6 and 16 But Not TGN38: Involvement of an Acidic Targetting Motif. *Molecular Biology of the Cell,* Volume 14, pp. 973-986.

Shi, J. & Kandror, K. V., 2005. Sortilin is Essential and Sufficient for the Formation of Glut4 Storage Vesicles in 3T3-L1 Adipocytes. *Developemtal Cell,* Volume 9, pp. 99-108.

Slot, J. W. et al., 1991. Translocation of the Glucose Transporter GLUT4 in Cardiac Myocytes of the Rat. *Proceedings of the National Academy of Sciences,* Volume 88, pp. 7815-7819.

Slot, J. W. et al., 1991. Immuno-localisation of the Insulin Regulatable Glucose Transporter in Brown Adipose Tissue of the Rat. *The Journal of Cell Biology,* Volume 113, pp. 123-135.

Somwar, R. et al., 2001. GLUT4 Translocation Precedes the Stimulation of Glucose Uptake by Insulin in Muscle Cells: Potential Activation of GLUT4 via p38 Mitogen-activated Protein Kinase. *Biochemical Journal,* Volume 359, pp. 639-649.

Song, X. M., Ryder, J. W., Kawano, Y. C. A. V. & Krook, A. Z. J. R., 1999. Muscle Fibre Type Specificity in Insulin Signal Transduction. *American Journal of Physiology,* Volume 277, pp. R1690-R1696.

Stenbit, A. E. et al., 1997. GLUT4 Heterozygous Knockout Mice Develop Muscle Insulin Resistance and Diabetes. *Nature Medicine,* Volume 3, pp. 1096-1101.

Stenmark, H. & Olkkonen, V. M., 2001. The Rab GTPase Family. *Genome Biology,* 2(5), pp. 1-7.

Stockli, J. et al., 2008. Regulation of Glucose Transporter 4 Translocation by the Rab Guanosine Triphosphate-Activating Protein AS160/TBC1D4 : Role of Phosphorylation and Membrane Association. *Molecular Endocrinology,* Volume 22, pp. 2703-2715.

Stone, S. et al., 2002. A Major Predisposition Locus for Severe Obesity, at 4p15-p14. *The American Journal of Human Genetics,* Volume 70, pp. 1459-1468.

Stone, S. et al., 2006. TBC1D1 is a Candidate for a Severe Obesity Gene and Evidence For a Gene/Gene Interaction in Obesity Predisposition. *Human Molecular Genetics,* Volume 15, pp. 2709-2720.

Sun, X. J. et al., 1991. Structure of the Insulin Receptor Substrate IRS-1 Defines a Unique Signal Transduction Protein. *Nature,* Volume 352, pp. 73-77.

Suzuki, K. & Kono, T., 1980. Evidence That Insulin Causes Translocation of Glucose Transport Activity to the Plasma Membrane From an Intracellular

Storage Site. *Proceedings of the National Academy of Sciences,* Volume 77, pp. 2542-2545.

Szekeres, F. et al., 2012. The Rab-GTPase Activating Protein TBC1D1 Regulates Skeletal Muscle Glucose Metabolism. *American Journal of Physiology, Endocrinology and Metabolism,* Volume 303, pp. E524-E533.

Tao, Y. et al., 2011. The Histone Methyltransferase Set7/9 Promotes Myoblast Differentiation and Myofibril Assembly. *The Journal of Cell Biology,* Volume 194, pp. 551-565.

Tasic, D. et al., 2003. Muscle Fibre Types and Muscle Morphometry in the Tibialis Posterior and Anterior of the Rat: A Comparative Study. *Medicine and Biology,* Volume 10, pp. 16-21.

Taylor, E. B. et al., 2008. Discovery of TBC1D1 as an Insulin-, AICAR-, and Contraction-stimulated Signalling Nexus in Mouse Skeletal Muscle. *The Journal of Biological Chemistry,* Volume 283, pp. 9787-9796.

Thong, F. S. L., Bilan, P. J. & Klip, A., 2007. The Rab GTPase-Activating Protein AS160 Integrates Akt, Protein Kinase C, and AMP-Activated Protein Kinase Signals Regulating GLUT4 Traffic. *Diabetes,* Volume 56, pp. 414-423.

Thorens, B. & Mueckler, M., 2009. Glucose Transporters in the 21st century. *American Journal of Physiology, Endocrinology and Metabolism,* Volume 298, pp. 141-145.

Tortorella, L. L. & Pilch, P. F., 2002. C2C12 Myotubes Lack an Insulin-responsive Vesicular Compartment Despite Dexamethosone-induced GLUT4 Expression. *American Journal of Physiology Endocrinology and Metabolism ,* Volume 283, pp. E524-E524.

Treebak, J. T. et al., 2009. A-769662 Activates AMPK b2-containing Complexes but Induces Glucose Uptake Through a PI3-kinase-dependant

Pathway in Mouse Skeletal Muscle. *American Journal of Physiology and Cell Physiology,* Volume 297, pp. C1041-C1052.

Treebak, J. T. et al., 2010. Identification of a Novel Phosphorylation Site on TBC1D4 Regulated by AMP-activated Protein Kinase in Skeletal Muscle. *American Journal of Physiology and Cell Physiology,* Volume 298, pp. C377-C385.

Tsuchiya, Y. et al., 2010. Palmitate-induced Down-regulation of Sortilin and Impaired GLUT4 Trafficking in C2C12 Myotubes. *The Journal of Biological Chemisty,* Volume 285, pp. 34371-34381.

Ukropcova, B. et al., 2005. Dynamic Changes in Fat Oxidation in Human Primary Myocytes Mirror Metabolic Characteristics of the Donor. *The Journal of Clinical Investigation,* Volume 115, pp. 1934-1941.

Vandesompele, J. et al., 2002. Accurate Normalisation of Real-time Quantitative RT-PCR Data by Genomic Averaging of Multiple Internal Control Genes. *Genome Biology,* Volume 3, pp. 1-12.

Vanhaesebroeck, B. & Alessi, D. R., 2000. The PI3K-PDK1 Connection: More than Just a Road to PKB. *Biochemical Journal,* Volume 346, pp. 561-576.

Verhey, K. J., Yeh, J.-I. & Birnbaum, M. J., 1995. Distinct Signals in the GLUT4 Glucose Transporter for Internalisation and for Targeting to an Insulin-responsive Compartment. *The Journal of Cell Biology,* Volume 130, pp. 1071-1079.

Verrier, L. et al., 2011. A New Isoform of the Histone Demethylase JMJD2A/KDM4A is Required for Skeletal Muscle Differentiation. *PLoS Genetics,* 7(6), pp. 1-16.

Vichaiwong, K. et al., 2010. Contraction Regulates Site-Specific Phosphorylation of TBC1D1 in Skeletal Muscle. *Biochemical Journal,* Volume 431, pp. 311-320.

Viollet, B. et al., 2009. Targeting the AMPK Pathway for the Treatment of Type 2 Diabetes. Volume 14, pp. 3380-3400.

Wang, Z. & Thurmond, D. C., 2009. Mechanisms of Biphasic Insulin-granule Exocytosis - Roles of the Cytoskeleton, Small GTPases and SNARE Proteins. *Journal of Cell Science,* 122(7), pp. 893-903.

Watson, R. T. & Pessin, J. E., 2006. Bridging the GAP Between Insulin-signalling and GLUT4 Translocation. *TRENDS in Biochemical Sciences,* Volume 31, pp. 215-222.

West, D. B. & York, B., 1998. Dietary Fat, Genetic Predisposition, and Obesity: Lessons From Animal Models. *The American Journal of Clinical Nutrition,* Volume 67, pp. S505-S512.

White, M. F., 2002. IRS Proteins and the Common Path to Diabetes. *American Journal of Physiology Endocrinology and Metabolism,* Volume 283, pp. E413-E422.

White, R. A., Pasztor, L. M., Richardson, P. M. & Zon, L. I., 2000. The Gene Encoding TBC1D1 with Homology to the Tre-2/USP6 Oncogene, BUB2 and cdc16 Maps to Mouse Chromosome 5 and Human Chromosome 4. *Cytogenetic and Genome Research,* Volume 89, pp. 272-275.

Wilson, C. M. & Cushman, S. W., 1994. Insulin Stimulation of Glucose Transport Activity in Rat Skeletal Muscle: Increase in Cell Surface GLUT4 as Assessed by Photolabelling. *Biochemical Journal,* Volume 299, pp. 755-759.

Witczak, C. A. et al., 2010. CAMKII Regulates Contraction- but not Insulin-induced Glucose Uptake in Mouse Skeletal Muscle. *American Journal of Physiology, Endocrinology and Metabolism,* Volume 298, pp. E1150-E1160.

Withers, D. J. et al., 1998. Disruption of IRS-2 Causes Type 2 Diabetes in Mice. *Nature,* Volume 391, pp. 900-904.

Wojtaszewski, J. F. P. et al., 2005. 5'AMP Activated Protein Kinase Expression in Human Skeletal Muscle: Effects of Strength Training and Type 2 Diabetes. *The Journal of Physiology,* Volume 564, pp. 563-573.

Woods, A. et al., 2003. Identification of Phosphoylation Sites in AMP-activated Protein Kinase (AMPK) for Upstream AMPK Kinases and Study of Their Roles by Site-directed Mutagenesis. *The Journal of Biological Chemistry,* Volume 278, p. 2843428442.

Wright, D. C., Geiger, P. C., Holloszy, J. O. & Han, D.-H., 2005. Contraction and Hypoxia-stimulated Glucose Transport is Mediated by a Ca2+-dependant Mechanism in Slow-twitch Rat Soleus Muscle. *American Journal of Physiology, Endocrinology and Metabolism,* Volume 288, pp. E1062-E1065.

Xu, Y. et al., 2011. Dual-mode of Insilin Action Controls GLUT4 Vesicle Endocytosis. *The Journal of Cell Biology,* Volume 193, pp. 643-653.

Yaffe, D. & Saxel, O., 1977. Serial Passaging and Differentiation of Myogenic Cells Isolated From Dystophic Mouse Muscle. *Nature,* Volume 270, pp. 725-727.

Yamamoto, D. L. et al., 2008. Myotube Formation on Micro-patterned Glass: Intracellular Organisation and Protein Distribution in C2C12 Skeletal Muscle Cells. *Journal of Histochemistry and Cytochemistry,* 56(10), pp. 881-892.

Yang, J. et al., 1992. Trafficking of Glucose Transporters in 3T3-L1 Adipocytes. *Biochemical Journal,* Volume 281, pp. 809-817.

Yang, J. & Holman, G. D., 1993. Comparison of GLUT4 and GLUT1 SubcellularTrafficking in Basal and Insulin-stimulated 3T3-L1 Cells. *The Journal of Biological Chemistry,* Volume 268, pp. 4600-4603.

Yang, J. & Holman, G. D., 2005. Insulin and Contraction Stimulate Exocytosis, but Increased AMP-activated Protein Kinase Activity Resulting from Oxidative

Metabolism Stress Slows Endocytosis of GLUT4 in Cardiomyocytes. *The Journal of Biological Chemistry,* Volume 280, pp. 4070-4078.

Yang, J. & Holman, G. D., 2006. Long-Term Metformin Treatment Stimulates Cardiomyocyte Glucose Transport through an AMP-Activated Protein Kinase-Dependant Reduction in GLUT4 Endocytosis. *Endocrinology,* 147(6), pp. 2728-2736.

Yan, K. S., Kuti, M. & Zhou, M.-M., 2002. PTB or not PTB - That is the Question. *FEBS Letters,* Volume 513, pp. 67-70.

Yoshida, N. et al., 1998. Cell Heterogeneity Upon Myogenic Differentiation: Down-regulation of MyoD and Myf-5 Generates 'Reserve Cells'. *Journal of Cell Science,* Volume 111, pp. 769-779.

Yu, P. B. et al., 2008. Dorsomorphin Inhibits BMP Signals Required for Embrogenesis and Iron Metabolism. *Nature Chemical Biology,* 4(1), pp. 33-41.

Zebedin, E. et al., 2004. Fibre-type Conversion Alters Inactivation of Voltage-dependant Sodium Currents in Mouse C2C12 Skeletal Muscle Cells. *American Journal of Physiology and Cell Physiology,* Volume 287, pp. C270-C280.

Zeigerer, A. et al., 2002. GLUT4 Retention in Adipocytes Requires Two Intracellular Insulin-regulated Transport Steps. *Molecular Biology of the Cell,* Volume 13, pp. 2421-2435.

Zeigerer, A., McBrayer, M. K. & McGraw, T. E., 2004. Insulin Stimulation of GLUT4 Exocytosis, but Not its Inhibition of Endocytosis, is Dependant on RabGAP AS160. *Molecular Biology of the Cell,* Volume 15, pp. 4406-4415.

Zhou, G. et al., 2001. Role of AMP-activated Protein Kinase in Mechanism of Metformin Action. *The Journal of Clinical Investigation,* Volume 108, pp. 1167-1174.

Zierath, J. R., Houseknecht, K. L., Gnudi, L. & Kahn, B. B., 1997. High-Fat Feeding Impairs Insulin-Stimulated GLUT4 Recruitment via an Early Insulin-Signalling Defect. *Diabetes,* Volume 46, pp. 215-223.

Zisman, A. et al., 2000. Targeted Disruption of the Glucose Transporter 4 Selectively in Muscle Causes Insulin Resistance and Glucose Intolerance. *Nature Medicine,* Volume 6, pp. 924-928.